EMERGING INFECTIOUS DISEASES®

EDITOR-IN-CHIEF
D. Peter Drotman

EMERGING INFECTIOUS DISEASES®

Vectorborne Diseases   November 2025

Synopses

Medscape
EDUCATION
ACTIVITY

Research

Dispatches

2122

EMERGING INFECTIOUS DISEASES®

November 2025

2168

About the Cover

Etymologia

Research Letters

2140

Haematospirillum jordaniae Infections after Recreational Exposure to River Water, Pennsylvania, USA, 2020

Melissa Dulcey, Katherine M. DeBord, Melissa E. Bell, Meghan T. Murray,
Adam M. Szewc, Kate Livingston, Brendan Headd, John R. McQuiston,
Eva Gordian-Rivera, Ben W. Humrighouse, Allison Longenberger, William A. Bower

Haematospirillum jordaniae was first identified as a human pathogen in 2016. In this article, we describe 4 patients who had *H. jordaniae* infections identified in 2020 and who had temporally and spatially linked environmental exposures. Three of the 4 patients reported leg injuries while participating in recreational river water activities in south-central Pennsylvania, USA. In 2024, we detected *H. jordaniae* in river samples collected at locations identified during patient interviews. All patients sought emergency department services for clinical assessment; however, the causative bacterial isolate was not initially identified. *H. jordaniae* was identified as the bacterial cause months after patient treatment and discharge. Although *H. jordaniae* infections are considered rare, the true occurrence is unknown. Additional information about the organism's ecology and environmental seasonality could guide public health messaging and increase awareness among healthcare providers.

*H*aematospirillum jordaniae is a slow-growing, gram-negative, rod-shaped bacterium that belongs to the alphaproteobacteria family Rhodospirillaceae. *H. jordaniae* was first identified as a human pathogen in 2016 by the Special Bacteriology Reference Laboratory (SBRL) at the Centers for Disease Control and Prevention (CDC) (1). SBRL identified 25 total *H. jordaniae* isolates that were sent from state health departments across the United States during 2000–2019. All 25 historical isolates were obtained from blood samples collected from adult men averaging 58 (range 39–78) years of age. Most of the clinical cases were identified during summer and fall months, suggesting a seasonal trend associated with *H. jordaniae* infection. In this article, we describe 4 patients who had *H. jordaniae* infections identified in 2020 and who had environmental exposures in a defined region of Pennsylvania, USA. We also describe the results of environmental testing for *H. jordaniae* conducted in the same area in 2024.

Methods

Identifying the Bacteria in Clinical Samples
Patient blood samples were sent to the Pennsylvania Department of Health (PADOH)'s Bureau of Laboratories for bacterial identification and to rule

Author affiliations: Centers for Disease Control and Prevention, Atlanta, Georgia, USA (M. Dulcey, K.M. DeBord, M.E. Bell, M.T. Murray, A.M. Szewc, K. Livingston, B. Headd, J.R. McQuiston, B.W. Humrighouse, W.A. Bower); Pennsylvania Department of Health, Harrisburg, Pennsylvania, USA (M. Dulcey, M.T. Murray, E. Gordian-Rivera, A. Longenberger)

out *Brucella* species, according to standard Laboratory Response Network protocols. After negative *Brucella* results and the inability to identify the isolates, bacterial isolates were then sent to SBRL at CDC for bacterial identification. We identified the bacterial isolates recovered from each patient using previously described methods for 16S rRNA gene sequence analysis and Clinical Laboratory and Standards Institute guidelines (1–3). We also used matrix-assisted laser desorption/ionization time-of-flight (MALDI-TOF) analysis as a secondary identification method. We performed MALDI-TOF analysis on a Biotyper SMART (Bruker) by using an in-house library containing reference spectra from 6 strains of *H. jordaniae*, which is publicly searchable through MicrobeNet (https://microbenet.cdc.gov). All isolates yielded a MALDI-TOF score of $\geq$2.0 for a reliable species-level identification as *H. jordaniae*.

Medical Information
We conducted emergency department (ED) medical chart reviews for all 4 patients. Public health officials conducted interviews with patients 1, 2, and 3. Patient 4 could not be reached for interview.

Environmental Sample Collection
We identified 3 water locations in Pennsylvania for environmental sampling on the basis of patient interviews. Patient 2 identified locations A and B as her entry and exit points in the creek on the day of injury, near where patient 1 also reported injury. Patient 3 identified location C as the location where the patient entered the river on the day of injury, ≈50 miles from locations A and B.

We collected four 1-L water samples from locations A and B once a month throughout 2024 and four 1-L water samples from location C for 7 months in 2024. We collected water samples from the river's surface, enabling the current to flow into the container without disturbing the river bottom sediment. At each sample collection site, we collected global positioning satellite coordinates, weather conditions, and water physiochemical measurements (pH, temperature, dissolved oxygen, conductivity, and specific conductance) by using a YSI Pro 2030 (YSI Incorporated).

Environmental Sample Processing and Testing
We shipped water samples to SBRL on cold packs on the day of sample collection. Because of resource constraints, a subset of the total number of collected samples were processed for DNA extraction. We filtered 1-L samples through MicroFunnel filter funnels containing a 0.22 µm filter (Cytiva), and we extracted

genomic DNA from the filters by using the DNeasy PowerWater Kit (QIAGEN) according to manufacturer instructions. We analyzed extracted filter genomic DNA by using previously published methods for a real-time quantitative PCR (qPCR) specific to *H. jordaniae* (*4*). Modifications of methods for the screening of the submitted water samples included using the previously published real-time qPCR with environmental samples and testing environmental genomic DNA extracted from water filters. We used 2 layers of controls, including positive (PCR amplification) and negative (nontemplate) controls for real-time qPCR, as well as positive and negative filter extraction controls, which aided in confirming that targeted DNA could be collected through experimental filter extraction.

Ethics

This study did not meet the definition of human subjects research as defined in the US Code of Federal Regulations, Title 45 Part 46. Therefore, this study was not subject to review by an institutional review board.

Case Series

Patient 1

Patient 1 was a 28-year-old man who reported a scratch to his right distal leg in September 2020 (Figure 1). The injury occurred while participating in a recreational water activity in a south-central Pennsylvania creek. Within 24 hours of the injury, redness developed on the medial aspect of the patient's right lower extremity. Two days later, swelling and pain developed at the location of the redness. The patient was initially treated by his primary care physician by telehealth appointment and prescribed

cephalexin. After treatment was initiated, the redness started to improve but then became worse and spread down the patient's leg, resulting in swelling of his ankle. The patient denied any fever or chills and was taking oral cephalexin (500 mg every 6 h for 10 days) as prescribed.

Ten days after the initial injury, the patient sought care at a local ED with a primary complaint of severe pain associated with the right lower extremity wound infection. Temperature was 37.1°C, heart rate 115 beats/min, respiratory rate 18 breaths/min, blood pressure 148/102 mm Hg, and oxygen saturation 99% on room air. Physical examination revealed swelling, tenderness, and erythema on the medial aspect of the right lower extremity from the ankle to halfway up the tibia. The patient's remaining physical examination findings were unremarkable. Laboratory results at admission revealed an elevated leukocyte count of 21,800 cells/µL (reference range 3,900–9,500 cells/µL) (Table).

The patient was given 1 dose of intravenous (IV) vancomycin (1.25 g) in the emergency room before being hospitalized for sepsis and cellulitis and started on IV vancomycin (1.5 g every 8 h) and IV clindamycin (600 mg every 8 h) antimicrobial therapy. Radiographs and ultrasound of the right ankle showed a moderate amount of soft tissue swelling surrounding the ankle that was consistent with cellulitis. No fluid collection was observed in the ankle to indicate a septic joint, and no radiopaque foreign body or acute osseous abnormalities were observed. The patient clinically improved, was discharged after 3 days of in-hospital treatment, and was prescribed a 7-day course of oral clindamycin (300 mg every 6 h). A blood sample obtained at admission was cultured, and a bacterial
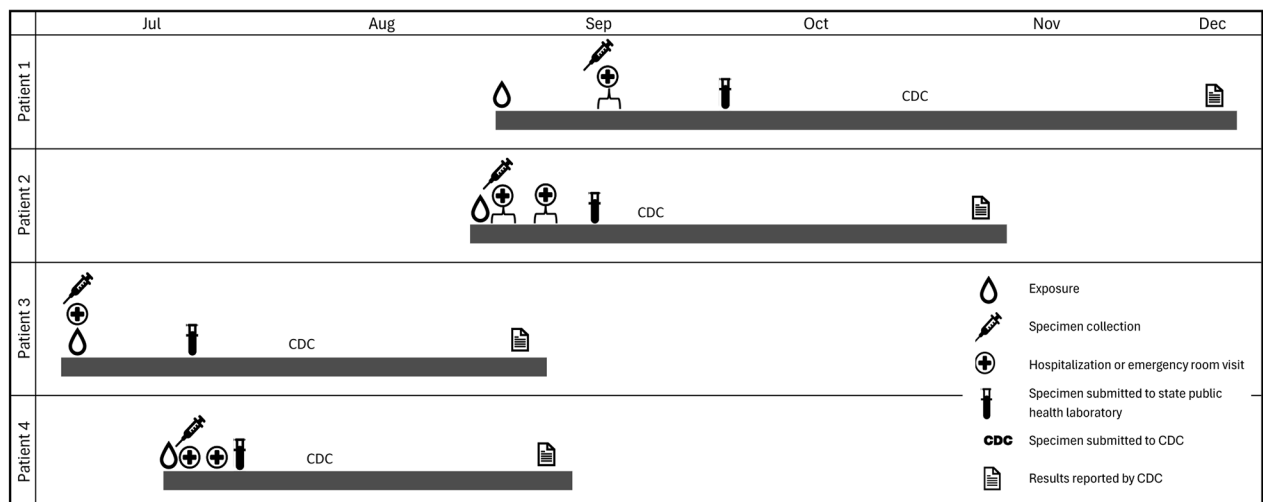
Figure 1. Clinical timeline of 4 patients with *Haematospirillum jordaniae* infections, Pennsylvania, USA, 2020. Three of the 4 cases were later determined to be associated with recreational freshwater exposure.

Table. Laboratory results during initial hospital admission of 4 patients with *Haematospirillum jordaniae* infections with recreational water exposure in 3 of 4 cases, Pennsylvania, USA, 2020*

Laboratory values	Patient 1	Patient 2	Patient 3	Patient 4
Leukocyte count, cells/µL	21,800 (3,900–9,500)	24,200 (3,900–9,500)	22,430 (4,000–10,800)	21,000 (4,000–11,000)
Neutrophil count, cells/µL	18,300 (1,800–7,400)	20,570 (1,800–7,400)	17,620 (1,800–7,700)	18,000 (1,700–7,800)
Platelets/µL	394,000 (140,000–366,000)	413,000 (140,000–366,000)	247,000 (140,000–400,000)	265,000 (140,000–400,000)
Creatinine, mg/dL	0.87 (0.7–1.3)	0.75 (0.6–1.2)	0.8 (0.6–1.2)	0.91 (0.7–1.3)
Hemoglobin, g/dL	15 (12.8–16.6)	13 (11.7–15.1)	15.3 (14.0–16.8)	14.3 (13–17.3)
Calculated eGFR non-African American, mL/min/1.73 m^2	117 ($\geq$90)	104 ($\geq$89)	>60 (>60)	>90.0 ($\geq$90)

*Values in parentheses are hospital laboratory reference values. eGFR, estimated glomerular filtration rate.

isolate was recovered; 16S rRNA gene sequence analysis showed the isolate to be most closely related to *H. jordaniae* (reference strain no. DSM 28903^T). A nearly full-length (1,406-bp) 16S rRNA gene sequence from the isolate shared 99.9% sequence similarity with DSM 28903^T. On the basis of Clinical and Laboratory Standards Institute guidelines (3), we identified the isolate (GenBank accession no. PX060169) as *H. jordaniae* 3 months after the patient's admission.

Patient 2

Patient 2 was a 34-year-old woman with a history of rheumatoid arthritis, hypothyroidism, idiopathic thrombocytopenic purpura, hypertension, and migraines. She reported hitting her left shin on a rock in August 2020 while participating in a recreational water activity in a south-central Pennsylvania creek (Figure 1). The patient reported redness and discomfort developing in the area the day after injury and severe pain of the lower leg around superficial abrasions on the left shin that developed 3 days later. The patient subjectively reported low-grade fever, without objective temperatures >100°F (37.8°C). Four days after the initial exposure, the patient was evaluated by her primary care physician, who was concerned that compartment syndrome might have developed and advised her to go to the ED for further evaluation.

During ED examination, the patient reported severe left lower leg pain. Temperature was 37.7°C, heart rate 121 beats/min, respiratory rate 18 breaths/min, blood pressure 150/108 mm Hg, and oxygen saturation 100% on room air. Physical examination revealed erythema and tenderness of the left lower extremity, and a 1 cm abrasion was located on the anterior aspect of the leg distal to the left knee. Edema of the left lower leg was also noted. The rest of the physical examination was unremarkable. Laboratory results at admission revealed an elevated leukocyte count of 24,200 cells/µL (reference range 3,900–9,500 cells/µL) (Table).

The patient was hospitalized for sepsis attributable to cellulitis and administered a single dose of IV ceftriaxone (1 g) in the ED and started on IV cefazolin antimicrobial therapy (2g every 8 h) after admission as treatment for potential group B *Streptococcus* infection. Radiographs of the patient's left lower fibula and tibia showed subcutaneous phleboliths (calcification of blood clots) likely unrelated to the injury and no radiopaque foreign body or acute osseous abnormalities. The patient clinically improved during hospitalization with decreased left leg pain, improved leukocyte count, and improved physical therapy evaluations. She was discharged after 2 days and prescribed an 8-day course of oral cephalexin (500 mg 4×/d).

Within 2 days of discharge, the blood cultures performed at admission were positive for unspecified gram-negative rod-shaped bacteria, and the patient was advised to return to the ED for evaluation. At admission, the patient reported improved symptoms with decreased redness and swelling at the site and an increased ability to ambulate on her left leg. She denied any fevers, chills, nausea, or vomiting. On physical examination, a slight warmth around the healing abrasions was noted, the erythema on her left leg had improved, and no edema was apparent. Repeat blood culture, lactic acid, basal metabolic panel, and complete blood count were performed. Other than a slightly elevated leukocyte count at 9,600 cells/µL (reference range 3,900–9,500 cells/µL), other values were unremarkable. The patient was hospitalized and treated with IV cefepime (2 g every 8 h); while hospitalized, the patient continued to clinically improve. She was discharged on day 3 with a 10-day course of oral levofloxacin (750 mg/d). The blood cultures from blood obtained during the second hospitalization were negative. Two months later, we identified the isolate from a blood sample obtained during the patient's initial hospitalization as *H. jordaniae* (GenBank accession no. PX060171). A nearly full-length (1,408-bp) 16S rRNA gene sequence from the isolate shared 99.9% sequence similarity with DSM 28903^T.

Patient 3

Patient 3 was a 36-year-old man with history of diabetes mellitus, obesity, and boils. He reported hitting his

leg in July 2020 while participating in a recreational water activity in a south-central Pennsylvania river (Figure 1). The patient sought care at the ED the day after the injury with pain, swelling, and erythema of the anterior aspect of the right leg.

At initial examination, the patient reported severe right lower leg pain. Temperature was 36.4°C, heart rate 106 beats/min, respiratory rate 16 breaths/min, blood pressure 164/76 mm Hg, and oxygen saturation 97% on room air. Physical examination showed a 10.5 cm area of poorly defined erythema, warmth, and tenderness of the anterior aspect of the right leg. No drainage, breakage of the skin, or crepitus of the limb's joints was noted. Laboratory results at admission demonstrated an elevated leukocyte count of 22,430 cells/μL (reference range 4,000–10,800 cells/μL) (Table).

The patient was administered a single dose of IV clindamycin (800 mg) for presumed bacterial infection. Radiographs of the right tibia and fibula showed chronic calcification of the diaphysis of the tibia, unchanged from a prior radiograph, and no signs of acute osseous abnormalities, radiopaque foreign body, or soft tissue gas. On the basis of the patient's age, comorbidities, laboratory results, imaging, and examination findings, the decision to treat as an outpatient with a primary care physician follow-up was made. The patient was discharged with a 10-day course of oral clindamycin (300 mg every 8 h).

Within 4 days of discharge, the blood culture performed at admission was positive for gram-negative rod-shaped bacteria. The patient was advised to return to the ED for evaluation and additional blood cultures. At admission, the patient reported feeling better with right leg improvement. He had slight tenderness and itchiness of the right leg, with pain only when walking and during palpation. Physical examination showed an increased warmth of the right anterior lower leg compared with the left leg and a central scabbed-over pinpoint wound on the right leg with mild erythema. Bloodwork revealed resolved leukocytosis; other blood values, radiographs, and urinalysis results were unremarkable. The patient was hospitalized and received IV cefepime (dose unknown) for bacteremia and cellulitis of the right lower extremity. While hospitalized, the patient clinically improved, and the redness of the right leg completely resolved. Three days after collection, preliminary results for the repeat blood cultures were negative. After consultation with an infectious disease doctor, the patient was discharged on a 10-day course of oral ciprofloxacin (500 mg every 12 h) and oral amoxicillin/clavulanate (500 mg/125 mg every 8 h) (length of course

unknown). The blood cultures obtained during hospitalization were negative after 5 days of incubation. Gram-negative rod-shaped bacteria were recovered by the hospital laboratory from blood cultures collected at the patient's initial ED visit. We identified the isolate as *H. jordaniae* 1.5 months after the patient's discharge (GenBank accession no. PX060170). A nearly full-length (1,408-bp) 16S rRNA gene sequence from the isolate shared 99.9% sequence similarity with DSM 28903[T].

Patient 4

Patient 4 was a 48-year-old man with history of fatty liver who sought care at the ED in July 2020 with a history of a fever up to 101°F (38.3°C), nausea, and left lower leg erythema with swelling of 1-day duration (Figure 1). The patient reported being at a cabin the prior 2 days and noticed bug bites and scratches develop on his legs while walking in shorts. Additional information about any water-related exposures for this patient are unknown as the patient was unable to be reached for an interview.

At initial examination, the patient had a fever of 38.6°C; heart rate was 111 beats/min, blood pressure 107/67 mm Hg, and an oxygen saturation of 97% on room air. Physical examination showed bug bites and erythema on the anterior distal shin of the left leg that did not extend to the knee or thigh. Mild edema was also noted in areas of erythema. Tachycardia was the only other major physical examination finding. Laboratory results at admission revealed an elevated leukocyte count of 21,000 cells/μL (reference range 4,000–11,000 cells/μL) (Table).

The patient was observed in hospital for cellulitis and administered a single dose of IV cefazolin (2g). Ultrasound of the left lower extremity revealed no signs of deep vein thrombosis. The patient's fever and tachycardia improved with IV fluids, ketorolac tromethamine, and acetaminophen. The patient was discharged ≈4 hours after admission with a 7-day course of oral sulfamethoxazole/trimethoprim (800 mg/160 mg every 12 h). Two months later, we identified an isolate from a blood sample obtained during the patient's ED treatment as *H. jordaniae* (GenBank accession no. PX060172). A nearly full-length (1,408-bp) 16S rRNA gene sequence from the isolate shared 99.9% sequence similarity with DSM 28903[T].

Environmental Testing

We collected 121 total water samples. We processed and extracted DNA from 67 (55%) samples: 23 from location A, 23 from location B, and 21 from location C. Of the 67 processed samples, 18 (27%) tested positive

for *H. jordaniae* by real-time qPCR. All positive samples were collected during July–October; 83% (n = 15) of positive samples were from location C, but all 3 sampling sites had >1 positive sample (Figure 2). During July–September, location C demonstrated an average cycle threshold value difference of 5.88 compared with locations A and B, representing almost a 2-log increase in bacterial load at location C compared with the other sampling locations. Water temperature ranged from 4.9° to 28.1°C throughout the year, with peak temperatures recorded in July and August.

Discussion

We identified 4 patients with *H. jordaniae* infections that were spatially and temporally linked in Pennsylvania in 2020. Through systematic environmental sampling over a 1-year period in 2024, we identified *H. jordaniae* in the implicated water sources for 3 of the 4 patients at the same time of year when the patients' exposures occurred.

Three of 4 patients reported leg injuries and freshwater exposure. Exposures occurred independently of one another while participating in recreational water activities in waterways that are tributaries of the Susquehanna River in south-central Pennsylvania. The fourth patient's exposure to freshwater is unknown; however, he did spend time outdoors during the same period. A handful of sporadic cases of *H. jordaniae* have been published previously (5–7), including 2 persons with documented freshwater exposure accompanied by an injury to the skin or soft tissue, similar to 3 patients reported in this article (5). Although we have limited epidemiologic details on *H. jordaniae* isolates submitted to CDC, most historical specimens were collected during July and August, which coincides with the timing of infections for the 4 case-patients presented in this article.

Environmental testing over a 1-year period at 3 locations where the patients reported entering or exiting the rivers suggest seasonality in the detection of

H. jordaniae. All positive environmental samples were collected during July–October, coinciding with the timing of the 4 patients' illnesses, as well as historical *H. jordaniae* infections. Despite those findings, information on the presence and persistence of *H. jordaniae* in the environment remains limited. Although this study is a systematic sampling and testing for *H. jordaniae* in the environment in Pennsylvania, the study was limited in scope. Because of limited resources, we were not able to process all samples collected or visit location C for all months of the year. The full geographic distribution of *H. jordaniae* in this area and its persistence in water remains unknown. Additional information about the organism's ecology and seasonality in the environment can guide future messaging efforts focused on disease prevention and increase awareness of the pathogen's transmission among healthcare providers and the public.

Although *H. jordaniae* infections are considered rare, the true occurrence is unknown. For the 4 patients in this cluster, the final identification of *H. jordaniae* as the bacterial cause of their infections did not occur until months after they were treated and discharged. Diagnosing an *H. jordaniae* infection can be challenging because of the difficulty in recovering the bacteria from primary specimens because of the slow growth and fastidious nature of the organism. Bacterial identification was attempted at the hospital or the PADOH laboratories before isolates were submitted to CDC, leading to additional logistical delays in final identification. Recently, laboratory methods for a sensitive, specific, and efficient real-time qPCR were published (4). Such methods could be used by state and local health departments to decrease time to diagnosis and to identify cases of *H. jordaniae* that would otherwise go undetected if specimens are not submitted to CDC. Taxonomic updates to bacterial databases for commercial platforms might also improve identification in hospital and state laboratories, decreasing the time for identification.
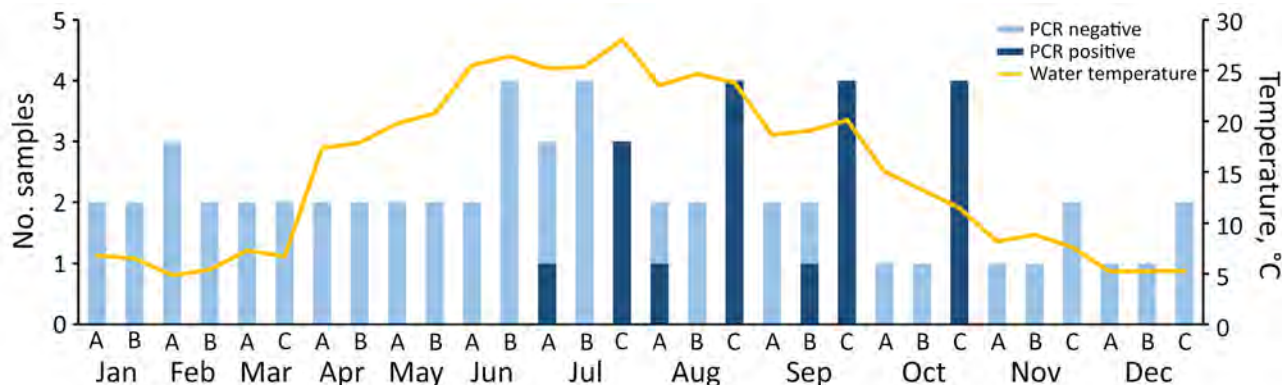
Figure 2. Environmental testing results for *Haematospirillum jordaniae* and water temperature measurements at 3 locations (A–C) in Pennsylvania, USA, 2024, in study of 4 patients with *H. jordaniae* infections from 2020 after recreational water exposure.

Information regarding *H. jordaniae* and its effects on human health remains limited. Although *H. jordaniae* infections are rare, this case series highlights freshwater exposure as a potential route of transmission. Clinicians should be vigilant in identifying bacterial infections and the potential for sepsis during midsummer and early fall when treating skin wounds that might be associated with freshwater exposure. In addition, *H. jordaniae* should be considered in the differential diagnosis for those patients when requesting bacterial identification from local public health laboratories. This request could expedite bacterial identification and provide a better estimate of the total number of *H. jordaniae* infections across the United States.

About the Author

Dr. Dulcey graduated from the Centers for Disease Control and Prevention's Epidemic Intelligence Service Program, where she worked at the Pennsylvania Department of Health on infectious disease epidemiology, prevention, and response. She has a decade of experience in One Health research and epidemiology in vectorborne and zoonotic diseases and environmental health.

References

1. Humrighouse BW, Emery BD, Kelly AJ, Metcalfe MG, Mbizo J, McQuiston JR. *Haematospirillum jordaniae* gen. nov., sp. nov., isolated from human blood samples. Antonie van Leeuwenhoek. 2016;109:493–500. https://doi.org/10.1007/s10482-016-0654-0
2. Morey RE, Galloway RL, Bragg SL, Steigerwalt AG, Mayer LW, Levett PN. Species-specific identification of *Leptospiraceae* by 16S rRNA gene sequencing. J Clin Microbiol. 2006;44:3510–6. https://doi.org/10.1128/JCM.00670-06
3. Clinical and Laboratory Standards Institute. Performance standards for antimicrobial susceptibility testing; twenty-fifth informational supplement (M100-S25). Wayne (PA): The Institute; 2015.
4. Szewc AM, Humrighouse BW, Livingston K, Gulvik CA, Nicholson AC, McQuiston JR. Detection of an emerging pathogen: a real time qualitative pcr assay targeting *Haematospirillum jordaniae* for EDTA whole blood and plasma clinical specimens. Diagn Microbiol Infect Dis. 2024;109:116310. https://doi.org/10.1016/j.diagmicrobio.2024.116310
5. Creech ZA, Truong GTD, Kenny DX, Butt DN, Li C, Cavalieri S, et al. Unusual freshwater-related infections caused by *Haematospirillum jordaniae*. Cureus. 2022;14:e25480. https://doi.org/10.7759/cureus.25480
6. Hovan G, Hollinger A. Clinical isolation and identification of *Haematospirillum jordaniae*. Emerg Infect Dis. 2018;24:1955–6. https://doi.org/10.3201/eid2410.180548
7. Pal E, Štrumbelj I, Kišek TC, Kolenc M, Pirš M, Rus KR, et al. *Haematospirillum jordaniae* cellulitis and bacteremia. Emerg Infect Dis. 2022;28:2116–9. https://doi.org/10.3201/eid2810.220326

Address for correspondence: Katherine M. DeBord, Centers for Disease Control and Prevention, 1600 Clifton Rd NE, Mailstop H24-12, Atlanta, GA 30329-4018, USA; email: wgr9@cdc.gov

Trichosporon austroamericanum Infections among Hospitalized Patients, France, 2022–2024

Emilie Burel, Catherine Sartor, Valérie Moal, Vincent Bossi, Jacques Sevestre,
Justine Solignac, Rémi Charrel, Marie Desnos-Ollivier, Stéphane Ranque, Estelle Menu

During 2022–2024, six cases of invasive fungal infection occurred among immunocompromised patients at Marseille University Hospital, Marseille, France. Matrix-assisted laser desorption/ionization time-of-flight mass spectrometry initially identified *Trichosporon inkin* fungi. However, phylogenetic analysis of intergenic spacer region 1 and whole-genome sequences revealed the genetically distinct species *T. austroamericanum*. Analysis of core genome and mitogenome from 6 patient isolates and 1 environmental isolate revealed substantial genetic diversity among *T. austroamericanum* strains, indicating a polyclonal outbreak. Furthermore, the mitochondrial genome emerged as a potential marker for intraspecies differentiation, which potentially could aid in epidemiologic investigations. Identified in 2024 but potentially underestimated, *T. austroamericanum* has since been reported in case clusters from hospital settings in France, highlighting the need for accurate fungal identification and suggesting previously identified *T. inkin* cases should be re-evaluated for *T. austroamericanum*. Clinical *T. austroamericanum* is emerging in hospital settings and should be included in the differential diagnosis of fungal infections.

Fungi belonging to various species of the genus *Trichosporon* can cause a wide range of infections, from superficial skin damage to serious systemic infections in immunocompromised persons, who can have high mortality rates (*1*). *Trichosporon*, which belongs to the Basidiomycota family, includes ≈20 species that are pathogenic to humans (*2*). Although *Cutaneotrichosporon cutaneum* and *T. asahii* are the predominant Basidiomycota species, new species have increasingly been described in human pathology since 2002 (*2*).

In 2024, a new Basidiomycota species, *T. austroamericanum*, was identified in a urine sample from a kidney transplant recipient in Brazil (*3*); the species was then detected in several clinical samples from France, South America, and Asia. *T. austroamericanum* and *T. inkin* have been confounded in the past before the species were distinguished through phylogenetic analysis of the intergenic spacer (IGS) 1

region and amplified fragment length polymorphism fingerprinting.

Ubiquitous in the environment, some *Trichosporon* species have been isolated from soil, leaf mold, and decayed wood (*4*). The environmental reservoirs of *T. inkin* and *T. austroamericanum* remain unknown. Moreover, emergence of hospital trichosporonosis cases caused by *T. asahii* have been described (*5*), highlighting hospital sources during epidemiologic and environmental investigations. Thus, *Trichosporon* species should not be overlooked in the hospital environment.

During July 2022–June 2024, the kidney transplant department of Marseille University Hospital, Marseille, France, recorded 4 cases of invasive fungal infection. Whole-genome sequencing (WGS) was initially performed on the first 3 reported cases by using matrix-assisted laser desorption/ionization time-of-flight (MALDI-TOF) mass spectrometry, which

identified the agent as *T. inkin*. Further investigation using other molecular methods revealed *T. austroamericanum* fungi as the causative agent. Because of the rarity of the species, we suspected a putative common source. Moreover, 2 other cases subsequently were diagnosed in patients admitted in cardiology and gastrointestinal surgery centers in 2 other hospitals of our institution. We investigated the sudden upsurge of trichosporonosis cases through WGS and phylogenetic analysis.

Materials and Methods

We prospectively identified patients over a 2-year period from 3 different sites of Marseille University Hospital system, referred to as hospitals A, B, and C. Our study included all patients with associated clinical signs of infection from whom *T. austroamericanum* fungi was isolated from sterile sites.

We collected retrospective medical data for each patient, when available, by using HOSPILINK DPI version 5.11.3P10.8.3 (Axigate Link, https://axigatelink.com) and processed data in an anonymized Excel 2013 file (Microsoft, https://www.microsoft.com). Data included demographic information, exposure factors, underlying diseases, and clinical signs and symptoms.

Inclusion and Ethics

We anonymized all identified *T. austroamericanum* strains recovered from clinical samples and stored them in Cryosysteme Protect bead tubes (Dutscher, https://www.dutscher.com) at −20°C. The hospital strain bank assigned a unique number to each sample: L0221, L0385, L0399, L0419, L0445, and L0458. The hospital routinely performed antifungal susceptibility testing by using the Sensititre YeastOne microdilution method (Thermo Fisher Scientific, https://www.thermofisher.com), according to the manufacturer's instructions.

This study was reviewed and approved by the Ethics Committee of Assistance-Publique-Hôpitaux de Marseille (approval no. CSE24-49) and the Assistance Publique Hôpitaux de Marseille Health Data Access Portal (approval no. PADS24-275). Patients were informed of the research and their nonopposition to the use of their data was collected. In accordance with those committees and current regulations, written informed consent was not required. All potentially identifying information was removed in compliance with International Committee of Medical Journal Editors guidelines.

Mycologic Investigation

From identified patients, we collected cryptococcal antigen in serum by using Cryptococcal Antigen Lateral Flow Assay (IMMY, https://www.immy.com) and Platelia *Aspergillus* Antigen (Bio-Rad Laboratories, https://www.bio-rad.com). In addition, the hospital's infection control team initiated an environmental investigation in 2023, which they continued in 2024 until the last infected patient was identified. The investigation focused on the rooms and units where the initial kidney transplant patients had been under care from the date of admission to discharge, including radiology, the intensive care unit (ICU), the urological surgery operating theater, and the dialysis unit. The team also investigated the nephrology unit, where patients were hospitalized for a week after kidney transplantation. The team collected air samples by using AESAP1075 Sampl'air Lite microbiological air sampler (AES Laboratories, https://www.chemeurope.com), collecting 330 liters on Sabouraud dextrose agar (SDA). The team collected water samples from faucets or showers in patients' rooms in 250-mL bottles containing sodium thiosulfate. The team also collected surface samples by using eSwab Liquid Amies Elution Swabs (Copan, https://www.copangroup.com).

Next-Generation Sequencing

We performed DNA extraction on pure subculture from SDA supplemented with gentamicin and chloramphenicol (Bio-Rad), using previously described methods (*6*). We sequenced genomic DNA by using a paired-end strategy. We barcoded and prepared samples by using the COVIDseq Test sample prep kit (Illumina, https://www.illumina.com) adapted for fungi, in which the tagmentation step fragmented and tagged the DNA. We used limited cycle PCR amplification (12 cycles) to complete the tag adapters and introduce dual-index barcodes. After purification on ITB beads (Illumina), we normalized libraries to the same molarity, then pooled those into a single library for sequencing on the NovaSeq 6000 (Illumina). We loaded the pooled single-strand library onto the reagent cartridge and then onto the instrument along with the flow cell. We conducted automated cluster generation and paired-end sequencing of dual index reads in a single 25-hour run of 2 × 150 bp.

We also performed nanopore sequencing on individually sequenced genomic DNA by using the PromethION 2 Solo or GridION and the LSK109 Ligation Kit on a FLO-PRO002 flow cell (all Oxford Nanopore Technologies, https://nanoporetech.com). The end-prep step fixes specific nucleotides to use for adapter ligation, after which we purified the DNA on magnetic beads (CleanNA, https://www.cleanna.com). We activated the flow cell by adding a flush buffer and a tether from Flow Cell Priming Kit EXP-FLP002

(Oxford Nanopore Technologies). We then loaded the libraries onto the flow cell for a 72-hour run.

Bioinformatics

We converted Illumina binary base call (BCL) files into fastq files by using bclconverter version 4.2.4 (Illumina). We used Trimmomatic version 0.39 (7) to trim reads to a minimum Phred quality of 33 and minimum read length of 36 bp. We trimmed nanopore raw reads by using ProwlerTrimmer (8), a Phred quality of 20–35, and minimum read length of 1,000 bp.

We obtained complete genomes from mixed de novo assembly of Illumina and nanopore reads by using Unicycler version 0.4.4 (9). We removed contigs <1,000 bp in length. We determined GC content and evaluated contamination by using ContEst16S (EZBio https://www.ezbiocloud.net). We assessed assembly quality by using BUSCO version 5.7.1 and the fungi_odb10 database (10).

We used the Burrows-Wheeler aligner (Galaxy version 2.3 plus galaxy0; https://usegalaxy.eu) (12) to map filtered reads to the reference genome CBS 17435 (11) from the CBS culture collection (https://wi.knaw.nl/fungal_table) hosted by the Westerdijk Fungal Biodiversity Institute (Utrecht, the Netherlands). We generated consensus sequences by using iVar consensus (Galaxy version 1.4.4 plus galaxy0) (13), with depth coverage of >10 reads and base quality of Q20. We aligned the resulting sequences by using MAFFT (Galaxy version 7.526 plus galaxy2) (14).

We calculated pairwise single-nucleotide polymorphism (SNP) distances by using SNP distance matrix (Galaxy version 7.526 plus galaxy2) and identified SNPs by using the Find SNP Sites command (Galaxy version 2.5.1 plus galaxy0) (15). We aligned concatenated SNP lists and analyzed with IQ-TREE version 2.4.0 (http://www.iqtree.org) plus galaxy1 to generate a maximum-likelihood phylogenetic tree, which we visualized on iTOL (https://itol.embl.de). We calculated genome coverage with a custom Python script (Python Software Foundation, https://www.python.org).

We isolated mitochondrial genomes into a single circular contig ≈40-kb in size and aligned contigs by using mauve version 2.4.0 (16). We oriented contigs from the cytochrome c oxidase 1 start codon. When necessary, we generated reverse complements using an online tool (https://reverse-complement.com/terms.html), then annotated genomes by using GeSeq (https://chlorobox.mpimp-golm.mpg.de/geseq.html).

We mapped trimmed Illumina reads against the reference IGS1 sequence (CBS 17435) using Burrows-Wheeler aligner (12) and obtained consensus sequences by using sam2consensus (https://github.com/edgardomortiz/sam2consensus). We used MAFFT (https://mafft.cbrc.jp/alignment/server/index.html) (13) to align sequences and performed subsequent phylogenetic analysis by using IQ-TREE with 1,000 bootstraps (17).

Maximum-Likelihood Core-Genome Phylogenetic Analysis

We constructed a core-genome tree by using the Galaxy platform. We masked repeats with RepeatMasker (Galaxy version 4.1.5 plus galaxy0) and annotated the assemblies by using the Maker annotation pipeline (18) with the Augustus predefined prediction model *Cryptococcus neoformans gattii* (Galaxy version 2.31.11 plus galaxy2). We derived the aligned core-genome from the resulting annotated general feature format files by using Roary in Galaxy version 3.13.0 plus galaxy3, then collected SNPs by using the Find SNP Sites tool (Galaxy Version 2.5.1 plus galaxy0). We used those SNPs to build the maximum-likelihood tree on IQ-TREE version 2.3.6 (built August 4, 2024) (17), under ModelFinder (19). We visualized trees by using the iTOL platform.

Results

Patient Data

By June 2024, a total of 6 patients with *T. austroamericanum* infection had been identified (Table 1). The patients' median age was 65.5 (range 55–83) years; 3 (50%) were male and 3 (50%) were female. Four patients were kidney transplant recipients who had clinical signs of an infection 2–4 months after transplantation; all 4 had scar dehiscence and subcutaneous abscesses, suggesting that the scar was the portal of entry.

The 2 other patients were immunocompetent. One (sample no. L0419) had been hospitalized in the cardiology department and was referred for a nephrology consultation during the time the outbreak was occurring. That patient had not undergone recent surgery. The other patient (sample no. L0445) experienced shock and acute respiratory distress syndrome after gastrointestinal surgery.

Of the 25 *T. austroamericanum*–positive samples, 16 (64%) were blood cultures from 2 patients, 3 were scar swab samples from 1 patient, 3 were abscess aspiration samples from 3 patients, and 3 were respiratory samples (2 bronchial aspirate and 1 bronchoalveolar lavage fluid) from 1 patient. All *T. austroamericanum* isolates exhibited similar antifungal susceptibility profiles (Table 2), and we

Table 1. Characteristics of patients from investigation of *Trichosporon austroamericanum* infections among hospitalized patients, France, 2022–2024*

Characteristics	Sample no.					
	L0221	L0385	L0399	L0419	L0445	L0458
Patient location						
Hospital	A	A	A	B	C	A
Hospital ward						
Kidney transplantation unit	Y	Y	Y	N	N	Y
Cardiac surgery	N	N	N	Y	N	N
Gastrointestinal surgery	N	N	N	N	Y	N
Clinical signs at time of positive culture						
Fever	Y	Y	N	N	N	N
Asthenia	Y	Y	N	Y	Y	N
Dyspnea	N	Y	N	N	Y	N
Digestive symptoms	N	N	N	N	Y	N
Scar dehiscence	Y	Y	Y	NA	NA	Y
Biology at time of positive culture						
Creatinine, µmol/L	271	128	103	177	80.7	216
C-reactive protein, mg/L	86	73	43	22	NP	1.3
Positive culture results						
Date of first positive culture	2022 Jul	2023 Apr	2023 Jun	2023 Dec	2024 Apr	2024 Jun
Days after transplantation	71	78	135	NA	NA	115
No. positive samples	4	11	1	5	3	1
Blood	0	11	0	5	0	0
Scar swab	3	0	0	0	0	0
Abscess aspiration	1	0	1	0	0	1
Respiratory sample	0	0	0	0	3	0
Microbiology						
Cryptococcal antigen	Positive	Positive	Positive	Negative	NP	Negative
Titer	160	5,120	20	–	–	–
Aspergillus antigen	Negative	NP	NP	NP	Negative	NP
Index	0.04	–	–	–	0.13	–
Outcome						
Death within 90 d	N	N	N	Y	Y	N
No. days after first positive culture	NA	NA	NA	30	30	NA
Treatment						
Posaconazole	N	Y	N	N	N	N
Voriconazole	Y	Y	Y	N	N	Y
Amphotericin B	N	Y	N	N	N	N
Surgical debridement	Y	Y	Y	NA	N	Y
Immunosuppressant reduction	Y	Y	N	NA	NA	Y

*NA, not applicable; NP, not performed; –, no data.

noted no significant difference related to date of isolate collection.

Mycological Investigation

The infection control team conducted an environmental survey in hospital A during April 20, 2023–July 19, 2024. In total, they collected 145 surface samples, 33 air samples, and 17 water samples in the urological surgery operating theater and the following patient units: the nephrology ICU, the kidney transplantation unit, the nephrology daycare, the radiology unit, and the dialysis unit. Samples were mainly collected from patient rooms, medical device storage area, and the decontamination room. All 195 samples were negative for *T. austroamericanum*. However, a *T. austroamericanum* strain was isolated from an air sample taken as part of a routine surveillance in a pediatric ICU of hospital B.

Table 2. Antifungal susceptibility testing of isolates from investigation of *Trichosporon austroamericanum* infections among hospitalized patients, France, 2022–2024*

Strain no.	MIC per antifungal agent, µg/mL								
	AMB	5-FC	FCZ	ITC	VRC	POS	CAS	MCF	AND
L0221	1	64	0.5	0.12	0.03	0.12	8	8	8
L0385	0.25	32	0.5	0.06	0.015	0.06	>8	>8	>8
L0399	0.25	16	1	0.06	0.015	0.12	>8	>8	>8
L0419	0.12	>64	1	0.06	0.015	0.06	>8	>8	>8
L0445	2	>64	1	0.12	0.03	0.25	>8	>8	>8
L0458	0.5	32	1	0.12	0.03	0.12	8	8	8

*AMB, amphotericin B; ANI, anidulafungin; CAS, caspofungin; FCZ, fluconazole; ITC, itraconazole; MIF, micafungin; VRC, voriconazole; POS, posaconazole; 5-FC, 5-Fluorocytosine.

Next-Generation Sequencing

Multilocus Sequence Typing

We initially performed WGS on the first 3 reported cases, which MALDI-TOF mass spectrometry had identified as *T. inkin*. To investigate genetic variations, we applied a multilocus sequence typing approach. We mapped sequences of *cytb*, *rpb1/2*, and *tef1* genes and the SSU and D1/D2 regions against the reference genome of *T. inkin* (GenBank accession no. MT801082). Although the sequences were identical among the isolates, notable differences from *T. inkin* emerged among isolates from those 3 cases. In addition, we observed high divergence between the strains from our investigation and the *T. inkin* reference mitochondrial genome and IGS1 marker, characterized by numerous point mutations, deletions, and insertions (Appendix Figure 1, https://wwwnc.cdc.gov/EID/article/31/11/25-0503-App1.pdf). The consistent mutation patterns across the strains, along with their divergence from *T. inkin*, strongly supported the classification of the isolates as a distinct taxonomic entity. That preliminary analysis served as the starting point for further investigation into the IGS1 region of the 6 patient-derived isolates. Phylogenetic analysis, which included 3 reference sequences provided by the National Reference Center for Invasive Mycoses and Antifungals (CNRMA) at Institut Pasteur (https://www.pasteur.fr), confirmed that the 7 strains (6 patient and 1 environmental) belonged to *T. austroamericanum* species (Figure 1).

WGS Typing

We conducted WGS typing to assess the clonal nature of the *T. austroamericanum* outbreak. Of the 7 genomes, 6 demonstrated excellent assembly quality and had contigs ranging from 12 to 31 (Table 3). Those assemblies showed consistent genome lengths of 20.8 to 21 Mb, and GC content was close to 61.31%. The BUSCO scores were all >96% (range 96.5%–97.4%), indicating highly complete and accurate assemblies. However, the assembly for strain L0445 stood out because it had a much higher number of contigs (1,051), a larger genome size of 26 Mb, and a higher GC content of 62.59%. That assembly also showed contamination with bacterial *Achromobacter xylosoxidans* 16S sequence, so we excluded it from further analyses.

The core genome consisting of 11,957 genes enabled construction of a phylogenetic tree from the extracted SNPs, which formed sequences with 542 nt sites and 196 parsimony-informative positions (Figure 2, panel A). Of the 542 sites, we observed 129 distinct site patterns, indicating a high level of sequence variation across the strains. Strains L0453 and L0221, separated by only 85 SNPs (Figure 2, panel B), were the closest in the tree. L0453, from the ICU air duct, also appeared near L0458, with a difference of 97 SNPs. In addition, we identified 7,668 shell genes, representing genes shared by a subset of strains, indicating genetic diversity beyond the core genome.

Whole-Genome SNP Analysis

We performed whole-genome SNP calling by mapping the Illumina reads of our strains against *T. austroamericanum* reference genome CBS 17435 (*11*). That method enabled us to include strain L0445, for which high-quality mapping data was available. Read mapping demonstrated high genome coverage quality across all 8 chromosomes and strict coverage exceeding 97% for all strains (minimum coverage 97.30% ±SD 0.00368%) and reaching up to 99.98% (±SD 0.00043%).

The resulting whole-genome SNP distance matrix revealed patterns consistent with the core genome analysis (Figure 3, panel A). Distances between the CBS 17435 reference and the clinical strains ranged from 447 to 1,085 SNPs. The smallest pairwise distance was 105 SNPs between L0385 and L0399, which were 2 isolates collected within 3 months of each other from the same hospital, supporting their close genetic relationship. The second closest group consisted of L0221, L0453, and L0458, which clustered together despite being collected in different years (Table 1). Most other pairwise distances ranged from ≈400 to >1,100 SNPs, including between L0445 and the rest of the isolates (≈1,070–1,186 SNPs), suggesting that L0445 is genetically more distant, consistent with its location at a hospital site geographically distant from the others.

Mitochondrial Genome

As a complementary approach, we analyzed the mitochondrial genome to assess its potential for discriminating between strains. We used mapping to obtain mitochondrial genomes of ≈44 kb from 3 *T. austroamericanum* reference strains from the CNRMA and the L0445 strain, then generated genomes of other 6 genomes through de novo assembly (Appendix Figure 2). Of note, synteny was identical between the de novo assembled mitogenomes.

The alignment of those mitochondrial genomes against the de novo assembled L0221 sequence revealed 4 distinct mutational profiles, including 3 among Marseille strains (Figure 4). Those profiles included 3 key mutated positions in the mitochondrial genome of the *cox3* (at position 22240), *apocytochrome*

Figure 1. Maximum-likelihood phylogenetic tree of IGS1 sequences from study of *Trichosporon austroamericanum* infections among hospitalized patients, France, 2022–2024. The tree includes strains isolated from 6 patients (red font) and 1 environmental sample (L0453, blue font), mapped against *T. austroamericanum* and related species from GenBank (https://www.ncbi.nlm.nih.gov/genbank) and the CBS culture collection (https://wi.knaw.nl/fungal_table). Bold font indicates reference strain CBS 17435. The clustering confirms that the patient and environmental strains belong to *T. austroamericanum* and form a distinct clade. The tree also shows the relationships between other *Trichosporon* species, such as *T. inkin*, *T. caseorum*, and *T. ovoides*, and other *T. austroamericanum* reference strains from the National Reference Center for Invasive Mycoses and Antifungals at Institut Pasteur (https://www.pasteur.fr). Bootstrap values are indicated at the nodes. Scale bar indicates nucleotide substitutions per site. IGS, intergenic spacer region.

b (at position 31837), and *trnL* (tRNA-Leu) (at position 39897) genes. The mutations provide clear genetic distinctions among the strains. For instance, strain CNRMA15 exhibited a unique mutation, C at position 22240, whereas other strains, such as L0221, have a G at that position (Figure 4, panel A). That analysis underscores the value of mitochondrial genome sequencing for identifying and distinguishing between

T. austroamericanum strains involved in this outbreak and future outbreaks.

The phylogenetic placement of mitochondrial genomes showed 4 distinct clades. L0221 and CNRMA15 formed a separate branch because of their unique SNP profiles. L0458 and L0453 were closely related, as seen in the core-genome analysis. Finally, L0385, L0419, L0399, L0445, CNRMA22, and CNRMA16

Table 3. Characteristics of isolates from investigation of *Trichosporon austroamericanum* infections among hospitalized patients, France, 2022–2024

Characteristics	Isolate no.						
	L0221	L0385	L0399	L0419	L0445	L0453	L0458
Contigs	14	12	16	13	1,051	31	24
Length, bp	20,873,347	20,931,201	21,007,957	20,906,681	26,088,532	20,871,584	20,893,304
% GC	61.3	61.31	61.31	61.31	62.59	61.31	61.31
Contamination	N	N	N	N	Y	N	N
BUSCO C-score, %	96.50	96.90	97.40	96.60	96.10	96.90	96.90

cluster together, and CNRMA 15 branches off the others (Figure 4, panel B).

Discussion

With ≈20 pathogenic species, *Trichosporon* spp. are the second leading cause of Basidiomycota infections in humans (2). Although rare, *Trichosporon* infections in solid organ transplant patients have previously been reported and should be considered in cases of breakthrough infection or echinocandin therapeutic failure (20). In this case series, 67% of patients with invasive *T. austroamericanum* infection were kidney transplant recipients. For all kidney transplant recipients, the starting point was infection at the graft scar that occurred within 2–4 months of transplantation, suggesting a common source of contamination at the time of surgery. Of note, 2 patients in 2 different hospitals also had invasive *T. austroamericanum* infections, thus challenging the common source assumption. However, we did not observe any major changes in the antifungal susceptibility profiles that would have contradicted the idea of a common origin or that would have reflected an evolution of the strain over time (Table 2).

T. austroamericanum was initially described in May 2024 by E.C. Francisco et al. (3). The first case we report appeared in July 2022, but because our database did not yet contain *T. austroamericanum* reference strains, the *Trichosporon* species were initially identified by MALDI-TOF mass spectrometry as *T. inkin*, a closely linked species. In the absence of a satisfactory reference genome, we focused on the *T. inkin* mitochondrial genome, the only genome available and well described in the literature (21). We observed considerable differences between the genomes of our strains, and the reference mitochondrial genome of *T. inkin* (Figure 5). The *T. austroamericanum* species described by Francisco et al. reinforced our analyses.

IGS1 is the region of interest for discriminating between different *Trichosporon* species (3,22,23).
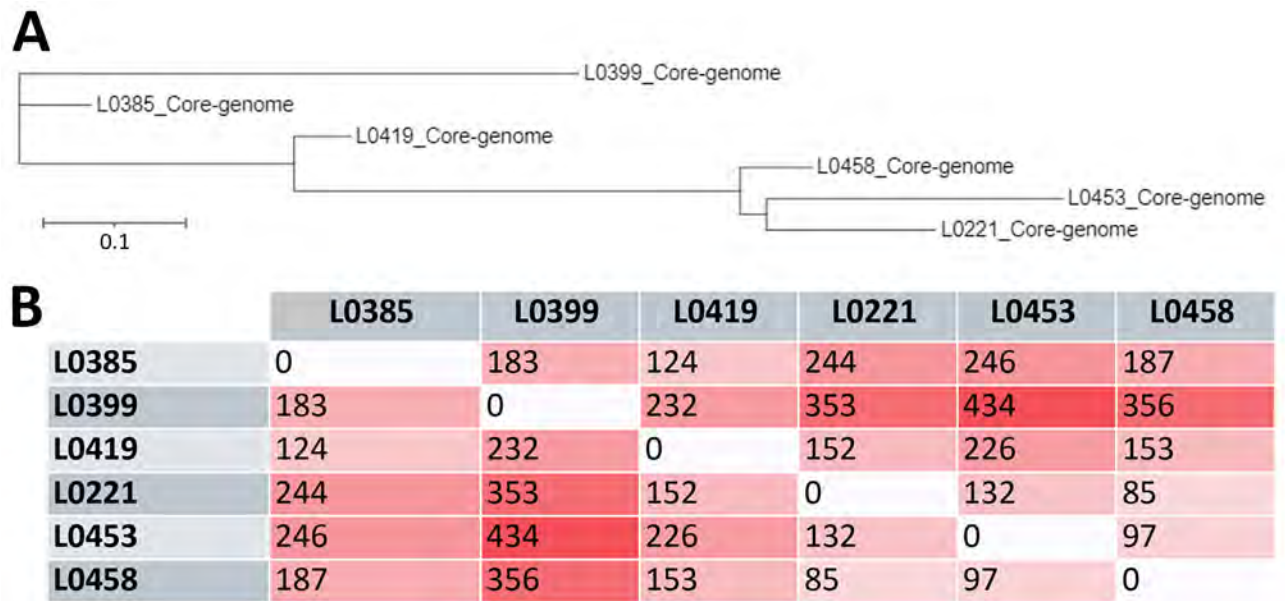
Figure 2. Core-genome phylogenetic relationships and single–nucleotide polymmorphism distance matrix from study of *Trichosporon austroamericanum* infections among hospitalized patients, France, 2022–2024. A) Phylogenetic tree based on the core genome of the analyzed strains showing the evolutionary relationship between strains. Distance between branches reflects the degree of genetic divergence on the basis of SNP variations in the core genome. Scale bar indicates nucleotide substitutions per site. B) Core-genome SNP distance matrix. Each value represents the number of SNPs that differ between genome pairs. Darker shades indicate greater distance.
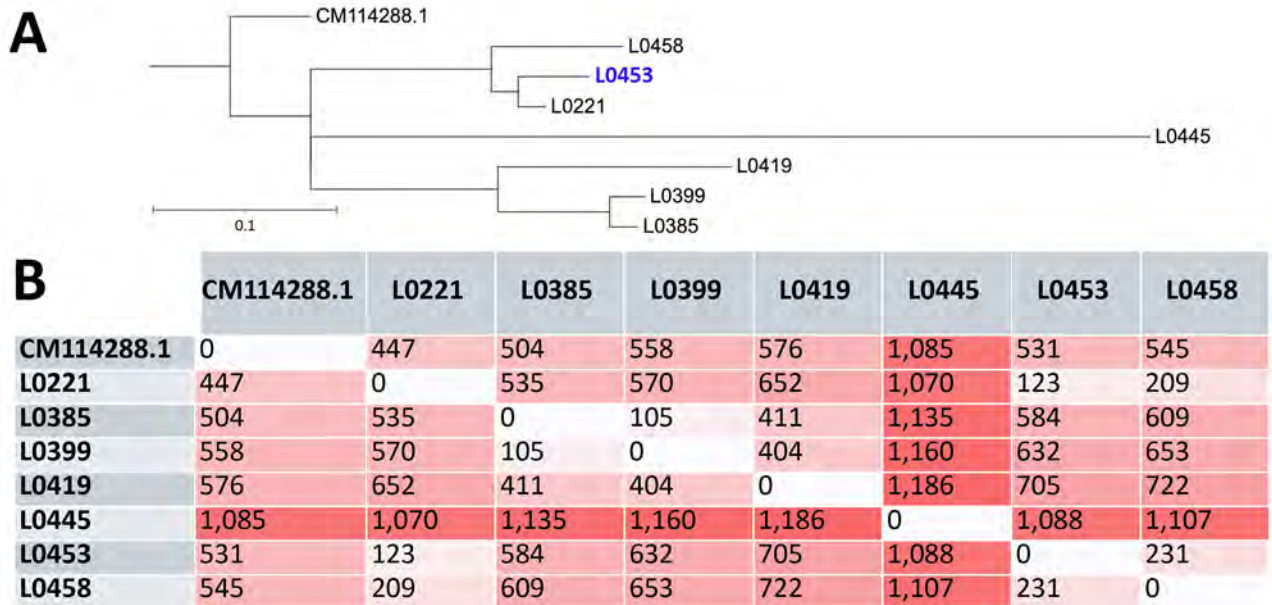
Figure 3. Whole-genome single–nucleotide polymmorphism-based phylogeny and distance matrix from study of *Trichosporon austroamericanum* infections among hospitalized patients, France, 2022–2024. A) Whole-genome phylogenetic tree of the analyzed strains. Blue font indicates reference strain; blue font indicates environmental strain. Scale bar indicates nucleotide substitutions per site. B) Whole-genome SNP distance matrix. Each value represents the number of SNPs that differ between genome pairs. Darker shades indicate greater distance.

Comparing the rRNA IGS1 region nucleotide sequences between our strains with the CNRMA *T. austroamericanum* strains enabled us to confirm the result of mitochondrial genome analysis and revealed that our hospital was facing an emergence of *T. austroamericanum*. Moreover, the mitochondrial genome showed 3 different profiles within the *T. austroamericanum* strains isolated in Marseille and 3 key mutation positions. The appearance of spontaneous mutations

has been described in the mitochondrial genome of certain phytopathogenic species, probably resulting from replication errors and the presence of mobile genetic elements (*24*).

We investigated a potential common origin through genomic analysis, as previously described (*25*). We produced complete genomes of *T. austroamericanum* by de novo WGS. Drawing inspiration from other epidemic investigations (*26,27*), we chose
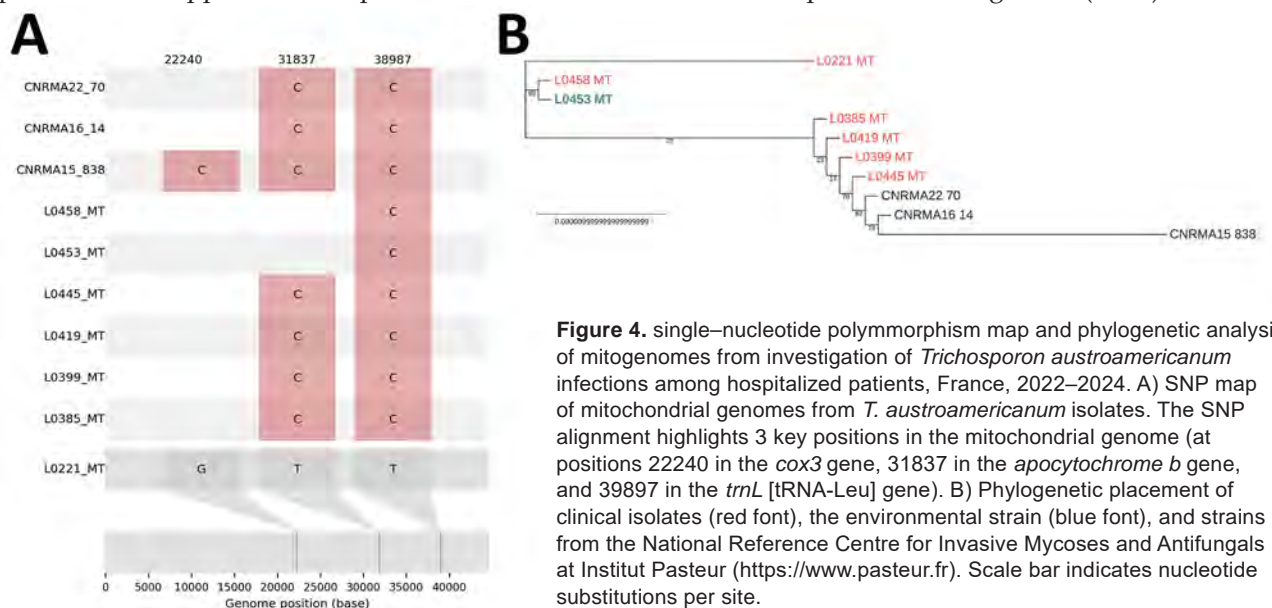
Figure 4. single–nucleotide polymmorphism map and phylogenetic analysis of mitogenomes from investigation of *Trichosporon austroamericanum* infections among hospitalized patients, France, 2022–2024. A) SNP map of mitochondrial genomes from *T. austroamericanum* isolates. The SNP alignment highlights 3 key positions in the mitochondrial genome (at positions 22240 in the *cox3* gene, 31837 in the *apocytochrome b* gene, and 39897 in the *trnL* [tRNA-Leu] gene). B) Phylogenetic placement of clinical isolates (red font), the environmental strain (blue font), and strains from the National Reference Centre for Invasive Mycoses and Antifungals at Institut Pasteur (https://www.pasteur.fr). Scale bar indicates nucleotide substitutions per site.

A

Trichosporon asahii CBS 8904
T. inkin MT801082
T. austroamericanum CBS 17435
L0445
L0385
L0419
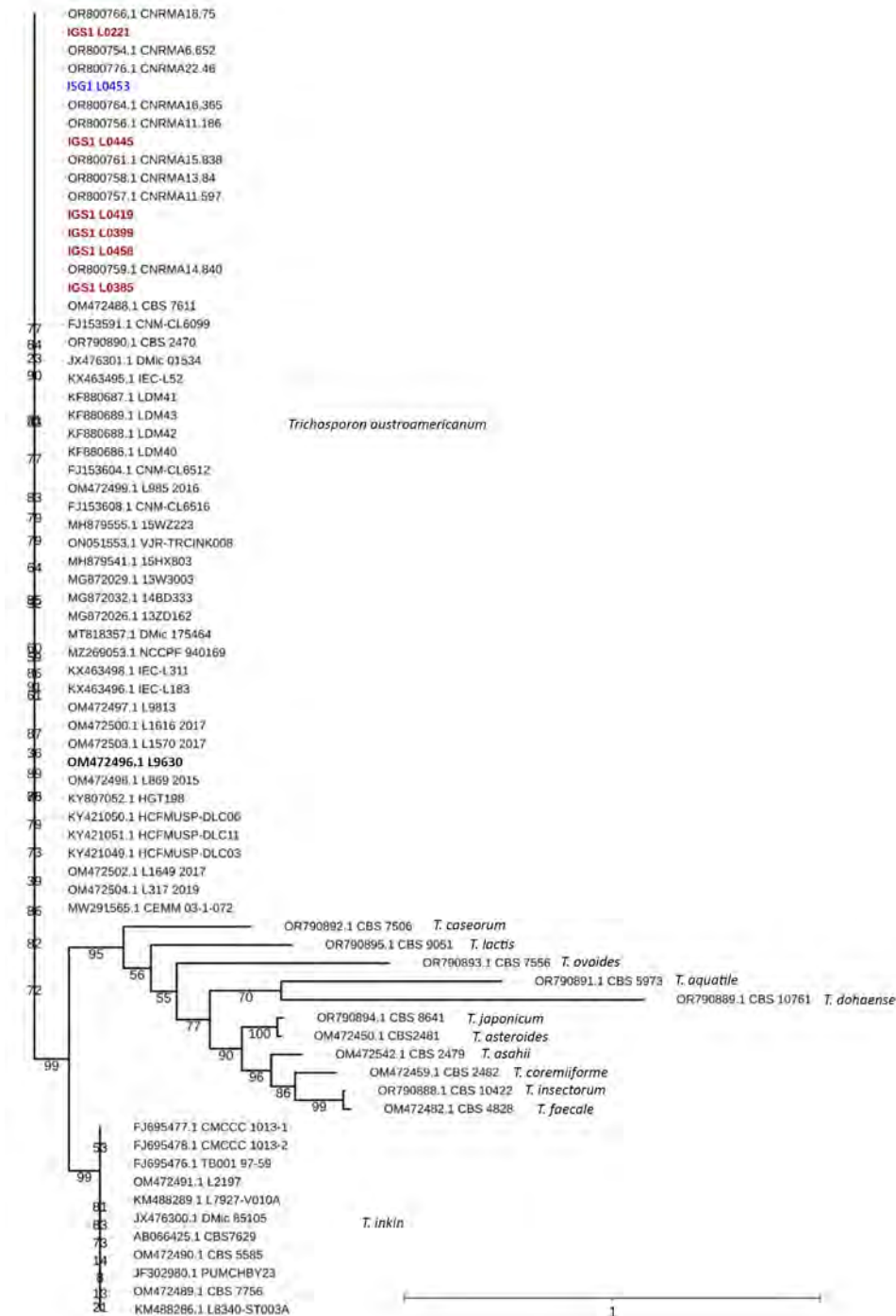L0399
L0221
L0453
L0458

B
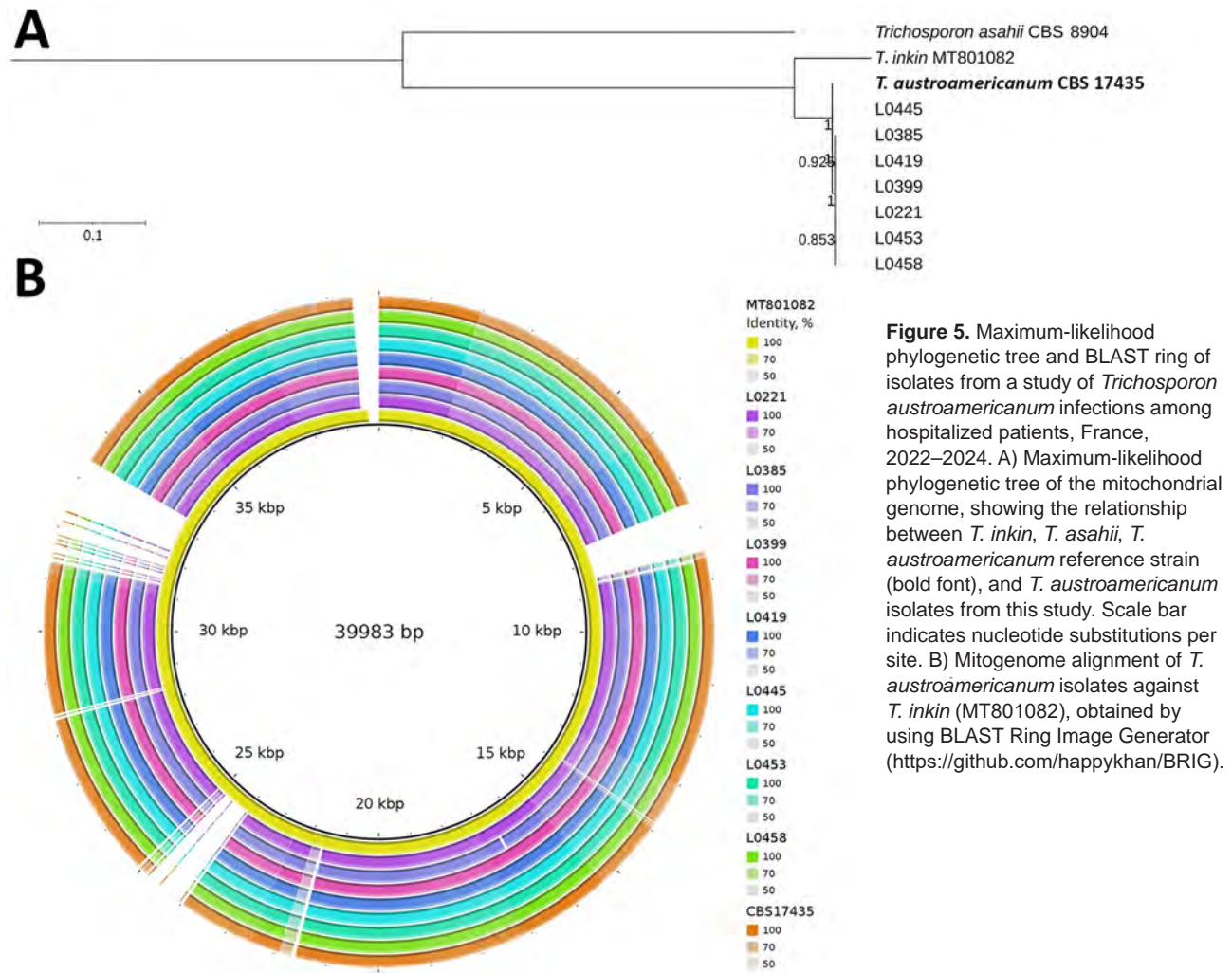
Figure 5. Maximum-likelihood phylogenetic tree and BLAST ring of isolates from a study of *Trichosporon austroamericanum* infections among hospitalized patients, France, 2022–2024. A) Maximum-likelihood phylogenetic tree of the mitochondrial genome, showing the relationship between *T. inkin*, *T. asahii*, *T. austroamericanum* reference strain (bold font), and *T. austroamericanum* isolates from this study. Scale bar indicates nucleotide substitutions per site. B) Mitogenome alignment of *T. austroamericanum* isolates against *T. inkin* (MT801082), obtained by using BLAST Ring Image Generator (https://github.com/happykhan/BRIG).

to target conserved sequences for a core-genome SNP typing approach (Figure 2). After publication of the *T. austroamericanum* CBS 17435 reference genome (*11*), we conducted a WGS and SNP analysis. Whole-genome SNP distances between the CBS 17435 reference strain from Brazil and our strains ranged from 447 to 1,186 SNPs. Of note, that range of differences was of the same order of magnitude as what we observed among the individual strains in our study, supporting the hypothesis of a polyclonal outbreak. Such an approach had already been used to identify clusters of 2 other basidiomycetes, *T. asahii* and *Rhodotorula* spp. (*28,29*).

No consensus regarding SNPs among fungal species exists because many strains are needed to study mutation rates, which is not always possible for rarer species. Thus, the cutoff point to determine whether strains are related seems to be set at <15 SNPs for *Candida auris* and 1,200 SNPs for other species, such as *Rhodotorula mucilaginosa* (*28,30*). Nevertheless, some

strains in our study were genetically much closer. L0385 and L0399 differed by only 105 SNPs and were isolated from the same site within a short interval, suggesting a recent common origin or persistence from an environmental reservoir (Figure 3).

Phylogenetic analysis of the mitochondrial genome, core genome, and whole genome showed similar results, highlighting the benefits of those phylogenetic analyses in epidemiologic fungal investigations. Although the core-genome analysis was based on only a limited number (11,957) of genes, it enabled distinguishing the species and obtaining a phylogenetic placement like that from whole-genome analysis.

The hospital's infection control team also conducted an environmental survey to identify a source of contamination, but investigations in the kidney transplant and nephrology departments did not reveal any common source of contamination. Investigations elsewhere have isolated *Trichosporon* species

from the hospital environment. One published study identified 53 patients with positive *T. asahii* cultures in a hospital in Jamaica, 4 of whom were hospitalized in an ICU and had invasive *T. asahii* infection (*5*). After an environmental investigation in that hospital, 10 surface swab samples from the patient rooms showed *T. asahii*, including samples from drawers, bed rails, faucets, and sinks (*5*). In our investigation, *T. austroamericanum* was isolated (no. L0453) from an air sample from a pediatric ICU at hospital B, but no infection or colonization with that microorganism was noted among patients from that unit. We found no epidemiologic link between that unit and the reported clinical case-patients, all of whom were treated in other hospitals. The lack of an epidemiologic link suggests that *T. austroamericanum* was part of the hospital environment. In our study, the whole-genome SNP analyses showed 123–1,088 SNPs difference between the clinical strains and the environmental strain. However, that finding does not exclude the possibility of multiple clonally unrelated strains circulating and acquired within hospital environmental reservoir.

The results of this study demonstrate that coregenome analysis can effectively differentiate *T. austroamericanum* strains, revealing a polymorphic species. Furthermore, the mitochondrial genome shows strong potential as an excellent marker for intraspecies differentiation. That approach is particularly valuable in the absence of available annotated genomes for *T. austroamericanum* and was supplemented and reinforced by the release of the reference genome CBS 17435 (*11*).

In conclusion, our findings suggest that certain previously deposited sequences identified as *T. inkin* should be re-evaluated for *T. austroamericanum* to account for the emergence of this newly described species. In addition, this study underscores the need for vigilance regarding *T. austroamericanum* infections, including the potential for nosocomial involvement.

The dataset generated for this study is available in the National Center for Biotechnology Information BioProject (https://www.ncbi.nlm.nih.gov/bioproject) database under accession nos. PRJDB20459 for mapped genomes and PRJNA1244900 for assemblies.

About the Author

Ms. Burel is a PhD student in genomics and bioinformatics at the University of Aix Marseille, France. Her research interests include intrahost viral evolution, in particular and more broadly, the genomic evolution of microbial genomes.

References

1. Miceli MH, Díaz JA, Lee SA. Emerging opportunistic yeast infections. Lancet Infect Dis. 2011;11:142–51. https://doi.org/10.1016/S1473-3099(10)70218-8
2. Menu E, Filori Q, Dufour JC, Ranque S, L'Ollivier C. A repertoire of the less common clinical yeasts. J Fungi (Basel). 2023;9:1099. https://doi.org/10.3390/jof9111099
3. Francisco EC, Desnos-Ollivier M, Dieleman C, Boekhout T, Santos DWCL, Medina-Pestana JO, et al. Unveiling *Trichosporon austroamericanum* sp. nov.: a novel emerging opportunistic basidiomycetous yeast species. Mycopathologia. 2024;189:43. https://doi.org/10.1007/s11046-024-00851-4
4. Sugita T, Nishikawa A, Ichikawa T, Ikeda R, Shinoda T. Isolation of *Trichosporon asahii* from environmental materials. Med Mycol. 2000;38:27–30. https://doi.org/10.1080/mmy.38.1.27.30
5. Fanfair RN, Heslop O, Etienne K, Rainford L, Roy M, Gade L, et al. *Trichosporon asahii* among intensive care unit patients at a medical center in Jamaica. Infect Control Hosp Epidemiol. 2013;34:638–41. https://doi.org/10.1086/670633
6. Menu E, Landier J, Prudent E, Ranque S, L'Ollivier C. Evaluation of 11 DNA automated extraction protocols for the detection of the 5 mains *Candida* species from artificially spiked blood. J Fungi (Basel). 2021;7:228. https://doi.org/10.3390/jof7030228
7. Bolger AM, Lohse M, Usadel B. Trimmomatic: a flexible trimmer for Illumina sequence data. Bioinformatics. 2014; 30:2114–20. https://doi.org/10.1093/bioinformatics/btu170
8. Lee S, Nguyen LT, Hayes BJ, Ross EM. Prowler: a novel trimming algorithm for Oxford Nanopore sequence data. Bioinformatics. 2021;37:3936–7. https://doi.org/10.1093/bioinformatics/btab630
9. Wick RR, Judd LM, Gorrie CL, Holt KE. Unicycler: Resolving bacterial genome assemblies from short and long sequencing reads. PLOS Comput Biol. 2017;13:e1005595. https://doi.org/10.1371/journal.pcbi.1005595
10. Simão FA, Waterhouse RM, Ioannidis P, Kriventseva EV, Zdobnov EM. BUSCO: assessing genome assembly and annotation completeness with single-copy orthologs. Bioinformatics. 2015;31:3210–2. https://doi.org/10.1093/bioinformatics/btv351
11. Francisco EC, Desnos-Ollivier M, Gerrits van den Ende B, Hagen F. De novo genome assembly and comparative genome analysis of the novel human fungal pathogen *Trichosporon austroamericanum* type-strain CBS 17435. Mycopathologia. 2025;190:33. https://doi.org/10.1007/s11046-025-00942-w

12. Li H, Durbin R. Fast and accurate short read alignment with Burrows-Wheeler transform. Bioinformatics. 2009;25:1754–60. https://doi.org/10.1093/bioinformatics/btp324

13. Grubaugh ND, Gangavarapu K, Quick J, Matteson NL, De Jesus JG, Main BJ, et al. An amplicon-based sequencing framework for accurately measuring intrahost virus diversity using PrimalSeq and iVar. Genome Biol. 2019;20:8. https://doi.org/10.1186/s13059-018-1618-7

14. Katoh K, Standley DM. MAFFT multiple sequence alignment software version 7: improvements in performance and usability. Mol Biol Evol. 2013;30:772–80. https://doi.org/10.1093/molbev/mst010

15. Page AJ, Taylor B, Delaney AJ, Soares J, Seemann T, Keane JA, et al. SNP-sites: rapid efficient extraction of SNPs from multi-FASTA alignments. Microb Genom. 2016;2:e000056. https://doi.org/10.1099/mgen.0.000056

16. Darling ACE, Mau B, Blattner FR, Perna NT. Mauve: multiple alignment of conserved genomic sequence with rearrangements. Genome Res. 2004;14:1394–403. https://doi.org/10.1101/gr.2289704

17. Minh BQ, Schmidt HA, Chernomor O, Schrempf D, Woodhams MD, von Haeseler A, et al. IQ-TREE 2: new models and efficient methods for phylogenetic inference in the genomic era. Mol Biol Evol. 2020;37:1530–4. https://doi.org/10.1093/molbev/msaa015

18. Cantarel BL, Korf I, Robb SMC, Parra G, Ross E, Moore B, et al. MAKER: an easy-to-use annotation pipeline designed for emerging model organism genomes. Genome Res. 2008;18:188–96. https://doi.org/10.1101/gr.6743907

19. Kalyaanamoorthy S, Minh BQ, Wong TKF, von Haeseler A, Jermiin LS. ModelFinder: fast model selection for accurate phylogenetic estimates. Nat Methods. 2017;14:587–9. https://doi.org/10.1038/nmeth.4285

20. Almeida Júnior JN, Song ATW, Campos SV, Strabelli TMV, Del Negro GM, Figueiredo DSY, et al. Invasive *Trichosporon* infection in solid organ transplant patients: a report of two cases identified using IGS1 ribosomal DNA sequencing and a review of the literature. Transpl Infect Dis. 2014;16:135–40. https://doi.org/10.1111/tid.12179

21. Liu Q, Wang X. Characterization and phylogenetic analysis of the complete mitochondrial genome of pathogen *Trichosporon inkin* (Trichosporonales: Trichosporonaceae). Mitochondrial DNA B Resour. 2021;6:803–5. https://doi.org/10.1080/23802359.2021.1882912

22. Araujo Ribeiro M, Alastruey-Izquierdo A, Gomez-Lopez A, Rodriguez-Tudela JL, Cuenca-Estrella M. Molecular identification and susceptibility testing of *Trichosporon* isolates from a Brazilian hospital. Rev Iberoam Micol. 2008;25:221–5. https://doi.org/10.1016/S1130-1406(08)70053-6

23. Sugita T, Nakajima M, Ikeda R, Matsushima T, Shinoda T. Sequence analysis of the ribosomal DNA intergenic spacer 1 regions of *Trichosporon* species. J Clin Microbiol. 2002;40:1826–30. https://doi.org/10.1128/JCM.40.5.1826-1830.2002

24. Mendoza H, Perlin MH, Schirawski J. Mitochondrial inheritance in phytopathogenic fungi–everything is known, or is it? Int J Mol Sci. 2020;21:3883. https://doi.org/10.3390/ijms21113883

25. Douglas AP, Stewart AG, Halliday CL, Chen SCA. Outbreaks of fungal infections in hospitals: epidemiology, detection, and management. J Fungi (Basel). 2023;9:1059. https://doi.org/10.3390/jof9111059

26. Aggelen HV, Kolde R, Chamarthi H, Loving J, Fan Y, Fallon JT III, et al. A core genome approach that enables prospective and dynamic monitoring of infectious outbreaks. Sci Rep. 2019;9:7808. https://doi.org/10.1038/s41598-019-44189-0

27. Menu E, Criscuolo A, Desnos-Ollivier M, Cassagne C, D'Incan E, Furst S, et al. *Saprochaete clavata* outbreak infecting cancer center through dishwasher. Emerg Infect Dis. 2020;26:2031–8. https://doi.org/10.3201/eid2609.200341

28. Huang JJ, Chen XF, Tsui CKM, Pang CJ, Hu ZD, Shi Y, et al. Persistence of an epidemic cluster of *Rhodotorula mucilaginosa* in multiple geographic regions in China and the emergence of a 5-flucytosine resistant clone. Emerg Microbes Infect. 2022; 11:1079–89. https://doi.org/10.1080/22221751.2022.2059402

29. Desnos-Ollivier M, Maufrais C, Pihet M, Aznar C, Dromer F; French Mycoses Study Group. Epidemiological investigation for grouped cases of *Trichosporon asahii* using whole genome and IGS1 sequencing. Mycoses. 2020;63:942–51. https://doi.org/10.1111/myc.13126

30. Mitchell BI, Kling K, Bolon MK, Rathod SN, Malczynski M, Ruiz J, et al. Identifying *Candida auris* transmission in a hospital outbreak investigation using whole-genome sequencing and SNP phylogenetic analysis. J Clin Microbiol. 2024;62:e0068024. https://doi.org/10.1128/jcm.00680-24

Address for correspondence: Estelle Menu, Assistance Publique Hôpitaux de Marseille (AP-HM), Service de Parasitologie-Mycologie, 19-21 Blvd Jean Moulin, Marseille 13005, France; email: estelle.menu@ap-hm.fr

Tickborne *Neoehrlichia mikurensis* in the Blood of Blood Donors, Norway, 2023

Hanne Quarsten, Charlotte N.B. Ryen, Linn K.T. Mørk, Christine Wennerås, Christine T. Steinsvåg

The tickborne bacterial pathogen *Neoehrlichia mikurensis* has been detected in <1% of blood donors in Sweden. *N. mikurensis* can give rise to asymptomatic persistent infections. Up to 25% of *Ixodes ricinus* ticks in southern Norway are infected with *N. mikurensis*. We investigated the incidence of *N. mikurensis* infection among blood donors in this region. We detected *N. mikurensis* in the blood of 45/499 (9%) blood donors by independent PCR methods; 69% of those were repeatedly positive 1–7 months after the first detection and tested negative after doxycycline treatment. We tested 8/19 adult recipients of potentially infected blood; none tested positive for *N. mikurensis* at the time of testing (191–301 days after transfusion). Our study identified a very high rate of infection with *N. mikurensis* in blood donors in Norway; whether infection can be transmitted by transfusion of blood products, however, remains unclear.

Neoehrlichia mikurensis is the cause of the infectious disease neoehrlichiosis. This tickborne bacterium is widespread in Europe and northern Asia. *Ixodes ricinus* ticks are the main vector in Europe. Infection prevalence varies from barely detectable to >20% (*1,2*); the southern coastline of Norway is a high-prevalence region, where up to 25% of ticks are infected with *N. mikurensis* (*3*).

N. mikurensis can cause a long-lasting infection with spiking fever. Immunosuppressed patients, predominantly those who have been treated with rituximab (anti–CD20/B cell) or splenectomized, are at risk of developing severe neoehrlichiosis (*4*). The target of this intracellular species of bacteria is human vascular endothelium (*5*). Severe neoehrlichiosis

may be accompanied by vascular events such as venous thromboembolism in immunocompromised persons and arteritis in immunocompetent persons (*6*). Molecular detection of *N. mikurensis* DNA by PCR is the only diagnostic test available because antibody tests have not yet been established and *N. mikurensis* does not grow in routine blood culture; it might grow in specialized cell culture. Neoehrlichiosis is underrecognized because of low awareness among clinicians and limited availability of microbiologic diagnostic methods (*4,7*).

A growing body of evidence suggests that *N. mikurensis* may give rise to asymptomatic infections, presumably persisting for months (*8–11*). It is not clear if persons with persistent asymptomatic *N. mikurensis* infection are at risk for activation of acute disease at a later stage. Carriage of *N. mikurensis* in the blood of asymptomatic healthy persons raises the possibility of *N. mikurensis* transmission through blood transfusion. Two retrospective studies have examined that issue. A study of blood donors in Sweden found that 0.7% of the donors had detectable levels of *N. mikurensis* DNA in the blood, yet no transmission of the infection could be established (*12*). A study of blood donors in Denmark found that none were infected by *N. mikurensis* (*13*).

The aim of this study was to investigate the prevalence of *N. mikurensis* in healthy blood donors living in southern Norway, an area highly endemic for *N. mikurensis* infection, and to analyze recipients of blood components from infected donors for possible infection with *N. mikurensis*. The Norwegian Regional Committee for Medical and Health Research Ethics, South-Eastern region, approved the study (reference no. 513442). All blood donors and blood recipients provided written informed consent, which included permission to collect information by approved questionnaires and to collect blood and analyze it for tickborne infections.

Author affiliations: Sørlandet Hospital, Kristiansand, Norway (H. Quarsten, C.N.B. Ryen, L.K.T. Mørk, C.T. Steinsvåg); Sahlgrenska Academy at the University of Gothenburg and Sahlgrenska University Hospital, Göteborg, Sweden (C. Wennerås)

Materials and Methods

Blood Donors and Blood Components

We recruited blood donors at the Department of Immunology and Transfusion Medicine at Sørlandet Hospital (Kristiansand, Norway) during March 20–June 15 (group 1, n = 381) and August 21–September 14, 2023 (group 2, n = 118) when they attended the hospital to donate blood. Each week, we invited all donors attending Monday–Thursday until up to 40 donors (usually ≈10 per day) were recruited per week. Blood donors answered a questionnaire at the time of study inclusion regarding health complaints the preceding year—pain, headache, dizziness, fever, night sweats, sleep problems, nausea or digestive problems, fatigue, and rash—as well as history of tick bites, tickborne infections, and antimicrobial treatment.

We collected EDTA blood and serum from all participants. Blood components (red blood cell or platelet concentrates) were produced in accordance with standard procedures. All blood components were leukocyte-reduced. No pathogen reduction technology was used.

DNA Extraction

We isolated DNA by MagNAPure 96 DNA or Viral NA Small Volume Kit (Roche, https://www.roche.com) from 200 µL of whole blood and plasma/buffy coat fractions of the blood from patients 1–4 days after sampling and plasma/buffy coat fractions of the blood from blood donors within 1 day of sampling. We collected plasma and buffy coat after centrifugation at $1,000 \times g$ for 12 minutes and concentrated to 200 µL by centrifugation at $10,000 \times g$ for 2 minutes. We added MS2 bacteriophage DNA to all samples before extraction to monitor for integrity of extraction and amplification by MS2-specific PCR (14). If the internal control system indicated inefficient DNA isolation from the plasma/buffy coat fractions of the blood donors, we performed additional extractions from thawed whole blood. We analyzed all index sample DNA after storage at −20°C; we tested some of the other samples before freezing.

Real-Time PCR

We tested all samples by real-time PCR for *N. mikurensis*; we conducted 2 independent assays targeting the *groEL* gene. The sequences, concentrations, and thermocycling conditions of the assays have previously been published (8). The protocols used 5 µL of DNA in a 15-µL reaction mixture consisting of 5 mM $MgCl_2$, 0.5 units uracil DNA-glycosylase

(Eurogentec S.A., https://www.eurogentec.com), and LightCycler FastStart DNA master mix (Roche) with primers and probes. The PCRs are validated for human diagnostics and are in routine use, 1 (CNM-I) at the national reference laboratory for *N. mikurensis* diagnostics at Sahlgrenska University Hospital (Göteborg, Sweden) and 1 (CNM-II) at the national reference laboratory for *Borrelia* diagnostics at Sørlandet Hospital, the site of this study. The CNM-I assay had been validated by using specimens from ≈180 patients in Sweden with confirmed neoehrlichiosis and 180 negative controls; all samples were verified by panbacterial 16S rRNA PCR and sequencing. The CNM-I and CNM-II assays show complete concordance with neoehrlichiosis patients in Norway, as demonstrated in a previous study involving 12 persons diagnosed with neoehrlichiosis (8).

We analyzed blood donor samples 1 time by each real-time PCR. If only 1 of the PCR methods was positive, we retested samples in triplicate by both methods. When ≥1 replicate was positive in the triplicate testing, we considered the donor positive. We tested confirmatory and posttreatment samples of blood donors and samples from blood recipients by both methods in triplicate.

Follow-Up of *N. mikurensis*–Positive Blood Donors

We informed blood donors by letter if *N. mikurensis* was detected in their blood and asked them to provide a new sample for retesting. If we detected *N. mikurensis* in a repeat blood sample, we treated the donors with antimicrobial drugs, retested them by PCR after completion of the course of treatment to ensure they had cleared the infection, and asked them to answer the enrollment questionnaire at the time of follow-up and posttreatment sampling.

Blood Recipients

All adult recipients of red blood cell or platelet components from *N. mikurensis*–positive donors who were alive at the time of the study received written information and invitation to participate in the study. We did not contact plasma recipients because only batch-processed virus-inactivated plasma (Octaplasma; Octapharma, https://www.octapharma.com) is used for transfusion in Norway, not single-donor plasma. We offered all blood recipients PCR testing, either for their participation in the study or as part of routine diagnostic procedure. Children <18 years of age were not eligible to participate in the study; however, we informed the attending hospital pediatrician if a child had been transfused with a blood component from a *N. mikurensis*–positive donor. We collected EDTA

blood and serum from the participating blood recipients. The included patients answered a questionnaire regarding health complaints the preceding year, immune status, medication, cardiovascular events, and history of tick bites, tickborne infections, and antimicrobial treatment.

Statistics

We used χ² (Table 1) and Fisher exact (Table 2) tests to compare categorical variables. We used statistics calculators (Social Science Statistics, https://www.socscistatistics.com) to perform Mann-Whitney U test to compare age and sex in different groups and analysis of variance for pairwise comparison to examine >2 means. We considered p values <0.05 to be significant.

Results

Blood Donors

The study included 499 blood donors, most of them living near or in Kristiansand city on the southern coast of Norway. The male-to-female ratio was 1.03:1, and the median age was 44 years (range 18–66 years). Most (82%) of the blood donors had a history of tick exposure. We noted no age-related difference in self-reported tick exposure among the blood donors; the average age was 42 years in those who reported no tick bites (n = 89), 41 years in those who reported 1–2 tick bites (n = 144), and 43 years in those who reported >2 tick bites (n = 266) over their lives. We observed no significant difference between the groups (p = 0.21).

Detection of *N. mikurensis* in Blood Donors

We analyzed DNA from the plasma/buffy coat (n = 490) or whole blood (n = 9) from blood donors by 2 different real-time PCR methods for detection of *N. mikurensis*. We detected *N. mikurensis* DNA in 45/499 (9.0%) of the blood samples (Figure 1). All 45 blood donors had PCR cycle threshold values >34. We first tested blood donor group 1 (n = 381) for *N. mikurensis* infection by PCR 2–5 months after the blood samples were drawn and group 2 (n = 118) 0–1 month after the blood samples were drawn (Table 1). The rate of *N. mikurensis* detection in index samples was the same in blood donors in early spring (March–April, 12/17

[71%]) as in late summer/autumn (August–September, 7/12 [58%]) (Table 1). In follow-up samples, drawn 1–7 months after the index sample, *N. mikurensis* DNA was detectable in 31/45 persons. The rate of donors repeatedly positive in follow-up sampling did not differ significantly in different seasonal periods; however, it was slightly lower among donors recruited in late summer (August–September). Out of the 31 repeatedly positive blood donors, 14 (45%) reported receiving tick bites between the first and second blood sampling, most during June–September.

Characteristics of Negative and Positive Blood Donors

The blood donors who tested positive for *N. mikurensis* were older (median age 52 years) than the blood donors who tested negative (median age 42 years) (p<0.001). We observed no significant difference by sex; 18/246 female and 27/253 male donors tested positive (p = 0.19). Moreover, the *N. mikurensis* positive group reported more tick bites in the year of the study than the noninfected group (p = 0.04) (Table 2). However, we observed no significant difference in overall history of tick exposure, history of Lyme borreliosis or tickborne encephalitis, or experienced health complaints between the groups (Table 2).

Follow-up of *N. mikurensis*–Positive Blood Donors

None of the infected donors experienced fever at the time of first blood sampling and donation. We offered treatment with doxycycline (200 mg/d for 3 weeks) and retesting by PCR after treatment to the 31 blood donors with *N. mikurensis* DNA detected in 2 repeated blood samples. We retested most (29/31) blood donors and did not detect *N. mikurensis* DNA in any of them. Some reported improvement in a few health complaints, but more than half (16/29) experienced no change in health after treatment (Table 2).

Testing of Recipients of Blood Components from *N. mikurensis* Positive Donors

We traced recipients of blood components donated by *N. mikurensis* PCR-positive donors. Two platelet concentrates from 1 of the donors had been sent to another hospital, but it is unknown whether they were transfused. Thirty-two of the 45 positive donors provided 39 blood component units that were

Table 1. Seasonal distribution of *Neoehrlichia mikurensis* DNA found in blood donors, Norway, 2023*

| Sample | No. (%) *Neoehrlichia mikurensis* DNA–positive blood donors | | | |
	March–April, n = 175	May–June, n = 206	August–September, n = 118	p value
Index sample	17 (9.7)	16 (7.8)	12 (10)	0.71
Follow-up sample	12 (6.9)	12 (5.8)	7 (5.9)	0.91
Difference, index to follow-up	5 (2.9)	4 (1.9)	5 (4.2)	0.63

*p values determined by χ² test.

Table 2. Characteristics of blood donors at study inclusion and after treatment with antimicrobial drugs in study of tickborne *Neoehrlichia mikurensis* in the blood of blood donors, Norway, 2023*

Reported data	No. (%) blood donors		p value
	N. mikurensis DNA negative	*N. mikurensis* DNA positive	
Tick bite in current year	97/454 (21)	16/45 (36)	0.04
History of tick bites	370/454 (82)	40/45 (89)	0.31
History of borreliosis/TBE†	38/454 (8.4)	6/45 (13)	0.27
Health complaints in previous 4 months			
Pain	10/451 (2.2)	1/44 (2.3)	>0.99
Headache	6/451 (1.3)	2/44 (4.6)	0.15
Dizziness	3/451 (0.7)	0/44 (0)	>0.99
Fever	0/451 (0)	0/44 (0)	>0.99
Night sweat	8/451 (1.8)	2/44 (4.6)	0.22
Sleep problems	11/450 (2.4)	1/44 (2.3)	>0.99
Nausea/digestive problems	0/451 (0)	0/44 (0)	>0.99
Fatigue	22/451 (4.9)	3/44 (6.8)	0.48
Rash	4/450 (0.9)	0/44 (0)	>0.99
Improvement of health complaints after treatment with antimicrobial drugs			
Pain		3/29 (10)	
Headache		4/29 (14)	
Dizziness		2/29 (6.9)	
Fever		1/29 (3.5)	
Night sweat		2/29 (6.9)	
Sleep problems		4/29 (14)	
Nausea/digestive problems		2/29 (6.9)	
Fatigue		3/29 (10)	
Rash		1/29 (3.5)	

*p values determined by Fisher exact test. TBE, tickborne encephalitis.
†History of borreliosis/TBE; 25 were reported as borreliosis, 19 were unspecified (either borrelioses or TBE) and none reported TBE.

given to 37 unique patients. Thirteen recipients had died by the time we traced the donations; we did not explore their cases further. Of the remaining 24 blood recipients, 5 were children and could not be included in the study. All of the remaining 19 patients had received red blood cell concentrates; 17 of them had received 1 unit, 1 of them 2 units from the same donor, and 1 recipient 1 red blood cell and 1 platelet concentrate from 2 different donors. The median time from donation to transfusion was 20 days (range 5–34 days). We invited all 19 recipients to participate in the study; 8 recipients provided blood samples for testing. Each had received 1 red blood cell concentrate from an infected donor. One had also received 1 platelet unit on a different date. Median time from transfusion to testing of recipients was 246 days (range 196–301 days). We did not detect *N. mikurensis* in any of the recipients. The median age of the 8 transfused patients was 69 years (range 27–79 years). None were immunosuppressed or reported fever at the time of blood sampling. Two patients experienced venous thrombosis, 1 patient in the arm about the same time as receiving blood and 1 few months after transfusion, but both tested negative for *N. mikurensis*. Five recipients self-reported treatment with antimicrobial drugs; 1 received treatment on 2 occasions. Three patients were treated with dicloxacillin, apocillin, and clindamycin, which are not effective against *N. mikurensis*. The type of drugs was not specified at 3 other occasions for 3 different patients. We could not exclude treatment with drugs active against *N. mikurensis*.

Discussion

We found high incidence (9%) of infection with *N. mikurensis* among blood donors from the Kristiansand region in southern Norway. We treated all repeatedly PCR positive blood donors (69%) with doxycycline; all tested negative after treatment. We did not establish transmission of infection in any of the recipients of blood components from the infected donors who were available for testing.

The observed rate of *N. mikurensis* infection was considerably higher than that reported in previous studies of blood donors in Sweden (0.7%) (*12*) and Denmark (0%) (*13*). The high rate of *N. mikurensis* in blood donors in our study may be partly explained by our region being highly endemic for *N. mikurensis* infections and with ≤25% *N. mikurensis*–infected ticks (*3*). The prevalence of *N. mikurensis* in ticks in the other Scandinavian countries varies (0% to >10%) and differs across locations (*5,15,16*). The donors in Sweden were recruited from 1 region (Kalmar); the blood donors in Denmark were recruited from all over Denmark. Most areas in Denmark have low prevalence, 0%–5%, of *N. mikurensis* infection in ticks (*15*).

More than 80% of the blood donors in our area had a history of tick bite, similar to the cohort of blood donors in Sweden (*12*). The high *B. burgdorferi* sensu lato seroprevalence of 18% in the blood

donor population and 22% in the adult population underscore the high exposure to ticks in the Kristiansand region (*17,18*). The prevalence of *N. mikurensis* antibodies in the population is, however, still unknown because of the lack of serologic assays for this emerging pathogen.

The very low (0.7%) or nonexistent prevalence of *N. mikurensis* in previous studies of blood donors (*12,13*) may reflect methodological issues regarding the type of blood tested (serum, plasma, or whole blood). The high prevalence of *N. mikurensis* infection in our study is to a certain extent a result of our strategy of isolating DNA from the buffy coat fraction of fresh whole blood. In that fraction, bacteria and leukocytes are concentrated, and the diagnostic sensitivity of *N. mikurensis* detection is optimized (*19*). Testing of plasma, serum, and frozen or nonconcentrated whole blood material is suboptimal and may reduce the overall sensitivity of the testing; those factors may affect the results of other studies on blood donors.

More than two thirds (31/45) of initial positive blood donors from Kristiansand were repeatedly positive for *N. mikurensis* DNA for up to 7 months after the first detection. This finding strengthens the notion that *N. mikurensis* may be associated with an asymptomatic carriage state, as reported in other studies (*8,10–12*). The infection rate among blood donors was as high in March–April, the first spring months in Norway when it is still cold and the vegetation is low, as in August–September when the grass is high and tick bites are more difficult to avoid. That finding indicates that a substantial proportion of donors had an ongoing infection from a previous tick bite rather than a recent one. Alternatively, a second positive test in donors may in a few cases be explained by reinfection; nearly half of the repeatedly positive donors reported a new tick bite between the index and follow-up samples. The tendency of *N. mikurensis* to cause a persistent infection will lead to an accumulation of positive persons over time, which may result in the high infection rates seen among blood donors and immunosuppressed patients in the Kristiansand region (*8*).

The *N. mikurensis*–infected blood donors did not report any signs of infection and were allowed to donate blood when they attended the blood bank. According to national guidelines in Norway, donors reporting an asymptomatic tick bite are prevented from donating blood for 4 weeks, whereas donors who have been treated for Lyme borreliosis must refrain from donation for 6 months. Our study shows that the current guidelines will not prevent *N. mikurensis*–infected blood donors from donating blood. Blood donors reported some common health complaints at the time of donation regardless of whether they tested positive for *N. mikurensis*. Headache and nightly sweats were more frequent in the infected donors but did not reach statistical significance. The donors who repeatedly tested positive for *N. mikurensis* DNA did not donate blood again until the
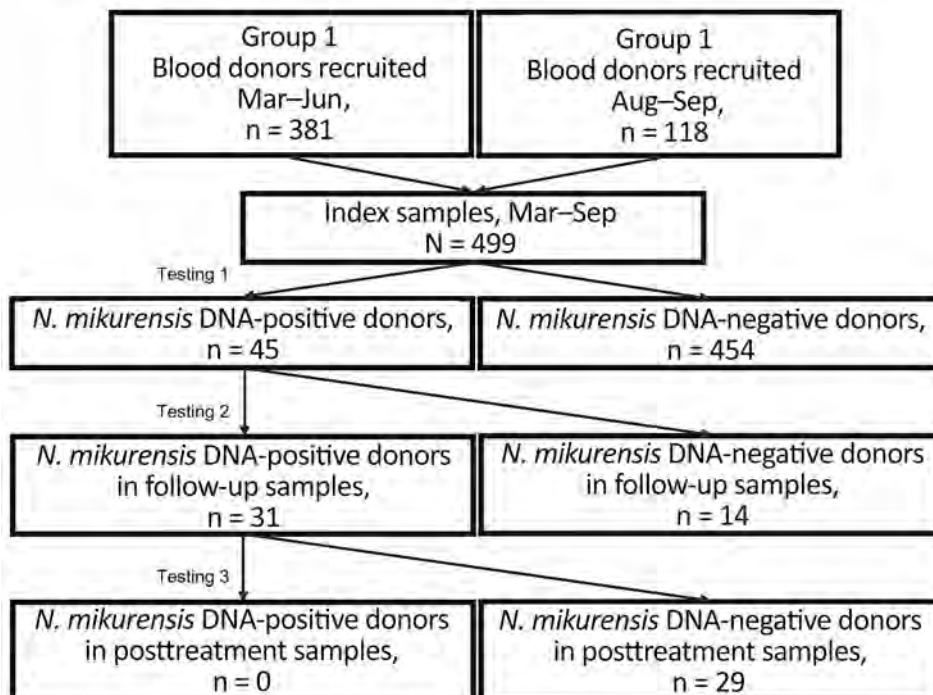
Figure. Flowchart of the study design and follow-up testing of *N. mikurensis*–infected blood donors in study of tickborne *Neoehrlichia mikurensis* in the blood of blood donors, Norway, 2023. Two patients did not provide blood samples for posttreatment testing.

N. mikurensis infection was eradicated by antimicrobial drug treatment. Some of the treated donors experienced relief from various types of reported health complaints after antimicrobial treatment. We could not verify in this study whether those results were causally related to *N. mikurensis* infection. Furthermore, antimicrobial therapy may have beneficial immunomodulatory effects besides killing of bacterial pathogens (*20*).

In our study, none of the recipients of blood from the infected blood donors tested positive for *N. mikurensis* by PCR. However, we tested only 8 of 19 traced recipients. Furthermore, we did not test the blood components of the *N.* mikurensis–infected blood donors for *N. mikurensis*. Our findings are consistent with the Sweden study in which 7 recipients of potentially *N. mikurensis*–infected blood also tested negative (*12*). The time from transfusion to testing of the recipients in both our study and the Sweden study was 2–13 months. The delayed testing might have reduced the probability of detecting transmission of infection because of either spontaneous recovery or adequate antimicrobial treatment. Acute disease caused by *N. mikurensis* has not been reported in children (*21*); we did not test the children receiving blood from *N. mikurensis* infected donors in this study.

All recipients of blood in our study received transfusions of leukocyte-reduced components. Leukocyte reduction of cellular blood components has been shown to lower the risk for transmission of tickborne *Anaplasma phagocytophilum*, which is known to infect granulocytes, although experimental models indicate that the risk is not eliminated (*22,23*). *N. mikurensis* is an intracellular bacterium with tropism for endothelial cells, similar to most *Rickettsia* spp. (*5,24*). In blood components, *N. mikurensis* might be present inside circulating endothelial cells, phagocytosed by neutrophils, or free in blood (*5,25*). In general, bacteria contaminating blood components may be removed by leukocyte reduction if they are phagocytosed or inside of cell types that aggregate in the leukocyte fraction or, if filtration is used in the process, if they attach to the filter matrix (*26*).

Red blood cell components are stored at 4°C. At low temperatures, contaminating extracellular bacterial species are not likely to replicate and their survival rate is often reduced. However, the intracellular bacterial pathogen *R. conorii* not only survived for 35 days in canine blood components stored at 4°C but also breached the leukocyte filter used and maintained infectivity (*27*). Platelet components are stored at room temperature, which increases the risk for bacterial growth and transmission of infection. Survival

of *N. mikurensis* in blood components should be investigated to clarify the ability of *N. mikurensis* to be transmitted via blood transfusion.

Immunosuppression, in particular B cell–depleting therapy (rituximab) or splenectomy, is the main risk factor for developing acute neoehrlichiosis (*21*). None of the study recipients traced after receiving blood products from *N. mikurensis*–infected donors were immunosuppressed and at a substantial risk of contracting disease. This condition could partly explain why *N. mikurensis* was not detected in their blood after transfusion. Still, we note that immunocompetent persons may also be vulnerable and in danger of contracting severe infection, given that 20% of neoehrlichiosis patients in Sweden were not immunocompromised (*6,21*).

It is too early to decide whether *N. mikurensis* can be transmitted by blood transfusion. However, the high incidence of *N. mikurensis* among blood donors in our highly endemic area is an alarming finding that requires further study. Many factors could influence the risk for transmission and the putative establishment of persistent infection with *N. mikurensis* bacteremia among blood recipients; among those are the ability of this emerging bacterial pathogen to stay alive during preparation and storage of the blood components.

About the Author

Dr. Quarsten is a researcher at Sørlandet Hospital, Kristiansand, Norway. Her primary interest is tickborne infections.

References

1. Portillo A, Santibáñez P, Palomar AM, Santibáñez S, Oteo JA. 'Candidatus Neoehrlichia mikurensis' in Europe. New Microbes New Infect. 2018;22:30–6. https://doi.org/10.1016/j.nmni.2017.12.011
2. Silaghi C, Beck R, Oteo JA, Pfeffer M, Sprong H. Neoehrlichiosis: an emerging tick-borne zoonosis caused by Candidatus Neoehrlichia mikurensis. Exp Appl Acarol. 2016;68:279–97. https://doi.org/10.1007/s10493-015-9935-y
3. Pedersen BN, Jenkins A, Paulsen KM, Okbaldet YB, Edgar KS, Lamsal A, et al. Distribution of *Neoehrlichia mikurensis* in *Ixodes ricinus* ticks along the coast of Norway: the western seaboard is a low-prevalence region. Zoonoses Public Health. 2020;67:130–7. https://doi.org/10.1111/zph.12662
4. Wennerås C. Infections with the tick-borne bacterium Candidatus Neoehrlichia mikurensis. Clin Microbiol Infect. 2015;21:621–30. https://doi.org/10.1016/j.cmi.2015.02.030
5. Wass L, Grankvist A, Bell-Sakyi L, Bergström M, Ulfhammer E, Lingblom C, et al. Cultivation of the causative agent of human neoehrlichiosis from clinical isolates identifies vascular endothelium as a target of infection. Emerg Microbes Infect. 2019;8:413–25. https://doi.org/10.1080/22221751.2019.1584017

6. Höper L, Skoog E, Stenson M, Grankvist A, Wass L, Olsen B, et al. Vasculitis due to *Candidatus* Neoehrlichia mikurensis: a cohort study of 40 Swedish patients. Clin Infect Dis. 2021;73:e2372–8. https://doi.org/10.1093/cid/ciaa1217

7. Quarsten H, Henningsson A, Krogfelt KA, Strube C, Wennerås C, Mavin S. Tick-borne diseases under the radar in the North Sea Region. Ticks Tick Borne Dis. 2023;14:102185. https://doi.org/10.1016/j.ttbdis.2023.102185

8. Quarsten H, Salte T, Lorentzen ÅR, Hansen IJW, Hamre R, Forselv KJN, et al. Tick-borne pathogens detected in the blood of immunosuppressed Norwegian patients living in a tick-endemic area. Clin Infect Dis. 2021;73:e2364–71. https://doi.org/10.1093/cid/ciaa971

9. Markowicz M, Schötta AM, Höss D, Kundi M, Schray C, Stockinger H, et al. Infections with tickborne pathogens after tick bite, Austria, 2015–2018. Emerg Infect Dis. 2021;27:1048–56. https://doi.org/10.3201/eid2704.203366

10. Welc-Falęciak R, Siński E, Kowalec M, Zajkowska J, Pancewicz SA. Asymptomatic "*Candidatus* Neoehrlichia mikurensis" infections in immunocompetent humans. J Clin Microbiol. 2014;52:3072–4. https://doi.org/10.1128/JCM.00741-14

11. Grankvist A, Sandelin LL, Andersson J, Fryland L, Wilhelmsson P, Lindgren PE, et al. Infections with *Candidatus* Neoehrlichia mikurensis and cytokine responses in 2 persons bitten by ticks, Sweden. Emerg Infect Dis. 2015;21:1462–5. https://doi.org/10.3201/eid2108.150060

12. Labbé Sandelin L, Olofsson J, Tolf C, Rohlén L, Brudin L, Tjernberg I, et al. Detection of *Neoehrlichia mikurensis* DNA in blood donors in southeastern Sweden. Infect Dis (Lond). 2022;54:748–59. https://doi.org/10.1080/23744235.2022.2087732

13. Gynthersen R, Ørbæk M, Høgdall E, Glintborg B, Ostrowski SR, Harritshøj L, et al. *Neoehrlichia mikurensis* is uncommon in rheumatological patients receiving tumour necrosis factor inhibitors and in blood donors: a retrospective cohort study. RMD Open. 2024;10:e003660. https://doi.org/10.1136/rmdopen-2023-003660

14. Dreier J, Störmer M, Kleesiek K. Use of bacteriophage MS2 as an internal control in viral reverse transcription-PCR assays. J Clin Microbiol. 2005;43:4551–7. https://doi.org/10.1128/JCM.43.9.4551-4557.2005

15. Kjær LJ, Klitgaard K, Soleng A, Edgar KS, Lindstedt HEH, Paulsen KM, et al. Spatial patterns of pathogen prevalence in questing *Ixodes ricinus* nymphs in southern Scandinavia, 2016. Sci Rep. 2020;10:19376. https://doi.org/10.1038/s41598-020-76334-5

16. Andersson M, Bartkova S, Lindestad O, Råberg L. Co-infection with *Candidatus* Neoehrlichia mikurensis and *Borrelia afzelii* in *Ixodes ricinus* ticks in southern Sweden. Vector Borne Zoonotic Dis. 2013;13:438–42. https://doi.org/10.1089/vbz.2012.1118

17. Thortveit ET, Aase A, Petersen LB, Lorentzen ÅR, Mygland Å, Ljøstad U. Human seroprevalence of antibodies to tick-borne microbes in southern Norway. Ticks Tick Borne Dis. 2020;11:101410. https://doi.org/10.1016/j.ttbdis.2020.101410

18. Mygland A, Skarpaas T, Ljøstad U. Chronic polyneuropathy and Lyme disease. Eur J Neurol. 2006;13:1213–5. https://doi.org/10.1111/j.1468-1331.2006.01395.x

19. Quarsten H, Grankvist A, Høyvoll L, Myre IB, Skarpaas T, Kjelland V, et al. *Candidatus* Neoehrlichia mikurensis and *Borrelia burgdorferi* sensu lato detected in the blood of Norwegian patients with erythema migrans. Ticks Tick Borne Dis. 2017;8:715–20. https://doi.org/10.1016/j.ttbdis.2017.05.004

20. Nau R, Tauber SC. Immunomodulatory properties of antibiotics. Curr Mol Pharmacol. 2008;1:68–79. https://doi.org/10.2174/1874467210801010068

21. Wennerås C, Wass L, Bergström B, Grankvist A, Lingblom C. Ten years of detecting *Neoehrlichia mikurensis* infections in Sweden: demographic, clinical and inflammatory parameters. Eur J Clin Microbiol Infect Dis. 2024;43:2083–92. https://doi.org/10.1007/s10096-024-04909-5

22. Proctor MC, Leiby DA. Do leukoreduction filters passively reduce the transmission risk of human granulocytic anaplasmosis? Transfusion. 2015;55:1242–8. https://doi.org/10.1111/trf.12976

23. Bilgin YM, van de Watering LM, Brand A. Clinical effects of leucoreduction of blood transfusions. Neth J Med. 2011;69:441–50.

24. Walker DH, Ismail N. Emerging and re-emerging rickettsioses: endothelial cell infection and early disease events. Nat Rev Microbiol. 2008;6:375–86. https://doi.org/10.1038/nrmicro1866

25. Pekova S, Vydra J, Kabickova H, Frankova S, Haugvicova R, Mazal O, et al. *Candidatus* Neoehrlichia mikurensis infection identified in 2 hematooncologic patients: benefit of molecular techniques for rare pathogen detection. Diagn Microbiol Infect Dis. 2011;69:266–70. https://doi.org/10.1016/j.diagmicrobio.2010.10.004

26. Bassuni WY, Blajchman MA, Al-Moshary MA. Why implement universal leukoreduction? Hematol Oncol Stem Cell Ther. 2008;1:106–23. https://doi.org/10.1016/S1658-3876(08)50042-2

27. Lucchese L, Ravagnan S, Da Rold G, Toniolo F, Wurzburger W, Mion M, et al. Survival of *Rickettsia conorii* in artificially contaminated whole and leukoreduced canine blood units during the storage period. Parasit Vectors. 2020;13:118. https://doi.org/10.1186/s13071-020-3991-9

Address for correspondence: Hanne Quarsten, Department of Medical Microbiology, Sørlandet Hospital, 4615 Kristiansand, Norway; email: hanne.quarsten@sshf.no

Two Independent Acquisitions of Multidrug Resistance Gene *lsaC* in *Streptococcus pneumoniae* Serotype 20 Multilocus Sequence Type 1257

Bernard Beall, Wuling Lin, Zhongya Li, Theresa Tran, Benjamin J. Metcalf,
Bridget J. Anderson, Keipp H. Talbot, Lesley McGee, Sopio Chochua

Among >25,000 invasive pneumococcal disease isolates recovered in US locations during 2015–early 2024 through population-based surveillance, we detected 17 case isolates carrying the *lsaC* gene, which has been shown to confer resistance to clindamycin in group B *Streptococcus*. Sixteen isolates carried the *mef*, *msrD*, *tetM*, and *lsaC* genes on a 29-kb mobile element acquired through an interspecies recombination event and were intermediately clindamycin resistant. One isolate acquired a 62-kb mobile element containing the *ermB*, *tetM*, and *lsaC* genes through a transposition event. All 17 cases were in adults, including 4 adults experiencing homelessness and 9 with substance abuse problems. All 17 *lsaC*-positive isolates shared a 5.2-kb *lsaC*-containing element precisely integrated within the conserved *oriT* site of their respective mobile element. Those 17 *lsaC*-positive strains were all serotype 20, multilocus sequence type 1257, and were recovered recently (2021–2024); isolates 1–16 represented emergent disease clusters in New York and Connecticut.

*S*treptococcus pneumoniae is a leading pathogen globally and is the most common cause of community-acquired pneumonia, bacterial meningitis, bacteremia, and otitis media. Macrolides are often used to treat pneumococcal respiratory infections, and their frequent use has led to increases of macrolide resistance and coselected lincosamide resistance in *S. pneumoniae* (*1*). Although β-lactam antibiotics are first-line treatments, established guidelines exist for using intravenous clindamycin to treat community-acquired bacterial pneumonia (CABP) (*2*).

The 2 major macrolide-resistance mechanisms in streptococci are 23S rRNA methylation by *erm* gene–encoded methylases (confers resistance to macrolides, lincosamides, and streptogramin B antibiotics) and removal of macrolides by the *mef/msrD*-encoded efflux pumps. In group B *Streptococcus* (GBS), 2 additional mechanisms conferring lincosamide resistance have been described: lincosamide modification by nucleotidyltransferases (*lnu* genes) (*3,4*), and the resistance to lincosamides, streptogramin A, and pleuromutilins conferred by the *lsaE*- or *lsaC*-encoded ATP-binding cassette (ABC) transporters (*5,6*). Streptogramin antibiotics have been used for skin infections caused by gram-positive species, and although pleuromutilins are primarily used for veterinary purposes (*7*), use of the pleuromutilin lefamulin has been approved by the US Food and Drug Administration for systemic treatment of CABP in adults (*8*). In a recent study (*9*), 211 strains of *S. pneumoniae* tested, including 105 that were penicillin resistant, were all lefamulin susceptible according to Clinical and Laboratory Standards Institute criteria (*10*), with MICs ≤0.25 µg/mL. In this study, we describe acquisitions of a conserved *lsaC*-containing element in pneumococci that appear to have been introduced through 2 independent mechanisms of horizontal transfer into the same serotype 20, multilocus sequence type (ST) 1257 (serotype 20/ST1257) strain lineage.

Materials and Methods

Active Bacterial Core Surveillance Data

We defined invasive pneumococcal disease (IPD) cases through isolating *S. pneumoniae* from a normally sterile site in an Active Bacterial Core surveillance (ABCs) (*11*) area resident. The surveillance sites included entire US states or selected counties in 10 states, representing ≈30–35 million persons during 2015–2024 (*11*). We reviewed case medical charts to obtain demographic information. We defined adults experiencing homelessness as adults documented as homeless or residing in a shelter, mission, medical respite, or church community center at the time of positive culture. This activity was reviewed by a Centers for Disease Control and Prevention (CDC) review board, was deemed not to be human participants research, and was conducted consistent with applicable federal law and CDC policy. ABCs sites obtained ethics approval from their state health department and academic partner institutional review boards as necessary.

ABCs Isolate Characterization

Isolates were assigned serotypes, multilocus STs, and resistance features employing short-read whole-genome sequencing as previously described within the CDC Pneumonia and Streptococcus Laboratory Branch (National Center for Immunization and Respiratory Diseases, Division of Bacterial Diseases) (*12,13*). We deposited genome sequences in the National Center for Biotechnology Information Sequence Read Archive (BioProject no. PRJNA284954). We used broth microdilution testing in the Pneumonia and Streptococcus Laboratory Branch as previously described (*14*) to verify resistance phenotypes predicted for clindamycin, erythromycin, tetracycline, and tiamulin. Tiamulin has the same mechanism of action as lefamulin, and the 2 antimicrobial drugs share closely similar MICs for pneumococci and for bacterial in vitro transcription-translation (*15*). Pneumococcal susceptibility to lefamulin corresponds to a MIC of <0.5 μg/mL according to Clinical and Laboratory Standards Institute guidelines (*10*).

Long-Read Sequencing

Long-read sequencing was conducted by the CDC Biotechnology Core Facility Branch (Office of Laboratory Systems and Response, Division of Core Laboratory Services and Response) to provide a single contig genome resource of a representative *lsaC*-positive isolate and to map the *lsaC* element; the PacBio Microbial Multiplexing procedure (Pacific Biosciences, https://www.pacb.com) was implemented. Genomic DNA extracted for short-read sequencing was also used to generate a representative single contig genome (isolate identifier 20234456). We generated libraries using the SMRTbell Express Template Prep Kit 3.0 and size-selected using a 0.45x Ampure bead cleanup (Pacific Biosciences) to remove small DNA (<5 kb). We sequenced final libraries for 30 hours after 30 minutes preextension times on the Sequel II using Sequel II Binding Kit 3.2 (Pacific Biosciences). We used PacBio HiFi reads in Flye v2.9 (*16,17*) to conduct de novo assembly for the genome size of 2.13 Mb and evaluated the assembled circularized contig by using BLAST + 2.9.0 (*18*). A coverage of 367 was obtained for the strain 20234456 genome, which we deposited into GenBank (accession no. CP178339).

Genomic Analyses

We used Prokka version 1.14.5 (*19*) to obtain annotated open reading frames and then used EasyFig version 2.2.3 (*20*) to align sequences and generate figures. We generated core-genomic maximum parsimony trees and pairwise single-nucleotide polymorphism (SNP) matrices from short-read bacterial genome sequences using kSNP3.0 with a kmer size of 19 (*21*). We used resultant core.tre files generated from kSNP3.0 to generate core-genomic pairwise SNP comparisons and phylogenetic diagrams using MEGA7 (*22*). We used the Proksee website (*23*) to generate a circular map of a representative *lsaC*-positive isolate and to predict mobile element genes using the mobileOG-db database (*24*). We used progressive Mauve (*25*) to generate aligned core genomes of representative serotype 20/ST1257 isolates and subjected core genome alignments to Gubbins (*26*) to identify recombinant regions.

Results

Serotype 20/ST1257 Invasive Pneumococcal Disease Isolate Phylogeny

Genomic sequence–based ABCs strain surveillance carried out during 2015–2023 (3 serotype 20/ST1257 isolates [1 *lsaC*-positive] were also included from 2024) included >25,000 genomes from invasive pneumococcal disease (IPD) case isolates recovered during this period. Of those, 17 IPD isolates recovered during 2020–early 2024 tested positive for the *lsaC* determinant (Table). All 17 *lsaC*-positive isolates were serotype 20/ST1257, were recovered from adults 34–84 years of age, and were among 367 serotype 20/ST1257 IPD isolates recovered during 2015–early 2024.

A single *lsaC*-positive isolate (isolate 17) recovered in Tennessee was *ermB+*/*tetM+* and was phylogenetically distinct from *lsaC*-positive isolates 1–16

recovered in New York and Connecticut that were positive for the *mef/msrD* macrolide efflux genes and *tetM* (Figure 1). The phylogenetic tree revealed 2 separate geographic clusters corresponding to New York and Connecticut. Twelve genomes (representing all 6 Connecticut isolates and 6 New York isolates) revealed a range of 2–20 pairwise SNP differences; the average was 11 SNPs. The genomes from 4 New York isolates recovered during 2022–2024 formed a separate subcluster (Figure 1); the pairwise SNP difference range was 5–14 SNPs (average of 9.5 SNPs).

Resistance Phenotypes

Isolate 17 was fully resistant to clindamycin (MIC >2 µg/mL) and erythromycin (MIC 4 µg/mL). Isolates 1–16 shared the clindamycin MIC of 0.5 µg/mL and erythromycin MICs of 2–8 µg/mL, compared with MICs of $\leq$0.12 µg/ml for clindamycin and erythromycin in control serotype 20/ST1257 isolate 20195631 and strain ATCC49619 (Table).

All 17 *lsaC*-positive isolates tested as susceptible to lefamulin (MIC range of $\leq$0.25–0.5 µg/mL). However, isolates 1–3 revealed MICs to both pleuromutilins that were above control values, and isolates 4–11 revealed MICs to 1 pleuromutilin that were above control values. Although inconclusive, those data are consistent with the *lsaC* gene conferring reduced susceptibility to pleuromutilins

compared with *lsaC*-negative strains, especially when considering that the *lsaC* determinant in isolates 1–16 appears to encode an active clindamycin efflux component conferring intermediate clindamycin resistance. Besides isolates 1–17, 5 serotype 20/ST1257 isolates carried resistance determinants, consisting of a single *ermB*-positive isolate, 2 *mef/msrD*-positive isolates, and 2 *tetM*-positive isolates, none of which were phylogenetically related to isolates 1–16 or isolate 17 (Figure 1).

Mobile Element Carrying Isolate 17 *lsaC* Gene

Examination of the region carrying the *lsaC* gene in isolate 17 revealed a complex 61-kb mobile element of the broad Tn916/Tn1545 conjugative transposon family (27) inserted within the 3′ end of the ribosomal protein gene *rplL* (corresponding to base 1,215,206 of the Tigr4 reference genome [GenBank accession no. CP000410]). That insertion revealed evidence of a transposition event shown by the tandem repeat of the 3′ 5 codons of the *rplL* gene at the distal end of the 61-kb element (Figure 2). That element shared its highest similarity to an element from *S. intermedius* (GenBank accession no. CP003858) with >98% sequence identity over the overlap (Figure 2). The *S. intermedius* insertion was also within the corresponding site of its *rplL* gene that shared 90.8% sequence identity with the isolate 17 *rplL* gene.

Table. Selected antibiotic phenotype testing for serotype 20 ST1257 *lsaC*-positive and control isolates in study of 2 independent acquisitions of multidrug resistance gene *lsaC* in serotype 20 ST 1257 *Streptococcus pneumoniae* isolates, United States*

| Isolate no.† | Laboratory ID no. | Resistance genotype | MIC, µg/mL (resistance)‡ | | | | | State |
			ERY	CLI	LEF§	TIA¶	TET	
C	ATCC49619	Negative	$\leq$0.12 (S)	$\leq$0.12 (S)	$\leq$0.25 (S)	$\leq$0.5	$\leq$0.25 (S)	NA
C	20195631	Negative	$\leq$0.06 (S)	0.12 (S)	ND	ND	$\leq$0.25 (S)	NA
C	20236374	*ermB*	4 (R)	>2	$\leq$0.25 (S)	1	$\leq$0.25 (S)	NA
17	20204687	*ermB*, *lsaC*, *tetM*	4 (R)	>2	$\leq$0.25 (S)	1	>8 (R)	TN
1–3	20228033, 20238465, 20246104	*lsaC*, *mef/msrD*, *tetM*	2–8 (R)	0.5 (I)	0.5 (S)	2	>8 (R)	NY
4	20242307	*lsaC*, *mef/msrD*, *tetM*	2–8 (R)	0.5 (I)	0.5 (S)	1	>8 (R)	CT
5–11	20223565, 20232253, 20232771, 20235035, 20235950, 20241474, 20243458	*lsaC*, *mef/msrD*, *tetM*	2–8 (R)	0.5 (I)	$\leq$0.25 (S)	2	>8 (R)	NY (5), CT (2)
12–15	20212635 20234456 20237578 20244259	*lsaC*, *mef/msrD*, *tetM*	2–8 (R)	0.5 (I)	$\leq$0.25 (S)	1	>8 (R)	CT (2), NY (2)
16	20232812	*lsaC*, *mef/msrD*, *tetM*	2–8 (R)	0.5 (I)	$\leq$0.25 (S)	$\leq$0.5	>8 (R)	NY

*C, negative control; CLI, clindamycin; CLSI, Clinical Laboratory Standards Institute; CT, Connecticut; ERY, erythromycin; I, intermediately resistant; ID, identification; LEF, lefamulin; NA, not applicable; ND, not done; R, resistant; S, susceptible; ST, sequence type; TET, tetracycline; TIA, tiamulin.
†Isolates 1–17 correlate to isolates described in text. All isolates listed are from Active Bacterial Core surveillance and are serotype 20/ST1257, except for ATCC49619.
‡Susceptible, intermediately resistant, or resistant as described in CLSI (10).
§LEF susceptibility is defined by CLSI as $\leq$0.5 µg/ml (10). Resistance values are currently undefined.
¶TIA susceptibility breakpoints have not been defined.
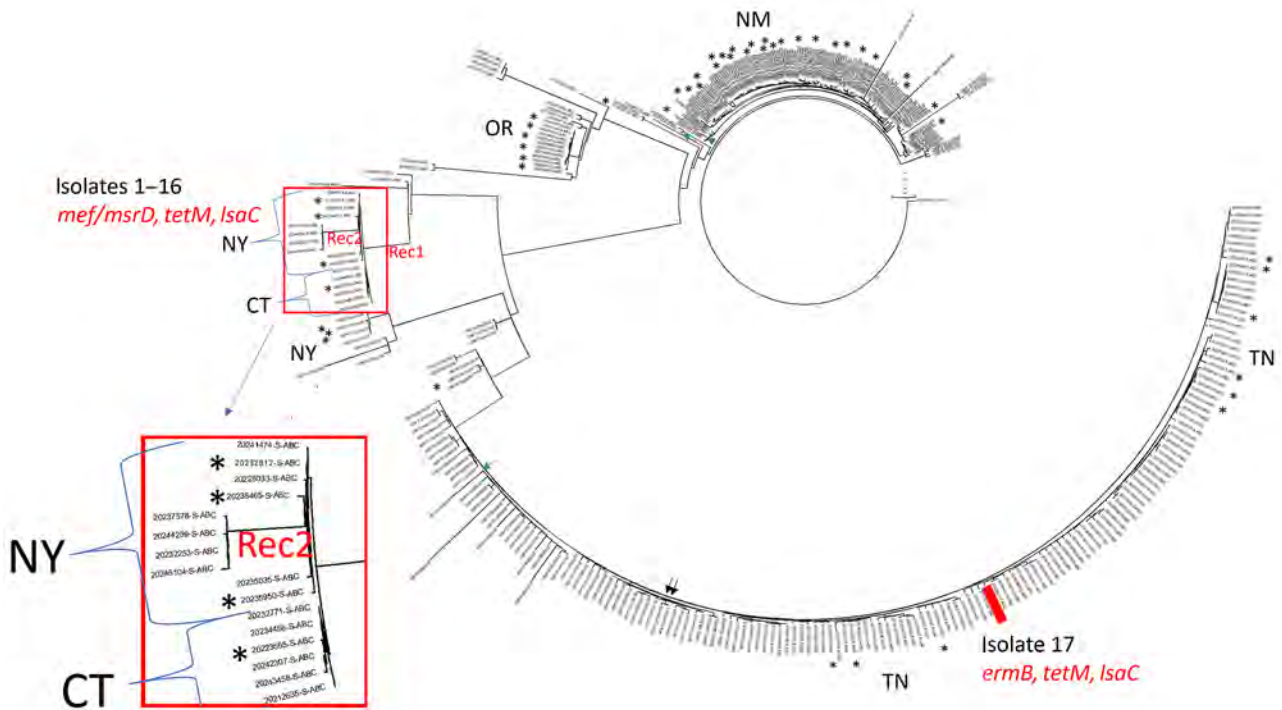
Figure 1. Core-genomic phylogeny of serotype 20/ST1257 invasive pneumococcal disease isolates recovered during 2015–2024 in study of 2 independent acquisitions of multidrug resistance gene *lsaC* in serotype 20/ST1257 *Streptococcus pneumoniae*, United States. Of 367 serotype 20/ST1257 invasive pneumococcal disease isolates recovered during 2015–2024, we included 358 with ≤200 short-read genome contigs in the phylogram. Only 3 year 2024 isolates, including 1 of the depicted *lsaC*-positive isolates 1–16, were included. There were 6,727 variable positions. Isolates 1–16 are indicated on a single branch with the red box divided into 2 subclusters specific to New York (10 isolates) and Connecticut (6 isolates) Active Bacterial Core surveillance sites. The 10-isolate New York subcluster has an inner subbranch of 6 isolates and outer subbranch of 4 isolates. The main branch containing isolates 1–16 and the outward New York subbranch are labeled with Rec, indicative of the disproportionate contribution of recombination to the long branch lengths. Asterisks indicate 50 isolates from adults experiencing homelessness. The remaining isolates were susceptible to antibiotics, except for 2 *mef/msrD*-positive isolates (green arrows), 2 *tetM*-positive isolates (black arrows), and 1 *ermB*-positive isolate (blue arrow). Isolate 17 (positive for *ermB*, *tetM*, *lsaC*) is indicated with a solid red rectangle. ST, sequence type.

Mitis Group Streptococcal Source of Mobile Element Carried by Isolates 1–16

Isolates 1–16 carried an identical 41-kb region that consisted of a 29-kb mobile element flanked by ≈12 kb of upstream and 1 kb of downstream divergent chromosomal sequence that shared 88% sequence identity with the corresponding region of serotype 20/ST1257 pansusceptible isolates (Figure 3). This flanking region and the predicted mobile element shared >99% sequence identity to its closest match in GenBank, *S. pseudopneumoniae* strain 315_SPSE (accession no. NZ_JVLX00000000) (Figure 4). The upstream crossover in this presumed homologous recombination event occurred just downstream of ribosomal protein gene *rpsD* (position 89,092 within *lsaC*-positive serotype 20/ST1257 strain 20234456) (Figure 5); the downstream crossover point corresponded to base 130,195 within putative transport protein gene *orf17*. Those positions corresponded to base 86,400 (upstream crossover) and 97,643 (downstream crossover) of the Tigr4 reference genome. *S. pseudopneumoniae* strain 315_SPSE was an outlier, in that the next 10 closest matches to the 12-kb flanking sequences, although representative of *S. pseudopneumoniae* and *S. mitis* strains, shared only ≈95% sequence identity to the 12-kb flanking sequence (Figure 6). The predicted 29-kb mobile element from isolates 1–16 shared high similarity in its overlap with the mobile element in isolate 16 except for presence of the 5.3 kb *mef/msrD* region and lack of the 2 kb *ermB* region (Figure 7, panel A).

5255-bp Integrative *lsaC* Element Shared by *lsaC*-Carrying Isolates

All 17 *lsaC*-positive isolates carried the complete 1,479-bp *lsaC* gene as part of a 5,255-bp integrative element also conserved with a counterpart locus in the GBS strain UCN70 (5) and predicted to carry genes encoding a site-specific integrase and a replication
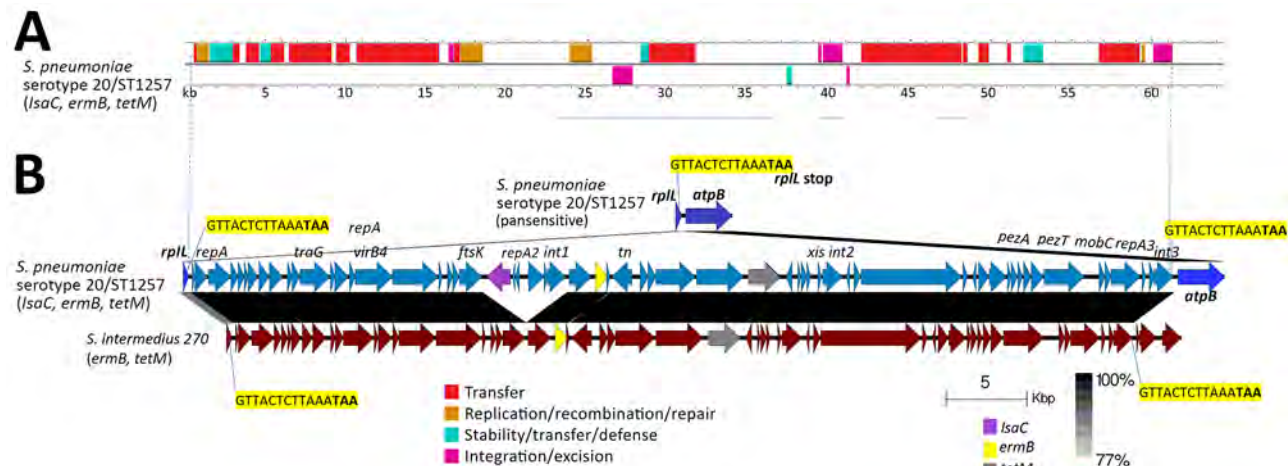
Figure 2. Complex mobile element within isolate 17 (positive for *ermB*, *tetM*, and *lsaC*) in study of 2 independent acquisitions of multidrug resistance gene *lsaC* in serotype 20/ST1257 *Streptococcus pneumoniae*, United States. A) Predicted mobile element genes and functions. B) The insertion site is depicted between *rplL* and *atpB* in pansusceptible genome serotype 20/ST1257 with *rplL* 3′ 15 bp target site highlighted in yellow. The alignment between corresponding genomic regions of isolate 17 and *S. intermedius* strain 270 is shown with 15 bp repeat of *rplL* 3′ end indicated upstream of genomic *atpB* gene in isolate 16 and upstream of unidentified open frames in *S. intermedius* 270. Although the *S. intermedius rplL* gene had an identical 15-bp terminus, it only shares 90% sequence identity with the pneumococcal *rplL* gene. The original EasyFig (*20*) output was modified to depict the interspecies homology between the 2 *rplL* homologs. Homology legend indicates range of 77%–100% sequence identity, depicting ≈90% sequence identity between the 2 different *rplL* alleles and >96% sequence identity between the 2 insertion elements. ST, sequence type.

initiation protein (Figure 7, panel A). The 5,255-bp isolate 1–16 *lsaC* element differed by 5 bp from isolate 17 and 10 bp from GBS UCN70. The isolate 1–16 *lsaC* allele differed from the isolate 17 *lsaC* allele by 2 missense substitutions, and those 2 alleles differed from GBS UCN70 *lsaC* allele by 1–2 missense substitutions. As described for related *lsaC* elements (*6*), each 5,255-bp element contained flanking homologous junctions (j1 and j2 in Figure 7, panel B) that shared repeated regions after a run of 6 Cs (j1) or preceding a run of 5–7

Gs (j2). Junctions j1 and j2 each shared overlapping sequence nearly identical to an *ori*T sequence motif shared by various related conjugative transposons, indicative of specific integration of the 3 different 5,255-bp *lsaC* elements within transposons harboring an identical *ori*T (Figure 7, panel B).

Features of Serotype 20/ST1257 Cases

Only 9 of the 367 serotype 20/ST1257 case-patients were <18 years of age; only 1 patient was <5 years of
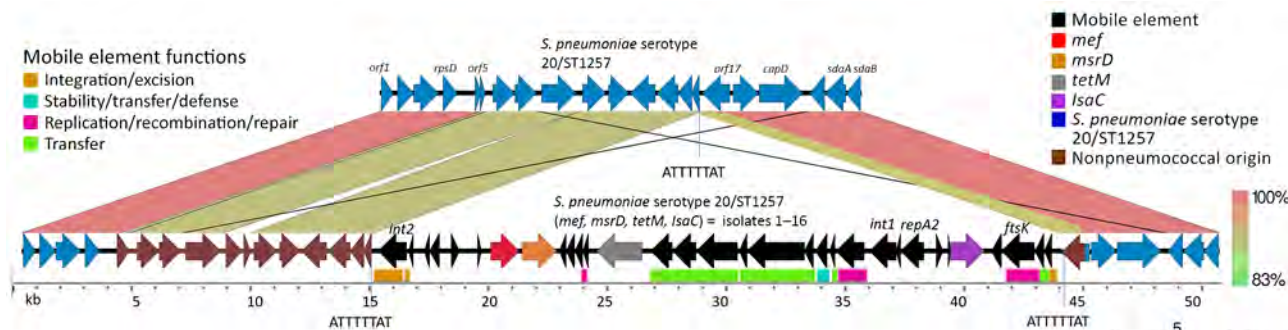
Figure 3. Introduction of isolate 1–16 mobile element into *Streptococcus pneumonae* serotype 20/ST1257 by a double crossover homologous transformation event in study of independent acquisitions of multidrug resistance gene *lsaC* in serotype 20/ST1257 *S. pneumoniae* isolates, United States. Crossover 1 occurred within *orf5* and crossover 2 occurred near the 5′ end of *orf17.* Apparent nonpneumococcal homolog genes in isolates 1–16 (serotype 20/ST1257 [*mef*, *msrD*, *tetM*, *lsaC*]) flanking the mobile element (*orf* 5–16) are indicated upstream in brown, as is most of *orf17* immediately downstream of the insertion element. These genes share <90% sequence identity with the parental strain lineage serotype 20/ST1257. The section corresponding to *orf17* has been modified from the original EasyFig (*20*) depiction to reflect more accurately the decreased homology between the 2 *orf17* alleles and the actual breakpoint in homology. The repeated 8-bp target site for the ancestral transposition event is indicated. Predicted mobile element genes and functions are indicated in the below grid corresponding to 15–44.2 kb of the entire isolate 1–16 region. *orf5* is indicated by 1 open reading frame in isolates 1–16 but is indicated by 2 short homologous reading frames in the parental strain (top). ST, sequence type.
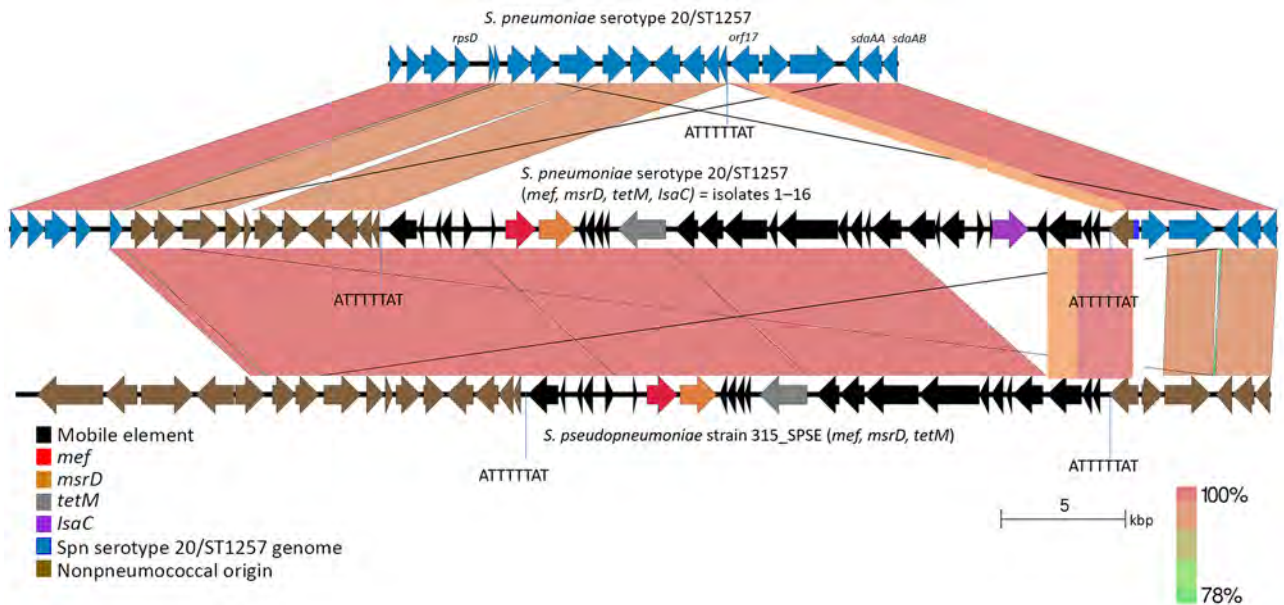
Figure 4. Near sequence identity shared between pneumococcal isolates 1–16 and *Streptococcus pseudopneumoniae* strain 315_SPE in mobile element insertion region in study of 2 independent acquisitions of multidrug resistance gene *lsaC* in serotype 20/ST1257 *S. pneumoniae*, United States. The near-identical region includes much of the mobile element itself, and flanking genes that diverge from pneumococcal parental recipient strain (top). The EasyFig (*20*) output homology was modified to reflect boundaries between marked homology differences between the 2 pneumococcal strains (focused upon *orf17* only) and between the middle pneumococcal strain and the below *S. pseudopneumoniae* strain (encompassing the last 3 *orf*s of the mobile elements and most of *orf17*). ST, sequence type.

age. Of the 357 case-patients with known residence status, 50 (14.0%) were adults experiencing homelessness, including 4 (23.5%) of the case-patients whose cases corresponded to 4 of the isolates 1–17. This finding is consistent with data from ABCs in 2018 and 2019 (*28,29*), in which serotype 20 made up the third highest proportion of cases among adults experiencing homelessness, surpassed only by serotypes 4 and 12F. Of serotype 20 cases, 14.9% were from adults experiencing homelessness in 2018 and 12.2% were from adults experiencing homelessness in 2019. Typical of serotypes more common among adults experiencing homelessness (*29*), 9 of the 17 serotype 20 *lsaC*-positive isolates were recovered from adults with substance use problems involving cocaine or methamphetamines (6 persons, 1 of which was an adult experiencing homelessness) or alcohol (2 persons).

Contribution of Interspecies and Intraspecies Recombination to Apparent Phylogenic Distance of Isolates 1–16 from Closest Pansensitive Ancestor

To assess temporal distances between *lsaC*-positive genetic progeny and their closest ancestors, we generated a core-genome phylogeny of serotype 20/ST1257 IPD isolates (Figure 1). Isolate 17 differed by only 12 SNPs from the closest pansensitive strains

(Figure 1). That finding is consistent with a recent transposition event in which the mobile element was precisely inserted within the genomic *rplL* gene (Figure 2). In contrast, the inner subbranch separating isolates 1–16 from its predicted most common ancestor showed a distance of ≈130 SNPs. The distance between closest pansensitive isolates (2 isolates recovered in Connecticut during 2015–2018) and the subcluster of 6 New York isolates within isolates 1–16 was 140–180 SNPs. Through recombination analysis of aligned genomes (*26*), all or most of this pairwise distance (152 SNPs) was introduced into the depicted phylogeny (Rec1 in Figure 1) by the single interspecies recombination event that introduced the resistance element along with ≈13 kb of nonpneumococcal flanking core-genomic sequence (Figures 3–5).

The 10 New York isolates (all recovered during 2022–2024) were additionally subdivided into 2 subclusters by 5 recombinant fragments uniformly present in the distal 4 isolates on the tree (data not shown). The most distal subcluster (consisting of isolates recovered during 2022–2024) displayed considerable distance (104–117 SNPs) from the other 6 New York isolates (recovered during 2022–2023). The 5 recombinant regions within the 4 distal subcluster isolates

Figure 5. Single contig genome of isolate 20234456 (*msrD*-positive, *mef*-positive, *tetM*-positive, *lsaC*-positive) representative of isolates 1–16 in study of 2 independent acquisitions of multidrug resistance gene *lsaC* in serotype 20/ST1257 *Streptococcus pneumoniae*, United States. Position 1 starts at the *dnaA* structural gene. CDSs and tRNA genes are indicated on the forward strand (outer band) and reverse strand (inner band). The genes approximating the location of the interspecies double-crossover event introducing the resistance element lie between the *rpsD* ribosomal protein gene and the putative transport gene *orf17*. The ribosomal protein gene *rplL* is also depicted near the 1.2-Mbp marker to show the approximate genomic location of the accessory element carrying the *ermB, tetM*, and *lsaC* determinants in isolate 17. Other determinants shown reflect potential genomic resistance determinants (all indicative of susceptibility in this genome according to bioinformatic pipeline output), including *folP/folA* (fluoroquinalones), *parC/gyrA* (sulfamethoxazole/trimethoprim), and *pbp2x/pbp1a/pbp2b* (β-lactam antibiotics). In addition, the multilocus sequence typing markers *spi-15, gki-8, aroE-15, ddl-31, xpt-31*, and *recp-18* define ST1257. CDS, coding sequences; ST, sequence type.
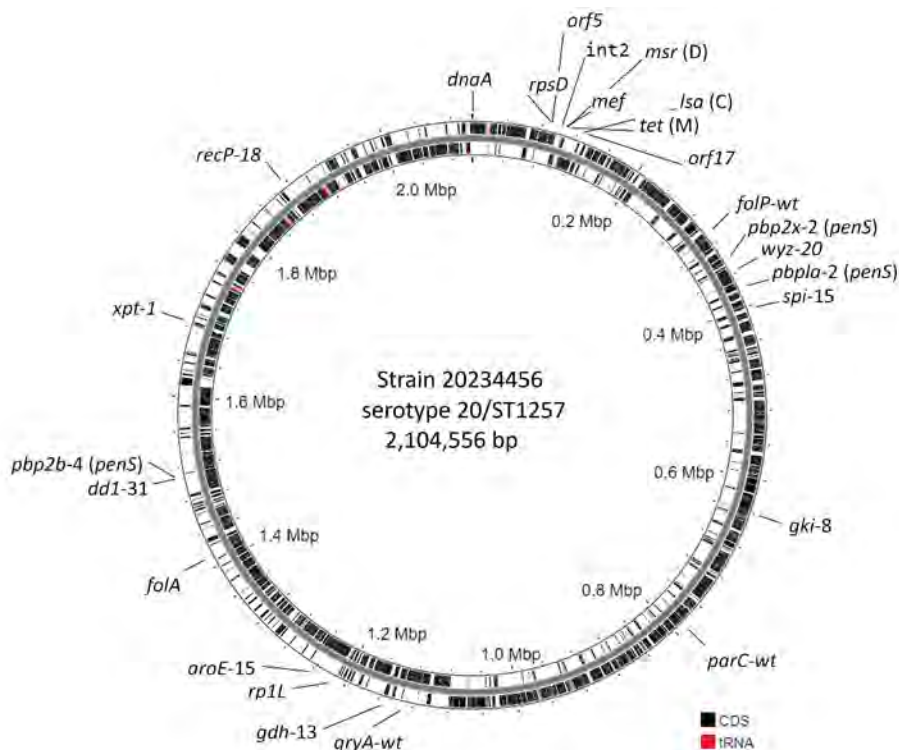
ranged from 750–9,020 bp in length and accounted for all or most of this entire SNP distance between the 2 subgroups (Rec2 in Figure 1); that finding was indicative of a close temporal distance between those 4 isolates and the 6 ancestral New York isolates.

Discussion

lsaC determinants have been described from GBS (*5,6*) and very recently have been reported from animal strains of *S. equisimilis* (*30*). In this study, we identified 2 independent introductions of *lsaC* into pneumococci where the determinant is present on 2 distinct mobile elements, 1 cocarrying *ermB* and *tetM*, and 1 cocarrying *mef, msrD*, and *tetM*. Within both mobile elements, the *lsaC* component element targeted *ori*T through a conserved mechanism first described in GBS (*6*). Within isolate 17, the large mobile element carrying *ermB* and *tetM* was likely to have been first introduced into the genome through transposition targeting the *rplL* 3′ 15-bp target, followed by *ori*T-targeted insertion of *lsaC*. Disruption of the *ori*T sequence would presumably prevent further high-frequency transposition of the composite transposon containing *ermB, tetM*, and *lsaC*. Because the mobile element observed within isolates 1–16 was introduced through interspecies homologous transformation (*31*) and not by conjugative transposition requiring an intact *ori*T, predicting whether the *lsaC* element was cocarried with other resistance genes or introduced subsequently is not possible. These 2 *lsaC* elements did not recently originate from the same donor bacterial strain; they differed by 5 SNPs, including 2 missense substitutions within the *lsaC* gene. The apparent *ori*T-targeting mechanism of *lsaC* horizontal transfer has the potential to include numerous bacterial species because of the ubiquity of conjugative elements sharing the *ori*T target for *lsaC* element insertion and the presence of transposition genes (site specific integrase/replication initiation) genes within the *lsaC* element itself.

Serotype 20 is one of the few serotypes that have an extremely high propensity for generating genomic clusters among IPD isolates recovered from adults, where a so-called clustering isolate differs from ≥1 isolates by ≤10 SNPs (*28,29,32,33*). The 23-valent pneumococcal polysaccharide vaccine introduced in 1983 contains a serotype 20 component; however, the immunity conferred by this vaccine decreases within a few years (*34*). Despite the introduction of highly effective pneumococcal protein-polysaccharide conjugate vaccines, starting

with the 7-valent vaccine (PCV7) in 2000, serotype 20 was not included within another licensed vaccine until the licensure of PCV21 in 2024 for adults 19–64 years of age with risk conditions for IPD and for those ≥65 years (*35*). The serotypes that have the highest proportions of clustering IPD isolates, such as 4, 12F, and 20, have the greatest propensity to cause IPD among adults experiencing homelessness and are rarely found in carriage (*35–39*). Those serotypes have been characterized as short carriage–duration serotypes (*40*) and rapidly spread between adults, causing IPD in vulnerable hosts shortly after acquisition in carriage (*40,41*). Serotypes such as 4, 12F, and 20 differ from serotypes often found in pediatric carriage, such as 35B and 19A (*35,36*) that are associated with relatively low frequencies of genomic clustering (*29*). The prevalence in IPD of such long duration–carriage serotypes as 35B and 19A appear directly related to their higher detection incidence in pediatric carriage (*35–37,39*); that observation is supported by the well-characterized herd effect of adult IPD prevention affected by high coverage of conjugate vaccines among the pediatric population (*41,42*).

Serotype 4, which has the highest propensity for both genomic clusters and causing IPD among adults experiencing homelessness, was recently found to acquire reduced susceptibility to vancomycin through the acquisition of a *vanG*-containing mobile element (*14*). The acquisitions of *vanG* and *lsaC* in pneumococci had not been reported before those very recent observations of their presence in the short carriage–duration serotypes. Another recent and unusual finding within those high-clustering serotypes was the generation of a serotype 12F to serotype 4 serotype-switch variant IPD cluster causing multiple IPD cases among adults experiencing homelessness (*32*). Recent increases (*45*) in the number of persons lacking permanent shelter (record numbers of 653,104 persons in 2023 and 771,480 persons in 2024) are likely to directly correlate to concurrent increases of IPD caused by high-clustering serotypes among adults experiencing disadvantages (*28,29,32,33,45,46*). Those increases might have contributed to unusual interspecies and intraspecies horizontal genetic transfer events involving those serotypes.

The acquisition of *lsaC* in isolate 17 is of potential medical significance, even though the strain is already fully clindamycin resistant through the presence of *ermB* on the same mobile element. Even though streptogramin A and pleuromutilin antibiotics are currently used primarily for veterinary purposes (*7*), the pleuromutilin lefamulin was recently approved for systemic use in cases of CABP in adults (*8*). Although all 17 isolates in this study were susceptible to lefamulin, 4 tested at the breakpoint of susceptibility, and 10 revealed MICs that were
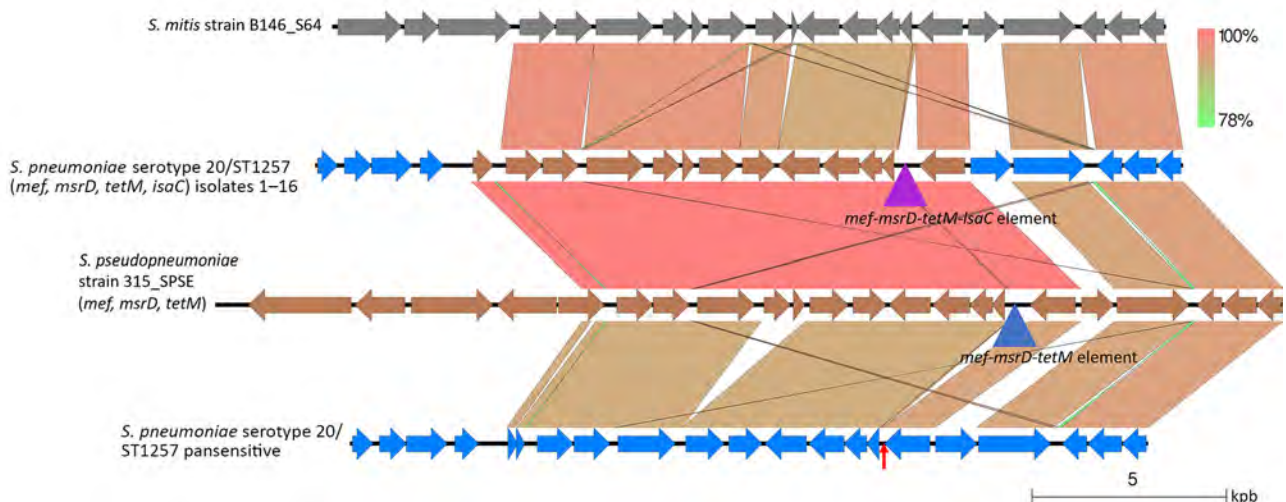
Figure 6. Alignments between *Streptococcus mitis* strain, pneumococcal isolates 1–16, *S. pseudopneumoniae* strain 315_SPSE, and pansusceptible serotype 20/ST1257 pneumococcal strain (bottom) in study of 2 independent acquisitions of multidrug resistance gene *lsaC* in serotype 20/ST1257 *S. pneumoniae*, United States. This alignment depicts representative homology between certain streptococcal strains recognized as *S. mitis* and the genome flanking the resistance element in strains 1–16. Also shown is the near identity to this region shown by *S. pseudopneumoniae* strain 315_SPSE. The mobile elements (triangles) in isolates 1–16 and *S. pseudopneumoniae* 315_SPSE correspond to the mobile elements depicted in Figure 4. The apparent nonpneumococcal genes (brown) flank the mobile element introduced by recombination into isolates 1–16. Red arrows indicates the genomic region in the serotype 20/ST1257 corresponding to the mobile element insertion site. ST, sequence type.
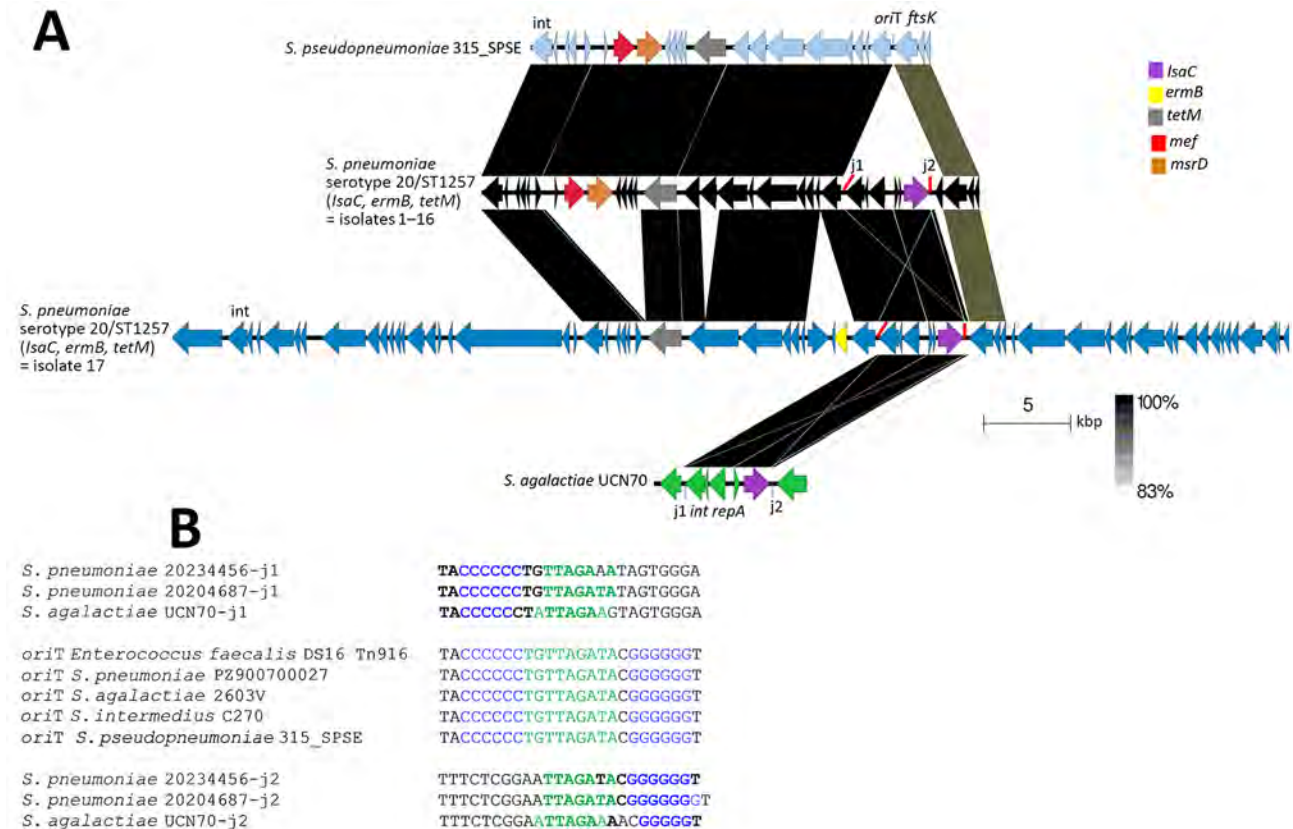
Figure 7. Related regions shared between the 2 pneumococcal *lsaC* elements from this study, the mobile element found in *S. pseudopneumoniae* 315_SP_SPSE, and the partial mobile element from GBS strain UCN70 in study of 2 independent acquisitions of multidrug resistance gene *lsaC* in serotype 20/ST1257 *S. pneumoniae*, United States. A) The *lsaC* element target site (*ori*T) is indicated in *S. pseudopneumoniae* 315_SP_SPSE, with partially homologous junctions (j1 and j2) of the *lsaC* elements in the 3 strains (isolate 1–16, isolate 17, and *S. agalactiae* UCN70). B) The identical *ori*T sequence shared between related mobile elements lacking *lsaC* from 5 different species is shown. *lsaC* element junction j1 shares homology with the 5' *ori*T sequence and junction j2 shares homology with the 3' *ori*T sequence. Purple indicates the shared C and G repeats; green indicates direct repeats between each of the 3 strains shared between their specific j1 and j2 sequences and homologous central *ori*T sequence. Bold indicates J1 and j2 bases shared with the *ori*T sequence. ST, sequence type.

above control values for the closely related pleuromutilin tiamulin. In view of the cross-resistance to clindamycin and pleuromutilins observed in GBS, it is reasonable to assume *lsaC*-conferred intermediate clindamycin-resistance and to suspect reduced pleuromutilin susceptibility in isolates 1–16. In isolates 1–16, the presence of *lsaC* would prevent the use of clindamycin for certain situations, such as strain penicillin resistance or patient allergy in CABP cases. The physical linkage of *lsaC* with other resistance genes also provides the obvious potential for coselection of the unrelated resistance determinants in bacterial strains.

Of note, isolates 1–16 appear to have recently emerged and are actively expanding within 2 different ABCs sites; the most recent isolate appeared within the small proportion of 2024 ABCs strain surveillance completed at that time. The apparent temporal distance shown between the isolate 1–16 lineage and pansusceptible serotype 20/ST1257 isolate is mainly artifactual because of SNPs introduced through recombination at the *lsaC* insertion region of the genome. This *lsaC*-positive cluster has continued to recently diversify; a 4-isolate subcluster revealed multifragment recombination, which appears to commonly occur in pneumococci from a single exposure to donor DNA (*32,48*).

The recent acquisitions of *lsaC* and *vanG* within invasive pneumococci highlight the granular nature of whole-genome sequence–based disease strain surveillance for detecting rare resistance gene acquisition events and for monitoring subsequent spread of such novel strains. With continued narrowing of available antibiotic choices for treating bacterial infections, maintaining this vigilance through long-term surveillance of invasive strains is key.

Acknowledgments

About the Author

Dr. Beall was a researcher at the Centers for Disease Control and Prevention during 1993–2021, where he focused on streptococcal strain characterization and invasive strain surveillance. He was the team lead of the Streptococcus Laboratory during 2004–2021 and since retirement continues to work with the laboratory as a scientific consultant.

References

1. Schroeder MR, Stephens DS. Macrolide resistance in *Streptococcus pneumoniae.* Front Cell Infect Microbiol. 2016;6:98. https://doi.org/10.3389/fcimb.2016.00098

2. Murphy PB, Bistas KG, Patel P, Le JK. Clindamycin. Treasure Island (FL): StatPearls Publishing; 2024 [cited 2024 Feb 28]. https://www.ncbi.nlm.nih.gov/books/NBK519574

3. de Azavedo JC, McGavin M, Duncan C, Low DE, McGeer A. Prevalence and mechanisms of macrolide resistance in invasive and noninvasive group B streptococcus isolates from Ontario, Canada. Antimicrob Agents Chemother. 2001;45:3504–8. https://doi.org/10.1128/AAC.45.12.3504-3508.2001

4. Achard A, Villers C, Pichereau V, Leclercq R. New *lnu*(C) gene conferring resistance to lincomycin by nucleotidylation in *Streptococcus agalactiae* UCN36. Antimicrob Agents Chemother. 2005;49:2716–9. https://doi.org/10.1128/AAC.49.7.2716-2719.2005

5. Malbruny B, Werno AM, Murdoch DR, Leclercq R, Cattoir V. Cross-resistance to lincosamides, streptogramins A, and pleuromutilins due to the *lsa*(C) gene in *Streptococcus agalactiae* UCN70. Antimicrob Agents Chemother. 2011;55:1470–4. https://doi.org/10.1128/AAC.01068-10

6. Douarre PE, Sauvage E, Poyart C, Glaser P. Host specificity in the diversity and transfer of *lsa* resistance genes in group B Streptococcus. J Antimicrob Chemother. 2015;70:3205–13. https://doi.org/10.1093/jac/dkv277

7. Schwarz S, Shen J, Kadlec K, Wang Y, Brenner Michael G, Feßler AT, et al. Lincosamides, streptogramins, phenicols, and pleuromutilins: mode of action and mechanisms of resistance. Cold Spring Harb Perspect Med. 2016;6:a027037. https://doi.org/10.1101/cshperspect.a027037

8. US Food and Drug Administration. Xenleta: highlights of prescribing information [cited 2019 Sep 16]. https://www.accessdata.fda.gov/drugsatfda_docs/label/2019/211672s000,211673s000lbl.pdf

9. Cao Y, Zhu J, Liang B, Guo Y, Ding L, Hu F. Assessment of lefamulin 20 µg disk versus broth microdilution when tested against common respiratory pathogens. Int J Antimicrob Agents. 2024;64:107366. https://doi.org/10.1016/j.ijantimicag.2024.107366

10. Clinical and Laboratory Standards Institute. Performance standards for antimicrobial susceptibility testing, 34th ed (M100-S34). Wayne, PA: The Institute; 2024.

11. ABCs Bactfacts Interactive Data Dashboard. Active bacterial core surveillance reports for 1997–2021 [cited 2024 Oct 13]. https://www.cdc.gov/abcs/bact-facts/data-dashboard.html

12. Metcalf BJ, Gertz RE Jr, Gladstone RA, Walker H, Sherwood LK, Jackson D, et al.; Active Bacterial Core surveillance team. Strain features and distributions in pneumococci from children with invasive disease before and after 13-valent conjugate vaccine implementation in the USA. Clin Microbiol Infect. 2016;22:60.e9–29. https://doi.org/10.1016/j.cmi.2015.08.027

13. Metcalf BJ. CDC streptococcal bioinformatics pipelines [cited 2023 Dec 1]. https://github.com/BenJamesMetcalf

14. Chochua S, Beall B, Lin W, Tran T, Rivers J, Li Z, et al. The emergent invasive serotype 4 ST10172 strain acquires vanG type vancomycin resistance element: a case of a 66-year-old with bacteremic pneumococcal pneumonia. J Infect Dis. 2025;231:746–50. https://doi.org/10.1093/infdis/jiae393

15. Paukner S, Riedl R. Pleuromutilins: potent drugs for resistant bugs—mode of action and resistance. Cold Spring Harb Perspect Med. 2017;7:a027110. https://doi.org/10.1101/cshperspect.a027110

16. Kolmogorov M, Yuan J, Lin Y, Pevzner PA. Assembly of long, error-prone reads using repeat graphs. Nat Biotechnol. 2019;37:540–6. https://doi.org/10.1038/s41587-019-0072-8

17. Lin Y, Yuan J, Kolmogorov M, Shen MW, Chaisson M, Pevzner PA. Assembly of long error-prone reads using de Bruijn graphs. Proc Natl Acad Sci U S A. 2016;113:E8396–405. https://doi.org/10.1073/pnas.1604560113

18. Camacho C, Coulouris G, Avagyan V, Ma N, Papadopoulos J, Bealer K, et al. BLAST+: architecture and applications. BMC Bioinformatics. 2009;10:421. https://doi.org/10.1186/1471-2105-10-421

19. Seemann T. Prokka: rapid prokaryotic genome annotation. Bioinformatics. 2014;30:2068–9. https://doi.org/10.1093/bioinformatics/btu153

20. Sullivan MJ, Petty NK, Beatson SA. Easyfig: a genome comparison visualizer. Bioinformatics. 2011;27:1009–10. https://doi.org/10.1093/bioinformatics/btr039

21. Gardner SN, Slezak T, Hall BG. kSNP3.0: SNP detection and phylogenetic analysis of genomes without genome alignment or reference genome. Bioinformatics. 2015;31:2877–8. https://doi.org/10.1093/bioinformatics/btv271

22. Kumar S, Stecher G, Tamura K. MEGA7: molecular evolutionary genetics analysis version 7.0 for bigger datasets. Mol Biol Evol. 2016;33:1870–4. https://doi.org/10.1093/molbev/msw054

23. Grant JR, Enns E, Marinier E, Mandal A, Herman EK, Chen C, et al. Proksee: in-depth characterization and visualization of bacterial genomes nucleic acids research. Nucleic Acids Res. 2023;51(W1):W484–92.

24. Brown CL, Mullet J, Hindi F, Stoll JE, Gupta S, Choi M, et al. mobileOG-db: a manually curated database of protein families mediating the life cycle of bacterial mobile

genetic elements. Appl Environ Microbiol. 2022;88:e0099122. https://doi.org/10.1128/aem.00991-22

25. Darling AE, Mau B, Perna NT. progressiveMauve: multiple genome alignment with gene gain, loss and rearrangement. PLoS One. 2010;5:e11147. https://doi.org/10.1371/journal.pone.0011147

26. Croucher NJ, Page AJ, Connor TR, Delaney AJ, Keane JA, Bentley SD, et al. Rapid phylogenetic analysis of large samples of recombinant bacterial whole genome sequences using Gubbins. Nucleic Acids Res. 2015;43:e15. https://doi.org/10.1093/nar/gku1196

27. Clewell DB, Flannagan SE, Jaworski DD, Clewell DB. Unconstrained bacterial promiscuity: the Tn916-Tn1545 family of conjugative transposons. Trends Microbiol. 1995; 3:229–36. https://doi.org/10.1016/s0966-842x(00)88930-1

28. Metcalf BJ, Chochua S, Walker H, Tran T, Li Z, Varghese J, et al. Invasive pneumococcal strain distributions and isolate clusters associated with persons experiencing homelessness during 2018. Clin Infect Dis. 2021;72:e948–56. https://doi.org/10.1016/j.bpg.2013.06.011

29. Beall B, Chochua S, Li Z, Tran T, Varghese J, McGee L, et al. Invasive pneumococcal disease clusters disproportionally impact persons experiencing homelessness, injecting drug users, and the western United States. J Infect Dis. 2022;226:332–41. https://doi.org/10.1093/cid/ciaa1680

30. Glambek M, Skrede S, Sivertsen A, Kittang BR, Kaci A, Jonassen CM, et al.; Norwegian Study Group on Streptococcus dysgalactiae. Antimicrobial resistance patterns in *Streptococcus dysgalactiae* in a One Health perspective. Front Microbiol. 2024;15:1423762. https://doi.org/10.3389/fmicb.2024.1423762

31. D'Aeth JC, van der Linden MP, McGee L, de Lencastre H, Turner P, Song J-H, et al.; GPS Consortium. The role of interspecies recombination in the evolution of antibiotic-resistant pneumococci. Elife. 2021;10:e67113. https://doi.org/10.7554/eLife.67113

32. Beall B, Chochua S, Metcalf B, Lin W, Tran T, Li Z, et al. Increased proportions of invasive pneumococcal disease cases among adults experiencing homelessness sets stage for new serotype 4 capsular-switch recombinant. J Infect Dis. 2025;231:871–82. https://doi.org/10.1093/infdis/jiae453

33. Beall B, Walker H, Tran T, Li Z, Varghese J, McGee L, et al. Upsurge of conjugate vaccine serotype 4 invasive pneumococcal disease clusters among adults experiencing homelessness in California, Colorado, and New Mexico. J Infect Dis. 2021;223:1241–9. https://doi.org/10.1093/infdis/jiaa501

34. Sankilampi U, Honkanen PO, Bloigu A, Leinonen M. Persistence of antibodies to pneumococcal capsular polysaccharide vaccine in the elderly. J Infect Dis. 1997;176:1100–4. https://doi.org/10.1086/516521

35. Kobayashi M, Leidner AJ, Gierke R, Farrar JL, Morgan RL, Campos-Outcalt D, et al. Use of 21-valent pneumococcal conjugate vaccine among U.S. adults: recommendations of the Advisory Committee on Immunization Practices—United States, 2024. MMWR Morb Mortal Wkly Rep. 2024;73:793–8. https://doi.org/10.15585/mmwr.mm7336a3

36. Huang SS, Hinrichsen VL, Stevenson AE, Rifas-Shiman SL, Kleinman K, Pelton SI, et al. Continued impact of pneumococcal conjugate vaccine on carriage in young children. Pediatrics. 2009;124:e1–11. https://doi.org/10.1542/peds.2008-3099

37. Sharma D, Baughman W, Holst A, Thomas S, Jackson D, da Gloria Carvalho M, et al. Pneumococcal carriage and invasive disease in children before introduction of the 13-valent conjugate vaccine: comparison with the era before 7-valent conjugate vaccine. Pediatr Infect Dis J. 2013;32:e45–53. https://doi.org/10.1097/INF.0b013e3182788fdd

38. Desai AP, Sharma D, Crispell EK, Baughman W, Thomas S, Tunali A, et al. Decline in pneumococcal nasopharyngeal carriage of vaccine serotypes after the introduction of the 13-valent pneumococcal conjugate vaccine in children in Atlanta, Georgia. Pediatr Infect Dis J. 2015;34:1168–74. https://doi.org/10.1097/INF.0000000000000849

39. Milucky J, Carvalho MG, Rouphael N, Bennett NM, Talbot HK, Harrison LH, et al.; Adult Pneumococcal Carriage Study Group. *Streptococcus pneumoniae* colonization after introduction of 13-valent pneumococcal conjugate vaccine for US adults 65 years of age and older, 2015–2016. Vaccine. 2019;37:1094–100. https://doi.org/10.1016/j.vaccine.2018.12.075

40. Kellner JD, McGeer A, Cetron MS, Low DE, Butler JC, Matlow A, et al. The use of *Streptococcus pneumoniae* nasopharyngeal isolates from healthy children to predict features of invasive disease. Pediatr Infect Dis J. 1998;17:279–86. https://doi.org/10.1097/00006454-199804000-00004

41. Metcalf BJ, Waldetoft KW, Beall BW, Brown SP. Variation in pneumococcal invasiveness metrics is driven by serotype carriage duration and initial risk of disease. Epidemics. 2023;45:100731. https://doi.org/10.1016/j.epidem.2023.100731

42. Domínguez-Hüttinger E, Boon NJ, Clarke TB, Tanaka RJ. Mathematical modeling of *Streptococcus pneumoniae* colonization, invasive infection and treatment. Front Physiol. 2017;8:115. https://doi.org/10.3389/fphys.2017.00115

43. Pilishvili T, Lexau C, Farley MM, Hadler J, Harrison LH, Bennett NM, et al.; Active Bacterial Core Surveillance/Emerging Infections Program Network. Sustained reductions in invasive pneumococcal disease in the era of conjugate vaccine. J Infect Dis. 2010;201:32–41. https://doi.org/10.1086/648593

44. Ahmed SS, Pondo T, Xing W, McGee L, Farley M, Schaffner W, et al. Early impact of 13-valent pneumococcal conjugate vaccine use on invasive pneumococcal disease among adults with and without underlying medical conditions—United States. Clin Infect Dis. 2020;70:2484–92. https://doi.org/10.1093/cid/ciz739

45. US Department of Housing and Urban Development. Annual homelessness assessment report [cited 2025 Sep 26]. https://www.huduser.gov/portal/datasets/ahar.html

46. Kellner JD, Ricketson LJ, Demczuk WHB, Martin I, Tyrrell GJ, Vanderkooi OG, et al. Whole-genome analysis of *Streptococcus pneumoniae* serotype 4 causing outbreak of invasive pneumococcal disease, Alberta, Canada. Emerg Infect Dis. 2021;27:1867–75. https://doi.org/10.3201/eid2707.204403

47. Navajo Epidemiology Center. Serotype 4 invasive pneumococcal disease (IPD) information for providers [cited 2024 Jul 22]. https://nec.navajo-nsn.gov/Projects-Reports/Infectious-Disease

48. Golubchik T, Brueggemann AB, Street T, Gertz RE Jr, Spencer CC, Ho T, et al. Pneumococcal genome sequencing tracks a vaccine escape variant formed through a multi-fragment recombination event. Nat Genet. 2012; 44:352–5. https://doi.org/10.1038/ng.1072

Address for correspondence: Bearnard Beall, Centers for Disease Control and Prevention, 1600 Clifton Rd NE, Mailstop C02, Atlanta, GA 30329-4018, USA; email: beb0@cdc.gov

Community-Driven, Text Message–Based COVID-19 Surveillance System, Los Angeles County, California, USA, 2020–2024

Jordan B. Braunfeld, Elizabeth Traub, Howard Chiou, Aryana T. Amoon, Christina Collins,
Allison Joyce, Justin Buendia, Prabhu Gounder, Annabelle de St. Maurice

Respiratory virus indicators were unreliable at the onset of the COVID-19 pandemic when testing availability was limited and residents with mild symptoms were advised to avoid unnecessary medical care. The Los Angeles County Department of Public Health (Los Angeles, California, USA) developed Angelenos in Action (AiA), a text message–based community syndromic surveillance system to monitor respiratory illness trends. Approximately 17,000 unique participants responded ≥1 time; 43% of participants continue to regularly respond to the survey. We assessed AiA's performance by measuring correlation coefficients with reported COVID-19 case counts (0.975), sentinel laboratory SARS-CoV-2 test positivity rate (0.762), and wastewater SARS-CoV-2 concentrations (0.861). AiA performed strongly against 3 comparator surveillance methods and correlated particularly well with raw case counts. A moderate correlation was also noted between influenza test positivity rate and AiA data, indicating the system has potential to detect respiratory illness besides COVID-19.

Even before the COVID-19 pandemic, a primary challenge with respiratory disease surveillance has been estimating the number of infections within the community, because counting every case of illness was not feasible. Public health officials have mitigated this limitation by using proxy indicators to detect rises in community incidence of disease. Commonly used proxies include sentinel laboratory data,

which examine the percentage of respiratory viral tests returning positive, and syndromic surveillance data, which tracks the percentage of emergency department (ED) visits for respiratory viral illness. As such, measuring the activity of respiratory diseases generally relies on ill persons seeking medical care and getting tested.

That approach to viral respiratory disease surveillance was disrupted during the COVID-19 pandemic. Early during the pandemic, to limit effects on the healthcare system and decrease individual risk, the public was asked to stay home and only seek care if severely ill (*1*). As a result, ED visit volume declined precipitously (*2*). In addition, SARS-CoV-2 testing availability was limited, and its use was often restricted to patients deemed sick enough to require medical care (*3*). The Los Angeles County (LAC) Department of Public Health (DPH), in Los Angeles, California, USA, identified the need to develop a system to gather timely, accurate, and relevant information about SARS-CoV-2 circulation in the community. In response, Angelenos in Action (AiA), a text message–based community syndromic surveillance system to track respiratory symptom trends, was created. AiA was modeled after long-running community surveys, such as Influenzanet and Outbreaks Near Me (*4*–*7*), and was intended to track trends in respiratory viral illness by measuring the number of persons reporting respiratory viral symptoms. The survey was intentionally focused on symptom reporting as a means of capturing illnesses of varying severity, including those cases mild enough to not require a medical visit.

For ≈4 years, AiA has provided data for LAC DPH. However, we wished to perform a comprehensive longitudinal analysis to ascertain whether it succeeded in reliably tracking communitywide COVID-19

activity. Our aim is to assess the performance of AiA as a method of tracking COVID-like illness (CLI) in LAC by observing its timeliness and accuracy in correlation to other measures of COVID incidence.

Materials and Methods

The symptom survey became available to all LAC residents >18 years of age on July 6, 2020. Recruitment for survey participants was performed with the intent to create a respondent panel that was demographically similar to the overall LAC population. Participant recruitment occurred during late summer and late fall of 2020. Participants were recruited primarily through digital advertising and social media advertising on Facebook (http://facebook.com). Two local radio stations recorded advertising spots that aired Monday through Wednesday for the first 2 weeks of the launch. Their websites and social media accounts displayed digital banners and posts about AiA during July 2020. Advertisements also ran on 2 local African American–focused digital newspapers. DPH generated press releases in both English and Spanish and advertised AiA through DPH social media accounts. An external marketing agency managed paid media. Recruitment materials were approved by the LAC DPH institutional review board. Enrollment has remained continuously open to all LAC residents. Project participation was initially limited only to those with a cell phone; however, an option to participate by email was added on December 20, 2021. Surveys were generated by Qualtrics (https://www.qualtrics.com) and sent by short message service. At the time of enrollment, participants were offered a choice of receiving the survey in English or Spanish. Participants provided their postal (ZIP) code to confirm residence in LAC and either a telephone number or an email address. Additional questions about age, sex, and race and ethnicity were optional. Participants may unsubscribe at any time by replying STOP to any AiA text message.

The symptom survey was distributed weekly and consisted of 1 question asking the respondent whether they were feeling well that day. If they reported not feeling well, 2 additional yes or no questions were asked. Participants were asked whether they were experiencing cough or shortness of breath and whether they were experiencing >2 of the following symptoms: headache, body ache, sore throat, fever, chills, or loss of sense of taste or smell (Figure 1). In consideration of the Council of State and Territorial Epidemiologists list of COVID-19 clinical symptoms at the time of the survey's development (8), respondents were considered to have CLI if they responded yes to both questions. Respondents who reported not feeling well, regardless of their responses to the symptom-specific questions, were instructed to contact their doctor.

Active respondents for each year were defined as those who submitted >1 survey during that Morbidity and Mortality Weekly Report (MMWR) surveillance year (MMWR week 40 of that calendar year through MMWR week 39 of the next calendar year) (9). To observe survey response trends over time, responses were tracked by MMWR week and plotted by MMWR surveillance year. To account for the 53rd week during the 2020–21 surveillance year, 2020 week 40 is an imputed average of the CLI rates during week 40 and week 41. The data for each remaining week
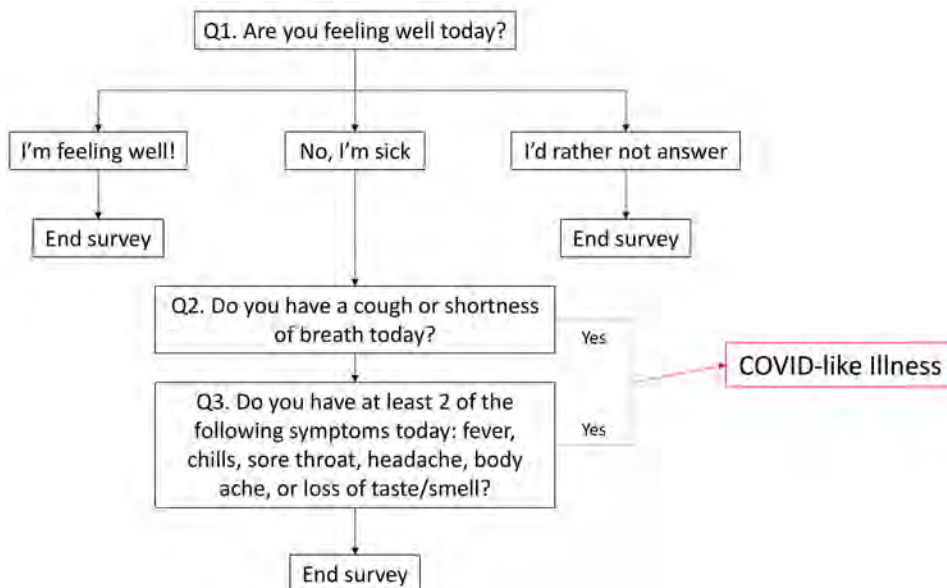

Figure 1. Survey question and response flow for the Angelenos in Action community-driven, text message-based COVID-19 surveillance system used in Los Angeles County, California, USA, 2020–2024. Red represents response pattern that results in the designation of COVID-like illness.

during 2020 were subsequently shifted 1 week backward. We chose to impute an average for week 40 and week 41 because there is historically little variation in respiratory viral activity during those weeks (10). We assessed survey population representativeness by comparing survey participant demographics with LAC demographic characteristics derived from the provisional population estimates prepared by Hedderson Demographic Services for the LAC Internal Services Department (11).

We compared trends in AiA's CLI rate with data from 3 other methods of COVID-19 surveillance used by LAC DPH during the pandemic; raw COVID-19 case counts, sentinel laboratory data, and wastewater surveillance data. We tabulated raw countywide case counts by mandatory laboratory and provider case reports to LAC; counts are described as 7-day rolling averages (12). We described sentinel laboratory data as weekly aggregates of the percentage of positive tests out of all tests performed for a given virus at the 7 LAC sentinel laboratories (10). We gathered sentinel laboratory data for SARS-CoV-2, influenza, and respiratory syncytial virus (RSV) testing. Wastewater surveillance for SARS-CoV-2 has been ongoing in LAC since January 9, 2022, and has involved all 3 LAC water treatment plants since September 12, 2022. Together, the 3 plants service ≈7.7 million of LAC's almost 10 million inhabitants. Each plant collects an average of 3 samples per week. We gathered wastewater surveillance data from the WastewaterSCAN dashboard (13,14). We describe wastewater SARS-CoV-2 RNA concentrations as a smoothed average of 5 consecutive samples after trimming the highest and lowest of the 5 samples.

We calculated CLI rates as the proportion of all responses in the AiA survey that fulfilled criteria for CLI. We calculated Pearson correlation coefficients to assess linear correlation between CLI rates and each of the 3 comparator metrics. The time frame during which CLI rates were calculated differed depending on the comparison being made. We reported CLI rates as 7-day rolling averages in comparison with daily case counts, weekly averages in comparison with sentinel laboratory data, and 7-day smoothed averages in comparison with wastewater surveillance data. Because symptoms of CLI overlap with similar respiratory illnesses, including influenza and RSV, Pearson correlation coefficients were also calculated between CLI rates and weekly LAC sentinel laboratory test positivity rates for influenza and RSV.

Because of prominent shifts in testing strategies and major changes to laboratory and provider reporting requirements in LAC throughout 2022, we calculated correlations between CLI rates and reported cases by using data from the opening of the survey through January 29, 2022. We calculated correlations between CLI rates and sentinel laboratory data for SARS-CoV-2 by using data from the opening of the survey through April 6, 2024. Because influenza viruses and RSV were essentially not circulating during the first year of the pandemic, we calculated supplemental correlations between CLI rates and sentinel laboratory data for influenza and RSV by using data collected during June 20, 2021–April 6, 2024. We calculated correlations between CLI rates and wastewater data by using data collected during January 9, 2022–April 6, 2024.

To determine if one system's data lagged another system, we calculated cross-correlation for each comparison by offsetting the data from 1 system by a discrete time interval and obtaining a new Pearson correlation coefficient. We repeated this process by shifting data 5 intervals forward and backward. The time interval used in the comparisons to case counts and to wastewater data was 1 day. The time interval used in the comparison to sentinel laboratory data was 1 week. If the offset data resulted in a higher Pearson correlation coefficient than in the original comparison, we determined there was a data lag.

This work was reviewed by Centers for Disease Control and Prevention and the LAC DPH Institutional Review Boards, was not considered human subjects research, and was conducted consistent with applicable federal law and Centers for Disease Control and Prevention policy. Consent from survey participants was obtained at the time of enrollment.

Results

AiA Participation
During July 6, 2020–April 6, 2024, a total of 20,033 unique adults received ≥1 symptom survey from AiA. The highest number of participants receiving a symptom survey in a week was 17,393 during the week starting December 26, 2021. The highest number of survey responses in 1 week was 11,061 during the week starting January 24, 2021 (Figure 2). There were 7,792 responses during the first week of the 2021–22 season, 7,022 responses during the first week of the 2022–23 season, and 5,493 responses during the first week of the 2023–24 season. The survey has received ≥1 response from 17,092 unique adults (Table 1). Respondents identifying as White composed 49.9% of all survey respondents and 51.3% of active respondents during the 2023–24 season, whereas 29.2% of all LAC residents identify as White. Respondents

Figure 2. Trends in the weekly number of responses to the Angelenos in Action community-driven, text message–based COVID-19 surveillance system by MMWR influenza season (*10*), Los Angeles County, California, USA, 2020–2024. The blue diamond represents the highest number of surveys submitted in any week since the survey opened. MMWR, Morbidity and Mortality Weekly Report.

identifying as Latino composed 29.2% of all survey respondents and 28.0% of active respondents during the 2023–24 season, whereas 45.9% of all LAC residents identify as Latino. Respondents ≥40 years of age composed 68.9% of all survey respondents and 78.3% of active respondents during the 2023–24 season, whereas 60.6% of all LAC residents are ≥40 years of age. Active respondents declined each year from a peak of 14,587 during the 2020–21 season to 7,388 during the 2023–24 season through the week ending April 6, 2024. When excluding the truncated 2019–20 and 2023–24 seasons, the average number

Table. Demographic characteristics of Los Angeles County adults and respondents to the Angelenos in Action community-driven, text message–based COVID-19 surveillance system, California, USA, 2020–2024*

	No. (%)		
Characteristics	Los Angeles County adult population	Respondents who answered ≥1 survey†	Active respondents‡ during 2023–2024 season†
Total	7,364,388	17,092	7,388
Age, y			
18–29	1,540,122 (20.9)	1,388 (8.1)	328 (4.4)
30–39	1,360,790 (18.5)	3,881 (22.7)	1,256 (17.0)
40–49	1,260,968 (17.1)	4,751 (27.8)	2,033 (27.5)
50–59	1,251,487 (17)	3,813 (22.3)	1,967 (26.6)
60–69	1,058,203 (14.4)	2,396 (14)	1,345 (18.2)
≥70	892,818 (12.1)	814 (4.8)	440 (6)
Not given	NA	49 (0.3)	19 (0.3)
Sex			
M	3,601,392 (48.9)	3,995 (23.4)	1,640 (22.2)
F	3,762,996 (51.1)	12,984 (76)	5,708 (77.3)
Not given	NA	70 (0.4)	23 (0.3)
Race			
American Indian	14,582 (0.2)	51 (0.3)	23 (0.3)
Asian	1,218,430 (16.5)	1,668 (9.8)	693 (9.4)
Black	590,152 (8)	493 (2.9)	250 (3.4)
Hawaiian/Pacific Islander	13,467 (0.2)	77 (0.5)	33 (0.4)
Latino	3,380,602 (45.9)	4,985 (29.2)	2,068 (28.0)
Multiracial	NA	845 (4.9)	379 (5.1)
White	2,147,155 (29.2)	8,530 (49.9)	3,792 (51.3)
Other	NA	238 (1.4)	77 (1)
Not given	NA	205 (1.2)	73 (1)

*NA, not available.
†Through April 6, 2024.
‡Active respondents are defined as those who submitted ≥1 survey during that year's Morbidity and Mortality Weekly Report influenza season (MMWR week 40 of that year through MMWR week 39 of the next year) (10).

of surveys submitted by respondents completing the survey $\geq$1 time in a year increased from 32.5 during the 2020–21 season to 33.9 during the 2022–23 season. (Appendix Table, http://wwwnc.cdc.gov/EID/article/31/11/25-0907-App1.pdf).

CLI Detection and System Comparisons

CLI rate increased each season from 2.2/1,000 responses during the 2019–20 season to 7.6/1,000 responses during the 2023–24 season (Appendix Table). CLI rate peaked during MMWR week 1 during both the 2020–21 season and the 2021–22 season (Figure 3). CLI rate peaked during MMWR week 48 during the 2022–23 season and MMWR week 52 during the 2023–24 season. When comparing AiA CLI rates to reported COVID-19 case count data, the Pearson correlation coefficient was 0.975 (Figure 4). When comparing AiA CLI rates to sentinel laboratory percent positivity data for SARS-CoV-2, the Pearson correlation coefficient was 0.762 (Figure 5). When comparing AiA CLI rates to wastewater surveillance data for SARS-CoV-2, the Pearson correlation coefficient was 0.861 (Figure 6). An increase in CLI rate was noted during May and June 2022 when no similar rise in wastewater detection of SARS-CoV-2 RNA was reported. Cross-correlation did not identify a data lag in any of those 3 comparisons. Additional comparisons of AiA CLI rates to sentinel laboratory percentage positivity data for RSV (Appendix Figure 1) produced a correlation coefficient of 0.094 and for influenza (Appendix Figure 2) produced a correlation coefficient of 0.508.

Discussion

During the first 4 years of the COVID-19 pandemic, AiA was able to reliably track population-level trends in symptomatic respiratory illness without a lag in data signal when compared with other commonly used surveillance methods. Data from AiA correlated well with data from the 3 comparator systems; the lowest correlation existed between AiA data and SARS-CoV-2 sentinel laboratory percentage positivity data. We noted multiple factors that might have contributed to the relatively weaker correlation. First, sentinel laboratory data was delivered in the form of once-weekly 7-day averages, so this comparison included fewer data points than either of the other 2 comparisons. Second, visual inspection of the data in this comparison shows that CLI increases from AiA data might have occasionally preceded percentage positivity increases from sentinel laboratory data. This effect was particularly apparent during the emergence of the highly infectious Delta variant during summer 2021 and during the winter 2022 seasonal increase. Last, although cross-correlation reassuringly displayed no overall lag in either dataset, this method might also be limited by the spacing of data points (i.e., a lag of <7 days might exist but would not be possible to detect by this method).

When other respiratory viruses resumed circulating at higher levels in late 2021, data from AiA continued to correlate well with COVID-19 data from other systems. However, AiA's CLI trends also appeared to have been affected by $\geq$1 other viruses. Whereas AiA showed a weak correlation with RSV sentinel

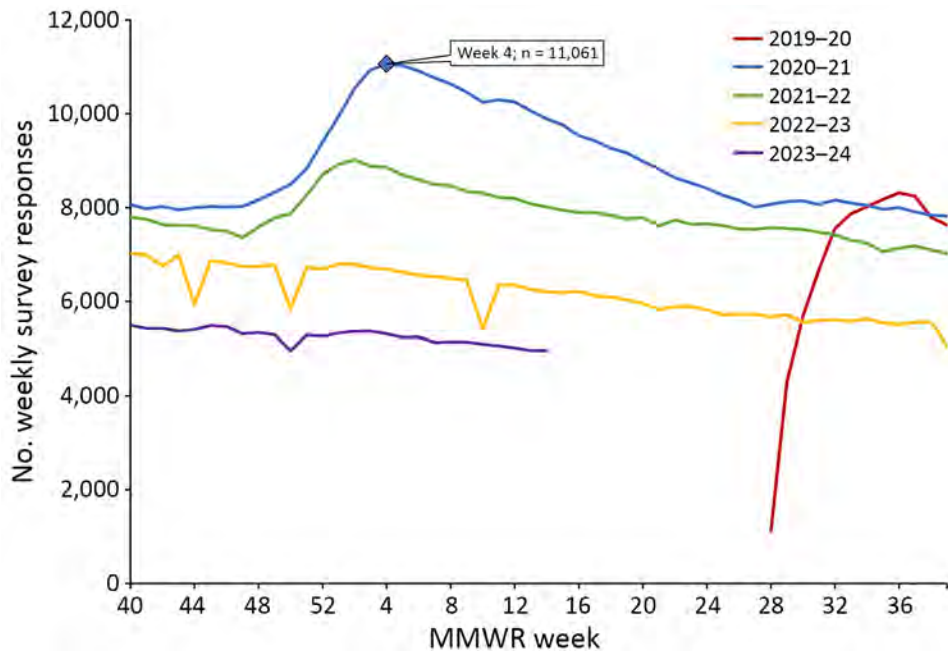**Figure 3.** Trends in COVID-like illness responses to the Angelenos in Action community-driven, text message–based COVID-19 surveillance system used in Los Angeles County, California, USA, 2020–2024, by MMWR influenza season (*10*). A response was designated as a COVID-like illness if the respondent indicated they were sick and answered yes to both symptom-specific questions. The colored diamonds correspond to the peak rate for each year. MMWR, Morbidity and Mortality Weekly Report; WK, week.

Figure 4. Trends of 7-day rolling average CLI response rate to the Angelenos in Action community-driven, text message–based COVID-19 surveillance system used in Los Angeles County, California, USA, 2020–2024, and 7-day rolling average Los Angeles County COVID-19 case counts during July 6, 2020–January 29, 2022. A response was designated as a CLI if the respondent indicated they were sick and answered yes to both symptom-specific questions. Pearson correlation coefficient = 0.975. CLI, COVID-like illness.

laboratory data (Appendix Figure 1), it showed a moderate correlation with influenza sentinel laboratory data (Appendix Figure 2). When examining periods of increased viral activity specifically, we noted that an instance of unseasonably high influenza activity during May and June 2022 appeared to correspond to a rise in CLI that preceded the increase in SARS-CoV-2 test positivity rates and SARS-CoV-2 wastewater concentrations observed later that summer. Further, when compared with peak SARS-CoV-2 test positivity rates, peak CLI rates appeared proportionally higher when influenza and SARS-CoV-2 were co-circulating (July 2022 and December 2022, and January and December 2023) than when SARS-CoV-2 was circulating alone (July 2021, January 2022, and August and September 2023). Those findings

Figure 5. Trends of weekly CLI response rate to the Angelenos in Action community-driven, text message–based COVID-19 surveillance system used in Los Angeles County, California, USA, 2020–2024, and weekly Los Angeles County sentinel laboratory SARS-CoV-2 percentage positivity during July 6, 2020–April 6, 2024. A response was designated as a CLI if the respondent indicated they were sick and answered yes to both symptom-specific questions. Pearson correlation coefficient = 0.762. Scales for the y-axes differ substantially to underscore patterns but do not permit direct comparisons. CLI, COVID-like illness.
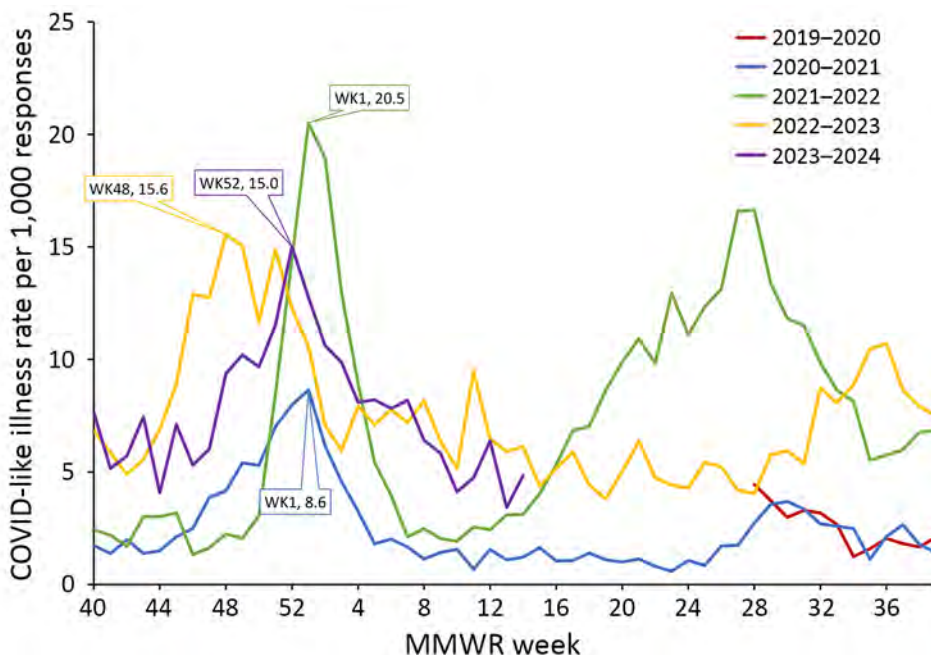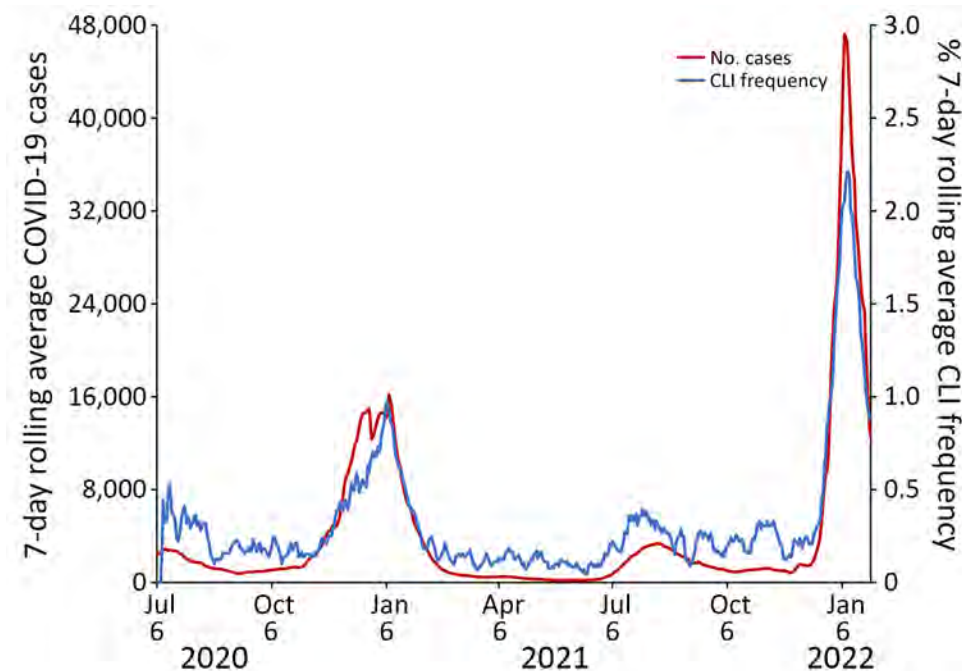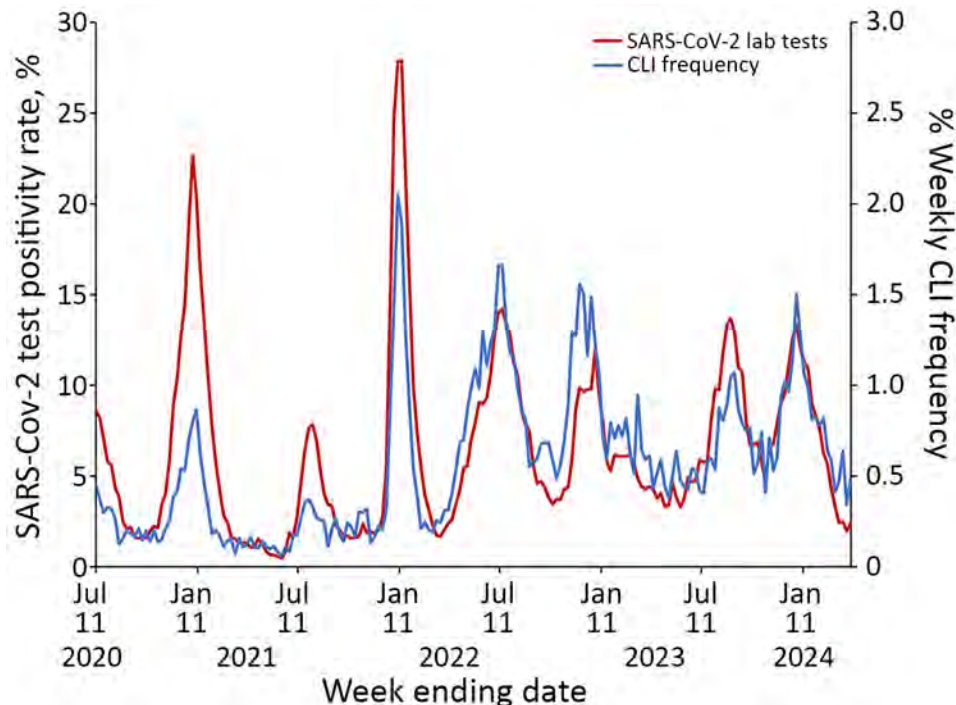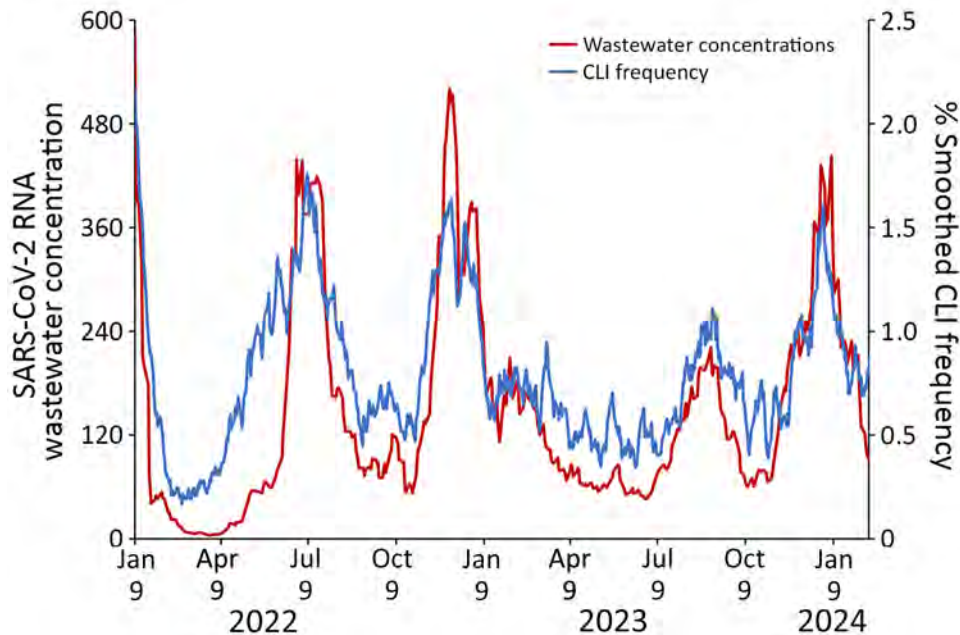
Figure 6. Trends of smoothed CLI response rate to the Angelenos in Action community-driven, text message–based COVID-19 surveillance system used in Los Angeles County, California, USA, 2020–2024, and trimmed and smoothed Los Angeles County SARS-CoV-2 RNA wastewater concentrations during January 9, 2022–April 6, 2024. A response was designated as a CLI if the respondent indicated they were sick and answered yes to both symptom-specific questions. Concentrations are normalized against values of a ubiquitous virus to account for stool flow rates and then multiplied by a factor of 10^6 (data not shown). Pearson correlation coefficient = 0.861. CLI, COVID-like illness.

indicate that AiA data might have been meaningfully influenced by influenza virus circulation, which is not surprising because of the overlap between typical influenza symptoms and the symptoms captured in the AiA symptom survey and highlights a limitation of the short survey format (15). This lower specificity means data from AiA must be interpreted in the context of other surveillance data and viral seasonality. However, it also demonstrated that AiA possesses potential to be used to detect respiratory illnesses beyond just COVID-19.

The simple data flow within AiA avoids the reporting delays inherent to the surveillance methods used before the pandemic. For example, electronic laboratory reporting data can take 3–4 days from specimen collection to test reporting. Syndromic surveillance requires appropriate medical record coding before reporting to public health, a process that can take 1–2 weeks. Because those systems rely on engagement with healthcare to capture cases, they are subject to additional delays attributable to the time from a patient first experiencing symptoms to their engagement with healthcare (4,16,17). For wastewater surveillance, the time required to collect and transport wastewater samples for testing introduces delays as long as 1–2 weeks. However, AiA delivers data with a remarkably short turnaround time, in as few as 24 hours after survey response. AiA's data collection is also independent of healthcare seeking, so it is not subject to delays from symptom onset to a medical visit. This attribute also enables AiA to capture complete data on those who do not seek medical care at all, which proved to be another strength, because most viral respiratory illnesses, COVID-19 included, do not prompt healthcare seeking (18–20). As a result, AiA's ability to rapidly display changes in disease activity and capture data regarding illnesses that did not require medical care made it particularly useful to DPH when the community health landscape was often rapidly changing.

LAC residents continue to participate in AiA >4 years after the pandemic started. Approximately 40% of all participants who responded since the survey's inception have participated in ≥1 of the weekly surveys during the 2023–24 season. Further, the average number of responses submitted by each active respondent has been consistently high and increased in each full season of the analysis, indicating that those who continued to engage with the survey did so with consistently high frequency (Appendix Table 1). This result might be partially attributable to AiA's text-based format and maximum of 3 questions per week, which placed minimal participation burden on respondents. This robust level of engagement was unexpected because no formal recruiting campaigns have occurred since January 2021, and there have been no participant retention campaigns. However, partially because of the absence of retention campaigns, overall participation has decreased. Modeling performed before the system's release and on the basis of ED influenza-like illness data before the pandemic indicated AiA would require 5,773 weekly responses to detect the presence of CLI above its baseline rate when SARS-CoV-2 was not in high

circulation. Weekly responses have not exceeded 5,773 since June 2023, which initially created concern about the reliability of data after this date. However, correlation with other surveillance metrics remained strong despite the lower number of responses. Existing differences between the survey's overall respondent population and the LAC population have become more dramatic during the most recent season, which could introduce further bias. The survey also does not account for illnesses among children, and those >60 years of age were underrepresented, which might partially explain its poor correlation with RSV data. Together, those trends indicate that the system's utility in identifying actionable increases of respiratory illness might be diminished and its representativeness and data quality can be improved.

Among the more consequential differences between AiA and its comparator systems is that AiA was the only system to measure symptomatic illness. This distinction is critical because the informational value of a positive COVID-19 test has changed as testing habits shifted throughout the pandemic, with asymptomatic testing becoming a more common strategy for controlling spread (21). However, the undetermined relevance of a positive test in an asymptomatic person made counting positive tests a less reliable metric of determining the community burden of disease. Later, the mass adoption of commercially available antigen tests made it easier for the public to rapidly determine if they had contracted the virus, but those test results were often not reported to public health authorities, creating an environment where case counts were likely underestimates of true disease counts. Pandemic fatigue and high relative costs of testing further contributed to creating uncertainty in the accuracy of raw case counts (22–24). Although AiA might not have always been able to determine the specific etiology of an illness, AiA's focus on detecting symptoms enabled it to remain reliable in detecting the magnitude of clinically apparent respiratory illness in the community.

Timely, accurate, and actionable data are crucial in the face of pandemic and seasonal viral respiratory illness. During the COVID-19 pandemic, when typical methods of obtaining data were impaired or inoperable, AiA provided data accurately and in a timely fashion. AiA was able to produce reliable results years into the pandemic despite waning participation and discordant demographic characteristics between respondents and the local population. AiA's community symptom survey approach enabled it to fill the surveillance gap by gathering data that were not captured by common surveillance methods but were still highly relevant to understanding the community burden of disease. Further, the principles of this survey methodology and the low relative cost of implementation could be adapted in low- and middle-income countries where mobile phone use is widespread but access to healthcare or laboratory testing might be limited. Our findings highlight the strengths of community participatory surveillance systems in monitoring emerging and endemic infectious diseases.

About the Author

Dr. Braunfeld is an infectious disease physician and Epidemic Intelligence Service Officer for the Centers for Disease Control and Prevention. His interests include measles and hepatitis A outbreak response and vaccination campaign assessments.

References

1. Executive Order N-33-20. March 19, 2020 [cited 2024 Dec 30]. https://www.gov.ca.gov/wp-content/uploads/2020/03/EO-N-33-20-COVID-19-HEALTH-ORDER-03.19.2020-002.pdf
2. Oskvarek JJ, Zocchi MS, Black BS, Celedon P, Leubitz A, Moghtaderi A, et al.; US Acute Care Solutions Research Group. Emergency department volume, severity, and crowding since the onset of the coronavirus disease 2019 pandemic. Ann Emerg Med. 2023;82:650–60. https://doi.org/10.1016/j.annemergmed.2023.07.024
3. Los Angeles County DPH Health Advisory: COVID-19 guidance—optimizing N95 supplies and managing mild illness. March 4, 2020 [cited 2024 Dec 30]. http://publichealth.lacounty.gov/eprp/lahan/alerts/LAHANVCOVID030420.pdf
4. van Noort SP, Codeço CT, Koppeschaar CE, van Ranst M, Paolotti D, Gomes MG. Ten-year performance of Influenzanet: ILI time series, risks, vaccine effects, and care-seeking behaviour. Epidemics. 2015;13:28–36. https://doi.org/10.1016/j.epidem.2015.05.001
5. Paolotti D, Carnahan A, Colizza V, Eames K, Edmunds J, Gomes G, et al. Web-based participatory surveillance of infectious diseases: the Influenzanet participatory surveillance experience. Clin Microbiol Infect. 2014;20:17–21. https://doi.org/10.1111/1469-0691.12477
6. Smolinski MS, Crawley AW, Baltrusaitis K, Chunara R, Olsen JM, Wójcik O, et al. Flu near you: crowdsourced symptom reporting spanning 2 influenza seasons. Am J

Public Health. 2015;105:2124–30. https://doi.org/10.2105/AJPH.2015.302696

7. Outbreaks Near Me. Who we are [cited 2024 Dec 30]. https://outbreaksnearme.org/us/en-US/who-we-are

8. Council of State and Territorial Epidemiologists. Standardized surveillance case definition and national notification for 2019 novel coronavirus disease (COVID-19) [cited 2024 Dec 30]. https://cdn.ymaws.com/www.cste.org/resource/resmgr/2020ps/Interim-20-ID-01_COVID-19.pdf

9. Centers for Disease Control and Prevention. MMWR weeks. 2013 [cited 2025 May 16]. https://stacks.cdc.gov/view/cdc/22305

10. RESPWatch | LA County DPH. Technical notes [cited 2024 Dec 30]. http://publichealth.lacounty.gov/acd/respwatch/index.htm#TechnicalNotes

11. County of Los Angeles, Internal Services Department, Information Technology Services, Geographic Information Systems Section. Los Angeles County population estimates (July 1, 2022) [cited 2024 Dec 30]. http://www.publichealth.lacounty.gov/epi/docs/2022-LAC-Population-8RE.pdf

12. Sunquest Public Health. Los Angeles County department of public health integrated reporting, investigation, and surveillance system (IRIS) and virtual confidentiality morbidity report (vCMR) [cited 2024 Dec 30]. http://dashboard.publichealth.lacounty.gov/covid19_surveillance_dashboard

13. Boehm AB, Wolfe MK, Bidwell AL, Zulli A, Chan-Herur V, White BJ, et al. Human pathogen nucleic acids in wastewater solids from 191 wastewater treatment plants in the United States. Sci Data. 2024;11:1141. https://doi.org/10.1038/s41597-024-03969-8

14. WastewaterSCAN. About the dashboard [cited 2024 Dec 30]. https://data.wastewaterscan.org/about

15. Uyeki TM, Hui DS, Zambon M, Wentworth DE, Monto AS. Influenza. Lancet. 2022;400:693–706. https://doi.org/10.1016/S0140-6736(22)00982-5

16. Wu Y, Xu S, Shen X, Cheng J, Chai J, Feng R, et al. Trajectories of symptoms and healthcare use following respiratory tract infections in rural Anhui, China: a cross-sectional study. J Infect Public Health. 2020;13:1939–45. https://doi.org/10.1016/j.jiph.2020.09.022

17. Moran KR, Fairchild G, Generous N, Hickmann K, Osthus D, Priedhorsky R, et al. Epidemic forecasting is messier than weather forecasting: the role of human behavior and internet data streams in epidemic forecast.

J Infect Dis. 2016;214(suppl_4):S404–8. https://doi.org/10.1093/infdis/jiw375

18. Peppa M, John Edmunds W, Funk S. Disease severity determines health-seeking behaviour amongst individuals with influenza-like illness in an internet-based cohort. BMC Infect Dis. 2017;17:238. https://doi.org/10.1186/s12879-017-2337-5

19. Galanti M, Comito D, Ligon C, Lane B, Matienzo N, Ibrahim S, et al. Active surveillance documents rates of clinical care seeking due to respiratory illness. Influenza Other Respir Viruses. 2020;14:499–506. https://doi.org/10.1111/irv.12753

20. Macinko J, Woolley NO, Seixas BV, Andrade FB, Lima-Costa MF. Health care seeking due to COVID-19 related symptoms and health care cancellations among older Brazilian adults: the ELSI-COVID-19 initiative. Cad Saude Publica. 2020;36(Suppl 3):e00181920. https://doi.org/10.1590/0102-311x00181920

21. Brook CE, Northrup GR, Ehrenberg AJ, Doudna JA, Boots M; IGI SARS-CoV-2 Testing Consortium. Optimizing COVID-19 control with asymptomatic surveillance testing in a university environment. Epidemics. 2021;37:100527. https://doi.org/10.1016/j.epidem.2021.100527

22. Huffman EM, Athanasiadis DI, Anton NE, Haskett LA, Doster DL, Stefanidis D, et al. How resilient is your team? Exploring healthcare providers' well-being during the COVID-19 pandemic. Am J Surg. 2021;221:277–84. https://doi.org/10.1016/j.amjsurg.2020.09.005

23. Nguyen N, Lane B, Lee S, Gorman SL, Wu Y, Li A, et al. A mixed methods study evaluating acceptability of a daily COVID-19 testing regimen with a mobile-app connected, at-home, rapid antigen test: implications for current and future pandemics. PLoS One. 2022;17:e0267766. https://doi.org/10.1371/journal.pone.0267766

24. de Meijere G, Valdano E, Castellano C, Debin M, Kengne-Kuetche C, Turbelin C, et al. Attitudes towards booster, testing and isolation, and their impact on COVID-19 response in winter 2022/2023 in France, Belgium, and Italy: a cross-sectional survey and modelling study. Lancet Reg Health Eur. 2023;28:100614. https://doi.org/10.1016/j.lanepe.2023.100614

Address for correspondence: Jordan B. Braunfeld, Los Angeles County Department of Public Health, 3530 Wilshire Blvd, Ste 700, Los Angeles, CA, 90010, USA; email: jordan.braunfeld@gmail.com

Isolation and Characterization of *Rickettsia finnyi*, Novel Pathogenic Spotted Fever Group *Rickettsia* in Dogs, United States

Praveen K. Korla,[1] Michael G. Karounos,[1] Sarah B. Clarke, Cynthia Robveille,
James M. Wilson, Edward B. Breitschwerdt, Adam J. Birkenheuer, Barbara A. Qurollo

In 2020, a novel spotted fever group *Rickettsia* was described in 3 clinically ill dogs in the United States. Using naturally infected canine blood, the novel *Rickettsia* sp. was isolated in epithelial (Vero E6) and mononuclear (DH82 and 030D) cell lines. The sequenced whole genome revealed a 1.27 Mb circular chromosome with 96.87% identity to *Rickettsia raoultii* on the basis of average nucleotide identity analysis. A maximum-likelihood phylogeny tree placed the novel *Rickettsia* in its own branch within the spotted fever group. Immunofluorescence revealed single rods localized along the membrane in epithelial cells and randomly distributed in the cytoplasm of mononuclear cells. We propose the name *Rickettsia finnyi* sp. nov., strain 2024-CO-Wats, which is available from national and international Rickettsial isolate reference collections. Fever and thrombocytopenia were among abnormalities in the 17 naturally infected dogs we describe, underscoring the pathogenic importance of *R. finnyi* sp. nov. and its potential public health relevance.

In 2020, a unique spotted fever group *Rickettsia* (SFGR), *Rickettsia* sp. 2019-CO-FNY, was identified in 3 clinically ill dogs in the southern and midwestern United States (*1*). Those dogs exhibited symptoms like those caused by *R. rickettsii*, the agent responsible for Rocky Mountain spotted fever (RMSF). SFGR are emerging tickborne pathogens infecting dogs and humans. Among tickborne pathogens infecting dogs, SFGR had the highest seroprevalence at 10.4% in the United States during 2004–2010 (*2*). The Centers for Disease Control and Prevention reported annual SFGR cases in humans in the United States increased substantially from 486 in 2000 to 6,248 in 2017 (*3*). Despite frequent exposure to

SFGR, gaps remain in our understanding of pathogenic *Rickettsia* spp., disease severity, and tick vectors.

In the United States, several SFGR species, including *R. parkeri*, *R. rickettsii*, and *R. rickettsii* subsp. *californica*, cause disease in humans (*4,5*). Among those species, *R. rickettsii* is the most virulent in dogs and humans and can be fatal without early antibiotic intervention (*6*). In addition to *R. rickettsii*, other SFGR species have been detected in dogs in the United States, including *R. montanensis*, *R. amblyommatis*, and *R. parkeri*, all of which caused asymptomatic infection (*7,8*). Until recently, *R. rickettsii* was the only SFGR known to cause disease in dogs in North America. Dogs with RMSF can demonstrate fever, lethargy, neurologic signs, and generalized or localized pain, like arthropathy (*9,10*). Clinical signs reported in dogs infected with *Rickettsia* sp. 2019-CO-FNY resembled those seen in RMSF, indicating the existence of additional virulent SFGR in the United States and underscoring the importance of expanded vectorborne disease surveillance for canine and human health.

In this study, we cultured and sequenced a novel, pathogenic SFGR, *Rickettsia* sp. 2019-CO-FNY. We identified *Rickettsia* sp. 2019-CO-FNY in 14 additional sick dogs and cultured it from 1 infected dog. On the basis of whole-genome sequencing (WGS) and imaging, we determined that *Rickettsia* sp. 2019-CO-FNY is a new *Rickettsia* species, which we propose naming *Rickettsia finnyi* sp. nov., strain 2024-CO-Wats.

Methods

Infected Dogs

All dogs naturally infected with *Rickettsia* sp. 2024-CO-Wats were identified after samples were

[1]These authors contributed equally to this article.

submitted to a veterinary diagnostic laboratory for canine comprehensive vectorborne disease testing. Signalment, sample collection date, and geographic location were included on submission forms. Attending veterinarians were asked to provide historical and clinical information. Ethical approval for animal use was not required for blood samples initially submitted for diagnostic testing; however, additional blood samples requested for *R. rickettsii* indirect immunofluorescence assay (IFA), posttreatment quantitative PCR (qPCR), and culture were approved under Institutional Animal Care and Use Committee protocol number 21–274. Analysis combined newly acquired data from 14 dogs with data from 3 dogs previously described (*1*).

Rickettsia Detection and Culture

The EDTA whole-blood sample used for culture was collected from a dog on April 25, 2024, by a veterinarian in Indiana, USA, and submitted to a veterinary diagnostic laboratory for comprehensive tickborne disease testing. The sample was received April 30, 2024, and stored at 4°C for 72 hours before testing. Tests consisted of qPCR for vertebrate GAPDH (internal control), *Anaplasma*, Apicomplexa, *Babesia*, *Bartonella*, *Ehrlichia*, hemotropic *Mycoplasma* and *Rickettsia*; IFA for *Babesia vogeli*, *Bartonella henselae*, *Bartonella koehlerae*, *Bartonella vinsonii* subsp. *berkhoffii*, *Ehrlichia canis*, and *Rickettsii* spp.; ELISA for antibodies to *Babesia gibsoni* and a SNAP 4DX Plus point-of-care ELISA (Idexx Laboratories, https://www.idexx.com) for *Dirofilaria immitis* antigen and species-specific antibodies to *E. canis*, *Ehrlichia ewingii*, *Anaplasma phagocytophilum*, *A. platys*, and *Borrelia burgdorferi* (*11–17*). *Rickettsia* sp. 2024-CO-Wats infection was confirmed with amplicon sequencing (GENEWIZ, http://www.genewiz.com) of the *Rickettsia* 23s-5s internal transcribed

spacer genus qPCR and a newly developed *R. finnyi* species-specific (sp-sp) hydrolysis probe-based qPCR (*1*) (Appendix, https://wwwnc.cdc.gov/EID/article/31/11/25-0681-App1.pdf).

We added blood from a dog naturally infected with *Rickettsia* sp. 2024-CO-Wats to continuously maintained cell cultures using a previously published protocol (*18*). In brief, we combined 100 µL of blood and sucrose-phosphate-glutamate in a 1:1 ratio for each inoculation of 5 replicate cultures of Vero E6 (VE6) and 3 replicate cultures of DH82 and 030D cells seeded in either 7 ml tissue culture tubes, 6-well plates, or T-25 flasks (Fisher Scientific, http://www.fishersci.com) (Appendix Table 1). Cultures were grown at 34°C with 5% CO_2 in either DMEM 5% FBS (VE6) or RPMI 1640 GlutaMAX 10% FBS (030D and DH82 cells) in a Biosafety Level 3 laboratory. We tested culture supernatants or cell suspensions from passages by qPCR and calculated fold changes in *Rickettsia* (Appendix). We performed retrospective qPCR and amplicon sequencing on stored culture DNA samples to assess a mutation acquired in a major facilitator superfamily (MFS) transporter gene (Appendix) (Table 1). We stained culture samples using the Gimenez method (*19*). We obtained images under oil immersion with an Olympus BX60 microscope and digital camera. We developed and performed an immunofluorescence technique on all 3 infected cell lines and acquired images with BZ-X810 Keyence (Appendix).

DNA Extraction and Whole-Genome Sequencing

We grew canine 030D and monkey VE6 cells infected with *Rickettsia* sp. 2024-CO-Wats in T25 flasks for DNA extraction (QIAGEN, https://www.qiagen.com). Sequencing was performed by the University of Delaware DNA Sequencing and Genotyping Center using Pacific Biosciences (https://www.pacb.com)

Table 1. Growth of *Rickettsia finnyi* sp. nov. strain 2024-CO-Wats in Vero E6, 030D, and DH82 cells monitored through changing Cq values in *Rickettsia* 23s-5s ITS and *R. finnyi*–specific M61 qPCRs in study of isolation and characterization of novel pathogenic spotted fever group *Rickettsia* in dogs, United States*

	Vero E6			030D			DH82		
Day	Sample	*Rickettsia* 23S-5S (Cq)	*R. finnyi* M61 probe (Cq)	Sample	*Rickettsia* 23S-5S (Cq)	*R. finnyi* M61 probe (Cq)	Sample	*Rickettsia* 23S-5S (Cq)	*R. finnyi* M61 probe (Cq)
3	VE6–5†	28.88	NA	030D-3†	33.32	NA	DH82–3†	31.35	NA
6	VE6–5†	28.88	NA	030D-3-P1†	35.13	NA	DH82–3-P1†	33.38	NA
10	VE6–5†	28.41	32.26	030D-3-P1†	30.37	34.52	DH82–3-P1†	32.83	35.76
13	VE6–5-P1†	30.40	34.28	030D-3 -P1†	30.86	34.45	DH82–3-P1†	28.93	32.60
20	VE6–5-P2†	21.41	25.88	030D-3-P2†	25.27	29.48	DH82–3-P2†	24.74	29.31
32	VE6–5-P4†‡	16.06	17.20	030D-3-P4†	20.35	21.67	DH82–3-P4†	19.49	22.78
57	NA	NA	NA	NA	NA	NA	DH82–3-P7†	18.70	NA
89	VE6–5-P7	12.81	NA	NA	NA	NA	NA	NA	NA
104	VE6–5-P9†‡	15.73	NA	030D-3-P15†	18.59	NA	DH82–3-P14†	18.93	NA

*Cq, quantification cycle; NA, not applicable; qPCR, quantitative PCR.
†qPCR performed to identify an MFS transporter single nucleotide mutation T→G.
‡MFS transporter single nucleotide mutation A→C present

Table 2. Date, location, signalment, and vectorborne disease diagnostic results from dogs naturally infected with *Rickettsia finnyi* sp. nov. strain 2024-CO-Wats in study of isolation and characterization of novel pathogenic spotted fever group *Rickettsia* in dogs, United States*

Dog no.	Date	State	Breed	Age, y/sex	*Rickettsia* 23S-5S ITS PCR (Cq, Mt)†	*R. rickettsii* IFA titer	Vectorborne disease co-infections, test type (titer)
1‡	2018 May 17	TN	MB	10/MC	37.7, 77.5°	1:512	None
2‡	2019 May 8	IL	BT	9/MC	39.1, 78°	1:256	None
	2019 May 15§				ND	1:8,192	
3‡	2019 Aug 28	OK	MB	9/MC	33.8, 77.5°	1:1,024	None
	2019 Sep 10§				ND	1:8,192	
4	2020 May 3	OK	V	8/MC	38.1, 78°	1:256	*Ehrlichia* SNAP4DxPlus
	2020 May 28§				ND	1:512	
5	2020 May 7	TX	MB	7/MC	34.5, 77°	1:512	*Mycoplasma hematoparvum* PCR+
6	2020 Jul 16	NC	KSD	2/FS	35.4, 77.5°	<1:32	*Bartonella henselae* IFA (1:64)
	2020 Aug 19§				ND	1:1,024	
7	2020 Aug 1	CO	ESS	12/FS	33.8, 77.5°	<1:32	*Babesia* sp. (Coco) PCR+
8	2022 May 23	KS	LR	4/MC	37.7, 77.5°	1:265	*Ehrlichia* SNAP4DxPlus
9	2022 May 24	MO	LR	6/M	38.3, 77.5°	1:2,048	None
	2022 Jun 17§				ND	1:8,192	
10	2023 May 5	KS	ASP	3/FS	33.9, 77.5°	<1:32	None
11	2023 May 5	KS	MB	13/MC	36.5, 77.5°	1:4,096	*Anaplasma* SNAP4DxPlus, *B. canis* IFA (1:256),
12	2023 Sep 13	AL	MB	8/MC	36.6, 78°	1:512	None
	2023 Oct 2§				ND	1:4,096	
13	2023 Sep 18	MO	LR	8/M	33.1, 77.5°	1:256	None
14	2023 Oct 10	IA	GR	5/FS	37.4, 78°	1:64	*Ehrlichia* SNAP4DxPlus, *E. canis* IFA (1:64)
	2023 Oct 19§				ND	1:4,096	
15¶	2024 Apr 25	IN	MB	9/M	28.8, 77°	1:1,024	None
16	2024 Oct 23	LA	TP	4/M	36.5, 77.5°	1:2,048	None
17	2025 May 14	LA	MB	8/MC	36.4, 77.5°	1:4,096	None

*ASP, American Staffordshire terrier; BT, Boston terrier; Cq, quantification cycle; ESS, English springer spaniel; FS, female spayed; GR, golden retriever; IFAT, indirect immunofluorescent antibody; ITS, internal transcribed spacer; KSD, Kangal shepherd dog; LR, labrador retriever; MC, male castrated; Mt, melting temperature; MB, mixed breed; ND, not detected; TP, toy poodle; VBD, vectorborne disease; V, Vizsla.
†Rickettsia 23S-5S ITS amplicons were Sanger sequenced and 100% identical to Rickettsia sp. strain 2019-CO-FNY.
‡Dogs described previously (*1*).
§Post doxycycline treatment.
¶Sample used for culturing.

Single-Molecule DNA for each culture DNA was sheared to 15 kb using the Megarupture 3 instrument (Diagenode, https://www.diagenode.com). SMRTbell DNA libraries were constructed according to the PacBio HiFi SMRTbell protocol using SMRTbell Express Template Prep Kit 3.0 and barcoded with the SMRTbell adaptor index plate 96A (Pacific Biosciences). AMPure PB beads were diluted at a 3.1× ratio to remove fragments <5 kb before sequencing and 1 SMRTcell was used to sequence the libraries on the Revio PacBio instrument for 30 hours.

Genome Assembly and Annotation
We assessed sequencing generated by PacBio HiFi circular consensus sequencing reads for quality using NanoPlot (*20*), aligned with host cell DNA, *Canis lupus familiaris* (030D) genomic DNA (Genbank no. GCA_000002285.4), and *Chlorocebus sabaeus* strain WHO RCB 10–87 (VE6) genomic DNA (Genbank no. GCA_015252025.1) using Minimap2 version 2.28 (*21*). We then filtered using SAMtools version 1.20

(*22*) and confirmed host DNA removal and coverage of the *Rickettsia* genome by using BAM file statistics. We assembled unmapped reads using Flye version 2.9.5 (*23*) and assessed quality using version 5.3 of the QUAST tool (*24*). We verified genome completeness and absence of plasmid sequences using Benchmarking Universal Single-Copy Orthologs tool version 5.8.0 and SourceFinder version 1.0 (*25*). We annotated the genome with the National Center for Biotechnology Information Prokaryotic Genome Annotation Pipeline.

Genomic and Phylogenetic Analysis
We directly compared the whole genomes of 37 *Rickettsia* spp. from GenBank, including 4 strains of *R. rickettsii* and 4 strains of *R. parkeri*, with the genome of 2024-CO-Wats (Appendix Table 2). We analyzed digital DNA-DNA hybridization (dDDH) with the Type Strain Genome Server (https://tygs.dsmz.de) (*26*) and determined average nucleotide identity (ANI) using the OrthoANI tool (*27*). We annotated 38

Rickettsia genomes with Prokka version 1.14.6 (default settings, *Rickettsia*-specific BLAST DB) (*28*). We identified orthologous core genes present in all genomes were identified using ProteinOrtho version 6.3.1 (*29*), aligned each gene at the nucleotide level with MAFFT version 7.526 (*30*), and concatenated into a matrix. We then performed maximum-likelihood phylogenetic inference with RAxML-NG version 1.2.1 (*31*) under a general time-reversible plus FC plus gamma 4m plus B model with per-partition parameter estimation. We mapped bootstrap support (500 replicates) onto the best maximum-likelihood tree, which was rooted with *Rickettsia bellii*.

Results

Infected Dogs

We compiled signalment, collection date and location, and vectorborne diagnostic results from the 17 *Rickettsia* sp. 2024-CO-Wats infected dogs (14 new and 3 previously described) (Table 2) (*1*). More than half the samples were collected in May (9/17, 53%), and many dogs (7/17, 41%) resided in Kansas, Missouri, or Oklahoma (Table 2). Two dogs were co-infected with *Babesia* sp. (Coco) or *Mycoplasma hematoparvum*, and 5 dogs were seroreactive for other vectorborne pathogens. Because of limited and inconsistent clinical data, dogs were not uniformly evaluated for each parameter. The most common abnormal findings were fever (n = 13), lethargy

(n = 13), and thrombocytopenia (n = 12) (Figure 1). Fourteen veterinarians administered doxycycline therapy (5–10 mg/kg every 12 hours) at the time of sample submission. One dog died before diagnosis and doxycycline therapy, and 1 was euthanized 1 day after starting doxycycline. One dog died because of nephrotic syndrome after treatment as previously described (*1*). Seven veterinarians sent additional samples for *Rickettsia* qPCR testing and *R. rickettsii* IFA. Results for all dogs tested for *Rickettsia* after doxycycline treatment were negative by qPCR, and all but 1 dog had a 4-fold or greater increase in *R. rickettsii* IFA titers (Table 2).

Rickettsia Culture and Visualization

The EDTA-whole blood sample used for culturing was qPCR-positive for *Rickettsia* by 23s-5s ITS qPCR (quantification cycle 28.7, melting temperature 77°C) and *R. finnyi*–specific probe-based qPCR (quantification cycle 31) (Table 2). Serum from the same dog was seroreactive by *R. rickettsii* IFA with a titer of 1:2,048. All other vectorborne tests were negative (Table 2). All 3 cell lines were infected with *Rickettsia* sp. 2024-CO-Wats and maintained over multiple passages (Table 1; Appendix Figure 2). Images of 2024-CO-Wats-infected 030D-P18 and VE6-P4 cells stained with Gimenez revealed red, small (≤0.5 by 2 μm), intracytoplasmic, randomly distributed rod-shaped bacteria (Figure 2). We visualized bacteria by immunofluorescence staining in 3 infected cell lines using serum from 2 dogs

A. Fever
B. Lethargy
C. Thrombocytopenia
D. Inappetence
E. Ticks on dog
F. Vomiting or diarrhea
G. Arthropathy
H. Elevated ALP or ALT
I. Anemia
J. Neutrophilia
K. Hyperglobulinemia
L. Abdominal pain
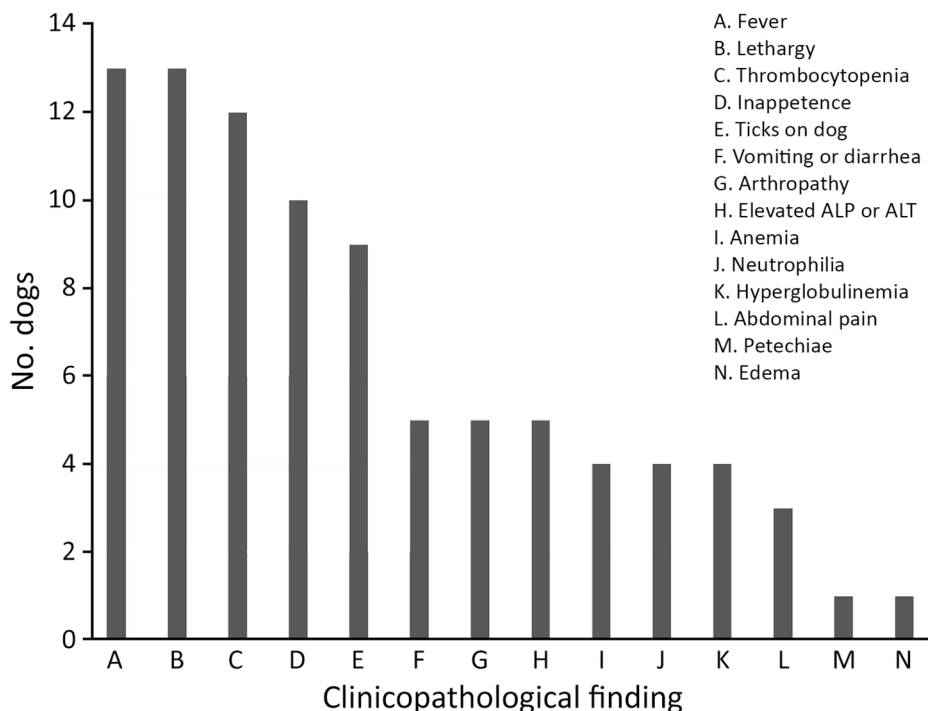M. Petechiae
N. Edema

Figure 1. Common clinicopathological findings in 17 dogs naturally infected with *Rickettsia finnyi* sp. nov. strain 2024-CO-Wats in study of isolation and characterization of novel pathogenic spotted fever group *Rickettsia* in dogs, United States. ALP, alkaline phosphatase; ALT, alanine transaminase.
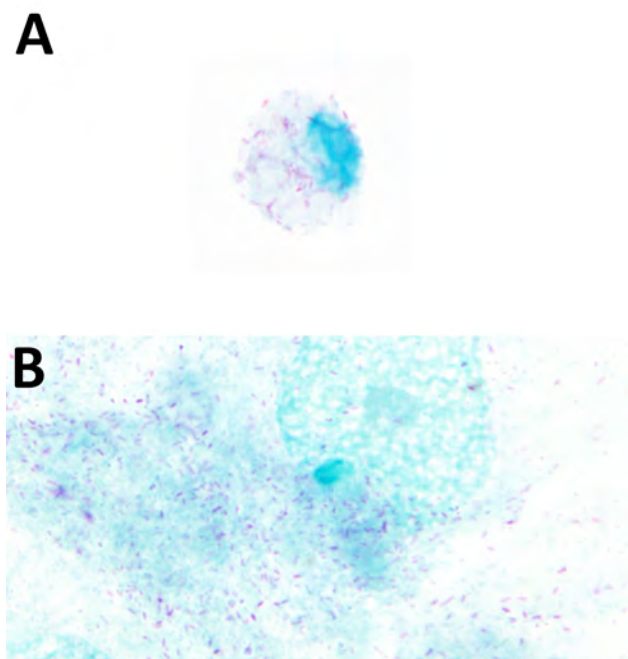
Figure 2. Microscopic images from study of isolation and characterization of *Rickettsia finnyi*, novel pathogenic spotted fever group *Rickettsia* in dogs, United States. Images depict *Rickettsia finnyi* sp. nov. strain 2024-CO-Wats–infected 030D canine mononuclear cells (A) and Vero E6 primate epithelial cells (B) stained with Giménez. Original magnification ×100. Image is white balance adjusted.

naturally infected with *Rickettsia* sp. 2024-CO-Wats (Figure 3). The staining did not differ between the 2 serum samples. The 030D-P9 (100% of cells), DH82-P8 (≈95%) and VE6-P2 (100%) cells were highly infected. The bacteria were in the cytoplasm as single rods or, less frequently, as clusters. In addition, we visualized aggregates of bacteria and, to a lesser extent, single bacilli on the cytoplasmic membrane of VE6 cells. We did not observe bacteria with nonreactive serum or with secondary antibody control.

Whole-Genome Sequencing, Assembly, and Annotation

We performed whole-genome sequencing using 1.33 μg (purity 1.92 A260/A280) of DNA from 030D cells infected with *Rickettsia* sp. 2024-CO-Wats and using 1.73 μg (purity 1.84 A260/A280) of DNA from VE6 cells infected with *Rickettsia* sp. 2024-CO-Wats. PacBio sequencing generated ≈1.5 million reads from infected 030D cells, where 1,481,022 reads were mapped to the host genome and removed leaving 16,333 unmapped reads. Approximately 4.6 million reads were generated from infected VE6 cells, where 3,030,649 reads were mapped to the host genome and removed, leaving 1,619,279 unmapped reads. We subsampled reads from VE6 cells and used 24,476

(2%) of the best quality reads for assembly. Flye generated a single, circularized contig of 1,270,764-bp with 32.3% G+C content for 2024-CO-Wats from both cultures. Mean genome coverage for 2024-CO-Wats was 174× from 030D and 261× from VE6 cultures. The assembled genomes showed 100% Benchmarking Universal Single-Copy Orthologs scores (genome completeness) using the Rickettsiales lineage. SourceFinder did not identify sequences originating from plasmids. Both genomes were deposited in Genbank as *Rickettsia* sp. 2024-CO-Wats cultured from 030D cells (accession no. CP170741) and *Rickettsia* sp. 2024-CO-Wats-2 from VE6 cells (accession no. CP187160). Both genomes were identical except a single nonsynonymous mutation at coordinate 646,406-bp (A/C) coding the 62nd amino acid in an MFS transporter protein (GenBank accession nos. XIA57199 and XRJ55031) changing the TTT (phenylalanine) in the 030D culture to TTG (leucine) in the VE6 culture. PCR and amplicon sequencing of the MFS transporter gene from cultures confirmed the mutation only occurred in VE6-P4 cells beginning on day 32 and was still present in VE6-P9 cells on day 104 (Table 1). The National Center for Biotechnology Information Prokaryotic Genome Annotation Pipeline identified 1,425 genes, 1,234 gene open-reading frames, 33 tRNAs, 3 rRNAs, and 4 ncRNAs.

Genomic and Phylogenetic Analysis

When compared with 37 *Rickettsia* spp. genomes, the 2024-CO-Wats genome was most similar to *R. raoultii* (GenBank accession no. CP098324); average nucleotide identity was 96.86% and dDDH was 70.6% (Appendix Table 2). ProteinOrtho identified 636 core orthologous genes, and phylogenetic analysis placed 2024-CO-Wats with its own distinct branch within the SFGR (Figure 4).

Discussion

We isolated and sequenced the genome of a novel, pathogenic SFGR (formerly *Rickettsia* sp. 2019-CO-FNY) from a clinically ill dog that we propose naming *Rickettsia finnyi* sp. nov. type strain 2024-CO-Wats. This novel *Rickettsia* was cultured and maintained over many passages proving viability in epithelial (VE6) and mononuclear (030D and DH82) cells. Whole-genome sequencing generated a small, circular genome (1.27 kb) from infected 030D and VE6 cell lines. The *Rickettsia* genome was identical except for 1 nucleotide mutation in the VE6 cultured strain in an MFS transporter protein gene. The difference resulted in a conservative hydrophobic-to-hydrophobic amino acid change (phenylalanine to leucine), which could affect substrate specificity and

transport efficiency, among other functions. The mutation could possibly have occurred in the VE6 culture because of different growth conditions or passage techniques. Genome alignment revealed it was most similar to *R. raoultii* (CP098324), with relatively small percentage differences between other SFGR species. Phylogenetic analysis of the genome sequence (CP170741) placed *R. finnyi* sp. nov. (2024-CO-Wats) on a distinct lineage within the spotted fever group, further supporting that it is a new species.

Criteria to designate a new *Rickettsia* sp. indicate that the genome must have an OrthoANI value of $\geq$83.63% compared with $\geq$1 *Rickettsia* species with a validly published name to be classified in the genus and a dDDH value of <92.3%, OrthoANI value of <99.19% identical with other known *Rickettsia* spp., or both to be considered a new species (*32*). *R. finnyi* sp. nov. (2024-CO-Wats) meets each of those criteria to be recognized as a new *Rickettsia* species. Genome comparisons revealed the highest results from both metrics was *R. raoultii* (CP098324) with a dDDH formula 2 value of 70.6% and OrthoANI measurement of 96.86%.

By both Gimenez staining and immunofluorescence, the morphology and cellular localization of *R. finnyi* sp. nov. (2024-CO-Wats) revealed characteristics consistent with pathogenic SFGR, including high quantities of bacillary-shaped intracellular bacteria and evidence of cell-to-cell expansion. In epithelial cells, *R. finnyi* sp. nov. (2024-CO-Wats) concentrated at the cytoplasmic membrane, likely representing direct transfer to neighboring cells, a well-documented mechanism used by SFGR for intracellular expansion

Figure 3. Microscopic images from study of isolation and characterization of *Rickettsia finnyi*, novel pathogenic spotted fever group *Rickettsia* in dogs, United States. Images depict *R. finnyi* sp. nov. strain 2024-CO-Wats–infected 030D canine mononuclear cells (A–C), DH82 canine histiocytic cells (D–F), and Vero E6 primate epithelial cells (G–I) detected by immunofluorescence using *R. finnyi* sp. nov.–seroreactive canine serum (dog 2, May 15 date from Table 2). Scale bar indicates 20 μm. SFGR nonreactive canine serum was used as a negative control. Green represents 2024-CO-Wats organisms. Blue represents nuclei of individual mammalian host cells (DAPI). SFGR, spotted fever group *Rickettsia*.
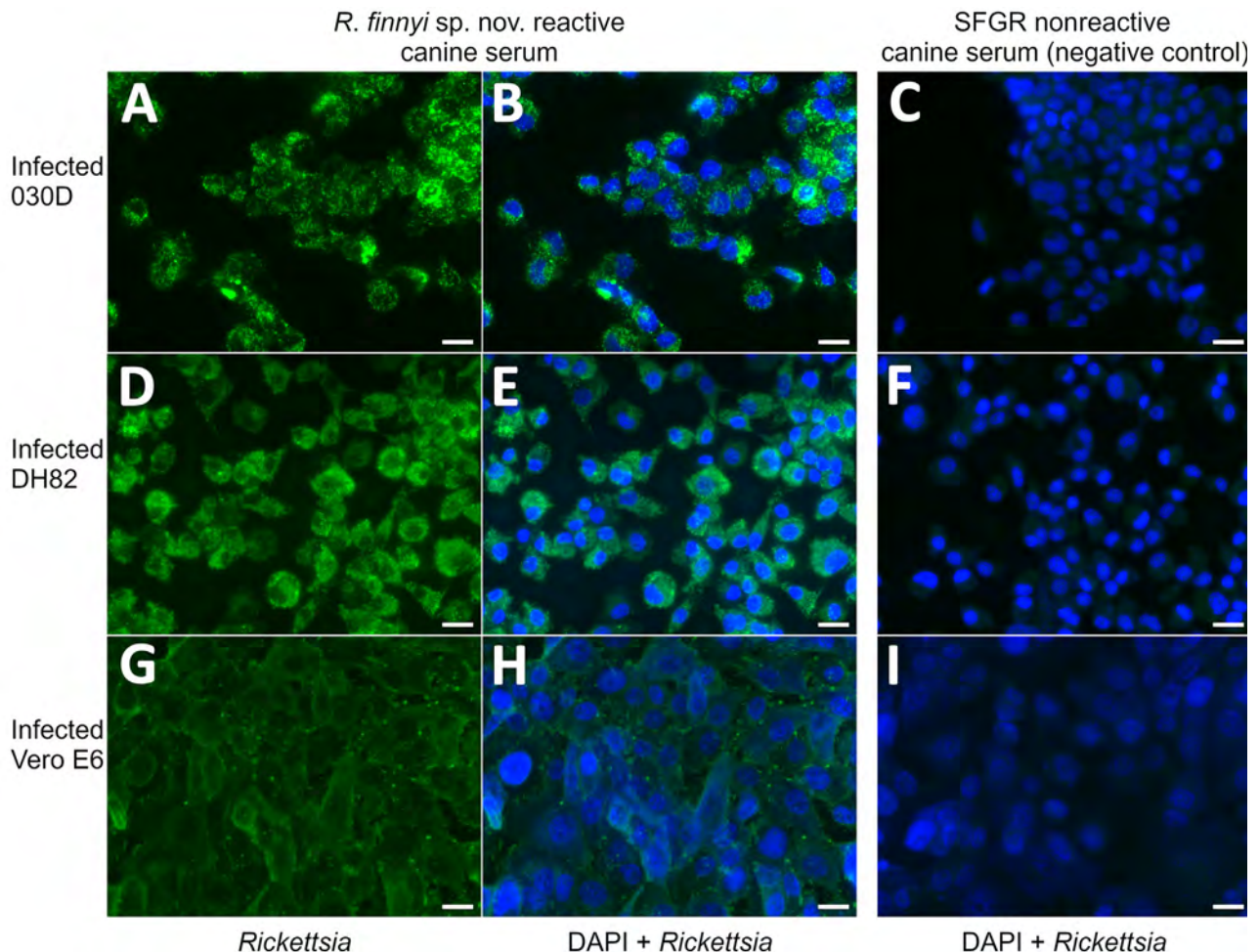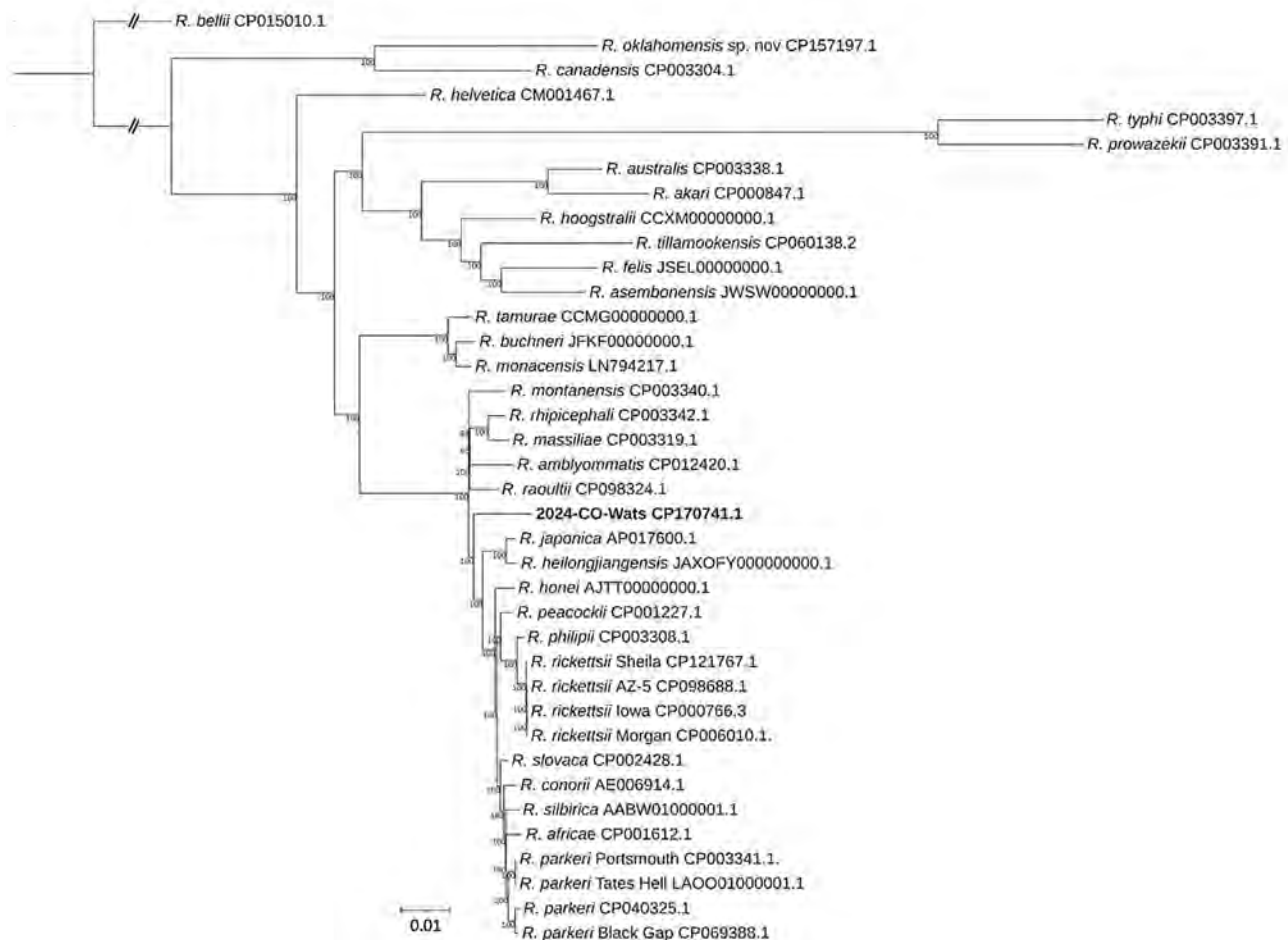
Figure 4. Phylogenetic tree from study of isolation and characterization of *Rickettsia finnyi*, novel pathogenic spotted fever group *Rickettsia* in dogs, United States. Tree depicts 38 *Rickettsia* spp., including *R. finnyi* sp. nov. strain 2024-CO-Wats (bold), which has its own distinct branch within the spotted fever group *Rickettsia*. A total of 636 orthologous core genes present in all genomes were aligned at the nucleotide level with MAFFT version 7.526 (*30*) and concatenated into a matrix. Maximum-likelihood phylogenetic inference was performed with RAxML-NG version 1.2.1 (*31*) under a general time-reversible plus FC plus gamma 4m plus B model with per-partition parameter estimation. Bootstrap support (500 replicates) was mapped onto the best maximum-likelihood tree, which was rooted with *R. bellii.*

(*33*). In contrast, the cytoplasmic localization observed in mononuclear cells is typical of obligate intracellular rickettsiae and provides supporting evidence that *R. finnyi* sp. nov. (2024-CO-Wats) is well adapted to survive in nonendothelial mammalian host cells (*34*).

In this study, we did not assess in vitro pathogenicity or cytopathic effects of *R. finnyi* sp. nov. (2024-CO-Wats); however, we documented growth for >104 days in 2 mononuclear cell lines. Previous studies have reported that pathogenic *Rickettsia* spp. can proliferate in nonendothelial cells, including leukocytes and macrophages, and that they exhibit enhanced intracellular survival in macrophage-like cells; the nonpathogenic *Rickettsia* spp. lacked this ability (*34–38*). *Rickettsia* spp. capable of proliferating in phagocytic cells have likely adapted mechanisms to evade host immunity and replicate before

invading endothelial cells. The prolonged survival of *R. finnyi* sp. nov. (2024-CO-Wats) in mononuclear cells, along with clinical signs observed in naturally infected dogs, provide evidence that it is pathogenic. Additional studies comparing transcription levels and posttranslational modifications of *R. finnyi* sp. nov. in phagocytic versus epithelial cells might help elucidate mechanisms of pathogenicity and cytologic variation.

Since our initial description in 2020 of 3 clinically ill dogs naturally infected with *R. finnyi* sp. nov., an additional 14 infected dogs have been identified. Historical and clinicopathological findings for most of the dogs included a combination of fever, lethargy, and thrombocytopenia, like those seen in *R. rickettsii* infections. Vectorborne co-infections could have contributed to the abnormalities or disease severity in

those dogs. However, the presence of similar abnormalities seen in the other dogs in our study without evidence of co-infections further supports the notion that *R. finnyi* sp. nov. is pathogenic in dogs.

Several *Rickettsia* spp., including *R. parkeri* and *R. rickettsii*, have been documented in both dogs and humans (*6,8,39*). Dogs serve as sentinels for human rickettsiosis, particularly RMSF, because they share similar clinical signs and exposure to the same ticks that transmit *R. rickettsii* (*6,39,40*). Antibodies to *R. finnyi* sp. nov. cross-react with *R. rickettsii* in IFA, as with most SFGR, making it challenging to accurately diagnose RMSF or other spotted fever rickettsiosises in dogs and humans. Furthermore, diagnostic PCRs specific to *R. rickettsii* might not detect novel *Rickettsia* spp. For example, *Rickettsia* sp. CA6269, which represents a novel *Rickettsia* sp. or subspecies of *R. rickettsii*, was detected in humans using broad-based *Rickettsia* qPCR screening after negative *R. rickettsii* and *R. typhi* sp-sp qPCR results (*41*). Studies are needed to determine whether *R. finnyi* sp. nov. can also infect and cause disease in humans.

R. finnyi sp. nov. (2024-CO-Wats) is likely transmitted by the lone star tick, *Amblyomma americanum*. Indeed, Noden et al. (*42*) reported amplified DNA sequences that were 100% identical with *Rickettsia* sp. 2019-CO-FNY in an *A. americanum* tick collected in 2018 in Oklahoma. Supporting possible exposure to *A. americanum* ticks, 1 *R. finnyi* sp. nov.–infected dog was co-infected with *Babesia* sp. coco, a protozoan pathogen detected in *A. americanum* ticks (*43,44*). Moreover, the geographic range of *A. americanum* ticks overlaps with areas in the United States where most infected dogs have been identified to date. Given the zoonotic potential of many *Rickettsia* spp., identifying the vectors and reservoir hosts of *R. finnyi* sp. nov. is essential toward understanding its transmission dynamics and potential public health impacts.

In conclusion, *Rickettsia finnyi* sp. nov. (fin'ny.i. N.L. gen. n. *finnyi*, named after Finny, the first infected dog, in recognition of companion dogs that have contributed to the discovery of novel pathogens) is proposed as a novel spotted fever group *Rickettsia*. Cells are small ($\leq$0.5 µm by 2 µm), rod-shaped intracytoplasmic bacteria that stain red using the Gimenez technique and grow in epithelial (Vero E6) and mononuclear (DH82 and 030D) cell lines. The circular genome is 1.27 Mb. This species has been identified in *A. americanum* ticks from Oklahoma and in dogs from the central and southeastern United States, where infection was associated with moderate to severe illness. The type strain is 2024-CO-Wats, isolated from a naturally infected dog in Tippecanoe County,

Indiana, in 2024. Cultures have been deposited in 2 curated rickettsial banks: the Centers for Disease Control and Prevention Rickettsial Isolate Reference Collection (WDCM 1093; accession no. RFI001), Atlanta, Georgia, USA; and the Collection de Souches de l'Unité des Rickettsies (WDCM 875; accession no. R5053), Marseille, France.

About the Author

Dr. Korla is a research associate at the North Carolina State College of Veterinary Medicine. His research interests include genome assembly and annotation, multi-omics data analysis and molecular modeling, and drug design. Mr. Karounos is a research specialist in the Department of Clinical Sciences at North Carolina State College of Veterinary Medicine. His research interests include acarology and bioinformatics.

References:

1. Wilson JM, Breitschwerdt EB, Juhasz NB, Marr HS, de Brito Galvão JF, Pratt CL, et al. Novel *Rickettsia* species infecting dogs, United States. Emerg Infect Dis. 2020;26:3011–5. https://doi.org/10.3201/eid2612.200272

2. Yancey CB, Hegarty BC, Qurollo BA, Levy MG, Birkenheuer AJ, Weber DJ, et al. Regional seroreactivity and vector-borne disease co-exposures in dogs in the United States from 2004–2010: utility of canine surveillance. Vector Borne Zoonotic Dis. 2014;14:724–32.

3. Centers for Disease Control and Prevention. Data and statistics on spotted fever rickettsiosis [cited 2025 Mar 25]. https://www.cdc.gov/rocky-mountain-spotted-fever/data-research/facts-stats/index.html

4. Paddock CD, Karpathy SE, Henry A, et al. *Rickettsia rickettsii* subsp. *californica* subsp. nov., the etiologic agent of Pacific Coast tick fever. J Infect Dis. 2025;231:849–58.

5. Rodino KG. Rickettsioses in the United States. Clin Microbiol Newsl. 2019;41:113–9. https://doi.org/10.1016/j.clinmicnews.2019.06.002

6. Nicholson WL, Allen KE, McQuiston JH, Breitschwerdt EB, Little SE. The increasing recognition of rickettsial pathogens in dogs and people. Trends Parasitol. 2010;26:205–12. https://doi.org/10.1016/j.pt.2010.01.007

7. Barrett A, Little SE, Shaw E. "Rickettsia amblyommii" and *R. montanensis* infection in dogs following natural exposure to ticks. Vector Borne Zoonotic Dis. 2014;14:20–5.

8. Grasperge BJ, Wolfson W, Macaluso KR. *Rickettsia parkeri* infection in domestic dogs, Southern Louisiana, USA, 2011. Emerg Infect Dis. 2012;18:995–7. https://doi.org/10.3201/eid1806.120165

9. Levin ML, Killmaster LF, Zemtsova GE, Ritter JM, Langham G. Clinical presentation, convalescence, and relapse of Rocky Mountain spotted fever in dogs experimentally infected via tick bite. PLoS One. 2014; 9:e115105. https://doi.org/10.1371/journal.pone.0115105

10. Gasser AM, Birkenheuer AJ, Breitschwerdt EB. Canine Rocky Mountain spotted fever: a retrospective study of 30 cases. J Am Anim Hosp Assoc. 2001;37:41–8. https://doi.org/10.5326/15473317-37-1-41

11. Cerreta AJ, Yang TS, Ramsay EC, Birkenheuer AJ, Rahoi D, Qurollo B, et al. Detection of vector-borne infections in lions and tigers at two zoos in Tennessee and Oklahoma. J Zoo Wildl Med. 2022;53:50–9. https://doi.org/10.1638/2020-0199

12. Ernst E, Qurollo B, Olech C, Breitschwerdt EB. *Bartonella rochalimae*, a newly recognized pathogen in dogs. J Vet Intern Med. 2020;34:1447–53. https://doi.org/10.1111/jvim.15793

13. Maggi RG, Birkenheuer AJ, Hegarty BC, Bradley JM, Levy MG, Breitschwerdt EB. Comparison of serological and molecular panels for diagnosis of vector-borne diseases in dogs. Parasit Vectors. 2014;7:127. https://doi.org/10.1186/1756-3305-7-127

14. Hegarty BC, Qurollo BA, Thomas B, Park K, Chandrashekar R, Beall MJ, et al. Serological and molecular analysis of feline vector-borne anaplasmosis and ehrlichiosis using species-specific peptides and PCR. Parasit Vectors. 2015;8:320. https://doi.org/10.1186/s13071-015-0929-8

15. Qurollo BA, Archer NR, Schreeg ME, Marr HS, Birkenheuer AJ, Haney KN, et al. Improved molecular detection of *Babesia* infections in animals using a novel quantitative real-time PCR diagnostic assay targeting mitochondrial DNA. Parasit Vectors. 2017;10:128. https://doi.org/10.1186/s13071-017-2064-1

16. Beall MJ, Mainville CA, Arguello-Marin A, Clark G, Lemieux C, Saucier J, et al. An improved point-of-care ELISA for the diagnosis of anaplasmosis and ehrlichiosis during the acute phase of tick-borne infections in dogs. Top Companion Anim Med. 2022;51:100735. https://doi.org/10.1016/j.tcam.2022.100735

17. Birkenheuer AJ, Levy MG, Breitschwerdt EB. Development and evaluation of a seminested PCR for detection and differentiation of *Babesia gibsoni* (Asian genotype) and *B. canis* DNA in canine blood samples. J Clin Microbiol. 2003;41:4172–7. https://doi.org/10.1128/JCM.41.9.4172-4177.2003

18. Condit ME, Jones E, Biggerstaff BJ, Kato CY. Procedure for spotted fever group *Rickettsia* isolation from limited clinical blood specimens. PLoS Negl Trop Dis. 2022;16:e0010781. https://doi.org/10.1371/journal.pntd.0010781

19. Ammerman NC, Beier-Sexton M, Azad AF. Laboratory maintenance of *Rickettsia rickettsii*. Curr Protoc Microbiol. 2008;Chapter 3:Unit 3A.5.

20. De Coster W, Rademakers R. NanoPack2: population-scale evaluation of long-read sequencing data. Bioinformatics. 2023;39:btad311. https://doi.org/10.1093/bioinformatics/btad311

21. Li H. Minimap2: pairwise alignment for nucleotide sequences. Bioinformatics. 2018;34:3094–100. https://doi.org/10.1093/bioinformatics/bty191

22. Danecek P, Bonfield JK, Liddle J, Marshall J, Ohan V, Pollard MO, et al. Twelve years of SAMtools and BCFtools. Gigascience. 2021;10:giab008. https://doi.org/10.1093/gigascience/giab008

23. Kolmogorov M, Yuan J, Lin Y, Pevzner PA. Assembly of long, error-prone reads using repeat graphs. Nat Biotechnol. 2019;37:540–6. https://doi.org/10.1038/s41587-019-0072-8

24. Mikheenko A, Saveliev V, Hirsch P, Gurevich A. WebQUAST: online evaluation of genome assemblies. Nucleic Acids Res. 2023;51(W1):W601–6. https://doi.org/10.1093/nar/gkad406

25. Aytan-Aktug D, Grigorjev V, Szarvas J, Clausen PTLC, Munk P, Nguyen M, et al. SourceFinder: a machine-learning-based tool for identification of chromosomal, plasmid, and bacteriophage sequences from assemblies. Microbiol Spectr. 2022;10:e0264122. https://doi.org/10.1128/spectrum.02641-22

26. Meier-Kolthoff JP, Carbasse JS, Peinado-Olarte RL, Göker M. TYGS and LPSN: a database tandem for fast and reliable genome-based classification and nomenclature of prokaryotes. Nucleic Acids Res. 2022;50(D1):D801–7. https://doi.org/10.1093/nar/gkab902

27. Lee I, Ouk Kim Y, Park S-C, Chun J. OrthoANI: an improved algorithm and software for calculating average nucleotide identity. Int J Syst Evol Microbiol. 2016;66:1100–3. https://doi.org/10.1099/ijsem.0.000760

28. Seemann T. Prokka: rapid prokaryotic genome annotation. Bioinformatics. 2014;30:2068–9. https://doi.org/10.1093/bioinformatics/btu153

29. Klemm P, Stadler PF, Lechner M. Proteinortho6: pseudo-reciprocal best alignment heuristic for graph-based detection of (co-)orthologs. Front Bioinform. 2023;3:1322477. https://doi.org/10.3389/fbinf.2023.1322477

30. Katoh K, Standley DM. MAFFT multiple sequence alignment software version 7: improvements in performance and usability. Mol Biol Evol. 2013;30:772–80. https://doi.org/10.1093/molbev/mst010

31. Kozlov AM, Darriba D, Flouri T, Morel B, Stamatakis A. RAxML-NG: a fast, scalable and user-friendly tool for maximum likelihood phylogenetic inference. Bioinformatics. 2019;35:4453–5. https://doi.org/10.1093/bioinformatics/btz305

32. Diop A, El Karkouri K, Raoult D, Fournier P-E. Genome sequence-based criteria for demarcation and definition of species in the genus *Rickettsia*. Int J Syst Evol Microbiol. 2020;70:1738–50. https://doi.org/10.1099/ijsem.0.003963

33. Teysseire N, Boudier JA, Raoult D. *Rickettsia conorii* entry into Vero cells. Infect Immun. 1995;63:366–74. https://doi.org/10.1128/iai.63.1.366-374.1995

34. Curto P, Santa C, Allen P, Manadas B, Simões I, Martinez JJ. A Pathogen and a non-pathogen spotted fever group *Rickettsia* trigger differential proteome signatures in macrophages. Front Cell Infect Microbiol. 2019;9:43. https://doi.org/10.3389/fcimb.2019.00043

35. Kristof MN, Allen PE, Yutzy LD, Thibodaux B, Paddock CD, Martinez JJ. Significant growth by *Rickettsia* species within human macrophage-like cells is a phenotype correlated with the ability to cause disease in mammals. Pathogens. 2021;10:228. https://doi.org/10.3390/pathogens10020228

36. Curto P, Simões I, Riley SP, Martinez JJ. Differences in intracellular fate of two spotted fever group *Rickettsia* in macrophage-like cells. Front Cell Infect Microbiol. 2016;6:80. https://doi.org/10.3389/fcimb.2016.00080

37. Voss OH, Gaytan H, Ullah S, Sadik M, Moin I, Rahman MS, et al. Autophagy facilitates intracellular survival of pathogenic rickettsiae in macrophages via evasion of autophagosomal maturation and reduction of microbicidal pro-inflammatory IL-1 cytokine responses. Microbiol Spectr. 2023;11:e0279123. https://doi.org/10.1128/spectrum.02791-23

38. Påhlson C, Lu X, Ott M, Nilsson K. Characteristics of in vitro infection of human monocytes, by *Rickettsia helvetica*. Microbes Infect. 2021;23:104776. https://doi.org/10.1016/j.micinf.2020.11.003

39. Kidd L, Hegarty B, Sexton D, Breitschwerdt E. Molecular characterization of *Rickettsia rickettsii* infecting dogs and people in North Carolina. Ann N Y Acad Sci. 2006;1078:400–9. https://doi.org/10.1196/annals.1374.079

40. Foley J, Backus L, López-Pérez AM. Focus on brown dog tick–transmitted Rocky Mountain spotted fever in dogs and people: shared threats and solutions [cited 2025 Apr 10]. https://avmajournals.avma.org/view/journals/javma/263/3/javma.24.11.0756.xml

41. Probert WS, Haw MP, Nichol AC, Glaser CA, Park SY, Campbell LE, et al. Newly recognized spotted fever group *Rickettsia* as cause of severe Rocky Mountain spotted fever-like illness, northern California, USA. Emerg Infect Dis. 2024;30:1344–51. https://doi.org/10.3201/eid3007.231771

42. Noden BH, Henriquez BE, Roselli MA, Loss SR. Use of an exclusion assay to detect novel rickettsiae in field collected *Amblyomma americanum*. Ticks Tick Borne Dis. 2022;13:101959. https://doi.org/10.1016/j.ttbdis.2022.101959

43. Bhosale CR, Wilson KN, Ledger KJ, White ZS, Dorleans R, De Jesus CE, et al. Ticks and tick-borne pathogens in recreational greenspaces in north central Florida, USA. Microorganisms. 2023;11:756. https://doi.org/10.3390/microorganisms11030756

44. Noden BH, Roselli MA, Loss SR. Effect of urbanization on presence, abundance, and coinfection of bacteria and protozoa in ticks in the US Great Plains. J Med Entomol. 2022;59:957–68. https://doi.org/10.1093/jme/tjab228

Address for correspondence: Barbara A. Qurollo, North Carolina State University, College of Veterinary Medicine, Department of Clinical Sciences, Research Bldg, Office 464, 1060 William Moore Dr, Raleigh, NC 27606, USA; email: baquroll@ncsu.edu

EID Podcast
Telework during Epidemic Respiratory Illness

The COVID-19 pandemic has caused us to reevaluate what "work" should look like. Across the world, people have converted closets to offices, kitchen tables to desks, and curtains to videoconference backgrounds. Many employees cannot help but wonder if these changes will become a new normal.

During outbreaks of influenza, coronaviruses, and other respiratory diseases, telework is a tool to promote social distancing and prevent the spread of disease. As more people telework than ever before, employers are considering the ramifications of remote work on employees' use of sick days, paid leave, and attendance.

In this EID podcast, Dr. Faruque Ahmed, an epidemiologist at CDC, discusses the economic impact of telework.

Visit our website to listen:
https://go.usa.gov/xfcmN

EMERGING INFECTIOUS DISEASES®

Monkeypox Virus Partial-Genome Amplicon Sequencing for Improvement of Genomic Surveillance during Mpox Outbreaks

Jiusheng Deng, Daisy McGrath, Kimberly Wilkins, Luis A. Haddock, Whitni Davidson,
Demi B. Rabeneck, Joseph Madden, Vaughn Wicker, Adrienne Amuri-Aziza,
Tony Wawina-Bokalanga, Placide Mbala-Kingebeni, Christina L. Hutson, Yu Li, Crystal Gigante

Mpox is a reemerging infectious disease caused by monkeypox virus (MPXV). Whole-genome sequencing provides comprehensive surveillance of MPXV but is challenging in resource-limited outbreak settings and on clinical samples with low viral load. We developed a low-cost, high-throughput partial-genome sequencing strategy and a freeware Nextflow pipeline for MPXV genomic surveillance. We targeted 2 genomic regions of MPXV by using short overlapping amplicons. This amplicon-based approach generated high-quality sequences over the 2 genomic regions from clinical specimens, including samples with low viral DNA and from formalin-fixed tissues. This partial-genome sequencing approach can determine MPXV subclades and offers an attractive strategy to lower cost and improve MPXV surveillance during outbreaks in mpox-endemic and -nonendemic countries.

Mpox is a reemerging infectious disease caused by monkeypox virus (MPXV) (1), a member of the genus *Orthopoxvirus* (2). MPXV has 2 distinct clades, clade I and clade II; each clade is further divided into 2 subclades (Ia and Ib, IIa and IIb) on the basis of genetic differences (3,4). Subclades can be further divided into multiple lineages (https://nextstrain.org/mpox/all-clades), such as lineages A.1, A.2, A.3, and B.1 inside clade IIb (4,5).

Mpox has become a new global challenge since the 2022 clade IIb outbreak that led to >100,000 cases across 115 nonendemic countries (6,7). In addition, the Democratic Republic of the Congo (DRC) and other countries in Africa have reported multiple escalating outbreaks of clade I MPXV over the past several years, including the first clade Ib mpox outbreak (8,9). The newly identified MPXV subclade Ib has spread within DRC and to neighboring countries (10,11), and travel-associated exportation has resulted in cases in multiple countries, including in Europe, Asia, and the Americas, through human-to-human close-contact transmission (12). Continued cases of clade IIb mpox outside of Africa and ongoing escalation of clade I mpox cases highlight the urgency for the international health community to monitor the disease and to strengthen surveillance of MPXV (7,13,14).

Advanced molecular techniques such as quantitative PCR (qPCR) and whole-genome sequencing (WGS) provide effective approaches for the surveillance of MPXV (15,16). The MPXV genome has a central conserved core region and 2 variable terminal regions with inverted terminal repeats at both ends (17). The 2 variable terminal ends contain clade- and subclade-specific genes, multicopy genes, and low-complexity repeat sequences (18), whereas the central core region of each clade has highly conserved genomic sequences encoding essential genes. Orthopoxvirus or MPXV generic qPCRs that target the conserved core region of the genome can rapidly and precisely detect MPXV DNA in samples (19); however, those methods might be unable to differentiate

Author affiliations: Chenega Enterprise Systems and Solutions, LLC, Chesapeake, Virginia, USA (J. Deng); Centers for Disease Control and Prevention, Atlanta, Georgia, USA (J. Deng, D. McGrath, K. Wilkins, L.A. Haddock, W. Davidson, D.B. Rabeneck, J. Madden, V. Wicker, C.L. Hutson, Y. Li, C. Gigante); University of Kinshasa, Kinshasa, Democratic Republic of the Congo (A. Amuri-Aziza, T. Wawina-Bokalanga, P. Mbala-Kingebeni)

clades or subclades of MPXV (*20*). The less-conserved genomic regions that might be targeted by clade- or subclade-specific PCR are more prone to generic drift and deletion mutations that have occurred in poxviruses (*21*).

WGS has been broadly used to generate consensus genomes and analyze MPXV genomic variation (*6,22*), becoming a critical tool for comprehensive surveillance to track circulating and emerging variants, drug resistance, and molecular evolution and to understand the transmission of MPXV (*7,23*). However, WGS requires expensive instruments and reagents, as well as samples with high viral load, limiting its use in resource-limited outbreak settings. The ≈200-kb double-stranded DNA genome of MPXV (*24*) introduces challenges for designing and optimizing efficient tiled primers for WGS of all 4 subclades. The conserved core region provides an optimal target for a pool of specific primers for partial-genome sequencing (PGS) of all subclades of MPXV.

In this study, we developed an amplicon-based PGS strategy by targeting 2 genomic regions in the central conserved core region of the MPXV genome (a 10-kb region and a 15-kb region) by using a portable MiniON sequencing device with low-cost Flongle flow cells from Oxford Nanopore Technologies (ONT) (https://nanoporetech.com). We evaluated the specificity of the PGS data to determine MPXV subclades in clinical specimens and the ability to sequence poor-quality specimens to improve the sensitivity of MPXV genomic surveillance.

Materials and Methods

Mpox Clinical Specimens

Mpox specimens used in this study included remainders of samples submitted to the Centers for Disease Control and Prevention (CDC) Poxvirus Laboratory (Poxvirus and Rabies Branch, Division of High-Consequence Pathogens and Pathology, National Center for Emerging and Zoonotic Infectious Diseases) for routine testing. CDC reviewed viral sequencing of the samples for genomic surveillance and deemed the study as nonresearch public health surveillance. No specimen collection was performed for this study. We subjected specimens from lesion swab or crust samples of patients to DNA extraction with an EZ1 & 2 DNA tissue kit on an EZ1 Advanced XL Instrument (QIAGEN, https://www.qiagen.com). We quantified DNA concentration on a Qubit 3 Fluorometer with a dsDNA high-sensitivity assay kit (Invitrogen, https://www.thermofisher.com).

qPCR

We performed qPCR on the DNA samples by using an Applied Biosystems 7500 Fast Dx PCR instrument with a TaqMan fast advanced master mix (Thermo Fisher Scientific, https://www.thermofisher.com) as previously described (*25*). We conducted reactions in 20-µL volumes. PCR profile was 95°C for 20 seconds, (95°C for 3 seconds, and 63°C for 30 seconds) for 40 cycles. We recorded cycle threshold (Ct) values of MPXV DNA samples.

MPXV Amplicon-based PGS

We designed 2 pools of overlapping primers for the 10-kb region (nucleotide position 29,632 to 40,271) (Appendix Table 1, https://wwwnc.cdc.gov/EID/article/31/11/25-0548-App1.pdf) and the 15-kb region (nucleotide position 72,243 to 86,891) (Appendix Table 2) amplicons against the respective genomic region of an MPXV reference sequence (GenBank accession no. ON563414.3) by using PrimalScheme (https://primalscheme.com). We produced amplicons by using multiplex PCR with either primer pool 1 or pool 2 (10 µM). PCR profile was 98°C for 1 minute, 98°C for 20 seconds, 60°C for 30 seconds, and 72°C for 1 minute for 24 cycles (for specimens with Ct ≤30) or 35 cycles (Ct >30) at 72°C for 2 minutes and a 4°C hold. PCR volume was 25 µL/reaction, including 12.5 µL Q5 High-Fidelity 2X Master Mix (New England Biolabs, https://www.neb.com), 2 µL primer pool, 5 µL DNA, and 5.5 µL PCR-grade H$_2$O. We verified amplicons on a 2% agarose gel by using a Gel Doc CR+ Molecular Imager (Bio-Rad Laboratories, https://www.bio-rad.com). We pooled amplicons for the 10-kb and the 15-kb regions for the same specimen together and purified them with AMPure XP beads (Beckman Coulter, https://www.beckman.com) at a volume ratio of 1:1, followed by end repairing, barcoding, and adaptor ligation with an ONT native barcoding 96 V14 kit (SQK-NBD114.96) according to the manufacturer's protocol. We loaded DNA libraries into Flongle FLO-FLG114 flow cells and performed amplicon sequencing, base calling, and demultiplexing on an MK1C Instrument (Oxford Nanopore).

Illumina DNA Library Sequencing

We prepared MPXV DNA libraries with an Illumina DNA prep kit and a Nextera DNA Unique Dual Indexes (Illumina, https://www.illumina.com) as described previously (*26*). We measured the concentrations of DNA libraries on the Qubit 3 Fluorometer. We determined the average sizes of libraries on a TapeStation 2400 instrument with a high-sensitivity D1000 kit (Agilent Technologies, https://www.agilent.com). We diluted DNA libraries to a concentration of 2 nM.

We loaded 20 µL of the pooled libraries at a final concentration of 750 pM into the NextSeq1000 cartridge for WGS by using a P2 300-cycle kit (Illumina).

Bioinformatic Analyses of PGS and WGS Data

Nanopore Data

We imported raw sequencing data into Geneious Prime 2023.2.1 (https://www.geneious.com). We aligned and mapped reads to clade IIb (GenBank accession no. ON563414.3) or clade I (GenBank accession no. KC257460) reference genomes by using Minimap2 version 2.24 (https://github.com/lh3/minimap2). We generated average sequence coverages and consensus sequences over the 10-kb and 15-kb regions of MPXV genomes per specimen. We manually identified single-nucleotide polymorphisms (SNPs) and insertions or deletions (indels) across the 2 regions in comparison with respective reference sequences. We used consensus sequences for MPXV clade and lineage assignment and phylogenetic analysis by using Nextclade 3.10.0 (https://clades.nextstrain.org).

Illumina Data (Metagenomic)

We processed raw data derived from Illumina sequencing through a custom-built workflow in the CLC Genomic Workbench 24.0 (QIAGEN). We extracted the mapped reads over the 10-kb and 15-kb genomic regions from the respective whole genomes. We compared sequence read depth and coverages over the 2 genomic regions derived from WGS with those from PGS.

Nextflow Pipeline

We built a new Nextflow pipeline specific for standardizing analysis of the 10-kb and 15-kb amplicon sequences under the Nextflow Workflow Manager (version 24.04.2) with Docker and Singularity as software containers (https://github.com/CDCgov/ONT-Seq-analysis) (Appendix Figure 1). In brief, we used SEQTK version 1.4-r122 (https://github.com/lh3/seqtk) to remove adapters and low-quality calls from base called reads. We trimmed reads with Trimmomatic version 0.39 (https://github.com/usadellab/trimmomatic) and mapped them to a reference sequence (GenBank accession no. NC_063383.1) by using Minimap2 version 2.28-r1209. We refined consensus sequences generated with Ivar consensus version 1.4.3 by using ONT's MEDAKA tool version 1.4.4. We assigned clades by using Nextclade module version 3.8.2 with additional mutation calls, phylogenetic placements, and quality checks specific for MPXV. We included custom scripts in the project repository to parse Nextclade output files, assign MPXV subclades, and summarize the resulting report into a more accessible format.

Results

Improved Sequence Read Depths and Coverages Using Amplicon-Based PGS Compared with WGS

We used 2 overlapping primer pools to generate amplicons over the 10-kb or the 15-kb regions (Figure 1, panel A). Amplicon size ranged from 310 bp to 489 bp, with an average of 393 bp (Appendix Tables 1, 2). To evaluate the performance of the amplicon-based PGS approach on MPXV clinical specimens, we measured read depths and sequence coverages over the 2 genomic regions of MPXV after performing 10-kb and 15-kb PGS on MPXV DNA isolated from 36 clinical specimens (20 clade IIb, 10 clade Ia, and 6 clade Ib) with Ct <30 (Table 1). More than 93% reads produced from each specimen corresponded to MPXV (Appendix Table 3). Bioinformatic analysis demonstrated that the 10-kb and 15-kb PGS generated high-sequence
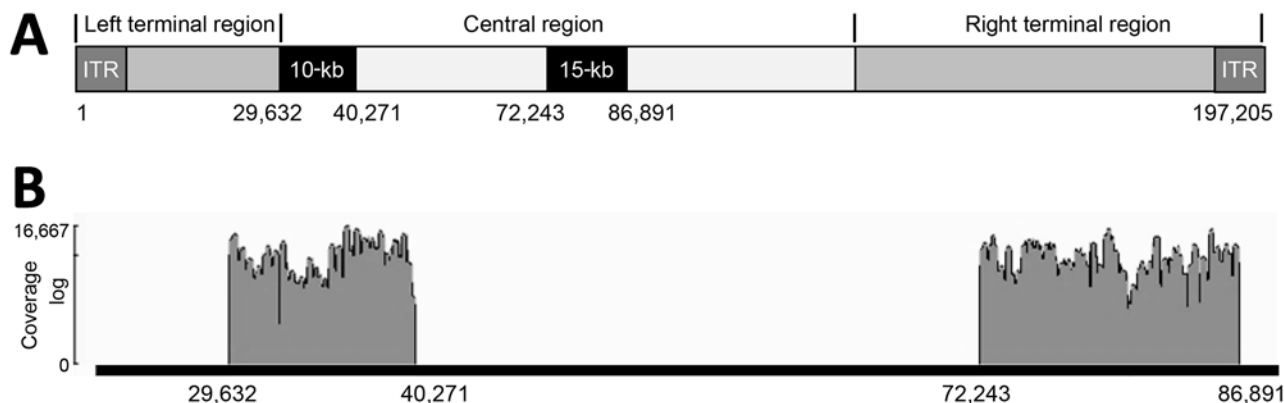

Figure 1. Locations and coverage of 10-kb and 15-kb amplicons of monkeypox virus for study of partial-genome amplicon sequencing for improvement of genomic surveillance during mpox outbreaks. A) Genomic positions of the 2 regions. B) Representative of sequence coverage over the 10-kb and 15-kb amplicons of monkeypox virus in clinical specimens. ITR, internal terminal repeat.

Table 1. Characteristics of MPXV specimens with Ct <30 and amplicon sequencing read depths over the 10-kb and 15-kb genomic region of MPXV for study of partial-genome amplicon sequencing for improvement of genomic surveillance during mpox outbreaks*

Specimen no.	Source/sample type	Country/year	DNA concentration, ng/μL	Ct	10-kb	15-kb
1	Back/lesion	USA/2024	4.7	19.8	1,279	554
2	Swab drag	USA/2024	5.6	22.7	840	408
3	Chest lesion	USA/2024	1.2	21.0	3,800	465
4	Lesion	USA/2024	4.3	22.6	1,455	324
5	Back/lesion	USA/2024	1.0	21.1	3,046	449
6	Leg/skin swab	USA/2024	8.4	20.1	1,625	328
7	Skin swab	USA/2024	1.0	22.0	1,417	487
8	Eye/swab drag	USA/2024	4.0	21.2	1,019	345
9	Penis/swab	USA/2024	10.7	19.2	1,097	464
10	Penis/skin swab	USA/2024	1.4	21.7	1,750	584
11	Penis/skin swab	USA/2024	9.3	19.9	2,760	479
12	Chest/skin swab	USA/2024	9.1	21.9	950	116
13	Back/skin swab	USA/2024	4.6	19.6	2,365	557
14	Hand/skin swab	USA/2024	22.0	20.5	1,870	461
15	Perianal/swab	USA/2024	2.9	21.3	1,259	432
16	Penis/skin swab	USA/2024	2.1	19.6	2,363	281
17	Perianal/swab	USA/2024	23.0	23.3	2,764	264
18	Penis/skin swab	USA/2024	1.0	20.8	1,673	652
19	Penis/lesion	USA/2024	10.9	21.5	932	241
20	Lesion	USA/2024	2.5	23.8	3,095	272
21	Crusts	DRC/2017	2.3	16.0	3,612	329
22	Vesicles	DRC/2017	1.9	16.0	1,819	1,231
23	Vesicles	DRC/2016	8.1	15.2	1,361	1,653
24	Vesicles	DRC/2017	16.0	16.7	1,421	1,607
25	Vesicles	DRC/2017	9.1	15.6	1,778	2,169
26	Crusts	DRC/2016	89.0	13.0	142	1,469
27	Vesicles	DRC/2017	62.0	18.0	797	1,056
28	Vesicles	DRC/2017	30.0	17.0	212	670
29	Vesicles	DRC/2017	28.0	22.3	1,180	762
30	Vesicles	DRC/2016	20.0	20.7	783	698
31	Swab	DRC/2024	0.8	22.6	2,022	1,520
32	Swab	DRC/2024	0.2	25.2	2,300	1,835
33	Swab	DRC/2024	6.0	17.7	1,856	1,339
34	Swab	DRC/2024	9.0	17.8	1,147	895
35	Swab	DRC/2024	0.2	25.1	1,907	1,532
36	Swab	DRC/2024	4.9	19.0	1,718	1,254

*Total DNA was extracted from MPXV specimens (n = 36) from different body sources of patients in USA in 2024 (nos. 1–20) or in DRC during 2016–2024 (nos. 21–36). DNA concentrations (ng/μL), MPXV Ct values, and read depths over the 2 genomic regions of MPXV genomes (10-kb and 15-kb) derived from amplicon sequencing on DNA samples included. Ct, cycle threshold; DRC, Democratic Republic of the Congo; MPXV, monkeypox virus; USA, United States.

read depths (Table 1) over the 2 regions of MPXV genomes (Figure 1, panel B), with an average read depth of 1,706 over the 10-kb region and 783 over the 15-kb region (Table 1). We observed complete target region coverage for all specimens (Appendix Table 3).

To test whether the 10-kb and 15-kb PGS could still give high read depth and sequence coverage over the 2 genomic regions in specimens containing low viral DNA, we performed PGS on 8 MPXV samples: 4 clade IIb samples with Ct >30 and 4 clade Ia samples diluted with DNase-free water at a ratio of 1:1,000 or 1:10,000 to produce Ct >30 as determined by qPCR (Table 2). The amplicon-based PGS yielded high-sequence read depth across the 2 genomic regions, having an average read depth of 521 over the 10-kb region and 436 over the 15-kb region (Table 2) and >95% sequence coverage for all specimens (Appendix Table 3), even though DNA was undetectable in some specimens (Table 2).

In contrast, metagenomic WGS on the same specimens produced low read depth over the 2 regions, having a maximum average read depth of 5.4 for either of the 2 regions and 12 for the whole MPXV genome (Table 2). Analysis of Ct value and coverage predicted complete target region coverage when MPXV Ct values were <31 (Appendix Table 3, Appendix Figure 2).

Next, we performed the 10-kb and 15-kb PGS on DNA isolated from formalin-fixed paraffin-embedded mpox clinical specimens, which are also challenging for WGS because of the fragmentation and cross-linking of DNA (27). Sequence analysis demonstrated that amplicon sequencing generated an average read depth of 792 over the 10-kb region and 694 over the 15-kb region for formalin-fixed specimens (nos. 41–45) (Table 3). Read depths were substantially lower with metagenomic WGS, which produced an average read depth of 11.2 over the whole genome (Table 3).

Table 2. Characteristics of MPXV specimens with Ct >30 and sequencing read depths over the 10-kb and 15-kb regions or the whole genome of MPXV for study of partial-genome amplicon sequencing for improvement of genomic surveillance during mpox outbreaks*

Specimen no. (dilution ratio)	Source/sample type	Country/year	DNA concentration, ng/μL	Ct	10-kb	15-kb	Genome
37	Penis/swab	USA/2024	14.30	35.3	587	703	10.0
38	Chin/swab	USA/2024	0.50	34.0	305	326	0.2
39	Swab	USA/2023	0.10	30.7	214	172	12.0
40	Swab	USA/2023	1.00	31.4	157	138	2.0
29 (1:1,000)	Vesicles	DRC/2017	0.02	32.3	950	310	0.4
29 (1:10,000)	Vesicles	DRC/2017	0.00	36.2	1,086	866	0.0
30 (1:1,000)	Vesicles	DRC/2016	0.02	30.0	544	613	0.0
30 (1:10,000)	Vesicles	DRC/2016	0.00	33.4	323	356	0.2

*Total DNA was extracted from MPXV specimens from different body sources of patients in USA during 2023–2024 (nos. 37–40) or in DRC during 2016–2017 (nos. 29–30). The 2 DNA samples from DRC were diluted with PCR-grade water at the ratio of 1:1,000 or 1:10,000. DNA concentrations (ng/μL), MPXV Ct values, and read depths over the 2 genomic regions (10-kb and 15-kb) derived from amplicon sequencing or over the whole genome (genome) of MPXV derived from metagenomic sequencing on DNA samples included. Ct, cycle threshold; DRC, Democratic Republic of the Congo; MPXV, monkeypox virus; USA, United States.

Identification of Genetic Variations in the 10-kb and the 15-kb Regions of MPXV Using Amplicon-Based PGS

Analyses of consensus sequences over the 10-kb and the 15-kb genomic regions (Appendix Table 4) demonstrated that amplicon-based PGS can identify many types of genetic variations in MPXV specimens from clade IIb, Ib, and Ia (Table 4; Appendix Table 5). Compared with reference sequence KC257460, the specimens showed multiple genetic variations, including 107 SNPs (28 unique) and 20 indels (2 unique) identified in 10 clade Ia specimens from DRC and 70 SNPs (13 unique) and 7 deletions (2 unique) detected in 6 clade Ib specimens from DRC (Table 4; Appendix Table 5). We detected 42 SNPs (14 unique) and 2 deletions in 20 clade IIb specimens from the United States (Table 4) compared with reference sequence ON563414.3. The deletions led to predicted amino acid changes in the encoded proteins (Appendix Table 5). Approximately 40% of the SNPs over the 10-kb and the 15-kb regions of MPXV genomes in the clade IIb specimens were GA>AA or TC>TT APOBEC3-like mutations (Table 4). However, most SNPs in the clade Ia or Ib specimens were not APOBEC3-driven mutations (Table 4), as expected when

using this clade Ia reference. The SNPs and indels affected 19 structural or functional genes, including OPG047, OPG048, OPG049, OPG053, OPG054, OPG055, OPG056, and OPG057 in the 10-kb region and OPG092, OPG094, OPG095, OPG097, OPG098, OPG101, OPG102, OPG103, OPG104, OPG105, and OPG0108 in the 15-kb region (Appendix Table 5). Affected genes OPG105 (72 SNPs) and OPG054 (37 SNPs) comprised ≈50% of SNPs over the 2 genomic regions of MPXV from 36 clinical specimens (Figure 2), result that align with previous findings (28). Moreover, the 10-kb amplicon was able to identify a nonsynonymous SNP (C184T) and a deletion (N267del) in OPG057 gene in a specimen (no. 8) (Appendix Table 5), variations that were previously associated with tecovirimat resistance (29).

In silico analysis of the 10-kb and the 15-kb regions from 88 published MPXV genome sequences revealed a pattern of conserved SNPs in different MPXV subclades (Figure 3; Appendix Table 6). Clades I and II could be separated by the 15 unique SNPs, clades Ia and Ib could be divided by the 4 SNPs, and clades IIa and IIb could be distinguished by 11 SNPs (Figure 3). This pattern of conserved SNPs indicated

Table 3. Characteristics of formalin-fixed (nos. 41–45) or inconclusive (nos. 46–48) MPXV specimens from the United States and sequencing read depths over the 10-kb and 15-kb regions or the whole genome of MPXV for study of partial-genome amplicon sequencing for improvement of genomic surveillance during mpox outbreaks*

Specimen no.	Source	Year	DNA concentration, ng/μL	Ct	10-kb	15-kb	Genome
41	Tissue	2022	39.4	17.1	576	347	9.6
42	Tissue	2022	6.3	17.1	981	1,065	0.1
43	Rectum	2023	56.4	17.4	794	977	17.9
44	Lung	2023	3.0	30.4	869	382	0.07
45	Tissue	2024	7.4	17.3	741	698	28.4
46	Swab	2024	0.0	37.1	69	1,391	NA
47	Swab	2024	0.0	37.3	15	691	NA
48	Swab	2024	0.0	37.2	359	1,092	NA
49	Swab	2024	0.0	38.4	25	155	NA

*Total DNA was extracted from formalin-fixed MPXV tissue specimens from different body sources of patients in the United States during 2022–2024 (nos. 41–45) or inconclusive specimens (nos. 46–49) with MPXV Ct >37. DNA concentrations (ng/μL), MPXV Ct values, and read depths over the 2 genomic regions (10-kb and 15-kb) derived from amplicon sequencing or over the whole genome (genome) of MPXV derived from metagenomic sequencing on DNA samples included. Whole-genome sequencing was not performed on 3 inconclusive specimens (nos. 46–48) or failed on specimen no.49; sequencing read depths over the whole genome of MPXV were not available. Ct, cycle threshold; MPXV, monkeypox virus; NA, not available.

Table 4. Genetic variants over the 10-kb and 15-kb genomic regions of MPXV in 36 clinical specimens for study of partial-genome amplicon sequencing for improvement of genomic surveillance during mpox outbreaks*

Specimen no.	Country	sSNP	nsSNP	Total SNPs†	Indels	Variants‡	SNP type§	SNPs
1–20	USA	15	27	42	2	44	GA>AA	17
							Other	25
21–30	DRC	90	17	107	20	127	GA>AA	22
							Other	85
31–36	DRC	60	10	70	7	77	GA>AA	23
							Other	47

*See Table 1. DRC, Democratic Republic of the Congo; indels, insertions and deletions; MPXV, monkeypox virus; nsSNP: nonsynonymous SNP; SNP, single-nucleotide polymorphism; sSNP, synonymous SNP. USA, United States.
†Total number of SNPs include sSNP and nsSNPs.
‡Variants include total number of SNPs plus indels.
§SNP type GA>AA (5′–3′) includes TC>TT (5′–3′).

the potential use of the 10-kb and the 15-kb regions for differentiation of MPXV subclades.

Correct Assignment of MPXV Subclades on the Basis of 10-kb and 15-kb Partial-Genome Sequences

To examine whether the 10-kb and 15-kb PGS could be used to determine MPXV subclades from clinical specimens, we imported the consensus sequences of the 2 genomic regions derived from amplicon-based PGS (Appendix Table 4) into the Nextclade web interface by using the Mpox virus (all clades) reference dataset. Clade assignment showed that MPXV in 29 specimens from the United States belonged to clade IIb lineage B. MPXV in 10 specimens from DRC were assigned to clade Ia; however, the other 6 specimens from DRC were assigned to clade Ib (Figure 4; Appendix Table 7). WGS conformed (with 100% agreement) all subclades and lineage assignments produced by the 10-kb and 15-kb PGS data (Appendix Table 7).

To increase the robustness of this evaluation, we also performed an in silico analysis of the 10-kb and the 15-kb regions extracted from 88 publicly available MPXV complete or near-complete genome sequences, including all subclades, and compared NextClade assignment of the 10-kb and the 15-kb regions to assignment using the whole-genome sequences. The partial-genome sequences were sufficient to produce correct assignments of subclade or lineages for all 88 sequences, including 25 clade Ia, 16 clade Ib, 12 clade IIa, and 35 clade IIb lineages A and B (Appendix Table 8).

To further validate the potential that the 10-kb and the 15-kb amplicons could be used to determine clade, subclade, or lineage information for inconclusive clinical specimens or specimens that had failed WGS, we selected 4 MPXV specimens (nos. 46–49) from the United States that had undetectable total DNA and MPXV Ct >37 (Table 3). For all 4 specimens, consensus sequences over the 10-kb and the 15-kb genomic regions produced from the 10-kb and 15-kb PGS successfully assigned clade IIb lineage B MPXV by Nextclade (Figure 4; Appendix Table 7).

Automated Bioinformatic Analysis of 10-kb and 15-kb PGS Reads Using ONT Sequencing

To build a cost-free bioinformatic workflow, improve reproducibility and accessibility, and enable automatic analyses of the 10-kb and the 15-kb amplicon sequences of MPXV, we developed a Nextflow pipeline (https://github.com/CDCgov/ONT-Seq-analysis) (Appendix Figure 1). The pipeline performed quality control and reference-based assemblies of Oxford Nanopore sequencing reads and generated consensus sequences independent of clade. By using the pipeline, we verified the clade, subclade, and lineage
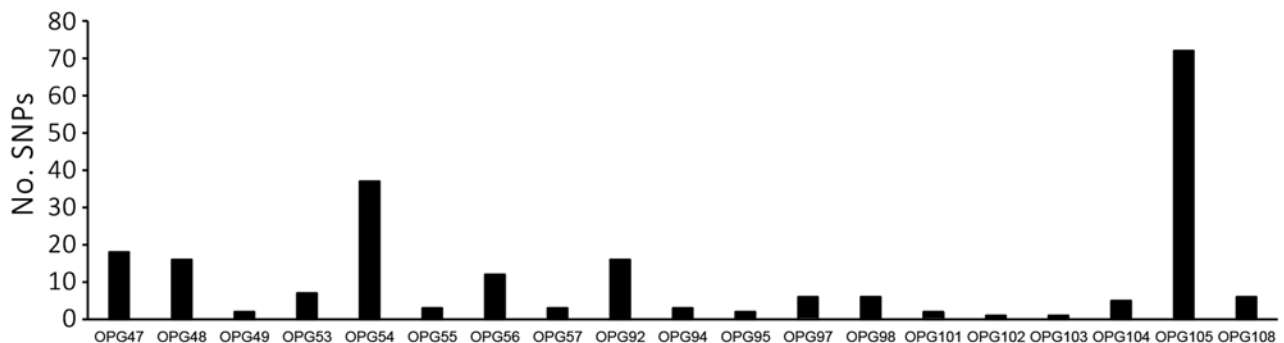

Figure 2. SNPs in the affected genes over the 10-kb and 15-kb genomic regions of monkeypox virus in 36 clinical specimens from United States and Democratic Republic of the Congo for study of partial-genome amplicon sequencing for improvement of genomic surveillance during mpox outbreaks. OPG, orthopoxvirus gene; SNP, single-nucleotide polymorphism.
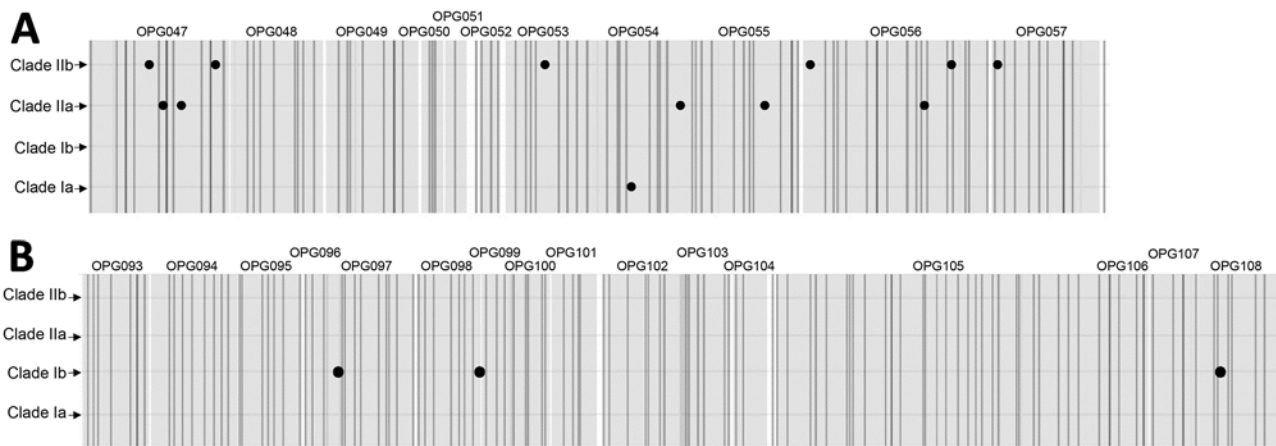
Figure 3. Conserved SNPs over the 10-kb and the 15-kb regions identified in silico among respective clades from 88 published moneypox virus genomes for study of partial-genome amplicon sequencing for improvement of genomic surveillance during mpox outbreaks. A) Unique SNPs over the 10-kb region. B) Unique SNPs over the 15-kb region. Large black points represent SNPs. Vertical shaded bars represent the binding sites of the amplicon primers. OPG, orthopoxvirus gene; SNP, single-nucleotide polymorphism.

assignments of MPXV genomes in the 49 clinical specimens, in addition to sublineage placements of 13 specimens (nos. 8–20) (Appendix Table 9).

Discussion

Genome sequencing is at the front line of MPXV surveillance and outbreak investigation for the smallpox virus–related pathogen of high public health importance (*7*). In this study, we demonstrate that an amplicon-based PGS produces robust sequence data that can determine the clades and subclades of MPXV from clinical specimens. This high-sensitivity and low-cost PGS represents an attractive strategy for high-throughput clade typing and MPXV genomic surveillance in resource-limited settings and for specimens with low viral load.

High-quality sequences are critical for effective MPXV genomic surveillance (*30*). Clinical specimens usually contain higher human DNA background than viral DNA that can degrade under suboptimal transport or storage (*30*). Unbiased metagenomic sequencing approaches generate most non-MPXV reads or low viral-specific reads when specimens have high MPXV Ct values, causing low coverage of the whole
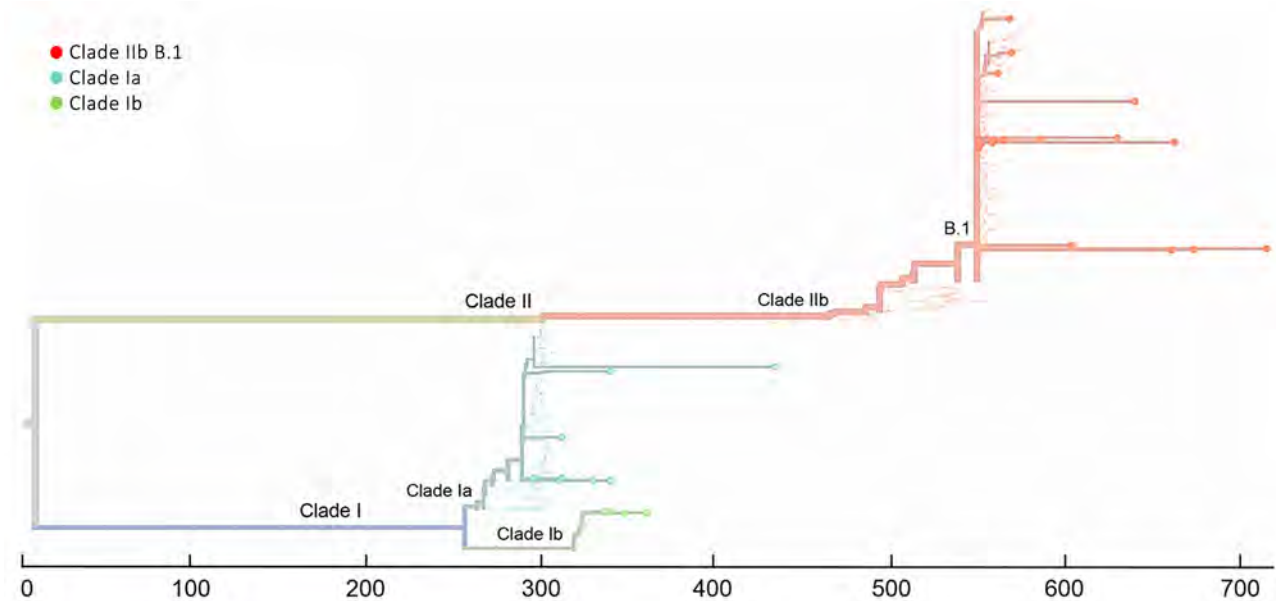

Figure 4. Amplicon-based phylogenetic assignment of monkeypox virus by 10-kb and 15-kb regions in Nextclade 3.10.0 (https://clades.nextstrain.org) for study of partial-genome amplicon sequencing for improvement of genomic surveillance during mpox outbreaks. Sixteen clinical specimens from Democratic Republic of the Congo were assigned to clade Ia or Ib, and 33 clinical specimens from United States were assigned to clade IIb lineage B.1.

MPXV genome, as demonstrated in this study. Several short-tiled (31) and long-tiled (32–34) amplicon-based WGS approaches have been developed to improve the sensitivity of MPXV WGS; however, such approaches also showed low success for samples with Ct >30, limiting potential use for specimens with low viral load. In this study, we conducted PGS by using short-tiled amplicons over the 10-kb and 15-kb regions of MPXV genome to improve PCR efficiency and lower primer dropout across the different clades. The approach selectively amplified the 2 genomic regions and yielded high read depth, even when the Ct values of MPXV specimens were >30.

Affordable MPXV genomic surveillance is critical to rapidly identify introduction of new lineages or emerging outbreaks (35). WGS is high-cost and resource-intensive and can be difficult for mpox-endemic regions or areas experiencing an outbreak to afford because of limited resources, capacity, or expertise. Amplicon-based WGS could be cost saving with ONT flow cells, but the number of specimens per run would be limited. In this study, we designed tiled primers that specifically target all 4 subclades of MPXV. We used the portable ONT MK1C sequencing platform with low-cost Flongle flow cells and native barcoding 96 V14 kit for PGS. One Flongle flow cell costs <$100 US and could be used for sequencing up to 40 specimens. The ONT native barcoding 96 V14 kit could be used for barcoding ≥288 specimens. The 10-kb and 15-kb amplicon-based PGS markedly reduced sequencing cost per specimen compared with WGS approaches. Thus, inexpensive amplicon-based PGS offers an attractive approach to complement WGS for largescale MPXV surveillance.

Bioinformatic resources and reproducibility can pose a barrier for MPXV surveillance. In this study, we described a freeware, open source, and accessible Nextflow pipeline for analyzing sequencing data produced by the 10-kb and 15-kb PGS strategy. The pipeline streamlines the entire process of amplicon sequencing data analysis, substantially reducing the need for manual intervention and the potential introduction of human errors. With detailed documentation and a feasible implementation strategy, our pipeline is suitable for varying levels of bioinformatic expertise. The pipeline's ability to simply differentiate clades and subclades either through the Nextclade output or the SNP panel will be incredibly valuable in outbreak investigations and epidemiologic studies.

Profiling whole-genome genetic variation and phylogenetic evolution is essential for MPXV genomic surveillance. Many types of genetic variations in MPXV genomes have been identified by WGS (23,36–39). In this study, we used amplicon-based PGS on the 10-kb and 15-kb regions of MPXV genomes and detected numerous SNPs and indels in the 2 genomic regions of MPXV from clinical specimens. The large proportion of SNPs in MPXV lineage B genomes from clade IIb were GA>AA, consistent with previous findings based on WGS (23,40,41), suggesting the 10-kb and 15-kb regions might be sufficient to identify changes in APOBEC-motif mutations, an indicator of sustained human-to-human transmission of an MPXV lineage. We also found that the 10-kb and 15-kb regions possess unique conserved SNPs that can distinguish clades Ia, Ib, IIa, and IIb. Our results strongly suggest that the 10-kb and 15-kb PGS approach could produce actionable information for public health MPXV surveillance, in which a subset of samples can be submitted to WGS for more detailed analysis.

The antiviral drug tecovirimat that has been widely used to treat MPXV infections in the United States works by blocking the viral envelope protein F13 and inhibiting viral release from MPXV-infected cells (42,43). However, long-term use of the drug could induce treatment-resistant nucleotide mutations or deletions of the OPG057 gene (29,42,44), resulting in the spread of tecovirimat-resistant MPXV variants (45). WGS and targeted gene sequencing have identified numerous SNPs or indels in OPG057 associated with tecovirimat resistance (29,42,43). In this study, the 10-kb and 15-kb amplicon-based PGS identified tecovirimat-resistant genetic variations in the OPG057 gene that correspond to amino acid A184T mutation and N267 deletion in F13 protein (29) in 1 clade IIb MPXV specimen. This finding indicates that amplicon-based PGS could be useful for monitoring antiviral drug-induced resistance of MPXV. Recent clinical trials have found no substantial benefit for patients treated with tecovirimat (46), which might limit usefulness of genetic monitoring in some situations; however, use in severe cases is still being evaluated.

In summary, our study demonstrated that the 10-kb and 15-kb PGS procedure has the advantages of cost-effectiveness, simplicity of use, and sufficient resolution to provide information needed for public health action, such as clade assignment and identification of drug resistance. Given the outbreaks of clade Ia, Ib, and IIb mpox in the past 3 years, this 10-kb and 15-kb PGS approach offers an attractive strategy to improve overall MPXV surveillance, which can help identify importations or new outbreaks early. Its low cost and high throughput potential is especially poised for use in low-resource and outbreak settings.

Acknowledgments

About the Author

Dr. Deng is a scientist in the Poxvirus and Rabies Branch, Division of High-Consequence Pathogens and Pathology, National Center for Emerging and Zoonotic Infectious Diseases, Centers for Disease Control and Prevention in Atlanta, USA. His research interests include partial- or whole-genome sequencing of monkeypox virus for mpox surveillance.

References

1. Gessain A, Nakoune E, Yazdanpanah Y. Monkeypox. N Engl J Med. 2022;387:1783–93. https://doi.org/10.1056/NEJMra2208860
2. Karagoz A, Tombuloglu H, Alsaeed M, Tombuloglu G, AlRubaish AA, Mahmoud A, et al. Monkeypox (mpox) virus: classification, origin, transmission, genome organization, antiviral drugs, and molecular diagnosis. J Infect Public Health. 2023;16:531–41. https://doi.org/10.1016/j.jiph.2023.02.003
3. Likos AM, Sammons SA, Olson VA, Frace AM, Li Y, Olsen-Rasmussen M, et al. A tale of two clades: monkeypox viruses. J Gen Virol. 2005;86:2661–72. https://doi.org/10.1099/vir.0.81215-0
4. Happi C, Adetifa I, Mbala P, Njouom R, Nakoune E, Happi A, et al. Urgent need for a non-discriminatory and non-stigmatizing nomenclature for monkeypox virus. PLoS Biol. 2022;20:e3001769. https://doi.org/10.1371/journal.pbio.3001769
5. Ulaeto D, Agafonov A, Burchfield J, Carter L, Happi C, Jakob R, et al. New nomenclature for mpox (monkeypox) and monkeypox virus clades. Lancet Infect Dis. 2023;23:273–5. https://doi.org/10.1016/S1473-3099(23)00055-5
6. Moss B. Understanding the biology of monkeypox virus to prevent future outbreaks. Nat Microbiol. 2024;9:1408–16. https://doi.org/10.1038/s41564-024-01690-1
7. Otieno JR, Ruis C, Onoja AB, Kuppalli K, Hoxha A, Nitsche A, et al. Global genomic surveillance of monkeypox virus. Nat Med. 2025;31:342–50. https://doi.org/10.1038/s41591-024-03370-3
8. McQuiston JH, Luce R, Kazadi DM, Bwangandu CN, Mbala-Kingebeni P, Anderson M, et al.; CDC 2024 Clade I Mpox Response Team. U.S. preparedness and response to increasing clade I mpox cases in the Democratic Republic of the Congo — United States, 2024. MMWR Morb Mortal Wkly Rep. 2024;73:435–40. https://doi.org/10.15585/mmwr.mm7319a3
9. Kibungu EM, Vakaniaki EH, Kinganda-Lusamaki E, Kalonji-Mukendi T, Pukuta E, Hoff NA, et al.; International Mpox Research Consortium. Clade I–-associated mpox cases associated with sexual contact, the Democratic Republic of the Congo. Emerg Infect Dis. 2024;30:172–6. https://doi.org/10.3201/eid3001.231164
10. Nolen LD, Osadebe L, Katomba J, Likofata J, Mukadi D, Monroe B, et al. Extended human-to-human transmission during a monkeypox outbreak in the Democratic Republic of the Congo. Emerg Infect Dis. 2016;22:1014–21. https://doi.org/10.3201/eid2206.150579
11. Vakaniaki EH, Kacita C, Kinganda-Lusamaki E, O'Toole Á, Wawina-Bokalanga T, Mukadi-Bamuleka D, et al. Sustained human outbreak of a new MPXV clade I lineage in eastern Democratic Republic of the Congo. Nat Med. 2024;30:2791–5. https://doi.org/10.1038/s41591-024-03130-3
12. Rahmani E, Bayat Z, Farrokhi M, Karimian S, Zahedpasha R, Sabzehie H, et al. Monkeypox: a comprehensive review of virology, epidemiology, transmission, diagnosis, prevention, treatment, and artificial intelligence applications. Arch Acad Emerg Med. 2024;12:e70. https://doi.org/10.22037/aaem.v12i1.2491
13. Wang JR. Mpox surveillance: the need for enhanced testing and genomic epidemiology. Lancet. 2024;404:1784–5. https://doi.org/10.1016/S0140-6736(24)02386-9
14. Kinganda-Lusamaki E, Amuri-Aziza A, Fernandez-Nuñez N, Makangara-Cigolo JC, Pratt C, Vakaniaki EH, et al. Clade I mpox virus genomic diversity in the Democratic Republic of the Congo, 2018–2024: predominance of zoonotic transmission. Cell. 2025;188:4–14.e6. https://doi.org/10.1016/j.cell.2024.10.017
15. Wawina-Bokalanga T, Vanmechelen B, Logist AS, Bloemen M, Laenen L, Bontems S, et al. A retrospective genomic characterisation of the 2022 mpox outbreak in Belgium, and in vitro assessment of three antiviral compounds. EBioMedicine. 2024;110:105488. https://doi.org/10.1016/j.ebiom.2024.105488
16. Roychoudhury P, Sereewit J, Xie H, Nunley E, Bakhash SM, Lieberman NAP, et al. Genomic analysis of early monkeypox virus outbreak strains, Washington, USA. Emerg Infect Dis. 2023;29:644–6. https://doi.org/10.3201/eid2903.221446
17. Shchelkunov SN, Totmenin AV, Safronov PF, Mikheev MV, Gutorov VV, Ryazankina OI, et al. Analysis of the monkeypox virus genome. Virology. 2002;297:172–94. https://doi.org/10.1006/viro.2002.1446
18. Yu Z, Zou X, Deng Z, Zhao M, Gu C, Fu L, et al. Genome analysis of the mpox (formerly monkeypox) virus and characterization of core/variable regions. Genomics. 2024;116:110763. https://doi.org/10.1016/j.ygeno.2023.110763
19. Li Y, Olson VA, Laue T, Laker MT, Damon IK. Detection of monkeypox virus with real-time PCR assays. J Clin Virol. 2006;36:194–203. https://doi.org/10.1016/j.jcv.2006.03.012

20. Lim CK, Roberts J, Moso M, Liew KC, Taouk ML, Williams E, et al. Mpox diagnostics: review of current and emerging technologies. J Med Virol. 2023;95:e28429. https://doi.org/10.1002/jmv.28429

21. Garrigues JM, Hemarajata P, Lucero B, Alarcón J, Ransohoff H, Marutani AN, et al. Identification of human monkeypox virus genome deletions that impact diagnostic assays. J Clin Microbiol. 2022;60:e0165522. https://doi.org/10.1128/jcm.01655-22

22. Wolf JM, Wolf LM, Fagundes PP, Tomm DMS, Petek H, Brenner A, et al. Molecular evolution of the human monkeypox virus. J Med Virol. 2023;95:e28533. https://doi.org/10.1002/jmv.28533

23. Gigante CM, Korber B, Seabolt MH, Wilkins K, Davidson W, Rao AK, et al. Multiple lineages of monkeypox virus detected in the United States, 2021–2022. Science. 2022;378:560–5. https://doi.org/10.1126/science.add4153

24. Alakunle E, Kolawole D, Diaz-Cánova D, Alele F, Adegboye O, Moens U, et al. A comprehensive review of monkeypox virus and mpox characteristics. Front Cell Infect Microbiol. 2024;14:1360586. https://doi.org/10.3389/fcimb.2024.1360586

25. Li Y, Zhao H, Wilkins K, Hughes C, Damon IK. Real-time PCR assays for the specific detection of monkeypox virus West African and Congo Basin strain DNA. J Virol Methods. 2010;169:223–7. https://doi.org/10.1016/j.jviromet.2010.07.012

26. Gigante CM, Weigand MR, Li Y. Orthopoxvirus genome sequencing, assembly, and analysis. Methods Mol Biol. 2025;2860:39–63. https://doi.org/10.1007/978-1-0716-4160-6_4

27. Steiert TA, Parra G, Gut M, Arnold N, Trotta JR, Tonda R, et al. A critical spotlight on the paradigms of FFPE-DNA sequencing. Nucleic Acids Res. 2023;51:7143–62. https://doi.org/10.1093/nar/gkad519

28. Wang L, Shang J, Weng S, Aliyari SR, Ji C, Cheng G, et al. Genomic annotation and molecular evolution of monkeypox virus outbreak in 2022. J Med Virol. 2023;95:e28036. https://doi.org/10.1002/jmv.28036

29. Gigante CM, Takakuwa J, McGrath D, Kling C, Smith TG, Peng M, et al. Notes from the field: mpox cluster caused by tecovirimat-resistant monkeypox virus—five states, October 2023–February 2024. MMWR Morb Mortal Wkly Rep. 2024;73:903–5. https://doi.org/10.15585/mmwr.mm7340a3

30. Aja-Macaya P, Rumbo-Feal S, Poza M, Cañizares A, Vallejo JA, Bou G. A new and efficient enrichment method for metagenomic sequencing of monkeypox virus. BMC Genomics. 2023;24:29. https://doi.org/10.1186/s12864-023-09114-w

31. Wu C, A R, Ye S, Ye F, Huo W, Lu R, et al. Rapid identification of full-length genome and tracing variations of monkeypox virus in clinical specimens based on mNGS and amplicon sequencing. Virol Sin. 2024;39:134–43. https://doi.org/10.1016/j.virs.2023.12.002

32. Brinkmann A, Pape K, Uddin S, Woelk N, Förster S, Jessen H, et al. Genome sequencing of the mpox virus 2022 outbreak with amplicon-based Oxford Nanopore MinION sequencing. J Virol Methods. 2024;325:114888. https://doi.org/10.1016/j.jviromet.2024.114888

33. Kwasiborski A, Hourdel V, Balière C, Hoinard D, Grassin Q, Feher M, et al. Direct metagenomic and amplicon-based Nanopore sequencing of French human monkeypox from clinical specimen. Microbiol Resour Announc. 2024;13:e0081123. https://doi.org/10.1128/MRA.00811-23

34. Chen NFG, Chaguza C, Gagne L, Doucette M, Smole S, Buzby E, et al. Development of an amplicon-based sequencing approach in response to the global emergence of mpox. PLoS Biol. 2023;21:e3002151. https://doi.org/10.1371/journal.pbio.3002151

35. Hill V, Githinji G, Vogels CBF, Bento AI, Chaguza C, Carrington CVF, et al. Toward a global virus genomic surveillance network. Cell Host Microbe. 2023;31:861–73. https://doi.org/10.1016/j.chom.2023.03.003

36. Rueca M, Tucci FG, Mazzotta V, Gramigna G, Gruber CEM, Fabeni L, et al. Temporal intra-host variability of mpox virus genomes in multiple body tissues. J Med Virol. 2023;95:e28791. https://doi.org/10.1002/jmv.28791

37. Piorkowski G, Ghosn J, Coppée R, Mailhé M, Ferré VM, Houhou-Fidouh N, et al. Genomic diversity of mpox virus in Paris area (France) during the 2022 outbreak. J Med Virol. 2023;95:e28853. https://doi.org/10.1002/jmv.28853

38. Orassay A, Berdigaliyev A, Sadvokassova D, Diassova A, Amin A, Cao W, et al. Recent advances on human mpox. New Microbes New Infect. 2023;51:101066. https://doi.org/10.1016/j.nmni.2022.101066

39. Masirika LM, Udahemuka JC, Schuele L, Ndishimye P, Otani S, Mbiribindi JB, et al. Ongoing mpox outbreak in Kamituga, South Kivu Province, associated with monkeypox virus of a novel clade I sub-lineage, Democratic Republic of the Congo, 2024. Euro Surveill. 2024;29:2400106. https://doi.org/10.2807/1560-7917.ES.2024.29.11.2400106

40. Isidro J, Borges V, Pinto M, Sobral D, Santos JD, Nunes A, et al. Phylogenomic characterization and signs of microevolution in the 2022 multi-country outbreak of monkeypox virus. Nat Med. 2022;28:1569–72. https://doi.org/10.1038/s41591-022-01907-y

41. O'Toole Á, Neher RA, Ndodo N, Borges V, Gannon B, Gomes JP, et al. APOBEC3 deaminase editing in mpox virus as evidence for sustained human transmission since at least 2016. Science. 2023;382:595–600. https://doi.org/10.1126/science.adg8116

42. Smith TG, Gigante CM, Wynn NT, Matheny A, Davidson W, Yang Y, et al. Tecovirimat resistance in mpox patients, United States, 2022–2023. Emerg Infect Dis. 2023;29:2426–32. https://doi.org/10.3201/eid2912.231146

43. Bapolisi WA, Krasemann S, Wayengera M, Kirenga B, Bahizire E, Malembaka EB, et al. Mpox outbreak—tecovirimat resistance, management approaches, and challenges in HIV-endemic regions. Lancet Infect Dis. 2024;24:e672–3. https://doi.org/10.1016/S1473-3099(24)00591-7

44. Lee M, Choi CH, Kim JW, Sim G, Lee SE, Shin H, et al. Prolonged viral shedding in an immunocompromised Korean patient infected with hMPXV, sub-lineage B.1.3, with acquired drug resistant mutations during tecovirimat treatment. J Med Virol. 2024;96:e29536. https://doi.org/10.1002/jmv.29536

45. Garrigues JM, Hemarajata P, Espinosa A, Hacker JK, Wynn NT, Smith TG, et al. Community spread of a human monkeypox virus variant with a tecovirimat resistance–associated mutation. Antimicrob Agents Chemother. 2023;67:e0097223. https://doi.org/10.1128/aac.00972-23

46. Ali R, Alonga J, Biampata JL, Kombozi Basika M, Maljkovic Berry I, Bisento N, et al.; PALM007 Writing Group. Tecovirimat for clade I MPXV infection in the Democratic Republic of Congo. N Engl J Med. 2025;392:1484–96. https://doi.org/10.1056/NEJMoa2412439

Address for correspondence: Crystal Gigante, Centers for Disease Control and Prevention, 1600 Clifton Road NE, Mailstop H23-4, Atlanta, GA 30329-4018, USA; email: lzu1@cdc.gov

Bjerkandera spp. Pulmonary Infection in Immunocompromised Hosts, Germany

Rosanne Sprute, Danila Seidel, Katrin Mehler, Zoé Westhues, Sarina K. Butzer,
Jannik Stemler, Oliver A. Cornely, Philipp Koehler

We report 3 cases of probable invasive pulmonary disease caused by *Bjerkandera* spp. fungi in immunocompromised patients in Germany. Accurate identification required internal transcribed spacer sequencing. Response to antifungal treatment varied. Our report underlines the pathogenic potential of *Bjerkandera* spp. and the importance of molecular diagnostics in rare fungal infections.

Common molds such as *Aspergillus* spp. and Mucorales are well-recognized pathogens in immunocompromised patients that cause life-threatening invasive fungal disease (IFD). Other environmental molds are frequently dismissed as contaminants in clinical specimens, yet growing evidence through clinical vigilance and advances in molecular techniques has revealed some as emerging threats in vulnerable populations (*1–2*). Many of those fungi are expected to remain unidentified because cultures stay negative without prolonged incubation for those organisms, and accurate identification requires molecular methods. Advanced molecular methods, such as cell-free DNA sequencing, hold promise as diagnostic tools but are not yet routinely available (*3,4*).

Bjerkandera spp., including *B. adusta* (syn. *Geotrichopsis mycoparasitica*) and *B. fumosa,* are filamentous basidiomycetes, wood-decaying fungi that have been isolated from dead hardwood trees in Europe and South America (*5*). *Bjerkandera* spp. have been linked to chronic cough, allergic bronchopulmonary mycosis, and hypersensitivity pneumonitis in humans (*6–8*). In addition, invasive sinonasal fungal disease by *B. adusta* was reported in a patient with uncontrolled type 2 diabetes, confirmed through histopathologic examination (*9*). We describe 3 patients in Germany with pulmonary infection and identification of *Bjerkandera* spp. in respiratory specimen that meet the European Organization for Research and Treatment of Cancer and the Mycoses Study Group Education and Research Consortium (EORTC/MSGERC) criteria for probable IFD, highlighting an emerging association between the basidiomycete and human invasive disease.

The Study

Patient 1 was a 32-year-old man who received allogeneic hematopoietic stem cell transplant (HSCT) for relapsed mediastinal T-cell lymphoma (Table). Nine months later, he experienced progressive dyspnea. The patient was on prednisolone (100 mg/d) immunosuppressive therapy and did not receive

Author affiliations: German Centre for Infection Research, Cologne, Germany (R. Sprute, D. Seidel, Z. Westhues, J. Stemler, O.A. Cornely); University of Cologne Faculty of Medicine and University Hospital Cologne Institute of Translational Research, Cologne Excellence Cluster on Cellular Stress Responses in Aging-Associated Diseases, Cologne (R. Sprute, D. Seidel, Z. Westhues, J. Stemler, O.A. Cornely, P. Koehler); University of Cologne Faculty of Medicine and University Hospital Cologne Department of Internal Medicine, Center for Integrated Oncology Aachen Bonn Cologne Duesseldorf and ECMM Excellence Center for Medical Mycology, Cologne (R. Sprute, D. Seidel, Z. Westhues, J. Stemler, O.A. Cornely, P. Koehler); University of Cologne Faculty of Medicine and University Hospital Cologne Department of Pediatrics, Division of Pediatric Infectious Diseases, Cologne (K. Mehler, S.K. Butzer); University of Cologne Faculty of Medicine and University Hospital Cologne, Department of Pediatrics, Division of Pediatric Oncology and Hematology, Cologne (S.K. Butzer); University of Cologne Faculty of Medicine and University Hospital Cologne, Clinical Trials Centre Cologne (ZKS Köln), Cologne (O.A. Cornely); University of Cologne Faculty of Medicine and University Hospital Cologne, Department of Internal Medicine, Division of Clinical Immunology, Cologne (P. Koehler)

DOI: https://doi.org/10.3201/eid3111.250878

Table. Characteristics of patients with probable invasive pulmonary disease by *Bjerkandera* spp., Germany*

Patient no.	Age, y	Time of diagnosis and department	Underlying condition and treatment	Antifungal prophylaxis	Radiology	Microbiology	Antifungal Treatment	Outcome
1	32	May 2017, inpatient hematology unit	Relapsed mediastinal T-cell lymphoma; allogeneic HSCT	None	Nodular infiltrates, ground-glass opacities	Mold culture from BAL fluid, *Bjerkandera* spp. identified by ITS sequencing†	Posaconazole	Deceased
2	82	Oct 2022, outpatient hematology department	AML, functional neutropenia; hydroxyurea	None	Nodular infiltrates, cavitary lesion	Mold culture from BAL fluid, *B. adusta* or *B. fumosa* identified by ITS sequencing‡	Voriconazole, isavuconazole	Unknown
3	4	Nov 2022, inpatient pediatric hematology unit	AML; HAM regimen	Micafungin	Nodular infiltrates, ground-glass opacities, cavitary lesion	Mold culture from tracheal aspiration, *B. adusta* or *B. fumosa* identified by ITS sequencing§	Voriconazole, liposomal AmB	Alive, secondary prophylaxis with voriconazole

*Microbiologic analyses were performed at the Institute of Medical Microbiology, Immunology, and Hygiene, University Hospital Cologne, Cologne, Germany. AmB, amphotericin B; AML, acute myeloid leukemia; BAL, bronchoalveolar lavage; HAM, high-dose cytarabine with mitoxantrone; HSCT, hematopoietic stem cell transplant, ITS, internal transcribed spacer.

†Other causes of infectious disease were ruled out by negative blood cultures; negative *Legionella* antigen from urine; negative culture from BAL including *Mycobacteria* and *Actinomyces* culture; negative results for *M. tuberculosis* complex, *Chlamydia pneumoniae*, *Mycoplasma pneumoniae*, *Legionella pneumophilia*, *Aspergillus* spp., Mucorales, *Pneumocystis jirovecii*, and *Toxoplasma gondii* by PCR from BAL; negative respiratory virus panel from BAL; and negative results on throat swab samples for viruses including influenza A, influenza B, parainfluenza, adenovirus, metapneumovirus, coronavirus, respiratory syncytial virus, rhinovirus, bocavirus, and enterovirus. There was no serologic evidence for *C. pneumoniae* or *M. pneumoniae* infection, no active hepatitis A–E, and negative results for cytomegalovirus, herpes simplex virus, varicella zoster virus, and parvovirus PCR from EDTA blood. We identified Epstein-Barr virus copies 14 IU/mL from EDTA blood, in control virus that was negative by PCR.

‡Other causes of infectious disease were ruled out by negative culture from BAL, including *Mycobacteria* and *Actinomyces* culture; negative results for *M. tuberculosis* complex, *C. pneumoniae, M. pneumoniae, L. pneumophilia, Aspergillus* spp., Mucorales, *Pneumocystis jirovecii*, and *Toxoplasma gondii* by PCR from BAL; negative influenza A, influenza B, parainfluenza, adenovirus, metapneumovirus, coronavirus, respiratory syncytial virus, rhinovirus, bocavirus, and enterovirus from BAL and throat swab samples; and negative *Legionella* and pneumococcal antigen from urine.

§Other causes of infectious disease were ruled out by negative blood cultures and urine cultures; negative culture from tracheal aspiration; negative *C. pneumoniae, L. pneumophilia, M. pneumoniae, Aspergillus* spp., Mucorales, *Pneumocystis carinii*, and *Toxoplasma gondii* by PCR from tracheal aspiration; and negative cytomegalovirus, human herpesvirus 6A, Epstein-Barr virus, influenza A, influenza B, parainfluenza, adenovirus, metapneumovirus, coronavirus, respiratory syncytial virus, rhinovirus, bocavirus, and enterovirus by PCR from tracheal aspiration.

antifungal drugs. Computed tomography (CT) of the chest showed new ground-glass opacities and nodular consolidations. Culture from bronchoalveolar lavage (BAL) fluid revealed a mold identified as *Bjerkandera* spp. by sequencing the internal transcribed spacer (ITS) 1/2 region in accordance with Clinical and Laboratory Standards Institute guidelines (*10*). We did not perform susceptibility testing because fungal growth on the testing media was insufficient. Results of Mucorales and *Aspergillus*-specific PCR from BAL fluid were negative. Serum was negative for galactomannan antigen. We did not perform BAL galactomannan testing. We identified no other potential causes of infectious diseases by culture, PCR, or serology (Table). We initiated empiric antimicrobial therapy with piperacillin/tazobactam for 2 weeks. The fungus was not considered clinically significant; no antifungal treatment was initiated. Immunosuppression was intensified on suspicion of lung graft-versus-host disease, but the patient's condition continued to deteriorate. We started antifungal therapy with posaconazole both as prophylaxis and targeted treatment of the probable IFD. Eight days later, we performed another BAL in which no fungus or other

infectious agent was detected. The patient died shortly afterward from respiratory failure. No autopsy was performed.

Patient 2 was an 82-year-old woman who was referred to the University Hospital Cologne with a diagnosis of acute myeloid leukemia 5 months before admission (Table). She had been treated with azacitidine monotherapy, but after allergic transfusion reaction to platelets, her cancer treatment was discontinued. At admission, the patient was experiencing hyperleukocytosis and neutropenia. We initiated cytoreductive treatment with hydroxyurea. A baseline chest CT scan revealed nodular infiltrates and a subpleural cavitary lesion, suggestive of fungal pneumonia (Figure 1). Of note, the patient had not received any antifungal prophylaxis other than trimethoprim/sulfamethoxazole. Bronchoscopy demonstrated purulent secretions. Results of galactomannan testing of BAL fluid were positive; culture yielded a preliminary phenotypic identification of *Geotrichum* spp. All other diagnostic work-up results were unremarkable (Table). Given the clinical significance of the mold identification, we pursued further species-level analysis. ITS sequencing identified the
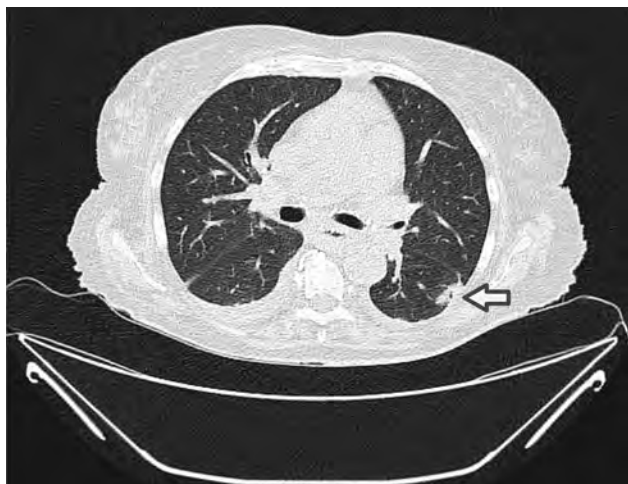
Figure 1. Chest computed tomography scan from an 82-year-old female patient with acute myeloid leukemia in study of *Bjerkandera* spp. pulmonary infection in immunocompromised hosts, Germany. Image depicts nodular infiltrates and a cavitary lesion (arrow) in the left lower lobe suggestive of fungal pneumonia. We cultured and identified a mold from bronchoalveolar lavage fluid as *Bjerkandera* spp. by internal transcribed spacer sequencing.

organism as either *B. adusta* or *B. fumosa* (*10*). *Aspergillus* PCR was negative. We could not perform antifungal susceptibility testing because of insufficient fungal growth. We initiated voriconazole therapy but switched to isavuconazole because the patient experienced visual disturbances. Follow-up chest CT scans at 2 and 5 weeks showed stable disease. After 5 weeks of antifungal therapy, we discontinued treatment and initiated posaconazole as secondary prophylaxis. No additional follow-up visits occurred.

Patient 3 was a 4-year-old boy with newly diagnosed acute myeloid leukemia who initially received cytarabine-based induction chemotherapy (Table). He experienced seizures secondary to cerebral

hemorrhage, requiring mechanical ventilation. After successful extubation, we resumed chemotherapy using a high-dose cytarabine and mitoxantrone regimen. He received micafungin (4 mg/kg 2×/wk) as antifungal prophylaxis. Subsequently, he experienced febrile neutropenia (temperature 39.2°C/102.6°F) that was unresponsive to empiric broad-spectrum antimicrobial treatment with meropenem and vancomycin, raising suspicion for IFD. We initiated voriconazole. Serum galactomannan test results were negative. A chest CT scan demonstrated nodular infiltrates and a new cavitary lesion radiographically consistent with a mold infection (Figure 2, panel A). We switched antifungal therapy to liposomal amphotericin B (L-AmB). Fungal culture from a tracheal aspirate yielded a mold with sterile mycelium, which we identified via ITS sequencing as *B. adusta* or *B. fumosa* (*10*). Other diagnostic assessments yielded no findings (Table). After 2 weeks of L-AmB therapy, the patient experienced severe hypokalemia, requiring a switch back to voriconazole. A follow-up CT scan performed 3 weeks later demonstrated a radiographic response to treatment (Figure 2, panel B). No further imaging was done. The patient continued voriconazole therapy for a total of 4 months.

Conclusions

We described 3 cases with probable invasive lung infections caused by *Bjerkandera* spp. in 2 adults and 1 pediatric patient with hematologic malignancies. We identified no other fungal pathogens or alternative infectious agents by culture, PCR, or serology. All cases met criteria for probable invasive pulmonary mold infection (*11*). Multidisciplinary teams discussed the possibility of contamination and likelihood of invasive disease by *Bjerkandera* spp. and concluded that the identification of *Bjerkandera* spp.

Figure 2. Chest computed tomography scan of a 4-year-old male patient with acute myeloid leukemia in study of *Bjerkandera* spp. pulmonary infection in immunocompromised hosts, Germany. The patient experienced fever unresponsive to antimicrobial treatment. A) Imaging revealed nodular infiltrates and surrounding ground-glass opacities in both lungs (arrow). *Bjerkandera* spp. was identified from tracheal aspiration. B) Follow-up

computed tomography scan after 4 weeks demonstrated regressive nodular lesions and the formation of a cavity in the right upper lobe (arrow).
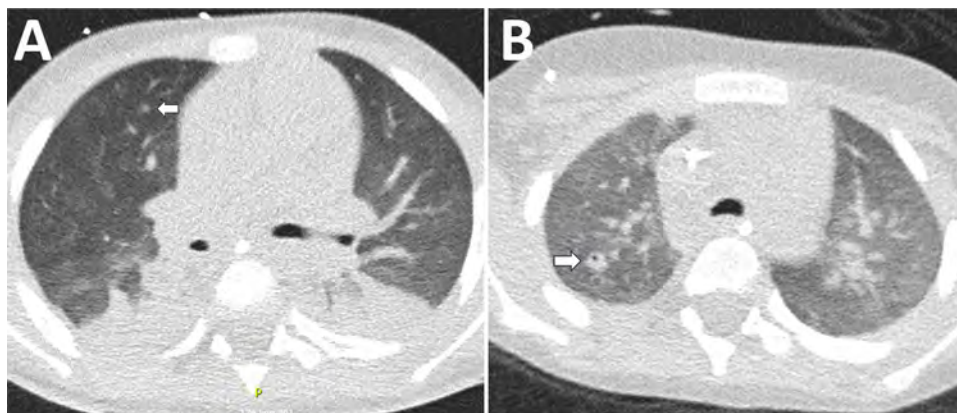
was consistent with an IFD in each case, warranting antifungal treatment.

We identified the fungus in all 3 cases by sequencing techniques, underlining the importance of molecular approaches in the evaluation of rare fungal infections. In patient 2, *B. adusta* was preliminary identified as *Geotrichum* spp. based on phenotypic appearance. *Geotrichum* spp. are environmental fungi that cause opportunistic infections in at-risk populations (*12*). Both fungi share phenotypic features such as whitish, fluffy to woolly colony morphology and wide-branching septate hyphae with formation of arthroconidia and only occasional formation of chlamydospores (Figure 3) (*6,13*). Therefore, reliable identification in filamentous basidiomycetes requires additional techniques such as matrix-assisted laser desorption/ionization time-of-flight mass spectrometry and sequencing methods. Sequence analysis of the ITS ribosomal DNA has better accuracy for species identification; however, for rare fungi, reference data may be incomplete or unavailable for both methods (*14*).

Guidance for clinical management of emerging IFD remains limited because IFD is rare and clinical manifestations vary. Susceptibility test results of 14 *B. adusta* isolates included high MIC for fluconazole and flucytosine and low MIC for AmB and newer triazoles (*15*). Clinical improvement with itraconazole treatment has been described (*14*) in cases with chronic cough associated with *Bjerkandera* spp., consistent with in vitro susceptibility findings. One reported case-patient with invasive rhinosinusitis caused by *Bjerkandera* was treated sequentially with L-AmB, posaconazole, and voriconazole, leading to clinical recovery (*9*). We used newer triazoles and L-AmB for treatment with variable responses. The lack of comprehensive susceptibility testing and outcome data limits definitive treatment recommendations for suspected IFD caused by *Bjerkandera* spp. Describing an unusual pathogen carries a risk for error. We were unable to demonstrate fungal growth in independent respiratory specimens or to obtain histologic proof of invasive growth from lung biopsy.

Our findings suggest that *Bjerkandera* spp. is a human pathogen causing invasive fungal pneumonia or other pulmonary infection in persons at risk, including the immunocompromised. Evaluating the clinical relevance of such infections must consider the degree of immunosuppression and the patient's future treatment plans.
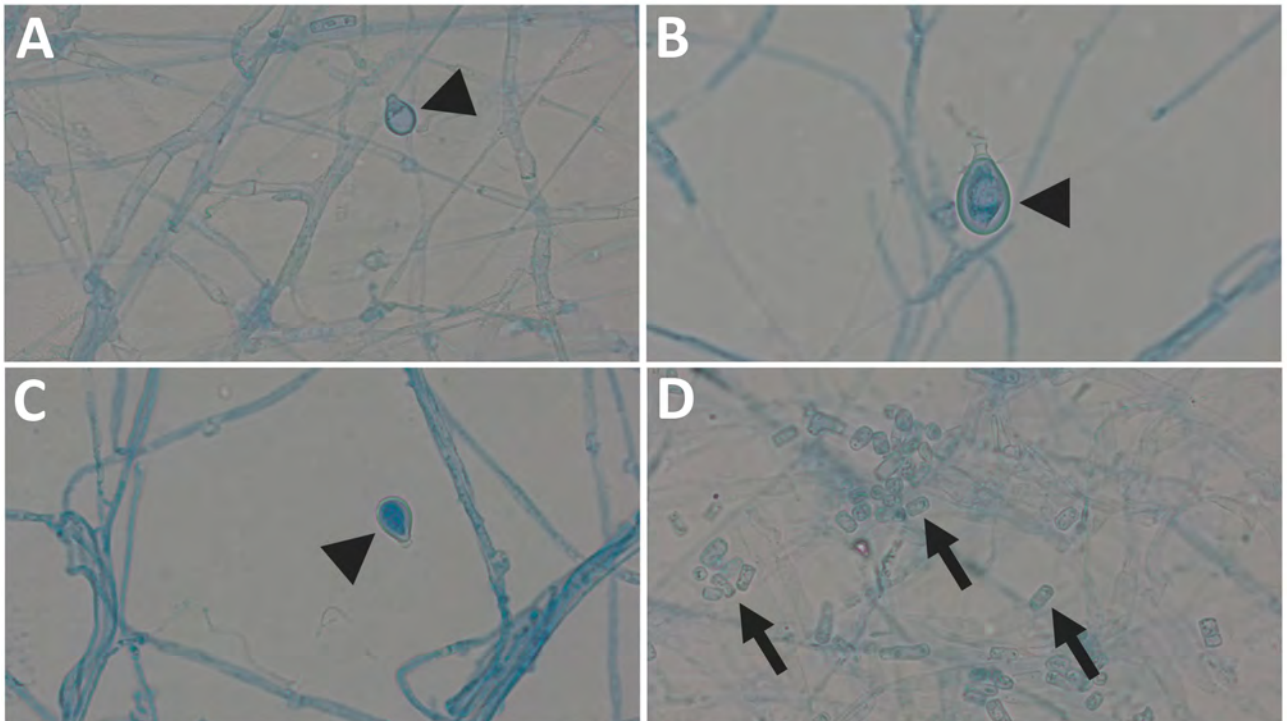

Figure 3. Images of *Bjerkandera* spp. formations from study of *Bjerkandera* spp. pulmonary infection in immunocompromised hosts, Germany. Slides are of lactophenol preparation (original magnification ×1,000). *Bjerkandera* spp. form white, yellowish-white, or tan colonies with a cottony to woolly texture on malt extract agar. The hyphae can be branched. Thin-walled, rectangular arthroconidia are formed via schizolytic dehiscence. In addition, ellipsoidal chlamydospores ≤10 μm long may develop. Arrowheads indicate chlamydospores (A–C), arrows indicate arthroconidia (D).

About the Author

Dr. Sprute is a physician-scientist at University Hospital Cologne specializing in translational approaches to the management of invasive fungal and other opportunistic infections. Her clinical and research focus centers on high-risk patients, particularly those with hematologic malignancies and in intensive care units.

References

1. Del Principe MI, Seidel D, Criscuolo M, Dargenio M, Rácil Z, Piedimonte M, et al.; FungiScope (Global Emerging Fungal Infection Registry); SEIFEM (Sorveglianza Epidemiologica Infezioni nelle Emopatie). Clinical features and prognostic factors of *Magnusiomyces* (*Saprochaete*) infections in haematology. A multicentre study of SEIFEM/Fungiscope. Mycoses. 2023;66:35–46. https://doi.org/10.1111/myc.13524
2. Sprute R, Salmanton-García J, Sal E, Malaj X, Rácil Z, Ruiz de Alegría Puig C, et al.; FungiScope ECMM/ISHAM Working Group. Invasive infections with *Purpureocillium lilacinum:* clinical characteristics and outcome of 101 cases from FungiScope and the literature. J Antimicrob Chemother. 2021;76:1593–603. https://doi.org/10.1093/jac/dkab039
3. Sprute R, Cornely OA, Chen SC, Seidel D, Schuetz AN, Zhang SX. All you need to know and more about the diagnosis and management of rare yeast infections. MBio. 2021;12:e0159421. https://doi.org/10.1128/mBio.01594-21
4. Sprute R, Seidel D, Cornely OA, Hoenigl M. EHA endorsement of the global guideline for the diagnosis and management of rare mold infection: an initiative of the European Confederation of Medical Mycology in cooperation with International Society for Human and Animal Mycology and American Society for Microbiology. HemaSphere. 2021;5:e519. https://doi.org/10.1097/HS9.0000000000000519
5. Motato-Vásquez V, Gugliotta AM, Rajchenberg M, Catania M, Urcelay C, Robledo G. New insights on *Bjerkandera* (Phanerochaetaceae, Polyporales) in the Neotropics with description of *Bjerkandera albocinerea* based on morphological and molecular evidence. Plant Ecol Evol. 2020;153:229–45. https://doi.org/10.5091/plecevo.2020.1667
6. Chowdhary A, Kathuria S, Agarwal K, Meis JF. Recognizing filamentous basidiomycetes as agents of human disease: a review. Med Mycol. 2014;52:782–97. https://doi.org/10.1093/mmy/myu047
7. Ogawa H, Tone K, Fujimura M, Makimura K. Central suppressant therapies in unexplained chronic cough patients whose sputum cultures yielded *Bjerkandera adusta*. Allergol Int. 2019;68:125–6. https://doi.org/10.1016/j.alit.2018.07.009
8. Tone K, Ogawa H, Gochi M, Nagano Y, Furube A, Inaki S, et al. Allergic bronchopulmonary mycosis associated with a novel pathogen: *Bjerkandera adusta*. Allergol Int. 2022;71:542–4. https://doi.org/10.1016/j.alit.2022.05.005
9. Kurata Y, Kimizuka Y, Yaguchi T, Ito K, Yamamoto T, Serizawa Y, et al. *Bjerkandera adusta* fungi as causative agent of invasive chronic rhinosinusitis. Emerg Infect Dis. 2025;31:355–8. https://doi.org/10.3201/eid3102.241275
10. Clinical Laboratory Standards Institute. Interpretive criteria for identification of bacteria and fungi by targeted DNA sequencing. 2nd edition (MM18). Wayne (PA): The Institute; 2018.
11. Donnelly JP, Chen SC, Kauffman CA, Steinbach WJ, Baddley JW, Verweij PE, et al. Revision and update of the consensus definitions of invasive fungal disease from the European Organization for Research and Treatment of Cancer and the Mycoses Study Group Education and Research Consortium. Clin Infect Dis. 2020;71:1367–76. https://doi.org/10.1093/cid/ciz1008
12. Chen SC, Perfect J, Colombo AL, Cornely OA, Groll AH, Seidel D, et al. Global guideline for the diagnosis and management of rare yeast infections: an initiative of the ECMM in cooperation with ISHAM and ASM. Lancet Infect Dis. 2021;21:e375–86. https://doi.org/10.1016/S1473-3099(21)00203-6
13. Zhu HY, Shang YJ, Wei XY, Groenewald M, Robert V, Zhang RP, et al. Taxonomic revision of *Geotrichum* and *Magnusiomyces*, with the descriptions of five new *Geotrichum* species from China. Mycology. 2024;15:400–23. https://doi.org/10.1080/21501203.2023.2294945
14. Tone K, Ogawa H, Alshahni MM, Kuwano K, Makimura K. Real-time PCR detection of the basidiomycetous fungus *Bjerkandera adusta*: a tool to identify itraconazole responder patients with unexplained chronic cough. Respiration. 2019;97:84–91. https://doi.org/10.1159/000492118
15. González GM, Sutton DA, Thompson E, Tijerina R, Rinaldi MG. In vitro activities of approved and investigational antifungal agents against 44 clinical isolates of basidiomycetous fungi. Antimicrob Agents Chemother. 2001; 45:633–5. https://doi.org/10.1128/AAC.45.2.633-635.2001

Address for correspondence: Rosanne Sprute, Institute of Translational Research, Herderstrasse 52, 50931 Cologne, Germany; email: rosanne.sprute@uk-koeln.de

etymologia

Cladophialophora carrionii
[klad´-ō-fī-əl-ō-for-ə kar´-ē-ō-nē-ī]

Dayane Moraes, Alexandre Melo Bailão, Mirelle Garcia Silva Bailão

Cladophialophora carrionii is a black fungus that causes chromoblastomycosis. The fungus was first reported in 1946 as *Fonsecaea pedrosoi* var. *cladosporium*. In 1954, mycologist Alfonso Trejos named this chromoblastomycosis agent *Cladosporium carrionii* n. sp. (Figure). Later, molecular phylogenetic analysis and morphologic traits (cladosporioid anamorphs and phialidic synanamorphs) supported its current placement in the genus *Cladophialophora*.

The term *Cladophialophora* is derived from the Greek words *klados* (branch) and *phiala* (flask or bottle) and the suffix *phora*, which means bearing or carrying, emphasizing that these structures produce and harbor the fungal spores. The specific epithet *carrionii* is in honor of the charismatic Puerto Rican mycologist Prof. Dr. Arturo I. Carrión, renowned for his contributions to medical mycology, particularly in the taxonomy and clinical understanding of dematiaceous fungal pathogens. Therefore, the full name *Cladophialophora carrionii* means a black flask-shaped fungus with branched conidia chains, named in honor of Dr. Carrión.
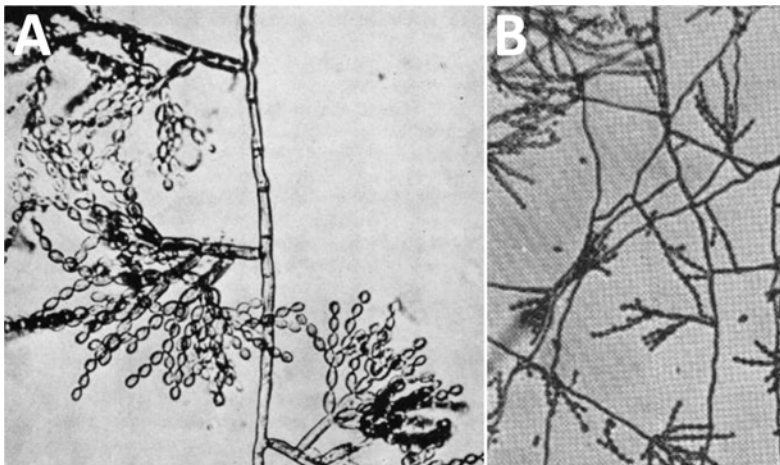
Figure. Images from early records of *Cladosporium carrionii*. A) *Fonsecaea pedrosoi* var. c*ladosporium* by F.W. Simson in 1946. B) *Cladosporium carrionii* n. sp. by A. Trejos in 1954.

Sources

1. Bensch K, Braun U, Groenewald JZ, Crous PW. The genus *Cladosporium*. Stud Mycol. 2012;72:1–401. https://doi.org/10.3114/sim0003
2. de Hoog GS, Guého E, Masclaux F, Gerrits van den Ende AH, Kwon-Chung KJ, McGinnis MR. Nutritional physiology and taxonomy of human-pathogenic *Cladosporium*-*Xylohypha* species. J Med Vet Mycol. 1995;33:339–47. https://doi.org/10.1080/02681219580000661
3. Simson FW. Chromoblastomycosis; some observations on the types of the disease in South Africa. Mycologia. 1946;38:432–49. https://doi.org/10.1080/00275514.1946.12024066
4. Trejos A. *Cladosporium carrionii* n. sp. and the problem of *Cladosporia* isolated from chromoblastomycosis. Rev Biol Trop. 1954;2:75–112.

Authors affiliation: Universidade Federal de Goiás (UFG), Goiânia, Brazil

Address for correspondence: Mirelle Garcia Silva Bailão, Universidade Federal de Goiás, Avenida Esperança s/n ICB2, sala 217, Laboratório de Biologia Molecular, Goiânia, Brazil; email: mgsbailao@ufg.br

Novel Dolphin Tupavirus from Stranded Atlantic White-Sided Dolphin with Severe Encephalitis, Canada, 2024

Oksana Vernygora,[1] Laura Bourque,[1] Megan Jones, Ole Nielsen,
Carissa Embury-Hyatt, Estella Moffat, Tonya Wimmer, Oliver Lung

We sequenced a novel rhabdovirus, *Tupavirus delphini* (dolphin tupavirus), from the brain of a stranded dead Atlantic white-sided dolphin with severe encephalitis in Canada. In situ hybridization linked presence of the virus to the animal's brain pathology and death. Our findings underscore the importance of monitoring marine mammals for unexpected pathogens.

Cetaceans (whales and dolphins) are ubiquitous in the world's oceans and are critical for monitoring oceanic ecosystem health (*1*). Despite their importance, little is known about diseases that affect free-ranging cetacean populations. Monitoring cetacean populations is challenging; consequently, much can be gained from necropsy examinations of dead, stranded animals. This study describes the discovery of a novel rhabdovirus species detected during the necropsy of an Atlantic white-sided dolphin (*Leucopleurus acutus*) found stranded on the Atlantic coast of Nova Scotia, Canada (Appendix 1 Figure 1, https://wwwnc.cdc.gov/EID/article/31/11/25-1203-App1.pdf).

Rhabdoviruses are a diverse group of enveloped single-stranded negative-sense RNA viruses that infect vertebrates, invertebrates, and plants. Most aquatic rhabdoviruses are described from ray-finned fish and amphibians; little is known about rhabdoviruses infecting marine mammals (*2*). Two species of rhabdoviruses are reported from cetaceans, dolphin rhabdovirus (*3*,*4*) and harbor porpoise rhabdovirus, neither of which was definitively linked to causing disease in their hosts (*5*). We characterized a novel rhabdovirus genome and used in situ hybridization to link viral infection with histopathologic lesions within the brain.

The Study

On October 27, 2024, a freshly dead Atlantic white-sided dolphin was found ashore on La Bloc Beach in the Cape Breton Highlands National Park, Nova Scotia, Canada. The carcass was well preserved with minimal scavenging or postmortem decomposition (Appendix 1 Figure 1) and demonstrated overall good nutritional condition (*6*). No significant lesions were identified from the carcass other than those from severe encephalitis. We conducted diagnostic PCR testing of frozen brain tissue for common pathogens known to cause encephalitis in marine mammals (avian influenza virus, cetacean morbillivirus, herpesvirus, *Brucella ceti*, *Sarcocystis* sp., and *Toxoplasma gondii*); results were negative.

Examination of transverse sections of the brain revealed multiple extensive areas of severe inflammation and necrosis primarily throughout the forebrain within the regions of the cingulate gyrus, internal capsule, thalamus, and temporal and parietal lobes of the neocortex. In situ hybridization showed consistent presence of viral RNA in the lesions (Figure 1). Regions of the brain that did not exhibit lesions were primarily within the midbrain and hindbrain. In affected regions, we observed generalized mild to severe expansion of the perivascular space

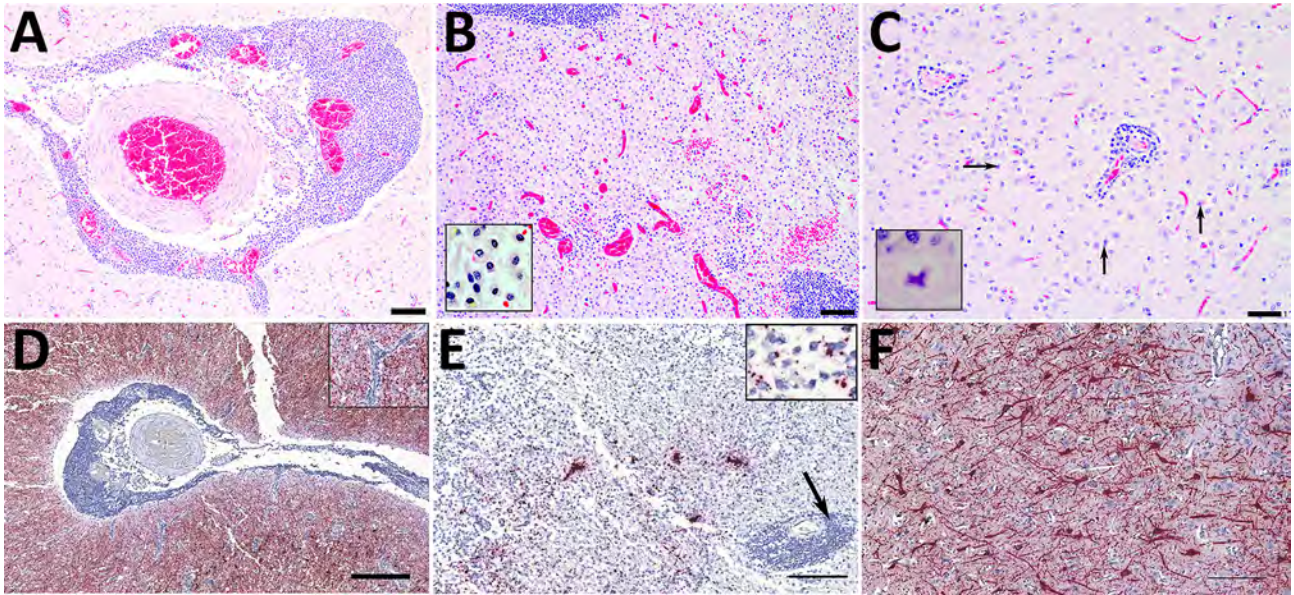[1]These authors contributed equally to this article.

Figure 1. Histopathology (A–C) and in situ hybridization (D–F) of brain tissue from stranded Atlantic white-sided dolphin infected with novel tupavirus, Canada. Histopathology images are stained with hematoxylin and eosin; cytoplasm and connective tissues appear pink, red blood cells red, and cell nuclei purple. A) Cross-section through an arteriole within the neuropil at the level of the internal capsule, depicting sometimes massive infiltration of perivascular (Virchow-Robin) space by large numbers of lymphocytes and plasma cells, fewer numbers of macrophages, and rare eosinophils. Scale bar indicates 100 µm. B) Cross-section through the cingulate gyrus at the level of the internal capsule, showing almost complete effacement of normal neuropil architecture by massive numbers of hypertrophied microglial cells. Also depicted are multiple arterioles with large perivascular cuffs of lymphocytes and plasma cells, as well as multiple areas of hemorrhage within the neuropil. Inset shows microglial cells. Scale bar indicates 100 µm. C) Section through neocortex exhibiting extensive infiltration of the neuropil by glial cells, which frequently form nodules surrounding necrotic neurons. Necrotic neurons are shrunken with hypereosinophilic cytoplasm and condensed, pyknotic nuclei (arrows). There are also multiple small arterioles with lymphoplasmacytic perivascular cuffs. Inset shows a necrotic neuron. Scale bar indicates 50 µm. D) Abundant viral RNA (red staining) in the area surrounding the affected arteriole. Staining is observed in the neuropil as well as some glial cells; however, endothelial cells are not infected (inset). No staining is observed within the perivascular inflammatory cells. Scale bar indicates 400 µm. E) Viral RNA in microglial cells and neuropil (inset) but not within perivascular cuffs (arrow). Scale bar indicates 200 µm.) Abundant viral RNA within neurons and dendrites. In situ hybridization, paraffin-embedded formalin-fixed tissue sections were performed with RNAScope 2.5HD Detection Reagent and custom probes targeting the 1275–2283 nt region of the viral genome (Bio-Techne Advanced Cell Diagnostics, https://www.bio-techne.com). Scale bar indicates 200 µm.

by lymphocytes and plasma cells and fewer macrophages and rare eosinophils (Figure 1, panel A). We observed intense positive staining for viral RNA in the surrounding neuropil but not in the perivascular inflammatory cells (Figure 1, panel D). In some areas, the normal tissue architecture was effaced by massive infiltration of hypertrophied microglial cells (Figure 1, panel B), many of which stained positive for viral RNA (Figure 1, panel E). In the neocortex, we noted glial nodules surrounding necrotic neurons (Figure 1, panel C), as well as neuronal cell bodies and dendrites within lesion areas that contained abundant viral RNA (Figure 1, panel F). All other tissues examined microscopically were either within normal limits or exhibited incidental lesions unrelated to the neuropathology described.

For whole-genome sequencing, we performed sample preparation and data processing (7) with modifications (Appendix 1). The complete 11,088-nt

dolphin tupavirus (DTV) genome we obtained (deposited into GenBank, accession no. PV683224) had a structure typical of rhabdoviruses comprising 5 major open reading frames (ORFs), nucleocapsid, phosphoprotein, matrix, glycoprotein, and RNA-dependent RNA polymerase (L) proteins, and a putative small hydrophobic protein between the matrix protein and glycoprotein, that encode proteins highly divergent from other rhabdoviruses (Table; Figure 2) (Appendix 1 Figure 2; Appendix 2 Table 1, https://wwwnc.cdc.gov/EID/article/31/11/25-1203-App2.xlsx) (8,9). Phosphoprotein contains a putative C protein in an overlapping reading frame. Each ORF of the DTV genome is flanked by conserved transcription initiation (UUGUC) and termination/polyadenylation (AWCU7) signals and an inferred untranscribed intergenic sequence (GG or GA). The L protein of DTV contains an LDSPL motif, a modification of the animal rhabdovirus

Table. Characteristics of highly divergent novel dolphin tupavirus protein sequences from the brain of a stranded dead Atlantic white-sided dolphin with severe encephalitis, Canada*

Protein	Nucleotide		Amino acid	
	Top match by BLASTn	% Identity	Top match by DELTA-BLAST	% Identity
Nucleocapsid	Wufeng *Rhinolophus pearsonii* tupavirus 1 (GenBank accession no. MZ328291.1)	68.54	Wufeng bat tupavirus 2 (GenBank accession no. WPV62772.1)	54.88
Phosphoprotein	NA	NA	Wufeng *Rhinolophus pearsonii* tupavirus 1 (GenBank accession no. UBB42388.1)	17.55
Matrix protein	NA	NA	Bat tupavirus CX1 (GenBank accession no. WGC86350.1)	32.68
SH protein	NA	NA	Durham virus (GenBank accession no. ADB88762)	33.33
Glycoprotein	NA	NA	Wufeng bat tupavirus 2 (GenBank accession no. WPV62776.1)	30.62
Polymerase	Wenzhou *Myotis laniger* tupavirus 1 (GenBank accession no. OM030290.1)	55.42	Klamath virus (GenBank accession no. AJR28401.1)	55.36

*Percentage amino acid identity for the SH protein was calculated by aligning it to the SH from Durham virus, the closest tupavirus to DTV, using a BLASTp algorithm (https://blast.ncbi.nlm.nih.gov/Blast.cgi). SH proteins have very low identity among the members of the genus (*7,8*). NA, not applicable; SH, small hydrophobic protein.

conserved motif (LNSPL), also found in Durham virus, another tupavirus (*10,11*).

Phylogenetic analysis of the complete L-protein sequences placed DTV within the genus *Tupavirus* (Figure 2). The closest BLAST (https://blast.ncbi.nlm.nih.gov/Blast.cgi) match to the assembled DTV genome was Wenzhou Myotis laniger tupavirus 1 (GenBank accession no. OM030290.1), with an overall genomewide nucleotide identity of 50.72%. Amino acid sequence divergence in the nucleocapsid protein between the DTV and the closest BLAST match (Wufeng bat tupavirus 2; accession no. OQ715690.1) was 45.12%. Amino acid sequence divergence between the DTV and the closest BLAST match was 69.38% (Wufeng bat tupavirus 2; accession no. OQ715690.1) in the G protein and 44.64% (Klamath virus; accession no. KM204999.1) in the L protein. Virus isolation with multiple passages for >1 month using 6 cell lines from diverse host species was unsuccessful, as indicated by the lack of visible cytopathic effect and negative results with a DTV PCR (Appendix 2 Table 3).

Conclusions

We report the identification and characterization of a novel rhabdovirus from the brain of a stranded Atlantic white-sided dolphin with severe encephalitis. DTV is genetically distinct from previously known cetacean rhabdoviruses, and phylogenetic analysis indicates a considerable gap between DTV and other tupaviruses, suggesting a substantial level of unsampled viral diversity within the group. Based on the presented genomic divergence, genome organization, phylogenetic placement, and host species, DTV complies with International Committee on Taxonomy of Viruses demarcation criteria as a new species within the genus *Tupavirus* (*10*).

Reports of rhabdoviruses in aquatic mammals are scarce. Their detection and discovery are hindered by numerous challenges presented by the environment, host biology, and postmortem decomposition; therefore, even single case reports of a new virus from an aquatic mammal host provide valuable information to enhance pathogen surveillance in aquatic environments.

Unlike the previous 2 cases of cetacean rhabdovirus infection, DTV was associated with signs of severe disease. The severity of encephalitis we described was striking, but not unique. Many pathogens, including morbillivirus and *Brucella ceti* bacteria, can cause encephalitis in marine mammals (*12*). Those agents and others were ruled out in this case through a series of PCR tests, further supporting DTV as the causative pathogen. Even so, we cannot totally rule out the presence of concurrent infections. DTV isolation in cultured cells was challenging and unsuccessful; however, it is critical for experimental infections in animal models that will support investigations into DTV's host range, tissue tropism, transmission, and pathogenicity. PCR screening and whole-genome sequencing methods for DTV could enable DTV surveillance. In addition, metagenomic sequencing of both affected and unaffected tissues might identify any co-infections.

The apparent preference of DTV for specific areas of the brain is reminiscent of rabies infection of terrestrial mammals, in which different host species exhibit unique patterns of lesion distribution in the brain; those patterns are an important criterion for disease recognition and diagnosis (*13*). A large

outbreak of rabies has been reported in cape fur seals (*Arctocephalus pusillus*) in South Africa, which likely originated as a spillover event from terrestrial canids (*14*). Before that event, rabies in marine mammals was considered vanishingly rare; 1 case had been reported in a ring seal (*Pusa hispida*) in Svalbard, Norway, in 1981 (*15*).

This work highlights the importance of responding to incidents involving dead marine animals and conducting thorough investigations and diagnostics. Such discoveries can compound conservation concerns for marine species. It is imperative to continue documenting and examining cetacean stranding incidents in Canada, including those involving species

Figure 2. Maximum-likelihood phylogenetic trees of novel dolphin tupavirus from stranded Atlantic white-sided dolphin, Canada, and reference rhabdoviruses. Trees were reconstructed based on the full-length amino acid sequences of the polymerase protein. All sequence records for the phylogenetic analysis were downloaded from GenBank (Appendix 2 Table 2, https://wwwnc.cdc.gov/EID/article/31/11/25-1203-App2.xlsx). Scale bars represent the estimated average number of substitutions per site. A) High-level phylogeny includes a subset of representative members across the *Rhabdoviridae* family (n = 438 sequence records) to determine the placement of the new virus within the family. Red text indicates rhabdoviruses of marine mammals, including the newly identified dolphin tupavirus; blue text indicates fish rhabdoviruses. The tree was rooted at the midpoint. B) Genus-level phylogeny provides a fine-level assessment of the phylogenetic affinities of the new virus within the *Tupavirus* genus. Red text indicates the sequence of the novel tupavirus; red shading highlights the *Tupavirus* clade in the phylogenetic tree. The phylogenetic bracket of the dolphin tupavirus includes a basal Durham virus and a large crown clade comprising the rest of the *Tupavirus* member viruses. Durham virus described from an American coot (*Fulica americana*) that demonstrated signs of severe disease associated with infection, including lesions

isolated to the central nervous system and consisting of severe cerebral necrosis and mononuclear inflammation similar to DTV. Support values at the nodes were determined by SSH-aLRT/Ultrafast bootstrap. *Tupavirus* genus tree was rooted to the outgroup members of the *Sunrhavirus* genus, Boteke, Sunguru, and Walkabout Creek viruses.
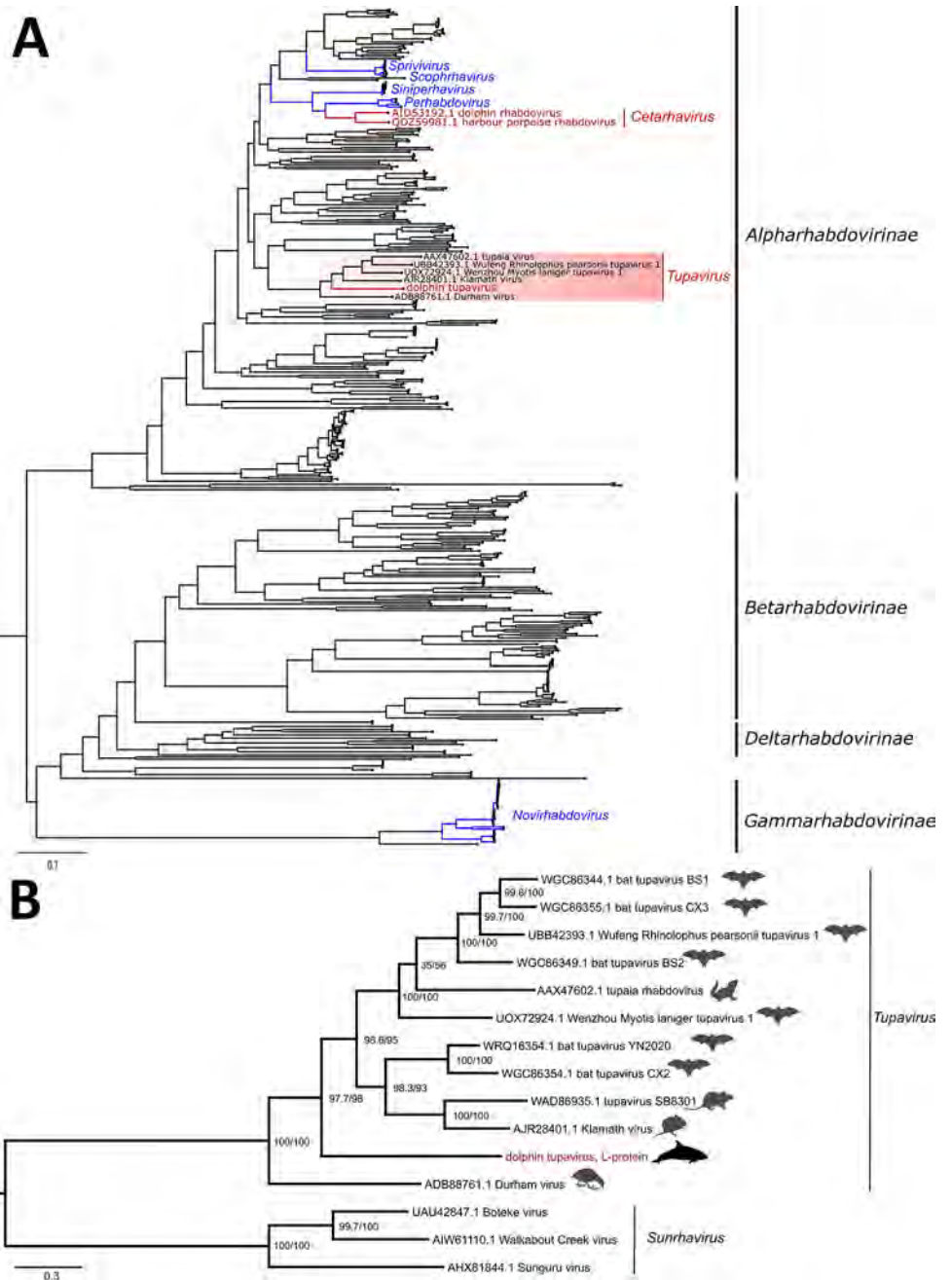
not considered to be a priority by federal government wildlife managers. Our work has provided histopathologic and molecular evidence linking a cetacean rhabdovirus to CNS pathology and supports further investigation to characterize DTV and its associated pathology and epidemiology.

About the Author

Dr. Vernygora is a research scientist at the National Centre for Foreign Animal Disease, Canadian Food Inspection Agency. Her research focuses on molecular identification and characterization of known, unknown, and unexpected animal viruses. Dr. Bourque is a wildlife pathologist that specializes in marine mammals. She works for the Canadian Wildlife Health Cooperative in Prince Edward Island, Canada.

References

1. Bossart GD. Marine mammals as sentinel species for oceans and human health. Vet Pathol. 2011;48:676–90. https://doi.org/10.1177/0300985810388525
2. Walker PJ, Bigarré L, Kurath G, Dacheux L, Pallandre L. Revised taxonomy of rhabdoviruses infecting fish and marine mammals. Animals (Basel). 2022;12:1363. https://doi.org/10.3390/ani12111363
3. Osterhaus ADME, Broeders HWJ, Teppema JS, Kuiken T, House JA, Vos HW, et al. Isolation of a virus with rhabdovirus morphology from a white-beaked dolphin (*Lagenorhynchus albirostris*). Arch Virol. 1993;133:189–93. https://doi.org/10.1007/BF01309754
4. Siegers JY, van de Bildt MWG, van Elk CE, Schürch AC, Tordo N, Kuiken T, et al. Genetic relatedness of dolphin rhabdovirus with fish rhabdoviruses. Emerg Infect Dis. 2014;20:1081–2. https://doi.org/10.3201/eid2006.131880
5. Emelianchik A, Rodrigues TCS, Subramaniam K, Nielsen O, Burek-Huntington KA, Rotstein D, et al. Characterization of a novel rhabdovirus isolated from a stranded harbour porpoise (*Phocoena phocoena*). Virus Res. 2019;273:197742. https://doi.org/10.1016/j.virusres.2019.197742
6. Geraci JR, Lounsbury VJ. Marine mammals ashore: a field guide for strandings. College Station (TX): Texas A&M University, Sea Grant College Program; 1993.
7. Vernygora O, Sullivan D, Nielsen O, Huntington KB, Rouse N, Popov VL, et al. *Senecavirus cetus* a novel picornavirus isolated from cetaceans represents a major host switching to the marine environment. Npj Viruses. 2024;2:33. https://doi.org/10.1038/s44298-024-00040-6
8. Allison AB, Palacios G, Travassos da Rosa A, Popov VL, Lu L, Xiao SY, et al. Characterization of Durham virus, a novel rhabdovirus that encodes both a C and SH protein. Virus Res. 2011;155:112–22. https://doi.org/10.1016/j.virusres.2010.09.007
9. Walker PJ, Firth C, Widen SG, Blasdell KR, Guzman H, Wood TG, et al. Evolution of genome size and complexity in the rhabdoviridae. PLoS Pathog. 2015;11:e1004664. https://doi.org/10.1371/journal.ppat.1004664
10. Walker PJ, Freitas-Astúa J, Bejerman N, Blasdell KR, Breyta R, Dietzgen RG, et al.; ICTV Report Consortium. ICTV virus taxonomy profile: Rhabdoviridae 2022. J Gen Virol. 2022;103:001689. https://doi.org/10.1099/jgv.0.001689
11. Kuzmin IV, Wu X, Tordo N, Rupprecht CE. Complete genomes of Aravan, Khujand, Irkut, and West Caucasian bat viruses, with special attention to the polymerase gene and non-coding regions. Virus Res. 2008;136:81–90. https://doi.org/10.1016/j.virusres.2008.04.021
12. Gulland FMD, Dierauf LA, Whitman KL, editors. CRC handbook of marine mammal medicine. 3rd edition. Boca Raton (FL): CRC Press; 2018.
13. Maxie M. Jubb, Kennedy, and Palmer's pathology of domestic animals. 6th edition. St. Louis (MO): Elsevier; 2016.
14. Winkler MP, Parker S. Rabies in seals: visitors to Cape Town marine areas urged to be alert. J Travel Med. 2024;31:taae106. https://doi.org/10.1093/jtm/taae106
15. Odegaard OA, Krogsrud J. Rabies in Svalbard: infection diagnosed in Arctic fox, reindeer and seal. Vet Rec. 1981;109:141–2. https://doi.org/10.1136/vr.109.7.141

Address for correspondence: Oliver Lung, National Centre for Foreign Animal Disease, Canadian Food Inspection Agency, 1015 Arlington St, Winnipeg, MB R3E 3M4, Canada; email: oliver.lung@inspection.gc.ca

Neoehrlichia mikurensis in Ticks and Tick-Bitten Persons, Sweden and Finland, 2008–2009

Emilia Hero, Malin Lager, Pia Forsberg, Per-Eric Lindgren, Anna J. Henningsson, Peter Wilhelmsson

By using PCR testing, we found *Neoehrlichia mikurensis* DNA in 1.1% of ticks removed from persons in Sweden and Finland. Symptoms developed in 2 immunocompetent persons. Despite low transmission risk, infection can occur after short tick attachment. Our findings highlight the need to consider *N. mikurensis* in patients with unexplained symptoms after tick bite.

N*eoehrlichia mikurensis* is an emerging tickborne pathogen, mainly transmitted by *Ixodes ricinus* ticks. The human infection known as neoehrlichiosis was first reported in Sweden in 2010 and has been documented in several countries in Europe (*1,2*). Neoehrlichiosis affects both healthy and immunocompromised persons, and more severe symptoms, such as vascular complications, are typically seen in immunocompromised patients (*3*). Diagnosis is challenging because of vague symptoms, low awareness, and lack of commercial diagnostic tests. PCR is the primary method of detection, because *N. mikurensis* is difficult to culture and no serologic tests are available. The true prevalence of *N. mikurensis* in humans and ticks remains unclear, although its DNA has been detected in both throughout Europe (*4,5*).

We investigated the prevalence of *N. mikurensis* after tick bites in northern Europe, aiming to detect its DNA in ticks and human blood and to assess symptoms among participants. The samples were originally collected in 2008–2009, when *N. mikurensis* was not yet recognized as a human pathogen and appropriate diagnostic tools were lacking; therefore, this analysis could not be conducted until recently. Despite being >15 years old, the data offer valuable insight into *N. mikurensis* ecology and transmission. Although epidemiology might have shifted, the underlying biologic mechanisms of pathogen transmission likely remain unchanged, ensuring continued relevance.

The Study

We analyzed data from the Tick-Borne Diseases (TBD) STING study (*6,7*), a prospective multicenter study conducted in Sweden and on the Åland Islands, Finland (Figure). During May 2008–November 2009, primary healthcare centers enrolled 1,425 healthy tick-bitten adults (≥18 years of age; median age 63, range 19–92) through public advertisements. The study was approved in 2008 by the Regional Ethical Review Board in Linköping, Sweden, and the Åland Health Care Ethics Committee.

At study inclusion, participants submitted removed tick(s), provided a blood sample, and completed a questionnaire on tick exposure, prior tickborne diseases, current health status, and medication use (*8*). Participants on antimicrobial drugs or immunosuppressive therapy were excluded. A follow-up visit 3 months later included providing a second blood sample and filling out a questionnaire about symptoms experienced since inclusion and if the participant had sought medical care (*8*). Medical records were reviewed when relevant. Participants also submitted any additional ticks found attached during the 3-month study period.

For this study, we photographed each tick and identified it by species, developmental stage, and sex. We estimated feeding duration for nymphs and adult females (*9*). We homogenized ticks, extracted total nucleic acids, and reverse-transcribed to cDNA (*7*). Participant plasma was collected in EDTA tubes (*6*), and we extracted DNA from participants whose ticks were PCR-positive for *N. mikurensis*.

We screened tick cDNA for *N. mikurensis* by using a SYBR Green real-time PCR targeting the *16S* rRNA gene (*10*) and confirming positive results by using a TaqMan real-time PCR targeting the *groEL* gene (*11*).

Author affiliations: Linköping University, Linköping, Sweden (E. Hero, P. Forsberg, P.-E. Lindgren, A.J. Henningsson, P. Wilhelmsson); Region Jönköping County, Jönköping, Sweden (M. Lager, P.-E. Lindgren, A.J. Henningsson, P. Wilhelmsson)

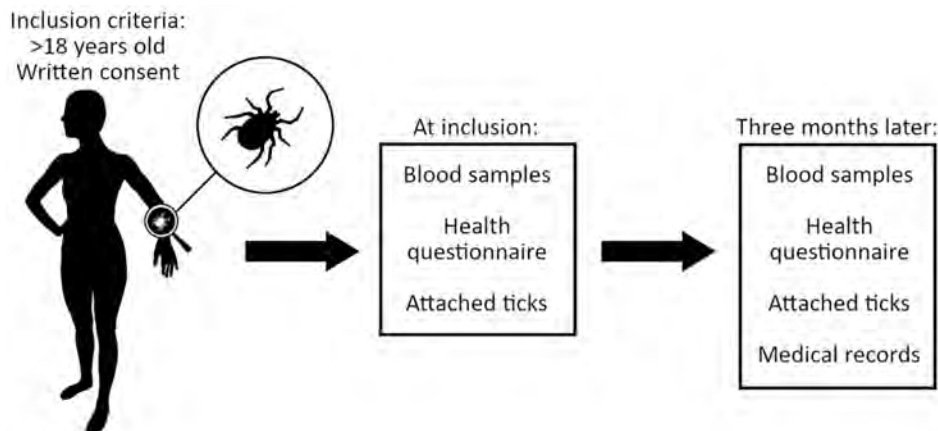**Figure.** Schematic overview of the Tick-Borne Diseases STING study during 2008–2009 in Sweden and Finland (*6*), in which tick-bitten persons ≥18 years of age gave written informed consent to participate, submitted removed tick(s), provided a blood sample, and completed a questionnaire. At a follow-up visit 3 months later, they provided a second blood sample and completed a second questionnaire. Any additional tick(s) found attached during the study period were also submitted and available medical records were reviewed.

We analyzed plasma DNA from participants bitten by positive ticks by using the same TaqMan assay. We confirmed PCR products by sequencing (Macrogen Inc., https://www.macrogen.com) and verified sequences with BLAST (https://blast.ncbi.nlm.nih.gov). We used a previously confirmed *N. mikurensis*-positive cDNA sample as a positive PCR control (*10*).

Of the 1,644 *I. ricinus* ticks analyzed, 18 (1.1%) were positive for *N. mikurensis* in both PCRs (Table 1). No DNA was found in larvae. Prevalence in nymphs was 1.1% and in adult females was 1.3%. The ticks were collected from participants in various regions in Sweden and on the Åland Islands (Appendix Table, http://wwwnc.cdc.gov/EID/article/31/11/24-1850-App1.pdf). Of the 18 participants bitten by PCR-positive ticks, 2 (11%) tested positive for *N. mikurensis* (Table 2).

The first positive participant was a 41-year-old otherwise healthy woman from southern Sweden who tested positive at inclusion. She had been bitten by a *N. mikurensis*–positive nymph that had fed for <24 hours. She reported symptoms including headache, fatigue, numbness, radiating pain, and myalgia. Eleven days later, she was bitten by another tick, which was not submitted for analysis. It was unclear whether her symptoms were related to the first or second tick bite. During the study period, she sought medical care for and was diagnosed with myalgia and calf muscle cramps, for which she was

treated with quinine tablets (100 mg) administered as needed.

The second positive participant was a 68-year-old otherwise healthy woman from south-central Sweden, who tested positive at the 3-month follow-up. She had been bitten by a *N. mikurensis*–positive nymph that had fed for ≈40 hours. She reported fatigue, neck pain, myalgia, and numbness but did not seek medical care. She was bitten by 3 additional ticks during the study period, of which only 1 was submitted to the TBD STING study; it tested negative for *N. mikurensis*.

Sequencing confirmed *N. mikurensis* DNA in both the ticks and the blood samples from the 2 participants. The remaining 16 participants bitten by PCR-positive ticks tested PCR-negative for *N. mikurensis* in both the inclusion and follow-up blood samples. Out of those participants, 9 reported no symptoms during the study period and 2 did not respond to the follow-up questionnaire. The remaining 5 reported nonspecific symptoms, including muscle and joint pain (n = 5), headache (n = 2), fatigue (n = 2), neck pain (n = 1), vertigo (n = 2), and numbness (n = 2).

Conclusions

We detected *N. mikurensis* DNA in 1.1% of *I. ricinus* ticks that had bitten humans in Sweden and Finland, indicating a low prevalence in the study areas compared with those reported in other regions of

Table 1. The prevalence of *Neoehrlichia mikurensis* determined in 1,644 *Ixodes ricinus* ticks collected from 1,425 humans who were bitten in Sweden or on the Åland Islands, Finland, during May 2008–November 2009

Developmental stage of the tick	Total no. ticks analyzed	No. (%) *N. mikurensis* PCR-positive ticks*
Adult females	392	5 (1.3)
Adult males	7	0
Nymphs	1,138	13 (1.1)
Larvae	69	0
Undetermined†	38	0
Total	1,644	18 (1.1)

*PCR-positive tick was defined as a tick that tested positive for *N. mikurensis* in both the SYBR Green and TaqMan real-time PCR assays.
†Tick developmental stage remains undetermined because of damages as previously described (*7*).

Table 2. Characteristics of participants with *Neoehrlicha mikurensis* DNA detected in their plasma in a study of ticks and tick-bitten persons, Sweden and Finland, 2008–2009.

Participant sex	Participant age, y	Tick developmental stage	Tick feeding time, h‡	PCR results§	Self-reported symptoms¶	Sought medical care
Female*	41	Nymph	<24	Positive/negative	Headache, fatigue, radiating pain, myalgia, numbness	Yes
Female†	68	Nymph	43	Negative/positive	Fatigue, neck pain, myalgia, numbness	No

*Participant was recruited to a primary healthcare center in southernmost Sweden (Appendix Figure, http://wwwnc.cdc.gov/EID/article/31/11/24-1850-App1.pdf).
†Participant was recruited to a primary healthcare center in south-central Sweden (Appendix Figure).
‡Estimation of the duration of blood feeding was calculated as described previously (*9*).
§Plasma samples collected during initial inclusion and then at follow-up visit.
¶Self-reported symptoms described in the questionnaire that was completed during the follow-up meeting 3 months after the tick bite.

Sweden (*10,12*). Two participants bitten by PCR-positive ticks also tested positive for *N. mikurensis* in blood samples and reported symptoms consistent with neoehrlichiosis, despite being immunocompetent. Those findings suggest that, although the overall risk for infection after a tick bite is low, transmission can still occur even after short tick attachment times (<24 h) and in persons without known immunosuppression.

The prospective design of the TBD STING study, large number of samples, and standardized follow-up strengthen the reliability of our findings. The use of a 2-tier PCR targeting the *16S* rRNA and *groEL* genes and then sequencing ensured high specificity of the detection assay. By linking infected ticks to the person they had bitten, the study provided an opportunity to assess the risk for transmission under natural conditions.

Although PCR detects bacterial DNA rather than viable organism, its sensitivity depends on having enough *N. mikurensis* DNA present in the blood sample. Because *N. mikurensis* likely causes low-level bacteremia because of its tissue tropism (*13,14*), the pathogen might not always be detectable in blood samples, leading to false-negative results and potential underdiagnosis. Therefore, the symptoms reported by PCR-negative participants bitten by positive ticks might be related to *N. mikurensis* exposure. Furthermore, PCR cannot detect seroconversion or immune responses, and the absence of serologic tools limits the ability of this study to identify resolved infections.

The absence of *N. mikurensis* DNA in tick larvae supports evidence that transovarial transmission is unlikely (*10,12,15*), whereas similar prevalence in nymphs and adult females suggests stable infection rates across stages, informing our understanding of pathogen maintenance in tick populations. The relevance of our results likely extends beyond the specific regions studied. Therefore, in areas where *N. mikurensis* has been detected in ticks, clinicians should consider this pathogen in the differential diagnosis of patients with unexplained symptoms after a tick bite.

About the Author

Dr. Hero is currently doing her residency in internal medicine at the Hospital of Kiruna. Her research interests include ticks and tickborne infections.

References

1. Welinder-Olsson C, Kjellin E, Vaht K, Jacobsson S, Wennerås C. First case of human "*Candidatus* Neoehrlichia mikurensis" infection in a febrile patient with chronic lymphocytic leukemia. J Clin Microbiol. 2010;48:1956–9. https://doi.org/10.1128/JCM.02423-09
2. Portillo A, Santibáñez P, Palomar AM, Santibáñez S, Oteo JA. '*Candidatus* Neoehrlichia mikurensis' in Europe. New Microbes New Infect. 2018;22:30–6. https://doi.org/10.1016/j.nmni.2017.12.011
3. Höper L, Skoog E, Stenson M, Grankvist A, Wass L, Olsen B, et al. Vasculitis due to *Candidatus* Neoehrlichia

mikurensis: a cohort study of 40 Swedish patients. Clin Infect Dis. 2021;73:e2372–8. https://doi.org/10.1093/cid/ciaa1217

4. Markowicz M, Schötta AM, Höss D, Kundi M, Schray C, Stockinger H, et al. Infections with tickborne pathogens after tick bite, Austria, 2015–2018. Emerg Infect Dis. 2021;27:1048–56. https://doi.org/10.3201/eid2704.203366

5. Jahfari S, Hofhuis A, Fonville M, van der Giessen J, van Pelt W, Sprong H. Molecular detection of tick-borne pathogens in humans with tick bites and erythema migrans, in the Netherlands. PLoS Negl Trop Dis. 2016;10:e0005042. https://doi.org/10.1371/journal.pntd.0005042

6. Wilhelmsson P, Fryland L, Lindblom P, Sjöwall J, Ahlm C, Berglund J, et al. A prospective study on the incidence of Borrelia burgdorferi sensu lato infection after a tick bite in Sweden and on the Åland Islands, Finland (2008–2009). Ticks Tick Borne Dis. 2016;7:71–9. https://doi.org/10.1016/j.ttbdis.2015.08.009

7. Wilhelmsson P, Lindblom P, Fryland L, Ernerudh J, Forsberg P, Lindgren PE. Prevalence, diversity, and load of Borrelia species in ticks that have fed on humans in regions of Sweden and Åland Islands, Finland with different Lyme borreliosis incidences. PLoS One. 2013;8:e81433. https://doi.org/10.1371/journal.pone.0081433

8. Wilhelmsson P, Lindblom P, Fryland L, Nyman D, Jaenson TG, Forsberg P, et al. Ixodes ricinus ticks removed from humans in Northern Europe: seasonal pattern of infestation, attachment sites and duration of feeding. Parasit Vectors. 2013;6:362. https://doi.org/10.1186/1756-3305-6-362

9. Gray J, Stanek G, Kundi M, Kocianova E. Dimensions of engorging Ixodes ricinus as a measure of feeding duration. Int J Med Microbiol. 2005;295:567–72. https://doi.org/10.1016/j.ijmm.2005.05.008

10. Labbé Sandelin L, Tolf C, Larsson S, Wilhelmsson P, Salaneck E, Jaenson TG, et al. Candidatus Neoehrlichia mikurensis in ticks from migrating birds in Sweden. PLoS One. 2015;10:e0133250. https://doi.org/10.1371/journal.pone.0133250

11. Grankvist A, Sandelin LL, Andersson J, Fryland L, Wilhelmsson P, Lindgren PE, et al. Infections with Candidatus Neoehrlichia mikurensis and cytokine responses in 2 persons bitten by ticks, Sweden. Emerg Infect Dis. 2015;21:1462–5. https://doi.org/10.3201/eid2108.150060

12. Andersson M, Bartkova S, Lindestad O, Råberg L. Co-infection with 'Candidatus Neoehrlichia mikurensis' and Borrelia afzelii in Ixodes ricinus ticks in southern Sweden. Vector Borne Zoonotic Dis. 2013;13:438–42. https://doi.org/10.1089/vbz.2012.1118

13. Wass L, Grankvist A, Bell-Sakyi L, Bergström M, Ulfhammer E, Lingblom C, et al. Cultivation of the causative agent of human neoehrlichiosis from clinical isolates identifies vascular endothelium as a target of infection. Emerg Microbes Infect. 2019;8:413–25. https://doi.org/10.1080/22221751.2019.1584017

14. Grankvist A, Jaén-Luchoro D, Wass L, Sikora P, Wennerås C. Comparative genomics of clinical isolates of the emerging tick-borne pathogen Neoehrlichia mikurensis. Microorganisms. 2021;9:1488. https://doi.org/10.3390/microorganisms9071488

15. Jahfari S, Fonville M, Hengeveld P, Reusken C, Scholte EJ, Takken W, et al. Prevalence of Neoehrlichia mikurensis in ticks and rodents from north-west Europe. Parasit Vectors. 2012;5:74. https://doi.org/10.1186/1756-3305-5-74

Address for correspondence: Peter Wilhelmsson, Linköping University, SE-581 83 Linköping, Sweden; email: peter.wilhelmsson@liu.se

Shifting Dynamics of Dengue Virus Serotype 2 and Emergence of Cosmopolitan Genotype, Costa Rica, 2024

Mauricio González-Elizondo, Dihala Picado Soto, Estela Cordero Laurent,
Francisco Duarte Martínez, Luiz Carlos Junior Alcantara, Vagner Fonseca, Jairo Andrés
Méndez Rico, Jose Lourenco, Leticia Franco, Marta Giovanetti,[1] Claudio Soto Garita[1]

Dengue remains a major public health challenge. In Costa Rica, we implemented nationwide genomic surveillance to track dengue virus serotype 2 cosmopolitan genotype emergence. Phylogenetic and eco-epidemiologic analyses revealed early detection, climate-driven spread, and spatial heterogeneity. Our findings underscore the need for integrated surveillance to guide adaptive responses to emerging arboviral threats.

Dengue fever, caused by mosquitoborne dengue virus (DENV), remains a major public health threat. DENV is primarily transmitted by *Aedes aegypti* mosquitoes (*1*). Rising global dengue incidence has been linked to climate change and urbanization (*2*).

In Costa Rica, DENV transmission has become increasingly complex. Dengue cases rose from 30,649 in 2023 (*2*) to 31,259 in 2024 (*1*); San José, Alajuela, and Puntarenas reported the highest incidence rates. Inciensa launched a nationwide DENV sequencing program in 2023, which confirmed simultaneous circulation of all 4 serotypes (DENV-1–4). That study was approved by the Pan-American Health Organization Ethics Review Committee (reference no. PAHO-2024-08-0029) and was conducted as part of routine arbovirus surveillance at Inciensa. In February 2024, that surveillance detected DENV-2 genotype II (cosmopolitan); by September genotype II had fully replaced genotype III, and the earliest cases were reported in coastal districts (*3*,*4*). Genotype II is associated with more severe clinical outcomes (*4*) and has been reported in Peru and Brazil since 2019 (*3*,*4*), raising concerns for regional spread. We investigated whether ecologic factors were contributing to DENV shifts in Costa Rica.

The Study

To assess ecologic drivers, we compared dengue incidence with a climate-driven suitability index, which integrates temperature- and humidity-dependent mosquito traits, such as biting rate, lifespan, and extrinsic incubation. Before 2022, dengue activity was irregular in Costa Rica but surged during 2022–2024 (Figure 1, panel A); we noted a moderate correlation ($r = 0.38$) between suitability and incidence during the 2022–2023 epidemic (Appendix 1, https://wwwnc.cdc.gov/EID/article/31/11/25-0746-App1.pdf). At the province level, correlations in 2022 were broadly consistent

(Figure 1, panel B), but in 2023, we observed stronger associations in Puntarenas and Limón, where the cosmopolitan genotype first appeared, suggesting ecologic and virologic factors converged to intensify local transmission (Figure 1, panel C).

Historically, DENV-1 and DENV-2 have been the predominant serotypes in Costa Rica, fluctuating in relative proportions. However, we observed a major shift in 2023–2024, characterized by co-circulation of all 4 serotypes, mirrored by emergence of DENV-4 in late 2022 and reemergence of DENV-3 in early 2023 after a 6-year absence (Appendix 1 Figure 1, panel A). The reemergence of DENV-3 aligns with the known ubiquitous serotype cycles observed every 7–9 years, and DENV-4 emergence aligns with its recent expansion in South America (1).
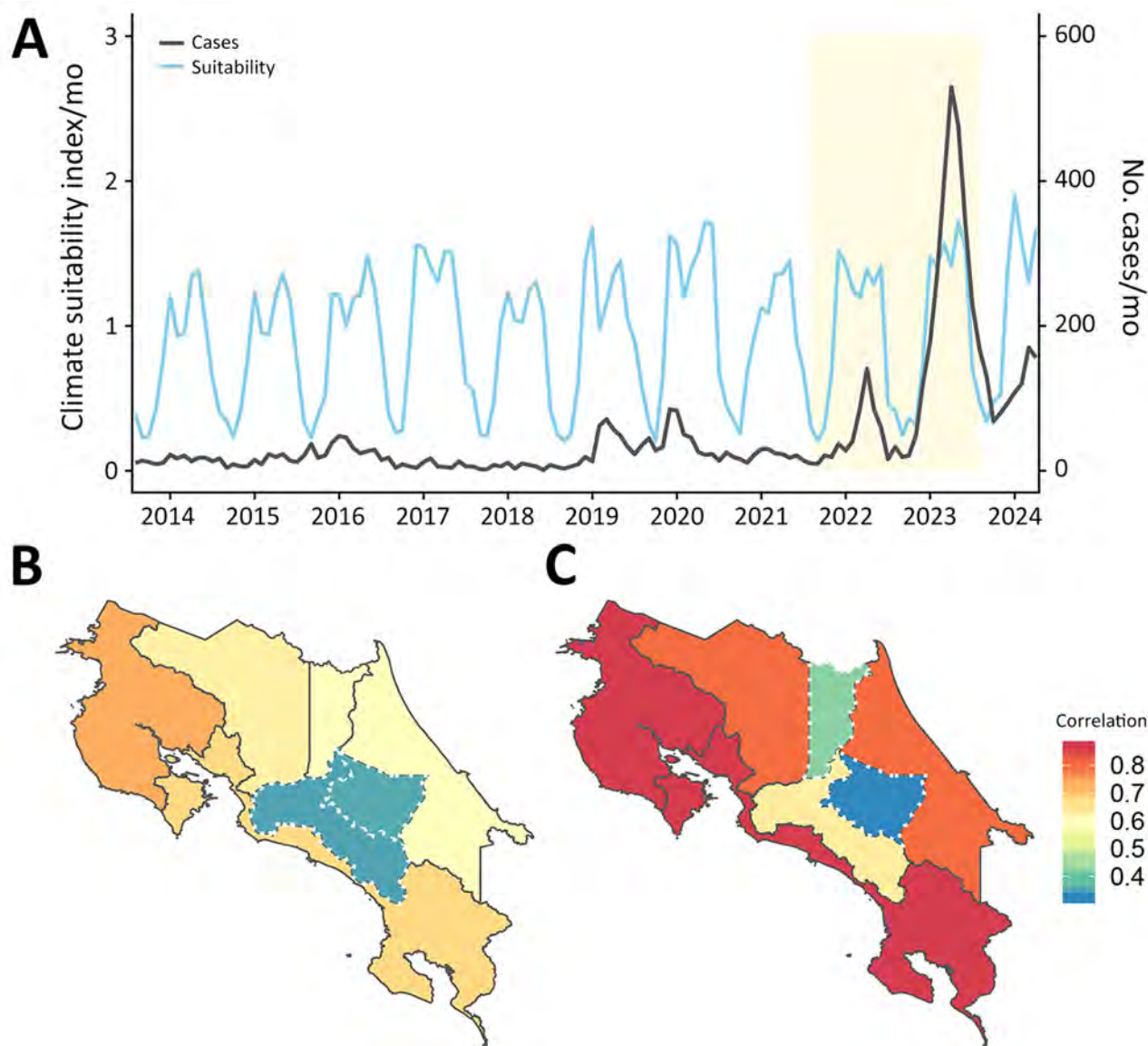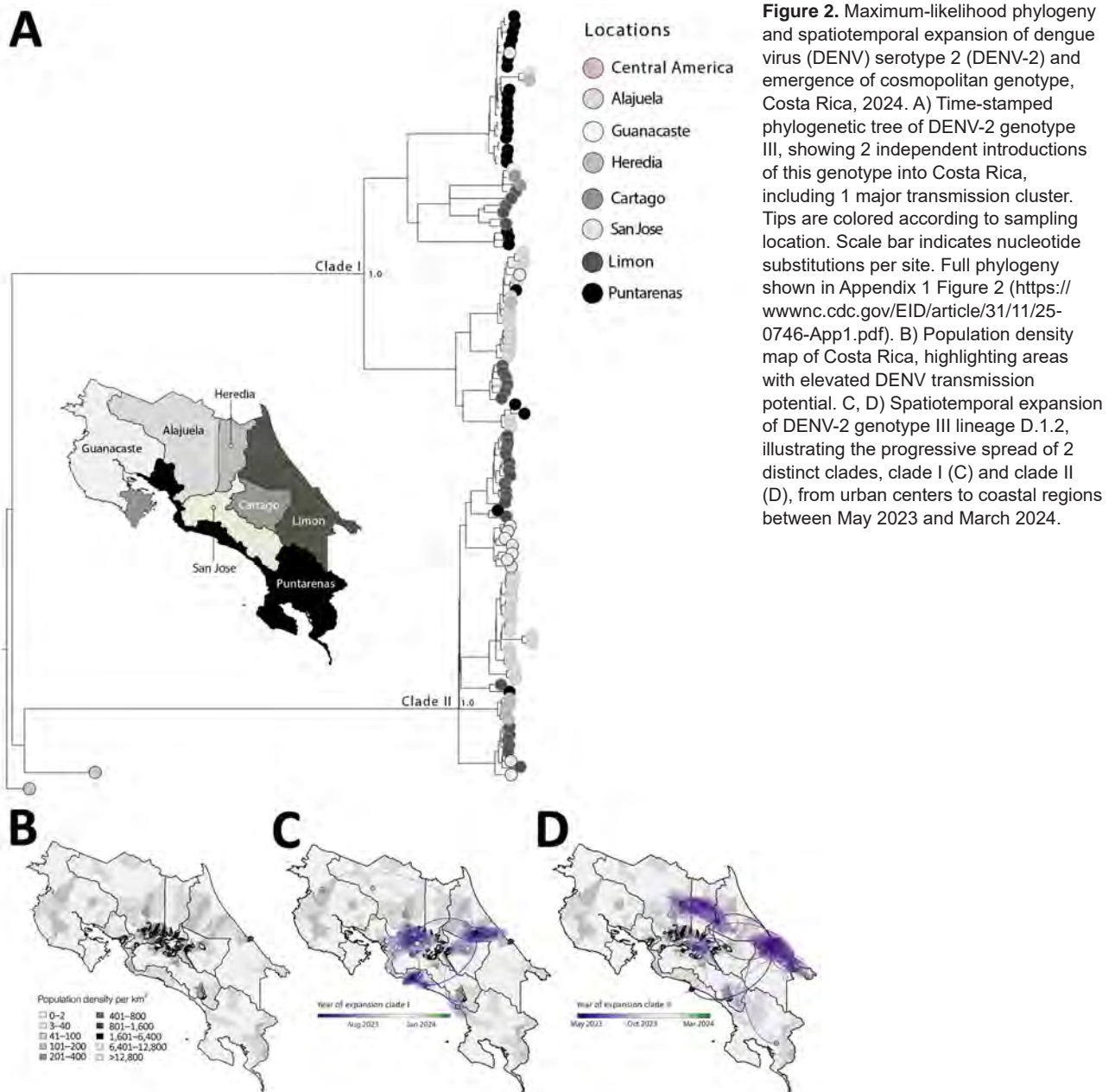

Figure 1. Temporal and spatial correlation between climate-driven suitability and dengue incidence from a study of shifting dynamics of dengue virus serotype 2 and emergence of cosmopolitan genotype, Costa Rica, 2024. A) Time series of monthly dengue cases and climate-driven suitability index for transmission during June 2014–November 2024. Shaded area (yellow) indicates the epidemic period during which enough cases with a clear seasonal signal were reported to enable an estimate correlation between suitability and incidence (Spearman r = 0.38; p<0.05). Scale bars for the y-axes differ substantially to underscore patterns. B, C) Province-level Spearman correlation values between monthly dengue incidence and climate suitability during 2022 (B) and 2023 (C). Warmer colors indicate stronger correlations. White dashed boundaries mark provinces with nonsignificant correlation (p>0.05) and solid dark gray boundaries indicate provinces with statistically significant correlation. In 2023, higher correlations were observed in eastern and coastal provinces where early cases of the dengue virus serotype 2 cosmopolitan genotype were detected.
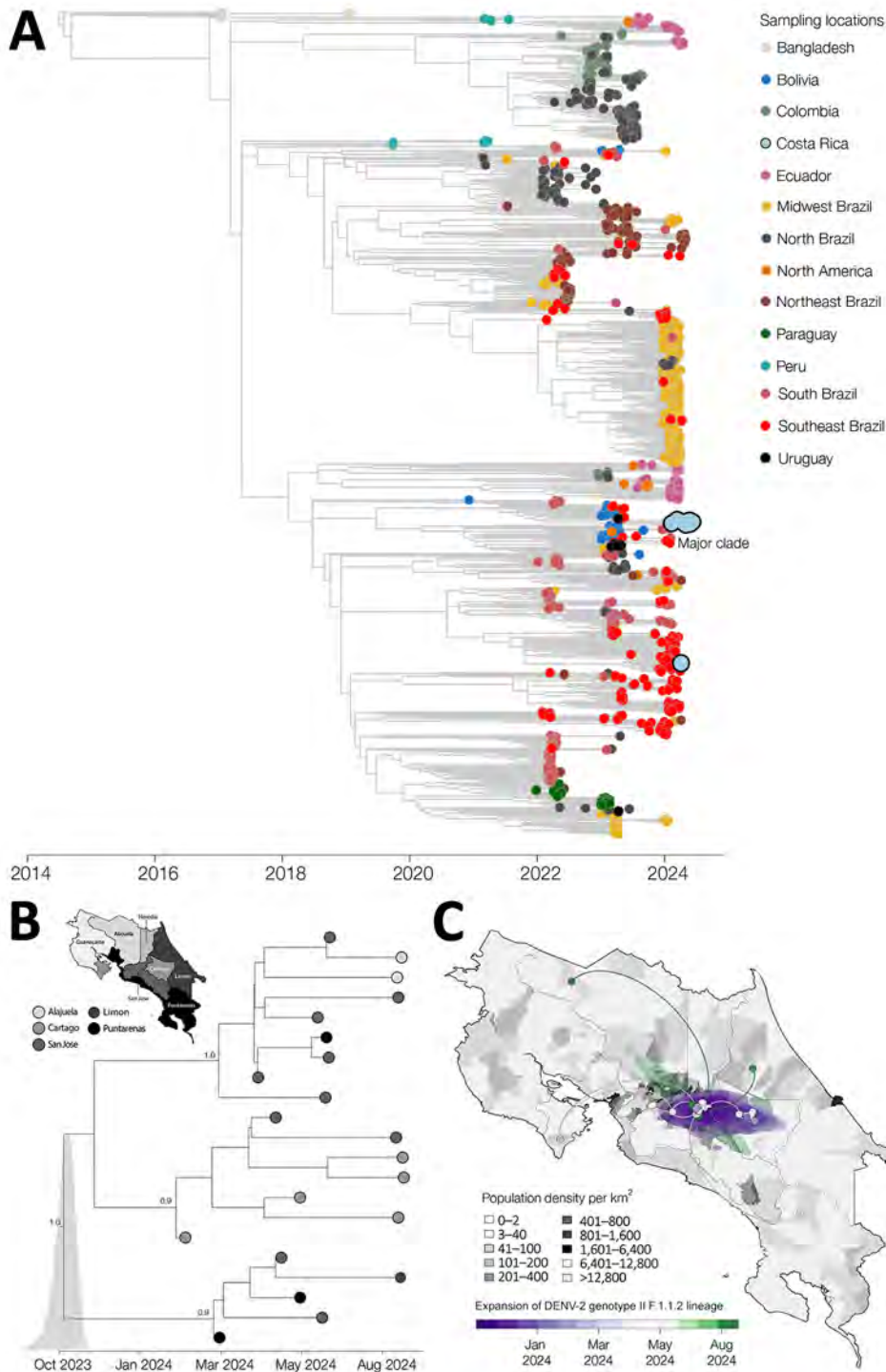
Figure 2. Maximum-likelihood phylogeny and spatiotemporal expansion of dengue virus (DENV) serotype 2 (DENV-2) and emergence of cosmopolitan genotype, Costa Rica, 2024. A) Time-stamped phylogenetic tree of DENV-2 genotype III, showing 2 independent introductions of this genotype into Costa Rica, including 1 major transmission cluster. Tips are colored according to sampling location. Scale bar indicates nucleotide substitutions per site. Full phylogeny shown in Appendix 1 Figure 2 (https://wwwnc.cdc.gov/EID/article/31/11/25-0746-App1.pdf). B) Population density map of Costa Rica, highlighting areas with elevated DENV transmission potential. C, D) Spatiotemporal expansion of DENV-2 genotype III lineage D.1.2, illustrating the progressive spread of 2 distinct clades, clade I (C) and clade II (D), from urban centers to coastal regions between May 2023 and March 2024.

To assess whether those serotype shifts were associated with longer-term changes in age distribution, we analyzed dengue case data spanning 2014–2024, the entire period of available national dengue surveillance. During the years with available dengue reports, age ranges among infected persons changed slightly, but we saw no quantifiably significant change over time (linear slope 0.17; p = 0.048) (Appendix 1 Figure 1, panel B). That estimate did not strongly support a substantial increase in the force-of-infection over time, which was supported by the relatively stable climate-driven suitability estimates (Figure 1). Force-of-infection should be mirrored by a decreasing age of reported infections; however, the age of infection increased slightly by 1.3 years for every extra circulating serotype (p<0.001), independent of year (Appendix Figure 1, panel B). That finding potentially indicates that serotype mixing increased the prevalence for secondary infections, which then occurred in older persons who were already seropositive.

Concurrently, we observed a marked change in circulating DENV-2 strains; the previously dominant genotype III was replaced by genotype II in early 2024 (Appendix 1 Figure 1, panel C). During May 2023–

August 2024, DENV-2 genotype III was more prevalent, particularly in Alajuela, San José, Puntarenas, and Limón, regions historically associated with high DENV transmission. Over time, however, genotype II became increasingly dominant, especially in San José, Cartago, and Alajuela, and genotype III declined. That pattern suggests a gradual replacement, potentially driven by selective advantage, immune escape, or repeated introductions from external sources.

After launching a nationwide genomic surveillance program, Inciensa generated 133 DENV-2 whole-genome sequences during 2023–2024. Using the dynamic DENV lineage classification system (*5*), we assigned 110 genotype III (Asian–American)

Figure 3. Time-scaled and spatiotemporal dynamics of dengue virus serotype 2 (DENV-2) and emergence of cosmopolitan genotype, Costa Rica, 2024. A) Time-scaled phylogenic reconstruction of global DENV-2 showing major clade in Costa Rica in 2024. Full phylogeny shown in Appendix 1 Figure 3 (https://wwwnc.cdc.gov/EID/article/31/11/25-0746-App1.pdf). B) Time-scaled phylogenetic reconstruction of the major DENV-2 genotype II clade, illustrating its expansion from Puntarenas, Limón, and Cartago in early 2024 (map inset). C) Spatiotemporal dynamics of the major DENV-2 genotype II clade in Costa Rica demonstrating its spread among provinces. DENV, dengue virus.

genomes to lineage D.1.2 and 23 genotype II (cosmopolitan) genomes to lineage F.1.1.2. Genotype III sequences were from 110 patients (mean age 38 years) across 7 provinces (Appendix 2 Table 1, https://wwwnc.cdc.gov/EID/article/31/11/25-0746-App2.xlsx); mean genome coverage was 92.6%, and mean cycle threshold was 22. Genotype II sequences were from 23 patients (mean age 38 years) in 5 provinces (Appendix 2 Table 2); mean coverage was 80%, and mean cycle threshold was 24. Phylodynamic analyses showed a well-supported monophyletic clade of DENV-2 genotype III in Costa Rica (Figure 2, panel A; Appendix 1 Figure 2), consistent with sustained local persistence after introduction events from Central America over the previous decade.

Maximum-likelihood phylogenetic reconstruction revealed cocirculation of 2 distinct clades within the DENV-2 genotype III D.1.2 lineage, here referred to as clades I and II (Figure 2, panel B). Although phylogenetically distinct, both clades belong to the same lineage. Phylogeographic analysis showed that early circulation was concentrated in Alajuela, Cartago, and San José, followed by expansion toward the coastal regions of Puntarenas and Limón. Clade I likely emerged in May 2023 (95% highest posterior density [HPD] April–late May 2023) (Figure 2, panel D) and spread from San José and Cartago to Puntarenas and Limón by early 2024. Clade II (Figure 2, panel E), detected as early as June 2023 with a similar HPD, displayed broader dispersal, including to the densely populated areas of Alajuela and San José. The spatial overlap of those sublineages with high-population regions (Figure 2, panel C) underscores the role of urban centers as transmission hubs enabling spread of DENV-2.

Further phylogenetic resolution of DENV-2 genotype II sequences revealed a distinct evolutionary trajectory compared with DENV-2 genotype III (Figure 3, panel A; Appendix 1 Figure 3), supporting the hypothesis of recent introduction followed by rapid establishment in Costa Rica. The time-stamped phylogenetic tree indicated that ≥2 independent introductions of the DENV-2 genotype II F.1.1.2 lineage likely occurred, potentially mediated by regional viral flow from countries in Latin America, including Bolivia and Brazil, and resulted in establishment of a well-supported monophyletic clade. Bayesian time-scaled phylogenetic analysis of that clade suggests emergence around October 2023, with a 95% HPD interval spanning from September to late November 2023. Early circulation was primarily concentrated in Puntarenas, Limón, and Cartago, then subsequently disseminated into San José, Alajuela, and Heredia (Figure 3, panel B). Reconstruction of viral dispersal for that major clade further highlighted its rapid establishment across densely populated areas (Figure 3, panel C). Initially detected in coastal and central provinces, the virus quickly spread into high-transmission hubs, particularly those characterized by high population density.

Conclusions

We used nationwide DENV genomic data and a suitability index to conduct an eco-epidemiologic assessment of dengue in Costa Rica. We documented replacement of DENV-2 Asian–American genotype by DENV-2 cosmopolitan genotype. Using sequencing, phylodynamics, and climate modeling, we showed how viral introductions, ecologic factors, and human mobility shaped transmission. Unlike other settings where genotype shifts were driven by immunity or fitness (6–8), we found no evidence of climate- or age-related increases. DENV-2 II, detected in early 2024, rapidly replaced DENV-2 genotype III despite declining circulation and did not show increased severity or deaths. At least 2 introduction events seeded widespread dissemination, consistent with patterns in Brazil and Southeast Asia (9,10). Now globally dominant, the cosmopolitan genotype has also been reported in Peru, Brazil, and Colombia (3,4,11). Its moderate correlation with climate suitability (r = 0.38) (2,12) and spread into urban centers (13–15) highlight how ecologic and mobility factors can amplify transmission. Those findings underscore the urgent need for real-time genomic surveillance integrated with environmental and mobility data to strengthen early dengue detection and targeted interventions.

About the Author

Dr. González-Elizondo is a researcher at the Centro Nacional de Referencia de Virología, INCIENSA, in Costa Rica. His work focuses on the genomic surveillance and molecular epidemiology of emerging and re-emerging viral pathogens of public health importance.

References

1. Pan-American Health Organization (PAHO). Dengue epidemiological situation in the region of the Americas: epidemiological week 40, 2025 [cited 2025 Mar 22]. https://www.paho.org/en/documents/dengue-epidemiological-situation-region-americas-epidemiological-week-08-2025
2. Nakase T, Giovanetti M, Obolski U, Lourenço J. Population at risk of dengue virus transmission has increased due to coupled climate factors and population growth. Commun Earth Environ. 2024;5:475. https://doi.org/10.1038/s43247-024-01639-6
3. García MP, Padilla C, Figueroa D, Manrique C, Cabezas C. Emergence of the cosmopolitan genotype of dengue virus serotype 2 (DENV2) in Madre de Dios, Peru, 2019. Rev Peru Med Exp Salud Publica. 2022;39:126–8. https://doi.org/10.17843/rpmesp.2022.391.10861
4. Giovanetti M, Pereira LA, Santiago GA, Fonseca V, Mendoza MPG, de Oliveira C, et al. Emergence of dengue virus serotype 2 cosmopolitan genotype, Brazil. Emerg Infect Dis. 2022;28:1725–7. https://doi.org/10.3201/eid2808.220550
5. Hill V, Cleemput S, Pereira JS, Gifford RJ, Fonseca V, Tegally H, et al. A new lineage nomenclature to aid genomic surveillance of dengue virus. PLoS Biol. 2024;22:e3002834. https://doi.org/10.1371/journal.pbio.3002834
6. Holmes EC, Twiddy SS. The origin, emergence and evolutionary genetics of dengue virus. Infect Genet Evol. 2003;3:19–28. https://doi.org/10.1016/S1567-1348(03)00004-2
7. Katzelnick LC, Gresh L, Halloran ME, Mercado JC, Kuan G, Gordon A, et al. Antibody-dependent enhancement of severe dengue disease in humans. Science. 2017;358:929–32. https://doi.org/10.1126/science.aan6836
8. Messina JP, Brady OJ, Golding N, Kraemer MUG, Wint GRW, Ray SE, et al. The current and future global distribution and population at risk of dengue. Nat Microbiol. 2019;4:1508–15. https://doi.org/10.1038/s41564-019-0476-8
9. Yu H, Kong Q, Wang J, Qiu X, Wen Y, Yu X, et al. Multiple lineages of dengue virus serotype 2 cosmopolitan genotype caused a local dengue outbreak in Hangzhou, Zhejiang Province, China, in 2017. Sci Rep. 2019;9:7345. https://doi.org/10.1038/s41598-019-43560-5
10. Colón-González FJ, Gibb R, Khan K, Watts A, Lowe R, Brady OJ. Projecting the future incidence and burden of dengue in Southeast Asia. Nat Commun. 2023;14:5439. https://doi.org/10.1038/s41467-023-41017-y
11. Colombia Instituto Nacional de Salud. Identification of the cosmopolitan genotype circulation of the dengue virus in Columbia [in Spanish] [cited 2025 Mar 22]. https://www.ins.gov.co/BibliotecaDigital/comunicado-tecnico-identificacion-de-la-circulacion-genotipo-cosmopolitan-del-virus-del-dengue-2-en-colombia.pdf
12. Salje H, Lessler J, Maljkovic Berry I, Melendrez MC, Endy T, Kalayanarooj S, et al. Dengue diversity across spatial and temporal scales: local structure and the effect of host population size. Science. 2017;355:1302–6. https://doi.org/10.1126/science.aaj9384
13. Kiang MV, Santillana M, Chen JT, Onnela JP, Krieger N, Engø-Monsen K, et al. Incorporating human mobility data improves forecasts of dengue fever in Thailand. Sci Rep. 2021;11:923. https://doi.org/10.1038/s41598-020-79438-0
14. Gubler DJ. Dengue, urbanization and globalization: the unholy trinity of the 21st century. Trop Med Health. 2011;39:3–11. https://doi.org/10.2149/tmh.2011-S05
15. Grubaugh ND, Ladner JT, Lemey P, Pybus OG, Rambaut A, Holmes EC, et al. Tracking virus outbreaks in the twenty-first century. Nat Microbiol. 2019;4:10–9. https://doi.org/10.1038/s41564-018-0296-2

Address for correspondence: Marta Giovanetti, Oswaldo Cruz Foundation Ringgold Standard Institution, Avenida Brasil 4.365, Rio de Janeiro 21040-360, Brazil; email: giovanetti.marta@gmail.com

Spiroplasma ixodetis in Ticks Removed from Humans, Sweden and Åland Islands, Finland

Malin Lager, Yousif Alkattan, Amanda Sandbacka Karlsson, Louise Fernström,
Anna Grankvist, Christine Wennerås, Marika Nordberg, Dag Nyman,
Per-Eric Lindgren, Pia Forsberg, Peter Wilhelmsson, Anna J. Henningsson

The prevalence of Spiroplasma ixodetis in ticks that have bitten humans in Sweden and in the Åland Islands, Finland, was 2.6%, with observed significant geographic differences between regions. The pathogen was not detected in blood samples from participants bitten by S. ixodetis–positive ticks, indicating low risk for transmission to humans.

Spiroplasma ixodetis, an emerging tickborne bacterium transmitted by Ixodes ricinus ticks, shows a prevalence range of 0.4%–3.0% in questing ticks (1,2) to 13.5% in ticks removed from humans in Europe (3). Human cases of S. ixodetis infection, spiroplasmosis, have been reported from Europe, including Sweden (4,5), in both immunocompetent and immunosuppressed patients; symptoms were more severe in immunosuppressed patients (4,6).

Low awareness, nonspecific symptoms similar to other tickborne infections, and potential co-infection with other tickborne pathogens contribute to misdiagnosis or underdiagnosis (7,8). Because S. ixodetis is an intracellular bacterium, culturing is difficult, and no serologic assays are available; the primary detection tool is PCR. We assessed the risk for human exposure to this pathogen by investigating the prevalence, geographic distribution, and potential coexistence with other tickborne pathogens in feeding ticks removed from humans in Sweden and in the Åland Islands, Finland.

The Study

This study is a part of the Tick-Borne Diseases (TBD) STING study, a prospective multicenter study in Sweden and in the Åland Islands, Finland. The study enrolled 2,327 healthy tick-bitten participants (>18 years of age) at primary healthcare centers (PHCs) in 4 geographic regions (9) (Figure 1) through public advertisements during 2008–2010. The Regional Ethics Review Board in Linköping, Sweden, and the Åland Health Care Ethics Committee approved the study.

We homogenized tick specimens, extracted total nucleic acids, and reverse-transcribed them to cDNA (9) (Appendix, https://wwwnc.cdc.gov/EID/article/31/11/25-0545-App1.pdf). We also extracted DNA from blood plasma collected at inclusion (at the time of the tick bite) and at follow-up 3 months later from participants bitten by a S. ixodetis–positive tick. We detected S. ixodetis in ticks and plasma using a species-specific TaqMan real-time PCR targeting a 170-bp fragment of the RNA polymerase β subunit (10), then performed nucleotide sequencing and verification with BLAST (https://blast.ncbi.nlm.nih.gov/Blast.cgi). We analyzed all S. ixodetis–positive ticks for the presence of nucleic acid from Borrelia burgdorferi sensu lato, B. miyamotoi, tick-borne encephalitis virus, Anaplasma phagocytophilum, Neoehrlichia mikurensis, Babesia spp., and Rickettsia spp. by real-time PCR (11) (Appendix Table 1).

The study consisted of 2,735 I. ricinus ticks: 1,823 nymphs, 689 adults, 118 larvae, and 105 ticks for
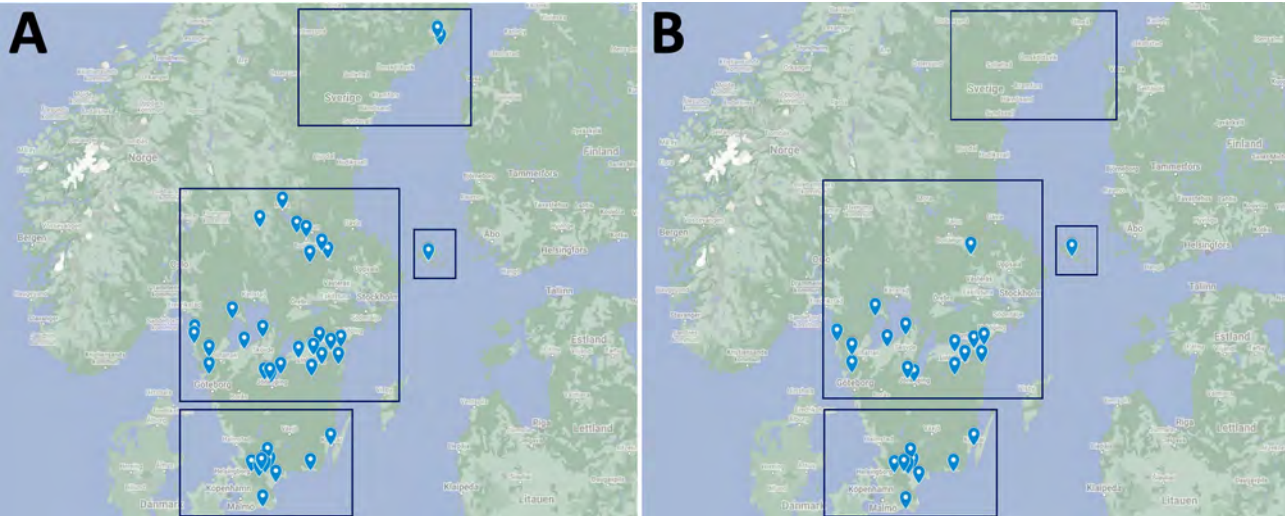
Figure. Locations of primary health care centers in study of *Spiroplasma ixodetis* in ticks removed from humans, Sweden and in the Åland Islands, Finland. Maps indicate all primary health care centers (A) and centers where *Spiroplasma ixodetis*–positive ticks were found (B) in 4 regions: northern Sweden (top boxes), southcentral Sweden (center left boxes), southernmost Sweden (bottom boxes), and the Åland Islands, Finland (center right boxes). Source: Google Maps (https://www.google.com/maps).

which we could not determine developmental stage (Table 1). The blood feeding time range was <24 to >72 hours (Appendix Table 2). Most (n = 1,156) ticks were collected in southcentral Sweden, followed by the Åland Islands (n = 950), southernmost Sweden (n = 605), and northern Sweden (n = 24) (Table 2). In total, 72 ticks (2.6%) were positive for *S. ixodetis*; of those, 60 showed $\geq$99.42% sequence identity with *S. ixodetis* strain sHm (GenBank accession no. AP026933.1). All plasma samples from study participants bitten by a *S. ixodetis*–containing tick yielded negative PCR results.

We found no statistical differences in the prevalence of *S. ixodetis* among the different developmental stages of the ticks (Table 1); however, we found a statistically significant difference in geographic distribution of *S. ixodetis*–positive ticks between southcentral Sweden and southernmost Sweden (p = 0.0004), southcentral Sweden and the Åland Islands (p = 0.00005), and southernmost Sweden and the Åland

Islands (p<0.00001). No ticks collected in northern Sweden were positive for *S. ixodetis*.

In total, 26 (36%) of the *S. ixodetis*–positive ticks contained $\geq$1 additional pathogens, mainly species in the *B. burgdorferi* s.l. complex (n = 14), of which most were *B. afzelii*. Coexistence of *S. ixodetis* and other tick-borne pathogens was less common. Fifteen of the ticks with coexisting pathogens were nymphs, and 11 were adult females. Three ticks carried 3 pathogens: *S. ixodetis*, *B. burgdorferi* s.l., and *N. mikurensis* (Appendix Table 2). We found no statistically significant difference between observed frequency (17%) and expected frequency (19%) for coexistence between *S. ixodetis* and *B. burgdorferi* s.l. bacteria, suggesting that coexistence does not appear more often than expected by chance based on the prevalences of the individual pathogens (p = 0.738). We found statistically significant differences in geographic distribution of ticks with coexistence, regardless of pathogens, between southcentral Sweden and southernmost Sweden (p = 0.0004), southcentral Sweden and the Åland Islands (p = 0.04), and southernmost Sweden and the Åland Islands (p<0.00001).

Table 1. Ticks testing positive for *Spiroplasma ixodetis*, by developmental stage, in study of *S. ixodetis* in ticks removed from humans, Sweden and Åland Islands, Finland

Developmental stage	Total no. (%)	No. (%) positive *
Larva	118 (4.0)	3 (2.5)
Nymph	1,823 (67)	44 (2.4)
Adult	689 (25)	22 (3.2)
F	654 (24)	21 (3.2)
M	35 (1.3)	1 (2.9)
Not determined†	105 (4.0)	3 (2.9)
Total	2,735 (100.0)	72 (2.6)

*Percentage calculated based on the number of *S. ixodetis*–positive ticks in relation to the total number of ticks in the study per developmental stage.
†Developmental stage could not be determined because of damage to ticks during removal from host.

Table 2. Distribution of collected and *Spiroplasma ixodetis*–positive ticks, by geographic region, Sweden and in the Åland Islands, Finland

Region	Total no. (%)	No. (%) positive *
Southcentral Sweden	1,156 (42)	31 (2.7)
Åland Islands, Finland	950 (35)	4 (0.42)
Southernmost Sweden	605 (22)	37 (6.1)
Northern Sweden	24 (1.0)	0

*Percentage calculated based on the number of *S. ixodetis*–positive ticks in relation to the total number of ticks in the study per region.

Conclusions

The overall prevalence of *S. ixodetis* in *I. ricinus* ticks removed from humans was 2.6%, with statistically significant differences in distribution between geographic areas. *S. ixodetis*–positive ticks were found in all developmental stages, including larvae, suggesting transovarial transmission of the bacterium. The prevalence in our study is consistent to previous studies showing a prevalence of 0.4%–3% in questing ticks (*1*,*2*). The number of ticks analyzed from northern Sweden was low, which can explain the negative results in this area. However, because of climate changes and raised temperatures, more suitable habitats for ticks and hosts might result in the spread of *S. ixodetis*–infected ticks into new areas (*12*). Few *S. ixodetis*–positive ticks were detected in the Åland Islands, an area with high tick density, highly endemic for *B. burgdorferi* s.l. and tick-borne encephalitis virus (*9*,*13*). That finding indicates that endemic areas for one pathogen may not be endemic for others.

The negative PCR results in plasma from participants who did not necessarily show symptoms related to tickborne diseases were consistent with a previous study (*3*). In that study, patients with influenza-like symptoms and erythema migrans also showed negative results in blood after being bitten by a tick carrying *S. ixodetis*. Even though *S. ixodetis* bacteria have been detected in blood (*4*), knowledge of the optimal time of sampling or the frequency of the pathogen in blood is limited. The inclusion sample was collected only days after the tick bite, perhaps before a potential bacteremia, and the follow-up sample was collected 3 months after a potential acute infection, which may be the reason for the negative outcome. No time lag for transmission has been established as of November 2025; because *S. ixodetis* is located in the midgut of the tick, we hypothesize that the time lag could be similar to that of *Borrelia* spp. transmission, 24–48 hours (*9*).

Most of the ticks carrying >1 pathogen contained both *S. ixodetis* and *B. burgdorferi* s.l. bacteria. That finding was not surprising because *Borrelia* spp. bacteria, mainly *B. afzelii*, are the most common pathogens found in questing ticks in Europe (*14*).

Our study used samples collected >15 years ago; although our findings might not reflect the current situation, they provide relevant epidemiologic insights into the prevalence and geographic distribution of *S. ixodetis*. Although we were unable to sequence all *S. ixodetis*–positive ticks, mainly because of high cycle threshold values (>35), we believe the real-time PCR findings are trustworthy because primers and probe are designed for species-specific detection.

Further studies are needed to expand our understanding of prevalence, geographic distribution, and the possibility of co-infection of tickborne *S. ixodetis*. Our results indicate low risk of being infected by *S. ixodetis* after a tick bite; however, spiroplasmosis and co-infections should be considered as differential diagnoses in cases of fever after a tick bite (*4*,*8*).

About the Author

Dr. Lager has a PhD in diagnostics of tickborne diseases at Linköping University. Her research interests concern molecular analyses of ticks, molecular and serological diagnostics of tickborne diseases on human samples, and the development of new molecular methods.

References

1. Olsthoorn F, Sprong H, Fonville M, Rocchi M, Medlock J, Gilbert L, et al. Occurrence of tick-borne pathogens in questing *Ixodes ricinus* ticks from Wester Ross, northwest Scotland. Parasit Vectors. 2021;14:430.
2. Subramanian G, Sekeyova Z, Raoult D, Mediannikov O. Multiple tick-associated bacteria in *Ixodes ricinus* from Slovakia. Ticks Tick Borne Dis. 2012;3:406–10.
3. Geebelen L, Lernout T, Tersago K, Terryn S, Hovius JW, Docters van Leeuwen A, et al. No molecular detection of tick-borne pathogens in the blood of patients with erythema migrans in Belgium. Parasit Vectors. 2022;15:27.
4. Eimer J, Fernström L, Rohlén L, Grankvist A, Loo K, Nyman E, et al. *Spiroplasma ixodetis* infections in immunocompetent and immunosuppressed patients after tick exposure, Sweden. Emerg Infect Dis. 2022;28:1681–5.
5. Matet A, Le Flèche-Matéos A, Doz F, Dureau P, Cassoux N. Ocular *Spiroplasma ixodetis* in newborns, France. Emerg Infect Dis. 2020;26:340–4.
6. Aquilino A, Masiá M, López P, Galiana AJ, Tovar J, Andrés M, et al. First human systemic infection caused by *Spiroplasma*. J Clin Microbiol. 2015;53:719–21.
7. Lernout T, De Regge N, Tersago K, Fonville M, Suin V, Sprong H. Prevalence of pathogens in ticks collected from humans through citizen science in Belgium. Parasit Vectors. 2019;12:550.
8. Madison-Antenucci S, Kramer LD, Gebhardt LL, Kauffman E. Emerging tick-borne diseases. Clin Microbiol Rev. 2020;33:e00083-18.
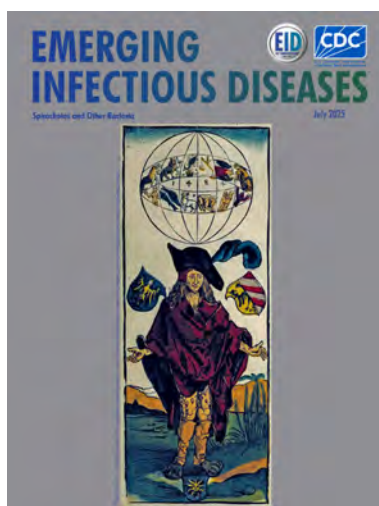
9. Wilhelmsson P, Lindblom P, Fryland L, Ernerudh J, Forsberg P, Lindgren PE. Prevalence, diversity, and load of *Borrelia* species in ticks that have fed on humans in regions of Sweden and Åland Islands, Finland with different Lyme borreliosis incidences. PLoS One. 2013;8:e81433.

10. Krawczyk AI, Van Duijvendijk GL, Swart A, Heylen D, Jaarsma RI, Jacobs FH, et al. Effect of rodent density on tick and tick-borne pathogen populations: consequences for infectious disease risk. Parasit Vectors. 2020;13:1–17

11. Gyllemark P, Wilhelmsson P, Elm C, Hoornstra D, Hovius JW, Johansson M, et al. Are other tick-borne infections overlooked in patients investigated for Lyme neuroborreliosis? A large retrospective study from south-eastern Sweden. Ticks Tick Borne Dis. 2021;12:101759.

12. Jaenson TG, Jaenson DG, Eisen L, Petersson E, Lindgren E. Changes in the geographical distribution and abundance of the tick *Ixodes ricinus* during the past 30 years in Sweden. Parasit Vectors. 2012;5:8.

13. Carlströmer Berthén N, Tompa E, Olausson S, Nyberg C, Nyman D, Ringbom M, et al. The AxBioTick study: *Borrelia* species and tick-borne encephalitis virus in ticks, and clinical responses in tick-bitten individuals on the Aland Islands, Finland. Microorganisms. 2023;11:1100.

14. Strnad M, Hönig V, Růžek D, Grubhoffer L, Rego ROM. Europe-wide meta-analysis of Bo*rrelia burgdorferi* sensu lato prevalence in questing *Ixodes ricinus* ticks. Appl Environ Microbiol. 2017;83:e00609-17.

Address for correspondence: Malin Lager (née Christiansson), Laboratory Medicine, Department of Clinical Microbiology, Ryhov County Hospital, SE-551 85 Jönköping, Sweden; email: malin.lager@rjl.se

---

July 2025

Spirochetes and Other Bacteria

EMERGING INFECTIOUS DISEASES®

Two Autochthonous Cases of Anaplasmosis, Washington, USA, 2022–2023

Hannah Schnitzler,[1] Mary Chan,[1] Jeni Nybo, Kelley Palmer-McGee, Zachary Doobovsky,
Ian Tracy, Siu-Kei Chow, Roumen B. Iordanov, Eugene H. Lee, Julianna R. Van Enk,
Elizabeth A. Dykstra, Beth A. Lipton, Hanna N. Oltean

We describe 2 cases of autochthonous human anaplasmosis in Washington, USA, where anaplasmosis has been rarely reported. Clinicians should consider anaplasmosis in the differential diagnosis for patients with compatible clinical symptoms after tick bite or time spent outdoors in an area where *Ixodes pacificus* ticks are present.

Anaplasmosis is a tickborne disease caused by *Anaplasma phagocytophilum*, a bacterium spread by some *Ixodes* spp. ticks (*1*). *I. pacificus*, the western black-legged tick, is the primary vector for *A. phagocytophilum* on the West Coast of the United States (*2*). Most patients with anaplasmosis experience moderate illness, including fever, malaise, headache, myalgia, nausea, vomiting, or diarrhea (*3–6*). The disease can progress to severe illness, with 31% of reported case-patients hospitalized, and rarely to death; the case-fatality rate is 0.3% in the United States (*7*). The risk for severe illness increases with advanced patient age, immunosuppression, and delayed diagnosis and treatment (*6,7*). Laboratory testing often shows transaminitis and cytopenias, including anemia, thrombocytopenia, and leukopenia (*3–6*). Peripheral blood smear tests may show morulae in granulocytes during acute illness, but that test is not a sensitive method for diagnosis (*4,8*). Definitive diagnosis relies on molecular testing, immunohistochemistry, or culture. Serologic testing is less specific (*4*).

The seasonality of human anaplasmosis cases in the United States coincides with vector activity. Nymphal *Ixodes* spp. ticks are active during March through early July; most anaplasmosis cases in the United States occur during May–August. A smaller peak in cases takes place during October–November, when adult *Ixodes* ticks are active (*9*).

In Washington, USA, the range of *I. pacificus* ticks encompasses western Washington and the eastern slopes of the Cascade mountains (*10*). Tick surveillance conducted by the Washington State Department of Health during 2011–2017 identified *A. phagocytophilum* in *I. pacificus* and *I. spinipalpis* ticks (*2*). Despite detection of *A. phagocytophilum* in ticks in the state, reports of autochthonous cases are rare but have been documented in canines with no recent travel outside of western Washington (*11*). We describe 2 reported human cases of autochthonous anaplasmosis in Washington.

The Case-Patients

In July 2022, an 81-year-old man (case-patient 1) visited an urgent care center with symptoms of fever (starting that day), shortness of breath, and dizziness. His medical history was notable for paroxysmal atrial fibrillation, congestive heart failure with dyspnea on exertion, pulmonary embolism, hypertension, dyslipidemia, and stroke. Bloodwork revealed thrombocytopenia (78,000 platelets/μL; reference range 140,000–400,000 platelets/μL), elevated aspartate aminotransferase (58 U/L; reference 10–35 U/L), and acute kidney injury with elevated blood urea nitrogen (32 mg/dL; reference 7–25 mg/dL) and creatinine

[1]These authors contributed equally to this article.

(1.51 mg/dL; reference 0.70–1.22 mg/dL). Treating physicians discharged the patient with instructions to return for care if his symptoms worsened.

The patient sought treatment at an emergency department 2 days later for worsening shortness of breath, fatigue, weakness, and fever reaching 103°F. His platelet count had worsened to 44,000 platelets/µL, and his aspartate aminotransferase level was 86 U/L. A computed tomography angiogram identified mild cardiomegaly and trace bilateral pleural effusion but no pulmonary embolism. Computed tomography of the abdomen and pelvis revealed unremarkable results, and results of a respiratory virus panel (Biofire Respiratory 2.1 Panel, https://www.biofiredx.com) were negative. The patient received a dose of ceftriaxone and was admitted to the hospital. Consultation with infectious disease specialists prompted blood sample collection for tickborne disease testing, and physicians initiated empiric doxycycline 3 days after admission. The patient showed improvement in platelet count and liver function on that day and was discharged. Five days after discharge, the patient's blood sample results returned positive for *A. phagocytophilum* by qualitative real-time PCR conducted at a commercial laboratory, and physicians prescribed a continued 10-day course of doxycycline. His symptoms resolved ≈1 month after discharge.

The commercial laboratory reported the patient's PCR results to the local health jurisdiction, who forwarded the sample to the Centers for Disease Control and Prevention (Atlanta, GA, USA), where real-time PCR and sequence analysis confirmed *A. phagocytophilum.* Upon interview, the patient reported no travel outside of Washington state and no tick detections or tick bites during the exposure period (5−21 days before symptom onset). Three weeks before symptom onset, the patient did visit Mason County, Washington, for several days and performed yard work in an area where a neighbor recently reported a tick bite. Public health officials presumed that location to be the patient's likely exposure location. Environmental investigation did not begin until April 2023, because nymphal ticks are not likely to be active in August; however, limited drag sampling in April revealed no ticks for collection.
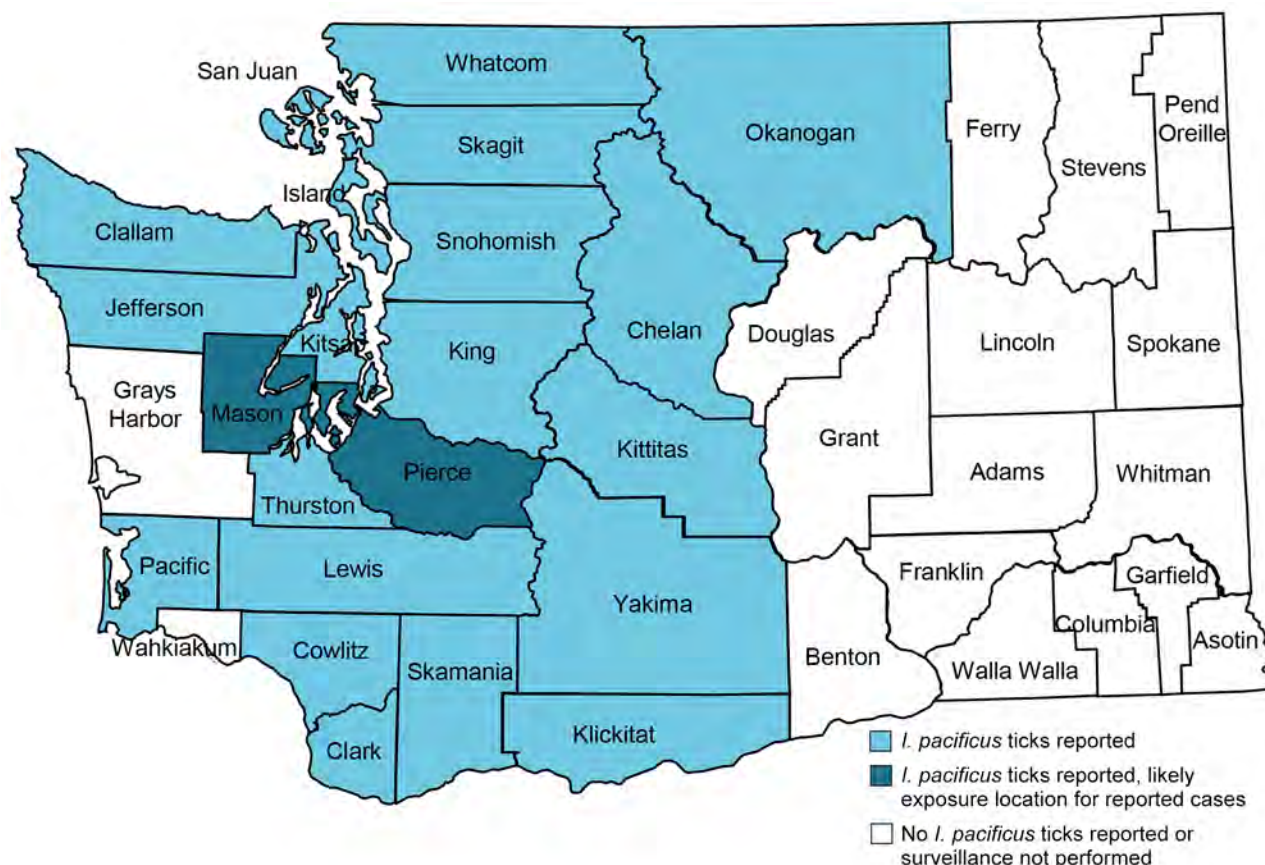

Figure. Geographic data from a study of 2 autochthonous cases of anaplasmosis, Washington, USA, 2022–2023. Blue indicates counties where health investigators have reported *I. pacificus* ticks (*12*); dark blue indicates counties of likely exposure for the 2 cases reported.

In June 2023, a woman (case-patient 2) residing in Washington began experiencing fever, back pain, neck stiffness, and headache. The woman had a history of psoriasis and hypothyroidism, managed with levothyroxine and a topical corticosteroid. Four days after symptom onset, she visited an urgent care center, where peripheral blood smear testing showed evidence of circulating, unidentified atypical cells and neutropenia, suggesting an infectious disease process or leukemia. Attending physicians discharged the patient with instructions to seek care if symptoms worsened. The woman visited an emergency department 2 days later, reporting fever, severe headache, back pain, and neck stiffness. Physicians admitted her to the hospital, where bloodwork revealed leukopenia (leukocytes 2,540/µL; reference range 4,000–12,000/µL), thrombocytopenia (platelets 96,000/µL reference 150,000–450,000/µL), anemia (erythrocytes 3.5 million/µL; reference 4–5.5 million/µL), and transaminitis (alanine transaminase 691 IU/L, reference 6–60 IU/L; aspartate aminotransferase 786 IU/L, reference 5–40 IU/L; alkaline phosphatase 435 IU/L, reference 28–126 IU/L). Computed tomography showed hepatosplenomegaly but no other abnormalities, and additional serologic testing showed negative results for cytomegalovirus, hepatitis (A, B, and C), HIV, and *Toxoplasma.* A respiratory virus panel (VERIGENE Respiratory Pathogens *Flex* Test, https://us.diasorin.com) and 2 sets of blood cultures revealed negative results. The patient tested positive for group A *Streptococcus* on throat culture and had low-level viremia with Epstein-Barr virus, although antibody testing was negative. An infectious disease specialist consulted on the day of admission recommended an extensive work-up for viral and tickborne diseases, and attending physicians initiated a course of cefepime and doxycycline the next day. A blood sample collected the day after admission tested positive for *A. phagocytophilum* via real-time PCR on day 6 of hospitalization, and physicians prescribed a continuing regimen of doxycycline for 10 days. Thrombocytopenia and leukopenia resolved 4 days after starting doxycycline, and physicians discharged the patient 10 days after admission, noting gradual improvement in symptoms.

The hospital laboratory reported the real-time PCR results for this patient to officials at the local health jurisdiction, who interviewed the patient. The patient reported hiking in multiple parks in Pierce County, but no travel outside of Washington during the exposure period. No environmental investigation took place because the patient did not report a tick bite and researchers could identify no single exposure location.

Conclusion

Washington is a low incidence region for tickborne diseases (2), posing a challenge for public health surveillance, prevention communication, and provider education. We charted the counties in Washington with documented *I. pacificus* tick presence and the suspected counties of exposure for the 2 human cases of anaplasmosis (Figure).

Clinicians should be aware of the local presence of *A. phagocytophilum* and the distribution of *I. pacificus* ticks in Washington. *I. pacificus* ticks can also transmit *Borrelia burgdorferi* sensu stricto, the causative agent of Lyme disease, and *Borrelia miyamotoi*, the causative agent of hard tick relapsing fever (2). Health officials have increased tick surveillance in Washington, noting increased *I. pacificus* ticks activity in spring and most ticks collected during March−May (2,13). To support prompt diagnosis and treatment of suspected tickborne disease among Washington residents, clinicians should consider travel history, exposure to tick habitats, seasonality in tick activity, and the patient's clinical manifestations. More robust tick surveillance in the state could help better define vector distribution, abundance, and infection risk to inform public health prevention messaging and provider education.

About the Author

Dr. Schnitzler is a zoonotic and vectorborne disease epidemiologist with the Washington State Department of Health, Office of Communicable Disease Epidemiology. Her research interests include the epidemiology and prevention of zoonotic and vectorborne diseases, using a One Health approach.

References

1. Chen SM, Dumler JS, Bakken JS, Walker DH. Identification of a granulocytotropic *Ehrlichia* species as the etiologic agent of human disease. J Clin Microbiol. 1994;32:589–95. https://doi.org/10.1128/jcm.32.3.589-595.1994
2. Dykstra EA, Oltean HN, Kangiser D, Marsden-Haug N, Rich SM, Xu G, et al. Ecology and epidemiology of tickborne

pathogens, Washington, USA, 2011–2016. Emerg Infect Dis. 2020;26:648–57. https://doi.org/10.3201/eid2604.191382

3. Bakken JS, Krueth J, Wilson-Nordskog C, Tilden RL, Asanovich K, Dumler JS. Clinical and laboratory characteristics of human granulocytic ehrlichiosis. JAMA. 1996;275:199–205. https://doi.org/10.1001/jama.1996.03530270039029

4. Biggs HM, Behravesh CB, Bradley KK, Dahlgren FS, Drexler NA, Dumler JS, et al. Diagnosis and management of tickborne rickettsial diseases: Rocky Mountain spotted fever and other spotted fever group rickettsioses, ehrlichioses, and anaplasmosis—United States. MMWR Recomm Rep. 2016;65:1–44. https://doi.org/10.15585/mmwr.rr6502a1

5. Bakken JS, Krueth J, Wilson-Nordskog C, Tilden RL, Asanovich K, Dumler JS. Clinical and laboratory characteristics of human granulocytic ehrlichiosis. JAMA. 1996;275:199–205. https://doi.org/10.1001/jama.1996.03530270039029

6. Bakken JS, Dumler S. Human granulocytic anaplasmosis. Infect Dis Clin North Am. 2008;22:433–48, viii. https://doi.org/10.1016/j.idc.2008.03.011

7. Dahlgren FS, Heitman KN, Drexler NA, Massung RF, Behravesh CB. Human granulocytic anaplasmosis in the United States from 2008 to 2012: a summary of national surveillance data. Am J Trop Med Hyg. 2015;93:66–72. https://doi.org/10.4269/ajtmh.15-0122

8. Schotthoefer AM, Meece JK, Ivacic LC, Bertz PD, Zhang K, Weiler T, et al. Comparison of a real-time PCR method with serology and blood smear analysis for diagnosis of human anaplasmosis: importance of infection time course for optimal test utilization. J Clin Microbiol. 2013;51:2147–53. https://doi.org/10.1128/JCM.00347-13

9. Centers for Disease Control and Prevention. Anaplasmosis—epidemiology and statistics [cited 2023 Oct 10]. https://www.cdc.gov/anaplasmosis/hcp/statistics/index.html

10. Eisen RJ, Eisen L, Beard CB. County-scale distribution of *Ixodes scapularis* and *Ixodes pacificus* (Acari: Ixodidae) in the continental United States. J Med Entomol. 2016;53:349–86. https://doi.org/10.1093/jme/tjv237

11. Poitout FM, Shinozaki JK, Stockwell PJ, Holland CJ, Shukla SK. Genetic variants of *Anaplasma phagocytophilum* infecting dogs in western Washington State. J Clin Microbiol. 2005;43:796–801. https://doi.org/10.1128/JCM.43.2.796-801.2005

12. Centers for Disease Control and Prevention. CDC tick surveillance data sets. December 2023 [cited 2024 Jan 4]. https://www.cdc.gov/ticks/surveillance/TickSurveillanceData.html

13. Washington State Department of Health. Washington tracking network—tick data dashboard. [cited 2023 Oct 10]. https://doh.wa.gov/data-and-statistical-reports/washington-tracking-network-wtn/tick-data/tick-dashboard

Address for correspondence: Hannah R. Schnitzler, Washington State Department of Health, 1610 NE 150th St, Shoreline, WA 98155, USA; email: hannah.schnitzler@doh.wa.gov

etymologia revisited

Schizophyllum commune

[skiz-of'-ĭ-ləm kom'-yoon]

Schizophyllum commune, or split-gill mushroom, is an environmental, wood-rotting basidiomycetous fungus. *Schizophyllum* is derived from "*Schíza*" meaning split because of the appearance of radial, centrally split, gill-like folds; "*commune*" means common or shared ownership or ubiquitous. Swedish mycologist Elias Magnus Fries (1794–1878) the Linnaeus of Mycology assigned the scientific name in 1815. German mycologist Hans Kniep in 1930 discovered its sexual reproduction by consorting and recombining genomes with any one of numerous compatible mates (currently >2,800).

Originally published in March 2022

References

1. Chowdhary A, Kathuria S, Agarwal K, Meis JF. Recognizing filamentous basidiomycetes as agents of human disease: a review. Med Mycol. 2014;52:782–97. https://doi.org/10.1093/mmy/myu047

2. Cooke WB. The genus *Schizophyllum*. Mycologia. 1961;53:575–99. https://doi.org/10.1080/00275514.1961.12017987

3. Greer DL. Basidiomycetes as agents of human infections: a review. Mycopathologia. 1978;65:133–9. https://doi.org/10.1007/BF00447184

4. O'Reilly P. *Schizophyllum commune*, split gill fungus, 2016 [cited 2021 Aug 23]. https://www.first-nature.com/fungi/schizophyllum-commune.php

5. Raper CA, Fowler TJ. Why study *Schizophyllum*? Fungal Genet Rep. 2004;51:30–6. https://doi.org/10.4148/1941-4765.1142

https://wwwnc.cdc.gov/eid/article/28/3/et-2803_article

Borrelia afzelii Hepatitis in Patient Treated with Venetoclax and Obinutuzumab, Switzerland

Gioele Capoferri, Raphael Battegay, Baptiste Hamelin, Peter M. Keller, Kirsten D. Mertz, Maja Weisser

We report *Borrelia afzelii* hepatitis in an immunosuppressed patient in Switzerland receiving anti-CD20 therapy and venetoclax. Diagnosis was made by metagenomic sequencing and PCR. This case underscores the need to consider Lyme borreliosis in unexplained hepatitis cases and highlights the value of molecular diagnostics in immunosuppressed patients when serologic test results are negative.

Lyme borreliosis (LB) presents a wide range of clinical manifestations across its stages. Early localized infection (stage 1) typically manifests as erythema migrans, whereas later stages involve systemic complications (*1,2*). In North America, *Borrelia burgdorferi* sensu stricto is the predominant causative agent (*3*). Possible manifestations of early dissemination are multiple erythema migrans, arthritis, or acute neuroborreliosis (*1,2*). In Europe, *B. afzelii* and *B. garinii* are more common causes (*3*); *B. afzelii* is the most frequent cause of erythema migrans, lymphocytoma, and acrodermatitis chronica atrophicans, and *B. garinii* primarily causes neuroborreliosis (*1,2*). Although mild hepatopathy occurs in up to 27% of LB cases in the United States (*4*) and in 14%–15% of cases in Europe (*5*), hepatic infection by *Borrelia* spp. is rare (*6*). We report a case of hepatic infection caused by *B. afzelii* in a patient in Switzerland with chronic lymphocytic leukemia (CLL) receiving venetoclax and obinutuzumab. Written informed consent for participation in this case report was obtained from the patient by the authors.

The Case

A 62-year-old white woman with CLL diagnosed in 2016 was managed with watchful waiting until late 2023, when biopsy-confirmed leukemia cutis

developed on her right shoulder. In March 2024, she began a chemotherapy regimen of obinutuzumab, a novel anti-CD20 monoclonal antibody, and venetoclax. One week later, she reported nonpruritic erythematous rashes on her legs; the first appeared on the right ankle, and additional rashes spread to the right and left leg. Clinically, multiple circular erythematous exanthemas with a maximum diameter of 10 cm were present on both legs (Figure 1). After 2 weeks, the rash on the left leg had further expanded, exhibiting discrete central clearing (Figure 1). In addition to that progression, similar new exanthemas appeared on the trunk and both arms (Figure 1). A skin biopsy showed a mild superficial and deep lymphocytic perivascular dermatitis (Figure 2, panel A). Initial test results for *Borrelia* IgM were negative; borderline IgG elevation was noted (10.78 AU/mL [reference <10 AU/mL]) (Diasorin, https://int.diasorin.com). Results of immunoblot (Virotech, http://www.virotechdiagnostics.com) were positive only for variable major protein-like sequence, expressed. Topical steroids were initiated for suspected morphea.

One month later, the exanthemas showed slight improvement, except for those on the right arm and upper chest (Figure 1). At that time, the patient began experiencing persistent fever of temperatures exceeding 38.5°C and elevated C-reactive protein (84 mg/L [reference <10 mg/L]); leukocyte and transaminase levels were within reference ranges, but cholestatic parameters were mildly elevated (gamma-glutamyl transferase 55 U/L [reference 6–40 U/L]; alkaline phosphatase 317 U/L [reference 35–105 U/L]). Results of a whole-body computed tomography scan were unremarkable. A drug fever was suspected; venetoclax and obinutuzumab were discontinued in June 2024. Three weeks later, the patient was hospitalized for persistent fever, worsening cholestatic parameters (gamma-glutamyl transferase189 U/L, alkaline phosphatase 804 U/L), new hepatitis (aspartate transferase
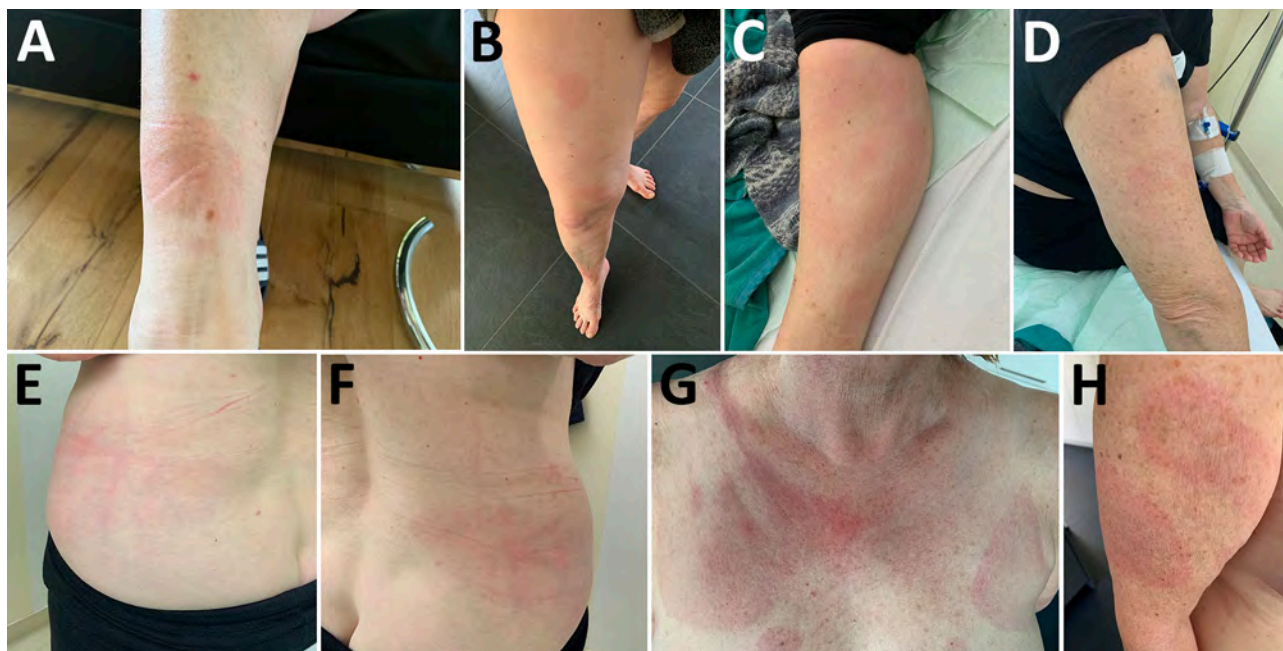
Figure 1. Evolution of cutaneous findings for reported case of early disseminated Lyme borreliosis with multiple erythema migrans and hepatitis in 62-year-old immunosuppressed patient treated with venetoclax and obinutuzumab, Switzerland. A) Oval erythematous rash on the anterior aspect of the right ankle, first lesion to appear (February 20, 2024). B) Right leg with 2 new additional circular/oval patches located on the anterior thigh and anterior knee (March 3, 2024). C–F) Worsening of the exanthemas, with expanding red rash and central clearing (targetoid appearance) on the left leg (C) and onset of red macules on the right arm (D) and the left (E) and right (F) posterolateral trunk (April 9, 2024). G–H) Macules on the décolleté (G) and evolution of cutaneous findings on the right arm, including the appearance of an additional macule (H) (April 27, 2024).

140 U/L [reference 11–34 U/L], alanine transaminase 80 U/L [reference 8–41 U/L]), and elevated C-reactive protein (120 mg/L). Results of serologic testing and PCR were negative for hepatitis B, C, and E; Epstein-Barr virus; cytomegalovirus; herpes simplex virus; adenovirus; HIV; *Bartonella henselae*; *Coxiella burnetii*; *Brucella* spp.; *Toxoplasma gondii*; *Schistosoma* spp.; *Leishmania* spp.; and dimorphic fungi. Results of blood cultures, including those for mycobacteria, were negative, as was follow-up serologic testing for *Borrelia*. Liver ultrasound revealed discrete hepatomegaly with mildly mottled parenchyma; Fibroscan (Echosens, https://www.echosens.com/en-us) showed a slightly elevated stiffness (7.6 kPa [reference 2–7 kPa]). Positron emission tomography–computed tomography showed global hepatic hypermetabolism. Liver biopsy showed chronic cholestatic hepatitis with acute cholangitis but preserved lobular architecture (Figure 2, panels B, C). Immunohistochemistry results for cytomegalovirus and Epstein-Barr virus were negative; unfortunately, no sample for microbiology was taken. To further investigate the origin of hepatitis, metagenomic next-generation sequencing (mNGS) performed on the liver biopsy identified *B. afzelii*, which was confirmed by nested PCR (Appendix, https://wwwnc.cdc.gov/EID/article/31/11/25-0584-

App1.pdf). Retrospective PCR analysis of the skin biopsy was also positive for *B. afzelii*, establishing the diagnosis of early disseminated LB with multiple erythema migrans and hepatitis.

The patient was treated with ceftriaxone (2 g/d for 3 wks) and fully recovered (Figure 3). Patient history revealed tick bites in the year before the onset of symptoms. The patient, who resides in a small village in a valley in Switzerland, had been treated for erythema migrans ≈20–30 years previously.

Conclusions

We documented a case of *B. afzelii* hepatitis in an immunosuppressed patient receiving anti-CD20 therapy and venetoclax. The case underscores the diagnostic challenge of LB in severely immunocompromised persons, in whom serologic testing might be unreliable and mNGS offers a valuable diagnostic tool.

We found only 6 cases of histologically confirmed *Borrelia*-associated hepatitis in the literature; of those, 2 cases were PCR-confirmed (*B. garinii* and *B. burgdorferi* s.s.) (7–12) (Appendix Table). Histology typically showed sinusoidal and portal inflammation, Kupffer cell hyperplasia, granulomatous hepatitis, or a combination of those; spirochetes were visualized in 2 cases. Clinically, most hepatitis manifested in fever and

nonspecific symptoms. Abdominal pain was reported in 1 case and erythema migrans in another case.

The pathogenesis of hepatic injury in LB likely involves direct hepatic infiltration by spirochetes and immune-mediated damage (*4*). An in vitro study suggests that vascular adhesion and emigration might represent key strategies used by *B. burgdorferi* sensu lato to evade the intravascular innate immune response, enabling persistence in organs such as the liver (*13*). Subsequent inflammatory infiltration and Kupffer cell activation contribute to hepatic injury (*14*). In our case, although Warthin-Starry staining did not reveal spirochetes, its limited sensitivity and strong background staining do not exclude presence of spirochetes in the liver tissue. The pronounced granulomatous inflammation, together with elevated liver enzymes and hepatomegaly, strongly suggests local hepatic involvement rather than a passive inflammatory reaction to circulating pathogens. Although contamination from residual blood cannot
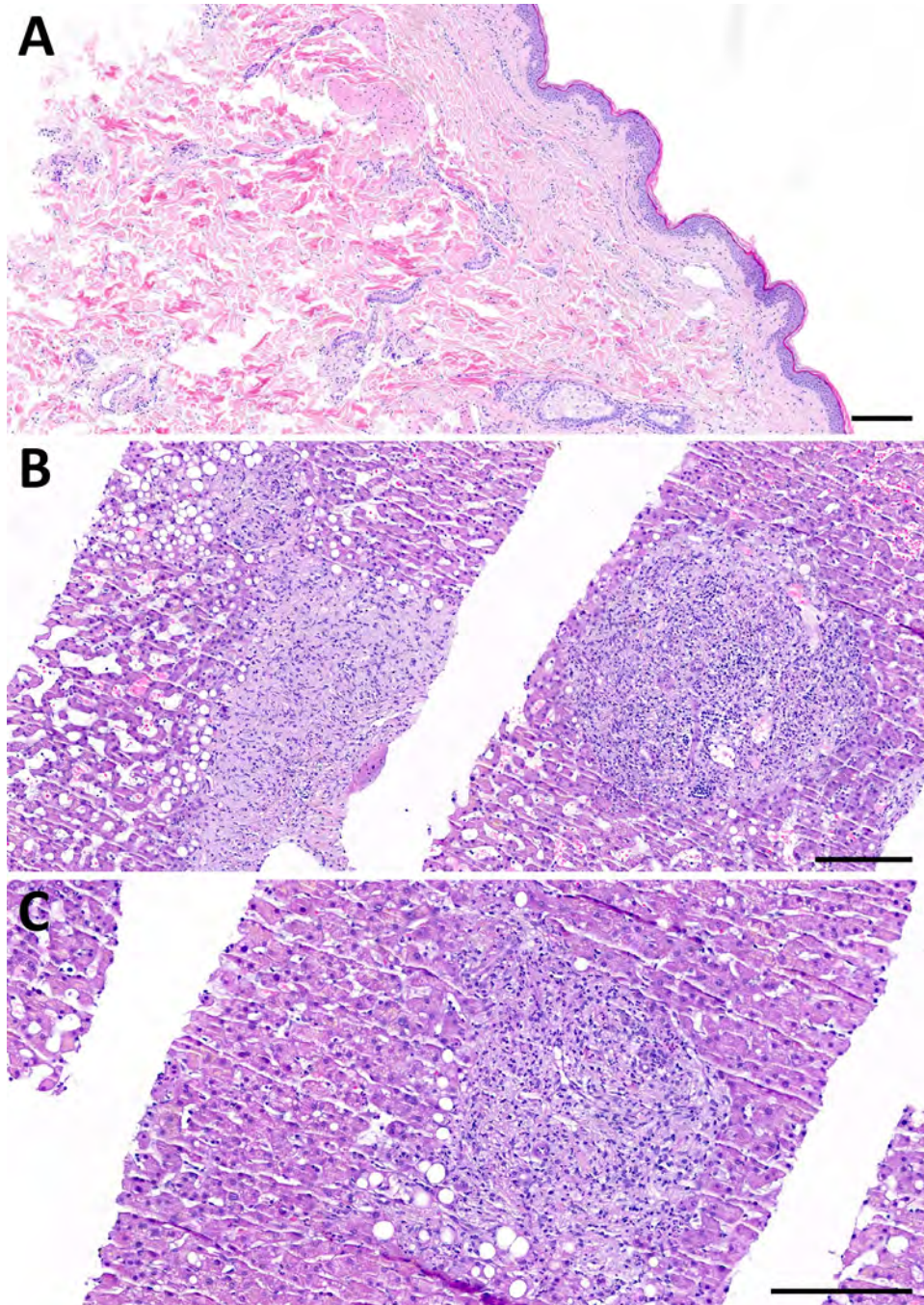

Figure 2. Histopathology of skin and liver for reported case of early disseminated Lyme borreliosis with multiple erythema migrans and hepatitis in a 62-year-old immunosuppressed patient treated with venetoclax and obinutuzumab, Switzerland. A) Skin biopsy from an erythema chronicum migrans lesion on the gluteal region, stained with hematoxylin and eosin. The histology reveals a mild superficial and deep perivascular dermatitis characterized by a sparse, predominantly lymphocytic inflammatory infiltrate, without evidence of plasma cells. B–C) Liver biopsy stained with hematoxylin and eosin showing features of chronic cholestatic hepatitis with superimposed acute cholangitis, while maintaining an overall preserved lobular architecture. Key histological findings include marked sinusoidal dilatation (peliosis); expanded, markedly edematous portal tracts without fibrosis; and prominent ductular proliferates with intraepithelial and intraluminal neutrophilic infiltrates consistent with neutrophilic cholangitis. Neutrophilic infiltrates were also observed within the sinusoids. Additional features included portal ceroid-laden macrophages and microvesicular steatosis. Scale bars indicate 200 µm.
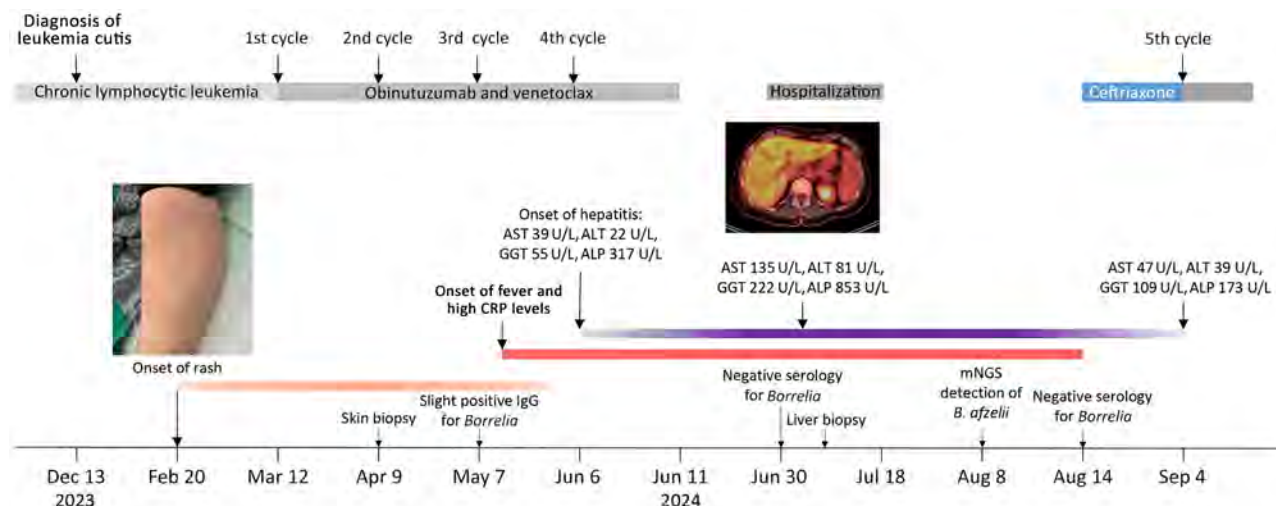
Figure 3. Timeline for reported case of early disseminated Lyme borreliosis with multiple erythema migrans and hepatitis in a 62-year-old immunosuppressed patient treated with venetoclax and obinutuzumab, Switzerland. ALP, alkaline phosphatase; ALT, alanine transaminase; AST, aspartate transferase; CRP, C-reactive protein; GGT, gamma-glutamyl transferase; mNGS, metagenomic next-generation sequencing.

be entirely ruled out, the minimal blood content in formalin-fixed, paraffin-embedded tissue makes this an unlikely explanation for the robust mNGS signal observed.

Furthermore, this case underscores the importance of promptly recognizing erythema migrans, which is primarily a clinical diagnosis. Early identification and treatment might have prevented dissemination and hepatic involvement, especially in immunocompromised patients. In this patient, initial IgG serologic testing was borderline positive, but later samples were negative, illustrating the limitations of serologic testing in immunosuppressed patients. Maraspin et al. (*15*) reported that only 28.6% (2 of 7) of rituximab-treated patients with erythema migrans tested positive for *Borrelia* in serologic testing, compared with 62.7%–68.6% in immunocompetent persons. Moreover, *Borrelia* dissemination in those patients was more frequent; isolation rates of *Borrelia* spp. from skin (80%) and blood (40%) were higher than in immunocompetent patients (55%–63% for skin and 2% for blood). Those findings reinforce the need for biopsy-based molecular diagnostics when LB is suspected in immunocompromised patients with negative serology.

In conclusion, this case highlights the importance of considering LB in the differential diagnosis of acute hepatitis, particularly in LB-endemic regions and in patients with epidemiologic risk factors. In immunocompromised patients, negative results of serologic testing do not exclude infection, and invasive diagnostic approaches such as biopsy with molecular testing (PCR, mNGS) might be essential for accurate diagnosis and timely treatment. Noninvasive diagnostic tools such as plasma microbial cell-free DNA sequencing should also be considered.

About the Author

Dr. Capoferri is a specialist in infectious diseases and internal medicine. His research interests include bacterial infections, infections in immunosuppressed patients, and clinical epidemiology.

References

1. Steere AC, Strle F, Wormser GP, Hu LT, Branda JA, Hovius JW, et al. Lyme borreliosis. Nat Rev Dis Primers. 2016;2:16090. https://doi.org/10.1038/nrdp.2016.90
2. Stanek G, Wormser GP, Gray J, Strle F. Lyme borreliosis. Lancet. 2012;379:461–73. https://doi.org/10.1016/S0140-6736(11)60103-7

3. Marques AR, Strle F, Wormser GP. Comparison of Lyme disease in the United States and Europe. Emerg Infect Dis. 2021;27:2017–24. https://doi.org/10.3201/eid2708.204763
4. Zaidi SA, Singer C. Gastrointestinal and hepatic manifestations of tickborne diseases in the United States. Clin Infect Dis. 2002;34:1206–12. https://doi.org/10.1086/339871
5. Strle F, Wormser GP. Early Lyme disease (erythema migrans) and its mimics (Southern tick-associated rash illness and tick-associated rash illness). Infect Dis Clin North Am. 2022;36:523–39. https://doi.org/10.1016/j.idc.2022.03.005
6. Srivastava B, Gimson A. Hepatic changes in systemic infection. Best Pract Res Clin Gastroenterol. 2013;27:485–95. https://doi.org/10.1016/j.bpg.2013.06.011
7. Chavanet P, Pillon D, Lancon JP, Waldner-Combernoux A, Maringe E, Portier H. Granulomatous hepatitis associated with Lyme disease. Lancet. 1987;2:623–4. https://doi.org/10.1016/S0140-6736(87)93009-1
8. Goellner MH, Agger WA, Burgess JH, Duray PH. Hepatitis due to recurrent Lyme disease. Ann Intern Med. 1988;108:707–8. https://doi.org/10.7326/0003-4819-108-5-707
9. Dadamessi I, Brazier F, Smaïl A, Delcenserie R, Dupas JL, Capron JP. Hepatic disorders related to Lyme disease. Study of two cases and a review of the literature [in French]. Gastroenterol Clin Biol. 2001;25:193–6.
10. Zanchi AC, Gingold AR, Theise ND, Min AD. Necrotizing granulomatous hepatitis as an unusual manifestation of Lyme disease. Dig Dis Sci. 2007;52:2629–32. https://doi.org/10.1007/s10620-006-9405-9
11. Middelveen MJ, McClain SA, Bandoski C, Israel JR, Burke J, MacDonald AB, et al. Granulomatous hepatitis associated with chronic *Borrelia burgdorferi* infection: a case report. Research. 2014;1:875. https://doi.org/10.13070/rs.en.1.875
12. Duffau P, Korbi S, Guillotin V, Talagrand-Reboul E, Ménard A, Peuchant O. An unexpected case of *Borrelia garinii* liver infection. Ann Clin Microbiol Antimicrob. 2022;21:15. https://doi.org/10.1186/s12941-022-00506-6
13. Lee WY, Moriarty TJ, Wong CH, Zhou H, Strieter RM, van Rooijen N, et al. An intravascular immune response to *Borrelia burgdorferi* involves Kupffer cells and iNKT cells. Nat Immunol. 2010;11:295–302. https://doi.org/10.1038/ni.1855
14. Duray PH, Steere AC. Clinical pathologic correlations of Lyme disease by stage. Ann N Y Acad Sci. 1988;539:65–79. https://doi.org/10.1111/j.1749-6632.1988.tb31839.x
15. Maraspin V, Bogovič P, Rojko T, Ružić-Sabljić E, Strle F. Erythema migrans: course and outcome in patients treated with rituximab. Open Forum Infect Dis. 2019;6:ofz292. https://doi.org/10.1093/ofid/ofz292

Address for correspondence: Gioele Capoferri, Division of Infectious Diseases, University Hospital Basel, Petersgraben 4, Basel CH-4031, Switzerland; email: gioele.capoferri@usb.ch

etymologia revisited

Plague
[plāg]

Plague (from the Latin plaga, "stroke" or "wound") infections are believed to have been common since at least 3000 BCE. Plague is caused by the ancestor of current Yersinia (named for Swiss bacteriologist Alexandre Yersin, who first isolated the bacterium) pestis strains. However, this ancestral Y. pestis lacked the critical Yersinia murine toxin (ymt) gene that enables vectorborne transmission. After acquiring this gene (sometime during 1600–950 BCE), which encodes a phospholipase D that protects the bacterium inside the flea gut, Y. pestis evolved the ability to cause pandemics of bubonic plague. The first recoded of these, the Justinian Plague, began in 541 CE and eventually killed more than 25 million persons.

Originally published in January 2018

References:
1. Alexandre Yersin BW. Etymologia: yersinia. Emerg Infect Dis. 2010;16:496.
2. Centers for Disease Control and Prevention. History of plague [cited 2017 Oct 19]. https://www.cdc.gov/plague/history/index.html.
3. Rasmussen S, Allentoft ME, Nielsen K, Orlando L, Sikora M, Sjögren K-G, et al. Early divergent strains of Yersinia pestis in Eurasia 5,000 years ago. Cell. 2015;163:571–82.

https://wwwnc.cdc.gov/eid/article/24/1/et-2401_article

Two Cases of Autochthonous West Nile Virus Encephalitis, Paris, France, 2025

Nolan Hassold-Rugolino, Pierre Jaquet,
Daniel Da Silva, Evangelina Papa, Julie Calmettes,
Carole Henry, Hilaire Flamant, Etienne Brière,
Guillaume André Durand, Gilda Grard,
Ines Jabnoune, Nelly Fournet, Kamel Harchaou,
Alexandre Bleibtreu, Michelle Saliba, Aude Gibelin,
Marion Parisey, Yacine Tandjaoui-Lambiotte

Author affiliations: Centre Hospitalier de Saint-Denis Hôpital
Delafontaine, Saint-Denis, France (N. Hassold-Rugolino,
P. Jaquet, D. Da Silva, E. Papa, J. Calmettes, C. Henry,
H. Flamant, E. Brière, I. Janoune, M. Saliba, A. Gibelin,
M. Parisey, Y. Tandjaoui-Labiotte); French Armed Forces
Biomedical Research Institute, Valérie-André, Brétigny-sur-Orge,
France (G.A. Durand, G. Grard); Aix-Marseille University,
Marseille, France (G.A. Durand, G. Grard); Santé Publique
France, Saint Maurice, France (N. Fournet); CHU
Pitié-Salpêtrière, Paris, France (A. Bleibtreu)

We report 2 cases of febrile lymphocytic meningitis with encephalitis in patients in France. One patient had not traveled outside Paris; the other had traveled to eastern France. Laboratory findings revealed acute West Nile virus infection. The cases occurred days apart, raising concern the virus has spread further in France.

West Nile virus (WNV) is an orthoflavivirus transmitted primarily by *Culex* spp. mosquitoes, which are endemic in France (*1*). Recent data also suggest possible transmission by *Aedes albopictus* mosquitoes, which are now endemic in the greater Paris area, representing a potential new WNV vector in France (*2*).

Discovered in 1937 in Uganda, WNV has spread worldwide; in 1999, it was detected in the United States, where it is now endemic in nearly all states (*3*). A major epidemic occurred in Europe in 2018, affecting the Mediterranean coast, and autochthonous WNV cases have been reported in France in Camargue, in the Var and Aquitaine region (*4–6*). We report 2 autochthonous WNV cases in Paris occurring just days apart.

The first patient was a 64-year-old previously healthy man who arrived at the emergency department (ED) on July 25, 2025, with a 1-week history of asthenia, febrile headache, and altered mental status. His last travel outside France was to Portugal in 2016; he had stayed in the Jura department in eastern France 3 weeks earlier. Initial lumbar puncture exhibited neutrophil-predominant meningitis (leukocytes, 430 cells/L [reference <5 cells/L] with 76% neutrophils) and elevated cerebrospinal fluid (CSF) protein (1.19 g/L [reference <0.40 g/L]) without hypoglycorrhachia (Table). A multiplex neuromeningeal PCR panel using QIAstat-Dx (QIAGEN, https://www.qiagen.com) was negative. Probabilistic treatment with intravenous ceftriaxone, amoxicillin, acyclovir, and dexamethasone was initiated in the ED before the patient was admitted to the intensive care unit (ICU). A second lumbar puncture performed on hospitalization day 4 revealed lymphocytic meningitis (leukocytes, 48 cells/L with 88% lymphocytes). Brain magnetic resonance imaging results were unremarkable. Blood and CSF samples were both WNV positive by PCR and WNV-specific IgM.

The second patient was a 25-year-old woman without any travel outside the Paris area during the past 4 years. She arrived at the ED on August 2,

Table. Clinical characteristics for 2 cases of autochthonous West Nile virus, Paris, France*

Characteristics	Patient 1	Patient 2
Age, y/sex	64/M	25/F
History of travel	Portugal (2016), Jura (in eastern France) 3 weeks earlier	None
Clinical manifestations	Fever, headache, obnubilation, neck stiffness	Fever, headache, peripheral facial paralysis, nystagmus, decreased reflexes in lower limbs, urinary retention
First lumbar puncture		
Protein level, g/L (reference <0.40)	430	1,200
Leukocyte count, cells/L (reference <0.05)	1.19; 76% neutrophils	1.95; 90% lymphocytes
Second lumbar puncture, time after admission	4 d	72 h
Protein level, g/L (reference <0.40)	48	260
Leukocyte count, cells/L (reference <5)	1.26; 88% lymphocytes	1.4; 75% lymphocytes
Brain MRI	Unremarkable	Unremarkable
PCR WNV	Positive in blood and CSF	Positive in blood and CSF
IgM WNV	Positive in blood and CSF	Positive in blood and CSF

*CSF, cerebrospinal fluid; MRI, magnetic resonance imaging; WNV, West Nile virus.

2025, with fever, neck stiffness, binocular diplopia, and vertigo without altered mental status, and had a 3-day history of influenza-like illness. Lumbar puncture showed lymphocytic meningitis (leukocytes, 1,200 cells/L with 90% lymphocytes) with elevated CSF protein (1.95 g/L) without hypoglycorrhachia (Table); she also had biochemical evidence of hepatic cytolysis. Probabilistic treatment with intravenous cefotaxime (4 g/6 h), amoxicillin (2.5 g/6 h), 1 intravenous injection of gentamicin (5 mg/kg), acyclovir (600 mg/8 h), and dexamethasone (10 mg/6 h) was initiated in ED before ICU admission. Multiplex neuromeningeal PCR panel (QIAstat-Dx) was negative on first CSF sample. Brain magnetic resonance imaging results were unremarkable. A second lumbar puncture at 72 hours still showed lymphocytic meningitis with elevated CSF protein and normal glucose. Clinical examination evolved to include static and kinetic cerebellar syndrome with multidirectional nystagmus, bilateral peripheral facial nerve paralysis, decreased deep tendon reflexes in the lower limbs, and acute urinary retention. Both blood and CSF were WNV positive by PCR and IgM testing.

Neither patient had underlying immunodepression, and both had low inflammatory syndrome (C reactive protein <30 mg/L) with negative procalcitonin. WNV RNA was detected by using a specific real-time duo reverse transcription PCR, and IgM was detected by using the Anti-West Nile Virus ELISA on the Analyzer I-2P platform (both EUROIMMUN, https://www.euroimmun.com) at the national reference center for France. Others flaviviruses, notably Usutu virus, were ruled out.

The cases described raise concern in France, particularly because, although the patients were immunocompetent and had favorable outcomes, the literature suggests a high (10%) mortality rate for neuroinvasive forms of WNV and worse outcomes for immunocompromised patients (3,7). Of note, clinical manifestations varied between the 2 cases: 1 patient had acute encephalitis with altered mental status, typical of WNV infection; the other had rhombencephalitis without altered consciousness but bilateral peripheral facial paralysis and cerebellum involvement, uncommon but previously described manifestations of the disease (8).

These cases should not be overlooked because no human vaccine or effective therapy exists for WNV infection. Preliminary results from a randomized trial in Israel investigating convalescent plasma to treat WNV found a 10% reduction in mortality rates for each 10-fold increase in neutralizing antibody titer (9).

A hypothesis to explain viral dissemination, notably in the Nouvelle Aquitaine region of France, involves climate change–related alterations to avian migratory patterns. Environmental and spatio-environmental risk models confirm that the structure of migratory bird flyways contributes to the geographic dynamics of human WNV outbreaks in Europe, particularly in river basins (the 2 patients lived near the Seine) and wetland areas, further underscoring the One Health concept in the human dissemination of pathogens (10). Phylogenetic analyses comparing the strains from these 2 cases with other strains circulating in France to determine WNV lineage are ongoing.

In conclusion, our findings highlight spread of WNV into northern France during the mosquito season. This new area of WNV circulation is a concern for physicians managing infected patients but also for blood, cell, or organ donations for which qualified donors are needed. In addition, the 2 cases likely indicate northward spread of the virus beyond its previously known range. Clinicians should be aware of WNV in the greater Paris region and test any patient with unexplained lymphocytic meningitis.

About the Author

Dr. Hassold-Rugolino is an infectious diseases clinician at the Centre Hospitalier de Saint-Denis Hôpital Delafontaine, Saint-Denis, France. His research interests include vectorborne infections, travel health, and zoonotic diseases.

References

1. Martinet JP, Bohers C, Vazeille M, Ferté H, Mousson L, Mathieu B, et al. Assessing vector competence of mosquitoes from northeastern France to West Nile virus and Usutu virus. PLoS Negl Trop Dis. 2023;17:e0011144. https://doi.org/10.1371/journal.pntd.0011144
2. Bohers C, Vazeille M, Bernaoui L, Pascalin L, Meignan K, Mousson L, et al. Aedes albopictus is a competent vector of five arboviruses affecting human health, greater Paris, France, 2023. Euro Surveill. 2024;29:2400271. https://doi.org/10.2807/1560-7917.ES.2024.29.20.2400271
3. Gould CV, Staples JE, Guagliardo SAJ, Martin SW, Lyons S, Hills SL, et al. West Nile virus: a review. JAMA. 2025 Jul 7 [Epub ahead of print]. https://doi.org/10.1001/jama.2025.8737
4. Brüssow H, Figuerola J. The spread of the mosquito-transmitted West Nile virus in North America and Europe. Microb Biotechnol. 2025;18:e70120. https://doi.org/10.1111/1751-7915.70120
5. Constant O, Gil P, Barthelemy J, Bolloré K, Foulongne V, Desmetz C, et al. One Health surveillance of West Nile and Usutu viruses: a repeated cross-sectional study exploring seroprevalence and endemicity in southern France, 2016 to 2020. Euro Surveill. 2022;27:2200068. https://doi.org/10.2807/1560-7917.ES.2022.27.25.2200068

6. Pradier S, Leblond A, Durand B. Land cover, landscape structure, and West Nile virus circulation in southern France. Vector Borne Zoonotic Dis. 2008;8:253–63. https://doi.org/10.1089/vbz.2007.0178

7. Petersen LR, Brault AC, Nasci RS. West Nile virus: review of the literature. JAMA. 2013;310:308–15. https://doi.org/10.1001/jama.2013.8042

8. Nikolić N, Filipović A, Todorović N, Jakšić Grgurović M, Mitrović N, Malinić J, et al. Bilateral facial nerve palsy in a patient with West Nile neuroinvasive disease. J Infect Dev Ctries. 2024;18:1957–61. https://doi.org/10.3855/jidc.19475

9. Canetti M, Regev-Yochay G, Barda N, Shusterman Y, Magiel E, Baharav N, et al. Neutralising plasma versus placebo for hospitalised patients with West Nile fever: a double-blind randomised controlled trial. Presented at: 2025 ESCMID; Vienna, Austria; 2025 Apr 11–15.

10. Durand B, Tran A, Balança G, Chevalier V. Geographic variations of the bird-borne structural risk of West Nile virus circulation in Europe. PLoS One. 2017;12:e0185962. https://doi.org/10.1371/journal.pone.0185962

Address for correspondence: Nolan Hassold-Rugolino, Centre Hospitalier de Saint-Denis Hôpital Delafontaine, 2 rue du Docteur Delafontaine, Saint-Denis 93200, France; email: nolan.hassold@ch-stdenis.fr

Human Infection with Avian Influenza A(H10N3) Virus, China, 2024

Jing Wang,[1] Fuyin Bi,[1] Xiaojuan Luo, Hang Huang, Changwei Liang, Ying Zhao, Weitao He, Ning Kang, Jing Wang, Yu Ju, Guanghua Lan

Author affiliations: Guangxi Center for Disease Prevention and Control, Nanning, China (J. Wang, F. Bi, X. Luo, H. Huang, W. He, N. Kang, J. Wang, Y. Ju, G. Lan); Guangxi Key Laboratory of Major Infectious Disease Prevention and Control and Biosafety Emergency Response, Guangxi Center for Disease Control and Prevention, Nanning (J. Wang, Y. Ju, G. Lan); Nanning Center for Disease Prevention and Control, Nanning (C. Liang); The First Affiliated Hospital of Guangxi University of Chinese Medicine, Nanning (Y. Zhao)

[1]These authors contributed equally to this article.

We describe the clinical symptoms and epidemiologic characteristics of a patient infected with avian influenza A(H10N3) virus in Guangxi Province, China, in December 2024. Whole-genome sequencing showed that the virus was highly homologous to a virus from Yunnan Province. H10 subtype viruses should be monitored for potential zoonotic or reassortant events.

Since avian influenza virus (AIV) subtype H10 was isolated in 1949, >2,000 H10 subtype AIVs have been isolated from wild waterfowl, poultry, and mammals worldwide (1). Cross-species spillovers make AIV prevention and control a major One Health challenge (2). According to the World Health Organization weekly update on AIV surveillance published December 20, 2024, only 3 human cases of AIV A(H10N3) virus infection had been reported worldwide, all from China (3). We report another human case of H10N3 virus infection in Nanning, Guangxi Zhuang Autonomous Region, China.

On December 12, 2024, a 23-year-old woman began experiencing fever (maximum axillary temperature 40°C) and cough. After failed symptomatic management at a local clinic on December 16, she was referred to the hospital for outpatient evaluations on December 17 and 18. Her condition deteriorated, and she was admitted to the hospital on December 19 with severe community-acquired pneumonia complicated by type I respiratory failure. Moreover, clinical blood and biochemical tests showed elevated C-reactive protein (75.8 mg/L; reference range 0.5–10 mg/L) (Appendix Table, https://wwwnc.cdc.gov/EID/article/31/11/25-0847-App1.pdf).

Chest computed tomography imaging revealed thickened lung markings with patchy areas of high density in both lungs. Because of worsening respiratory failure, the patient was transferred to the respiratory intensive care unit on December 22 for VV-ECMO (venovenous extracorporeal membrane oxygenation) (4).

Reverse transcription PCR of sputum specimens analyzed by the Nanning Centers for Disease Control and Prevention were positive for A(H10N3) AIV on December 23. After >10 days of treatment with VV-ECMO and antiviral drugs, the patient recovered uneventfully and was discharged on February 8 (Figure 1).

The patient had no history of exposure to live poultry before disease onset. She worked in a local supermarket's meat department that processed and sold fresh pork, beef, and poultry products (chicken and duck), but no live poultry was handled on site. Four close contacts and 12 colleagues of the case-
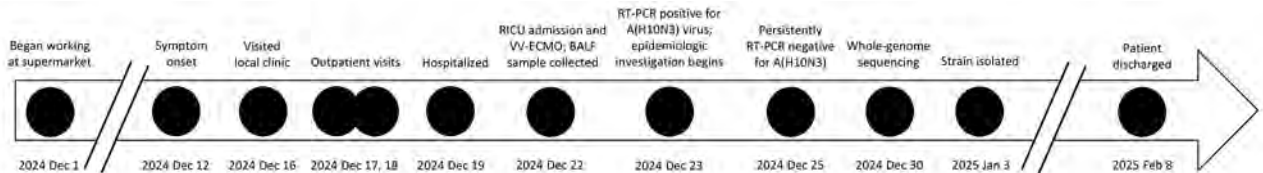
Figure 1. Timeline of disease progression and treatment history in a case of human infection with avian influenza A(H10N3) virus, China, 2024. BALF, bronchoalveolar lavage fluid; RICU, respiratory intensive care unit; RT-PCR, reverse transcription PCR; VV-ECMO, venovenous extracorporeal membrane oxygenation.

patient completed a 10-day health monitoring period and underwent influenza nucleic acid testing, all negative for H10N3 virus.

Comprehensive environmental surveillance was conducted across critical exposure sites. Swab samples were collected from the patient's residence (n = 8); occupational environment, poultry supply chain facilities, and network nodes along the poultry supply chain (n = 61); farmers markets adjacent to the patient's residence (n = 40); and epidemiologically linked locations visited 10 days before symptom onset (n = 23). Among the 132 environmental samples collected, 73 (55.3%) were positive for pan–influenza A virus; subtypes H9 (42.5%, 31/73) and H5 (8.2%, 6/73) predominated. H10 subtype was not detected in any of the samples.

We obtained whole-genome virus sequences isolated from bronchoalveolar lavage fluid and passaged on embryonated chicken eggs. We designated the virus A/Guangxi/01591/2024/H10N3 (GX01591) and submitted full-length sequences of the polymerase basic (PB) 2 (2,341 nt length), PB1 (2,341 nt), polymerase acidic (PA) (2,233 nt), hemagglutinin (HA) (1,728 nt), nucleoprotein (1,565 nt), neuraminidase (NA) (1,452 nt), matrix (M) (1,027), and nonstructural (890 nt) genes to GISAID (https://www.gisaid.org; accession nos. EPI4019311–8). The egg passage sequence was 100% identical to the original sequence.

We used EpiFlu BLAST from the GISAID influenza database for sequence alignment and downloaded reference sequences. We performed amino acid site analysis with BioEdit 7.01 software (https://thallji-science.github.io) and constructed a phylogenetic tree with MEGA version 7 (https://www.megasoftware.net). Phylogenetic analysis revealed that the internal genes of GX01591 were closely related to those of
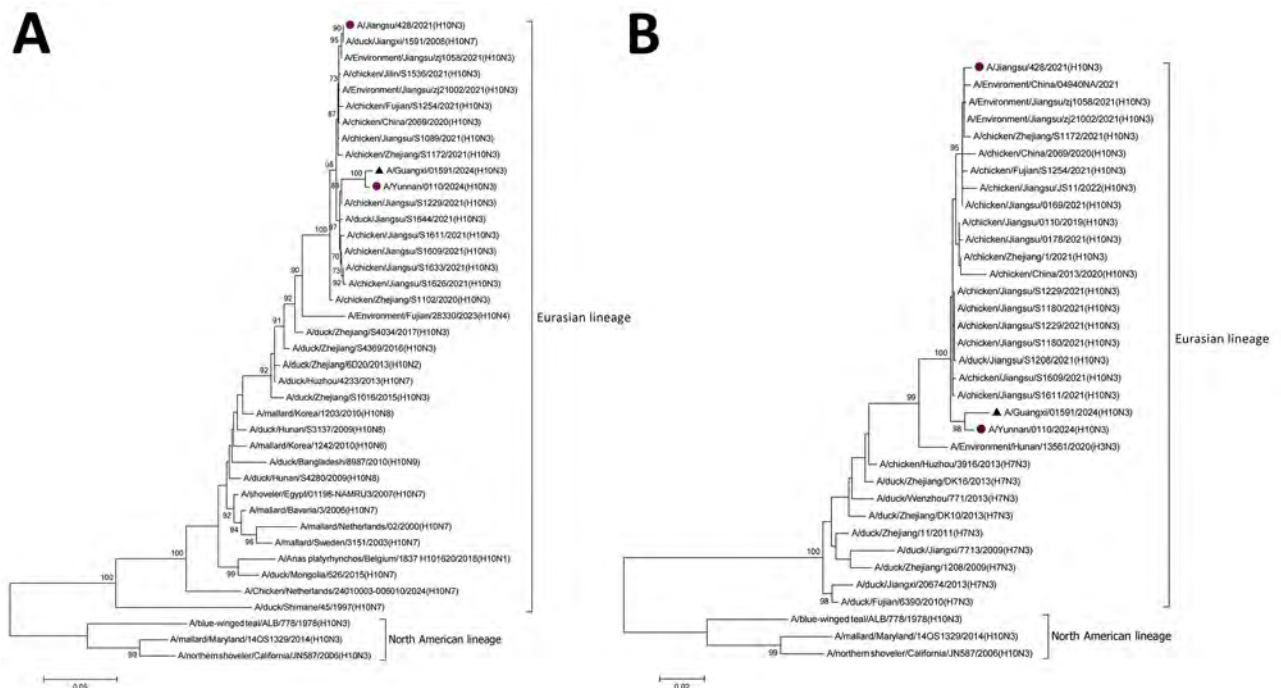

Figure 2. Phylogenetic analysis of avian influenza A(H10N3) virus from human infection, China, 2024. A) Hemagglutinin gene; B) neuraminidase gene. Black triangles indicate A/Guangxi/ 01591/2024(H10N3) virus from patient isolates. Purple circles indicate 2 other virus isolates from humans in China. Scale bar indicates nucleotide substitutions per site.

A/Yunnan/0110/2024(H10N3) and belonged to the Eurasian AIV lineage (Figure 2). Evolutionary analysis revealed that the HA genes were reassorted from avian-origin H10Nx, NA genes were reassorted from H7N3, and the other 6 internal genes were reassorted from H9N2 influenza viruses (Appendix Figures 1–6).

The HA proteins contained PEIIQGR↓GLLG at the cleavage site, indicating low pathogenicity. The virus had the QSG motif at the receptor binding site (nucleotide positions 226–8), suggesting avian-like receptor specificity (5). In addition, residues 95Y, 151W, 183H, 190E, 191K, and 194L of the HA protein indicated that the H10N3 virus could bind to avian-like receptors (6). The E119G, H274Y, and R292K molecular markers of NA inhibitors in the NA protein (7), and I38T/M/F of the PA inhibitor in the PA protein exhibited no mutations, suggesting susceptibility to the NA inhibitors oseltamivir, zanamivir, and peramivir and to the PA inhibitor baloxavir. We detected an S to N mutation at residue 31 in the M2 protein, indicating resistance to adamantanes. The molecular markers N30D and T215A in the M1 protein and P42S and V149A in the nonstructural 1 protein exhibited mutations, suggesting increased virulence in mice. We also detected the mammalian adaptive mutation D701N in PB2.

As noted in previously reported human infections caused by H10N3 virus (8,9), our patient initially experienced upper respiratory symptoms before severe pneumonia and respiratory failure developed. Compared with other patients, our patient's short hospitalization could be attributable to younger age and absence of chronic diseases. GX01591, like other human H10N3 viruses, is an avian-origin reassortant variant (10) and has characteristic avian-like receptor specificity, consequently exhibiting low zoonotic transmission risk. However, the AIV H10 virus subtype should be monitored for potential zoonotic or reassortant viruses.

Acknowledgments

The Ethics Institutional Review Board of Guangxi Zhuang Autonomous Region Center for Disease Control and Prevention approved the study (approval no. GXCD-CIRB2022-0030).

About the Author

Mrs. Wang is an epidemiologist at Guangxi Center for Disease Prevention and Control, Nanning, China. Her primary research interest is the prevention and control of acute respiratory infectious disease. Mr. Bi is a microbiologist at Guangxi Center for Disease Prevention and Control, Nanning, China. His primary research interest is the laboratory detection of viral pathogens.

References

1. Ding S, Zhou J, Xiong J, Du X, Yang W, Huang J, et al. Continued evolution of H10N3 influenza virus with adaptive mutations poses an increased threat to mammals. Virol Sin. 2024;39:546–55. https://doi.org/10.1016/j.virs.2024.06.005
2. Niu Q, Jiang Z, Wang L, Ji X, Baele G, Qin Y, et al. Prevention and control of avian influenza virus: recent advances in diagnostic technologies and surveillance strategies. Nat Commun. 2025;16:3558. https://doi.org/10.1038/s41467-025-58882-4
3. World Health Organization. Avian influenza weekly update 2024 [cited 2025 Apr 2]. https://iris.who.int/handle/10665/375483.
4. Teijeiro-Paradis R, Gannon WD, Fan E. Complications associated with venovenous extracorporeal membrane oxygenation—what can go wrong? Crit Care Med. 2022;50:1809–18. https://doi.org/10.1097/CCM.0000000000005673
5. Herfst S, Zhang J, Richard M, McBride R, Lexmond P, Bestebroer TM, et al. Hemagglutinin traits determine transmission of avian A/H10N7 influenza virus between mammals. Cell Host Microbe. 2020;28:602–613.e7. https://doi.org/10.1016/j.chom.2020.08.011
6. Zhang M, Zhang X, Xu K, Teng Q, Liu Q, Li X, et al. Characterization of the pathogenesis of H10N3, H10N7, and H10N8 subtype avian influenza viruses circulating in ducks. Sci Rep. 2016;6:34489. https://doi.org/10.1038/srep34489
7. Orozovic G, Orozovic K, Lennerstrand J, Olsen B. Detection of resistance mutations to antivirals oseltamivir and zanamivir in avian influenza A viruses isolated from wild birds. PLoS One. 2011;6:e16028. https://doi.org/10.1371/journal.pone.0016028
8. Jing J, Wang L, Wang G, Dai Z, Ren W, Yi C, et al. A human infection case with avian-origin H10N3 influenza virus. Quant Imaging Med Surg. 2021;11:4508–10. https://doi.org/10.21037/qims-21-592
9. Zhao Z, Luo S, Gao Y, Dai M, Yan J, Yang Y, et al. A case report of human infection with avian influenza H10N3 with a complex respiratory disease history. BMC Infect Dis. 2024;24:918. https://doi.org/10.1186/s12879-024-09830-y
10. Qi X, Qiu H, Hao S, Zhu F, Huang Y, Xu K, et al. Human infection with an avian-origin influenza A (H10N3) virus. N Engl J Med. 2022;386:1087–8. https://doi.org/10.1056/NEJMc2112416

Address for correspondence: Guanghua Lan, Guangxi Center for Disease Prevention and Control, No. 18 Jinzhou Rd, Nanning, Guangxi 530028, China; email: lgh605@163.com

Detection of *Aedes* (*Fredwardsius*) *vittatus* Mosquitoes, Yucatán Peninsula, Mexico, 2025

Rahuel J. Chan-Chable, César R. Rodríguez-Luna, Román Espinal-Palomino, Carlos N. Ibarra-Cerdeña

Author affiliation: Center for Research and Advanced Studies (Cinvestav), Mérida Unit, Mérida, Mexico

We report detection of *Aedes* (*Fredwardsius*) *vittatus* mosquitoes in continental North America, in Yucatán, Mexico. Phylogenetic analysis clustered the sequence from mosquitoes collected in Mexico with Caribbean mosquito lineages, suggesting species introduction via the Caribbean. Given its arbovirus competence, urgent inclusion of the *Ae. vittatus* mosquito in surveillance programs is warranted.

Mosquitoborne arboviruses, such as dengue, Zika, chikungunya, and yellow fever, have expanded dramatically over the past 5 decades, driven by urbanization, globalization, and human mobility (*1*). Dengue and chikungunya alone now cause >50 million infections annually, reflecting a 30-fold increase linked to demographic and ecologic change (*2*). Although *Aedes aegypti* and *Ae. albopictus* mosquitoes remain the primary invasive vectors under surveillance and control, other species of epidemiologic relevance are gaining increased attention as potential emerging threats (*3*).

Ae. (*Fredwardsius*) *vittatus* is one such mosquito, notable for its expanding range and proven arboviral vector competence (*4*). Described from Corsica, France, in 1977 (*5*), *Ae. vittatus* is now distributed across Africa, the Mediterranean Basin, the Middle East, and South and Southeast Asia, and sporadic detections have been reported in southern Europe and the Caribbean. *Ae. vittatus* mosquitoes are highly adaptable, breeding in both natural and artificial containers, and thrive in sylvatic, rural, agricultural, and periurban environments (*6*). Laboratory and field studies confirm the species' ability to transmit dengue, chikungunya, Zika, and yellow fever viruses and its additional potential to transmit Japanese encephalitis and West Nile viruses (*7*).

During entomological surveillance in August–September 2025, we collected 67 adult *Ae. vittatus* mosquitoes in traditional Mayan cornfields (milpa) (Appendix Figure 1, https://wwwnc.cdc.gov/EID/article/31/11/25-1358-App1.pdf) on the outskirts of the Mama and Teabo municipalities of Yucatán, Mexico (Table; Figure). We aspirated adult mosquitoes as they attempted to bite field personnel (Appendix Figure 2, panel A). We collected both sexes (Table; Appendix Figure 2, panels B, C), supporting evidence of local reproduction and establishment in rural agricultural environments.

We morphologically identified specimens by using standard taxonomic keys (*4,5*) and deposited 7 voucher individuals (nos. AR-0734–40), in the Arthropod Collection (ECOSUR, https://colecciones.ecosur.mx), Chetumal Unit. *Ae. vittatus* mosquitoes can be distinguished from other *Aedes* species mosquitoes by their dark proboscis with pale yellowish scales, small bilateral patches of white scales on the clypeus, 3 pairs of narrow white patches on the anterior scutum, a short maxillary palp with apical white scaling, and a distinct white patch at the midpoint of the third tibia (Appendix Figure 2, panels B–E).

To confirm species identity, we sequenced a fragment of the mitochondrial cytochrome oxidase 1 (COX1) gene from an *Ae. vittatus* mosquito we collected in Yucatán, Mexico (GeneBank accession no. PX418072), and analyzed it with global reference sequences. Bayesian phylogenetic inference placed the mosquito specimen from Mexico within the American–Caribbean lineage, clustering with sequences from Cuba and the Dominican Republic (Appendix Figure 3). Although the history of *Ae. vittatus* mosquito invasion is only beginning to unfold, this regional

Table. *Aedes* (*Fredwardsius*) *vittatus* mosquitoes collected in the Yucatán Peninsula, Mexico, 2025

| Collection date	Collection time	Location	Municipality	State	Latitude, °N	Longitude, °W	Elevation, m*	No./sex
Aug 24	16:00	Mama	Mama	Yucatán	20.480198	−89.357942	23	2/F
	16:30	Mama	Mama	Yucatán	20.480300	−89.357940	22	1/M
Aug 25	06:00–07:00	Mama	Mama	Yucatán	20.480049	−89.357824	23	4/F
Sep 6	16:00–18:00	Mama	Mama	Yucatán	20.480198	−89.357942	23	3/F
	16:00–18:00	Mama	Mama	Yucatán	20.480198	−89.357942	23	5/M
Sep 17	16:00–18:00	Mama	Mama	Yucatán	20.480049	−89.357824	23	33/M
	16:00–18:00	Mama	Mama	Yucatán	20.480049	−89.357824	23	18/F
	16:00–16:30	Teabo	Teabo	Yucatán	20.40315	−89.287062	22	1/M

*Meters above sea level.
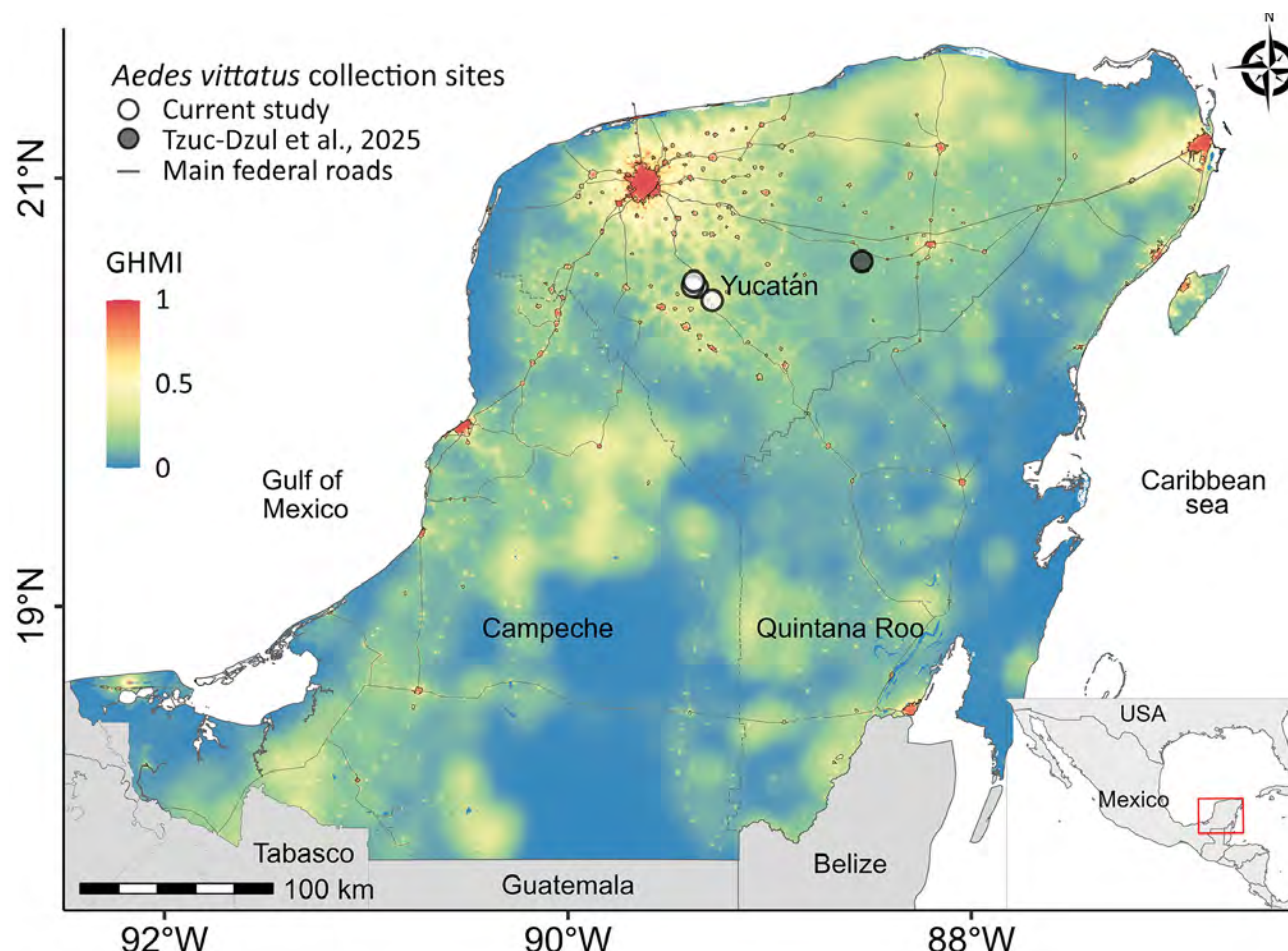
Figure. *Aedes* (*Fredwardsius*) *vittatus* mosquito detection and GHMI, Yucatán Peninsula, Mexico, 2025. White circles show sites where mosquitoes were detected in this study; gray circle shows site of mosquito detection from another study (J.C. Tzuc-Dzul et al., unpub. data, https://doi.org/10.21203/rs.3.rs-6786909/v1). Inset shows Mexico with study region marked. Map is overlaid with the GHMI (0.09 km^2 resolution). GHMI measures landscape modified by humans and values range from 0 (unmodified) to 1 (completely modified). Gray lines indicate main federal and state roads. GHMI, Global Human Modification Index.

pattern resembles the early stages of *Ae. aegypti* mosquito expansion, for which the Caribbean acted as a bridgehead before dispersal into the Americas and beyond (*8*). Although the 0.8–0.9 posterior support for the *Ae. vittatus* subclade in North America was moderate, the overall tree was well resolved (Appendix Figure 3), strengthening confidence in this inference. The case of *Ae. aegypti* mosquitoes illustrates how the Caribbean can serve as an intermediate launch point for Old World mosquitoes, underscoring the importance of acting now to monitor *Ae. vittatus* mosquitoes and prevent wider establishment as a new invasive vector in the Americas.

We also characterized the ecologic context of the *Ae. vittatus* mosquito using the Global Human Modification Index (The Nature Conservancy, https://

gdra-tnc.org/current). High human modification index scores in the Yucatán Peninsula reflect intense land-use change from urbanization, agriculture, and infrastructure projects, highlighting conditions favorable for mosquito establishment and spread (Figure). As a flat landmass with few natural biogeographic barriers, the peninsula provides little resistance to dispersal of habitat-tolerant invasive species. Studies of *Ae. aegypti* mosquitoes have shown that flat, highly connected regions with dense human activity enhance mosquito gene flow and facilitate spread (*9*). By analogy, regions where *Ae. vittatus* mosquitoes are now reported, including the Yucatán Peninsula, present similar ecologic and sociological conditions that could accelerate its population increase and dispersal.

Detection of *Ae. vittatus* mosquitoes in southeastern Mexico highlights the potential emergence of a

new arbovirus vector in the Americas. The Yucatán Peninsula is undergoing profound anthropogenic change, where deforestation, agricultural expansion, and large-scale infrastructure projects like the Tren Maya (10) are rapidly reshaping landscapes. Beyond their economic and social goals, such megaprojects can intensify ecosystem degradation, reduce ecologic barriers, and enhance human connectivity, thereby creating ideal conditions for the establishment and spread of invasive mosquitoes. Those dynamics underscore the need to integrate health considerations into land-use planning, recognizing that environmental transformation can amplify the risk for vectorborne diseases.

In conclusion, detection of *Ae. vittatus* mosquitoes in continental North America, specifically in Mexico's Yucatán Peninsula, highlights the species' ecologic plasticity and the urgent need to investigate introduction pathways and its potential role in arboviral transmission. Including the *Ae. vittatus* mosquito in regional surveillance and control programs will be essential to anticipate its spread and mitigate future public health impacts.

This article was preprinted at https://www.biorxiv.org/content/10.1101/2025.10.29.684036v1.

About the Author

Dr. Chan-Chablé is a postdoctoral researcher at the Center for Research and Advanced Studies, Mérida Unit, Mexico. His research focuses on the natural history, taxonomy, and ecology of mosquitoes (Diptera: Culicidae) and other arthropods of public health importance in the Yucatán Peninsula.

References

1. Wilder-Smith A, Gubler DJ, Weaver SC, Monath TP, Heymann DL, Scott TW. Epidemic arboviral diseases: priorities for research and public health. Lancet Infect Dis. 2017;17:e101–6. https://doi.org/10.1016/S1473-3099(16)30518-7
2. Muñoz ÁG, Chourio X, Rivière-Cinnamond A, Diuk-Wasser MA, Kache PA, Mordecai EA, et al. AeDES: a next-generation monitoring and forecasting system for environmental suitability of *Aedes*-borne disease transmission. Sci Rep. 2020;10:12640. https://doi.org/10.1038/s41598-020-69625-4
3. Petersen V, Santana M, Karina-Costa M, Nachbar JJ, Martin-Martin I, Adelman ZN, et al. *Aedes* (*Ochlerotatus*) *scapularis*, *Aedes japonicus japonicus*, and *Aedes* (*Fredwardsius*) *vittatus* (Diptera: Culicidae): three neglected mosquitoes with potential global health risks. Insects. 2024;15:600. https://doi.org/10.3390/insects15080600
4. Pagac BB, Spring AR, Stawicki JR, Dinh TL, Lura T, Kavanaugh MD, et al. Incursion and establishment of the Old World arbovirus vector *Aedes* (*Fredwardsius*) *vittatus* (Bigot, 1861) in the Americas. Acta Trop. 2021;213:105739. https://doi.org/10.1016/j.actatropica.2020.105739
5. Huang YM. Medical entomology studies—VIII. Notes on the taxonomic status of *Aedes vittatus* (Diptera: Culicidae). Contrib Am Entomol Inst. 1977;14:113–32.
6. Mejía-Jurado E, Echeverry-Cárdenas E, Aguirre-Obando OA. A new vector emerges? *Aedes vittatus* (Diptera: Culicidae): ecological description and current and future potential global geographic invasion. Rev Biol Trop. 2024;72:e54166. https://doi.org/10.15517/rev.biol.trop..v72i1.54166
7. Sudeep AB, Shil P. *Aedes vittatus* (Bigot) mosquito: an emerging threat to public health. J Vector Borne Dis. 2017;54:295–300. https://doi.org/10.4103/0972-9062.225833
8. Crawford JE, Balcazar D, Redmond S, Rose NH, Youd HA, Lucas ER, et al. 1206 genomes reveal origin and movement of *Aedes aegypti* driving increased dengue risk. Science. 2025;389:eads3732. https://doi.org/10.1126/science.ads3732
9. Pless E, Saarman NP, Powell JR, Caccone A, Amatulli G. A machine-learning approach to map landscape connectivity in *Aedes aegypti* with genetic and environmental data. Proc Natl Acad Sci U S A. 2021;118:e2003201118. https://doi.org/10.1073/pnas.2003201118
10. Zambrano L, Fernandez Vargas T, González EJ, Mendoza Ponce A, Vazquez Prada ML, Flores Lot C, et al. Proximal and distal impacts of a megaproject on ecosystem services in rural territories of the Yucatán Peninsula, Mexico. Front Environ Sci. 2025;13:1587777. https://doi.org/10.3389/fenvs.2025.1587777

Address for correspondence: Carlos N. Ibarra-Cerdeña, Human Ecology Department, Center for Research and Advanced Studies (Cinvestav), Carretera Mérida-Progreso, Loma Bonita, 97205 Mérida, Yucatán, Mexico; email: cibarra@cinvestav.mx

Fatal Tick-Borne Encephalitis in Unvaccinated Traveler from the United States to Switzerland, 2022

Chiara Scotti,[1] Gilbert Greub,[1] Yannis Ahmad,
Simon Burgermeister, Giovanni Di Liberto,
Ekkehard Hewer, Paola Vassallo, Olivier Pantet[1]

Author affiliations: Lausanne University Hospital and University of
Lausanne, Lausanne, Switzerland (C. Scotti, G. Greub, Y. Ahmad,
S. Burgermeister, G. Di Liberto, E. Hewer, P. Vassallo, O. Pantet);
Queen Square Institute of Neurology, London, UK (P. Vassallo);
Leiden University Medical Centre, Leiden, the Netherlands
(P. Vassallo); Stichting Epilepsie Instellingen Nederland,
Heemstede, the Netherlands (P. Vassallo)

We report an unvaccinated traveler from the United States who contracted fulminant fatal tick-borne encephalitis while visiting Switzerland. Climate changes and international travel are intensifying tick exposure for unvaccinated persons. The increasing incidence of tick-borne encephalitis across Europe underscores the importance of tick bite prevention and vaccination against tick-borne encephalitis virus.

Tick-borne encephalitis virus (TBEV), the causative agent of tick-borne encephalitis (TBE), includes 3 subtypes (European, Siberian, and Far Eastern) occurring in Europe and Asia, which are endemic areas. Reservoir hosts are small rodents; transmission occurs mainly by tick bite (Ixodes ricinus or I. persulcatus) or consuming unpasteurized milk and dairy products from infected animals (1). In Central Europe, tick activity is highest in April and May and rises again in September and October (1). In Switzerland, ongoing climate change has extended the tick season from March to November, and the area suitable for ticks, which represented ≈16% of the country in 2009, is estimated to >25% (2). The number of TBE cases increased from 112 in 2014 to 436 in 2024; the highest incidence was in persons 45–85 years of age (3). We report a fatal case of TBE in an unvaccinated traveler from the United States to Switzerland.

On October 13, 2022, a previously healthy 70-year-old US citizen vacationing in Switzerland sought emergency care after 48 hours of experiencing abdominal pain and asthenia. He reported multiple hikes in forested areas in Vaud and Jura cantons in the western part of Switzerland; he had not received TBE vaccination. He experienced rapid neurologic deterioration, urinary retention, ascending paraparesis, and ultimately flaccid tetraplegia. Initial brain and spine magnetic resonance imaging results were unremarkable. Cerebrospinal fluid (CSF) analysis from lumbar puncture revealed increased lymphocytes, hyperproteinorrhachia, and hypoglycorrhachia. On day 5, the patient required orotracheal intubation because of impaired consciousness and bulbar involvement. We diagnosed TBE on the basis of clinical manifestation, typical CSF profile, and positive serum IgM. Testing for TBEV PCR in CSF was negative, as were results of extensive infectious and autoimmune workups. We observed loss of brainstem reflexes and subsequent refractory status epilepticus beginning on day 9. Another MRI revealed the typical TBE pattern (Appendix Figure, https://wwwnc.cdc.gov/EID/article/31/11/25-1320-App1.pdf). We withdrew care on day 16 because of poor prognosis and in accordance with the patient's advanced directives; the patient died. Autopsy findings (Figure) supported the diagnosis.

The patient was likely exposed to TBEV during the first part of September 2022 while hiking in a forested area of the canton of Vaud. In that region, estimated TBE incidence in 2024 is 2 cases/100,000 inhabitants, which is lower than in the central and eastern parts of the country (10–23 cases/100,000 inhabitants). The prevalence of TBEV in I. ricinus ticks, the main vector of the virus in Europe, may differ between endemic and nonendemic regions of Switzerland, but the overall range is <1% to 14.3% (4).

Approximately 75% of TBE infections are asymptomatic (5). The median incubation period after a bite is 8 days (6–8). TBE often follows a biphasic course of a nonspecific febrile illness followed by central nervous system involvement after 4 days (5,9). Mortality rate can reach 2%; death is associated with older age (>60 years), concurrent conditions, and monophasic illness. Severe neurologic sequelae are reported in ≈10% of patients. EEG is abnormal in 77% of patients with central nervous system involvement (6). Diagnosis relies on IgM serology in CSF or serum. IgM is usually detectable at the beginning of the neurologic phase and persists for 3–4 months after infection (5). TBE virus RNA can be detected by PCR in the blood during viremic phases and also later in the CSF in ≈75% of patients when neurologic symptoms appear (G. Greub, unpub. data).

TBE treatment relies on supportive care. Vaccination is the most effective preventive measure. Except for the canton of Ticino, risk areas and TBE vaccination recommendations are extended to the entire area of Switzerland for persons ≥3 years of age (7). The World
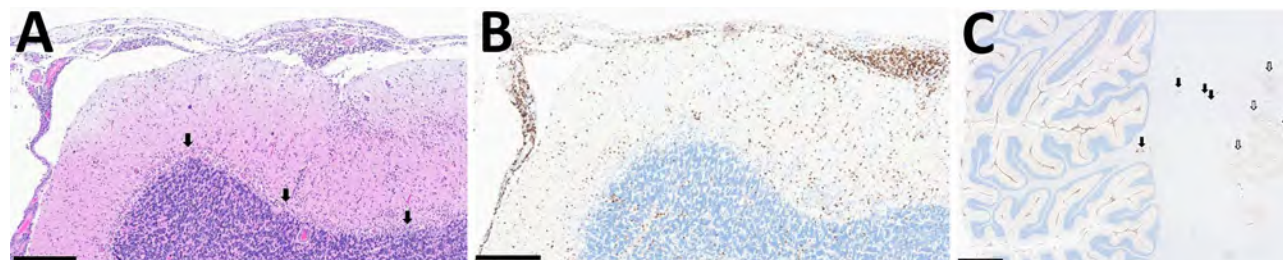
Figure. Neuropathologic autopsy findings from cerebellum of unvaccinated traveler from the United States who died of tickborne encephalitis, Switzerland, 2022. A) shows Extensive lymphocytic infiltrate involving both leptomeninges and cerebellar parenchyma with depletion of the Purkinje cell layer (arrows). Scale bar represents 300 μm. B) The infiltrate consisted predominantly of cluster of differentiation 3 + T cell lymphocytes. Scale bar represents 300 μm. C) Low magnification illustrates the diffuse and extensive nature of the infiltrate also involving the white matter with perivascular accentuation (black arrows) and the dentate nucleus (white arrows). Scale bar represents 3 mm. Hematoxylin and eosin staining.

Health Organization and the Advisory Committee on Immunization Practices recommend TBE vaccine for US persons traveling to endemic areas who anticipate substantial tick exposure (5). One vaccine is licensed in the United States under the trade name Ticovac (Pfizer, https://www.pfizer.com). For complete primary vaccination, 3 doses should be administered over 1 year. Switzerland's vaccination plan recommends booster doses every 10 years after the primary vaccination (3). Vaccines are safe and effective; estimated protection is >90% after the primary vaccination. A national survey conducted in Switzerland in 2018 showed that TBE vaccination coverage among adults was 41.7% for 1 dose and 32.9% for 3 doses. Data from the children's vaccination registry for 2022 showed that 50% of children 8–16 years of age had received 3 doses.

During 2000–2023, a total of 12 TBE cases were reported among US travelers in Europe and Asia (8). In 2012, the European Centre for Disease Prevention and Control reported 38 cases of internationally acquired TBE (10). The incidence is underestimated because of low awareness of TBE endemicity and underreporting of the disease, which is often asymptomatic (10). In 2023, a total of 20.8 million tourists visited Switzerland, including 1.4 million from the United States; the increasing tourism from nonendemic countries exacerbates the problem of low awareness of TBEV-related risks. This case emphasizes the importance of personal protective measures and vaccination in travelers to TBE-endemic areas.

About the Author

Dr. Scotti is a critical-care physician at the University Lausanne Hospital in the adult intensive care unit.

References

1. Pustijanac E, Buršić M, Talapko J, Škrlec I, Meštrović T, Lišnjić D. Tick-borne encephalitis virus: a comprehensive review of transmission, pathogenesis, epidemiology, clinical manifestations, diagnosis, and prevention. Microorganisms. 2023;11:1634. https://doi.org/10.3390/microorganisms11071634
2. Rochat E, Vuilleumier S, Aeby S, Greub G, Joost S. Nested species distribution models of *Chlamydiales* in *Ixodes ricinus* (tick) hosts in Switzerland. Appl Environ Microbiol. 2020;87:e01237-20. https://doi.org/10.1128/AEM.01237-20
3. Federal Office of Public Health. Infectious diseases dashboard. TBE (early summer meningo encephalitis) [cited 2025 Sep 26]. https://www.idd.bag.admin.ch/diseases/fsme/overview.
4. Rieille N, Bressanelli S, Freire CC, Arcioni S, Gern L, Péter O, et al. Prevalence and phylogenetic analysis of tick-borne encephalitis virus (TBEV) in field-collected ticks (*Ixodes ricinus*) in southern Switzerland. Parasit Vectors. 2014;7:443. https://doi.org/10.1186/1756-3305-7-443
5. Hills SL, Poehling KA, Chen WH, Staples JE. Tick-borne encephalitis vaccine: recommendations of the Advisory Committee on Immunization Practices, United States, 2023. MMWR Recomm Rep. 2023;72:1–29. https://doi.org/10.15585/mmwr.rr7205a1
6. Lindquist L, Vapalahti O. Tick-borne encephalitis. Lancet. 2008;371:1861–71. https://doi.org/10.1016/S0140-6736(08)60800-4
7. Federal Office of Public Health (FOPH). Tick-borne encephalitis (TBE) [cited 2025 Sep 26]. https://www.bag.admin.ch/en/tick-borne-encephalitis-tbe
8. Hills SL, Gould CV. Tick-borne encephalitis. In: CDC Yellow Book 2026: health information for international travel. Oxford University Press; 2025 [cited 2025 Sep 26]. https://www.cdc.gov/yellow-book/hcp/travel-associated-infections-diseases/tick-borne-encephalitis.html
9. Riccardi N, Antonello RM, Luzzati R, Zajkowska J, Di Bella S, Giacobbe DR. Tick-borne encephalitis in Europe: a brief update on epidemiology, diagnosis, prevention, and treatment. Eur J Intern Med. 2019;62:1–6. https://doi.org/10.1016/j.ejim.2019.01.004
10. Steffen R. Epidemiology of tick-borne encephalitis (TBE) in international travellers to Western/Central Europe and conclusions on vaccination recommendations. J Travel Med. 2016;23:taw018. https://doi.org/10.1093/jtm/taw018

Address for correspondence: Gilbert Greub, Institute of Microbiology, University Hospital Center and University of Lausanne, Rue du Bugnon 48, 1011, Lausanne, Switzerland; email: gilbert.greub@chuv.ch

Crimean-Congo Hemorrhagic Fever Virus in Cattle and Ticks, Israel

Nir Rudoler, Marisol Rubinstein-Guini, Asael Roth, Victoria Indenbaum, Oran Erster, Yaniv Lustig, Elad Eliahoo

Author affiliations: Ministry of Agriculture and Food Security, Beit Dagan, Israel (N. Rudoler, M. Rubinstein-Guini, A. Roth, E. Eliahoo); Ministry of Health, Ramat-Gan, Israel (V. Indenbaum, O. Erster, Y. Lustig); Sheba Medical Center, Ramat-Gan (V. Indenbaum, O. Erster, Y. Lustig); Tel Aviv University Faculty of Medical and Health Sciences, Tel Aviv, Israel (Y. Lustig)

We conducted a nationwide serologic and molecular survey to elucidate the epidemiologic status of Crimean-Congo hemorrhagic fever virus in Israel. We found serologic and molecular evidence of virus circulation in the country. Future human cases could be prevented by increasing public awareness and implementing public health measures.

Crimean-Congo hemorrhagic fever virus (CCHFV) is an enveloped segmented negative-sense RNA virus belonging to the *Nairoviridae* family of the *Bunyavirales* order (*1*). The virus is the etiologic agent of Crimean-Congo hemorrhagic fever (CCHF), a severe tickborne zoonotic illness with a wide geographic distribution, infecting ≈10,000–15,000 humans annually worldwide (*2*). Ticks, primarily of the genus *Hyalomma*, are considered the vector and the reservoir of CCHFV (*3*). CCHFV can infect various animal hosts, including livestock, that, although remaining asymptomatic, can act as amplifying hosts of the virus (*4*). CCHFV is transmitted to humans primarily through the bite of an infected tick but also by direct contact with blood or body fluids of infected animals or humans or through improperly sterilized medical equipment (*1*).

Neither CCHFV infection in humans nor positive serologic test results in humans or in animals were previously reported in Israel. However, outbreaks of the disease and seropositivity among livestock have been reported in neighboring countries (*5*). Moreover, the main vector of CCHFV, the *Hyalomma marginatum* tick, is endemic in Israel (*6*). Hence, the risk for CCHFV emergence in Israel is considered high, and undetected viral circulation might already exist in specific regions of the country (*6*).

During April 2024–February 2025, we sampled whole blood, serum specimens, and ticks from 19 beef cattle herds from different regions in Israel. We tested serum samples by using an ELISA commercial kit (ID Screen CCHF Double Antigen Multi-species; Innovative Diagnostics, https://www.innovative-diagnostics.com). We classified the ticks morphologically and extracted RNA to identify CCHFV presence (Appendix, https://wwwnc.cdc.gov/EID/article/31/11/25-0622-App.pdf).

Sixteen beef cattle herds had serologic evidence of prior exposure to CCHFV; seropositivity ranged from 3% to 100% (Table). We detected virus exposure eliciting an immune response in locations across Israel (Figure). Those serologic results are comparable with

Table. Seroprevalence of Crimean-Congo hemorrhagic fever virus in cattle, Israel, April 2024–February 2025

Site of sampling (district)	No. sampled animals	No. (%) seropositive	Average age of sampled animals, y
Kidmat Tzvi (Golan Heights)	34	17 (50)	8.3
Merom Golan (Golan Heights)	39	14 (35.9)	9.3
Ramat Magshimim (Golan Heights)	39	6 (15.4)	8.6
Keshet (Golan Heights)*	30	0	<2
Keshet (Golan Heights)	20	20 (100)	8.08
Ortal (Golan Heights)	25	22 (88)	8.8
Gazit (Yizrael Valley)	30	9 (30)	7.7
Zipori (Yizrael Valley)	17	5 (29.4)	7.05
Alonim (Yizrael Valley)	31	1 (3.2)	2[†]
Na'aura (Gilboa)	21	6 (28.6)	7.5
Nurit (Gilboa)	22	1 (4.7)	5[†]
Gal'ed (Ramat Menashe)	33	10 (30.3)	5.8
Ein Yaakov (Western Galilee)	24	19 (79.1)	8.5
Shetula (Western Galilee)	24	2 (8.3)	2.5
Lapidot (Western Galilee)	30	2 (6.6)	11.8
Kochav Hayarden (Jordan Valley)*	17	0	<2
Kfar Szold (Hula Valley)	30	1 (3.3)	3[†]
Sha'alabim (Gezer)	32	27 (84)	5.7
Avi'ezer (Adulam)*	9	0	<2
Binyamina (Haifa)	29	19 (65.5)	6.07
Total no. samples	536	181 (34)	

*Heifers only.
†Estimated average age provided by owner.

rates reported in CCHFV-endemic countries with confirmed human cases, such as Turkey (Türkiye) (*7*) and Pakistan (*8*). Consistent with prior publications linking older age with seropositivity (*9*), the age of the sampled animals from the 2 herds that were seronegative was <2 years. Moreover, although all serum samples from the heifers (<2 years of age) of the Keshet herd (Golan Heights) were seronegative, subsequent
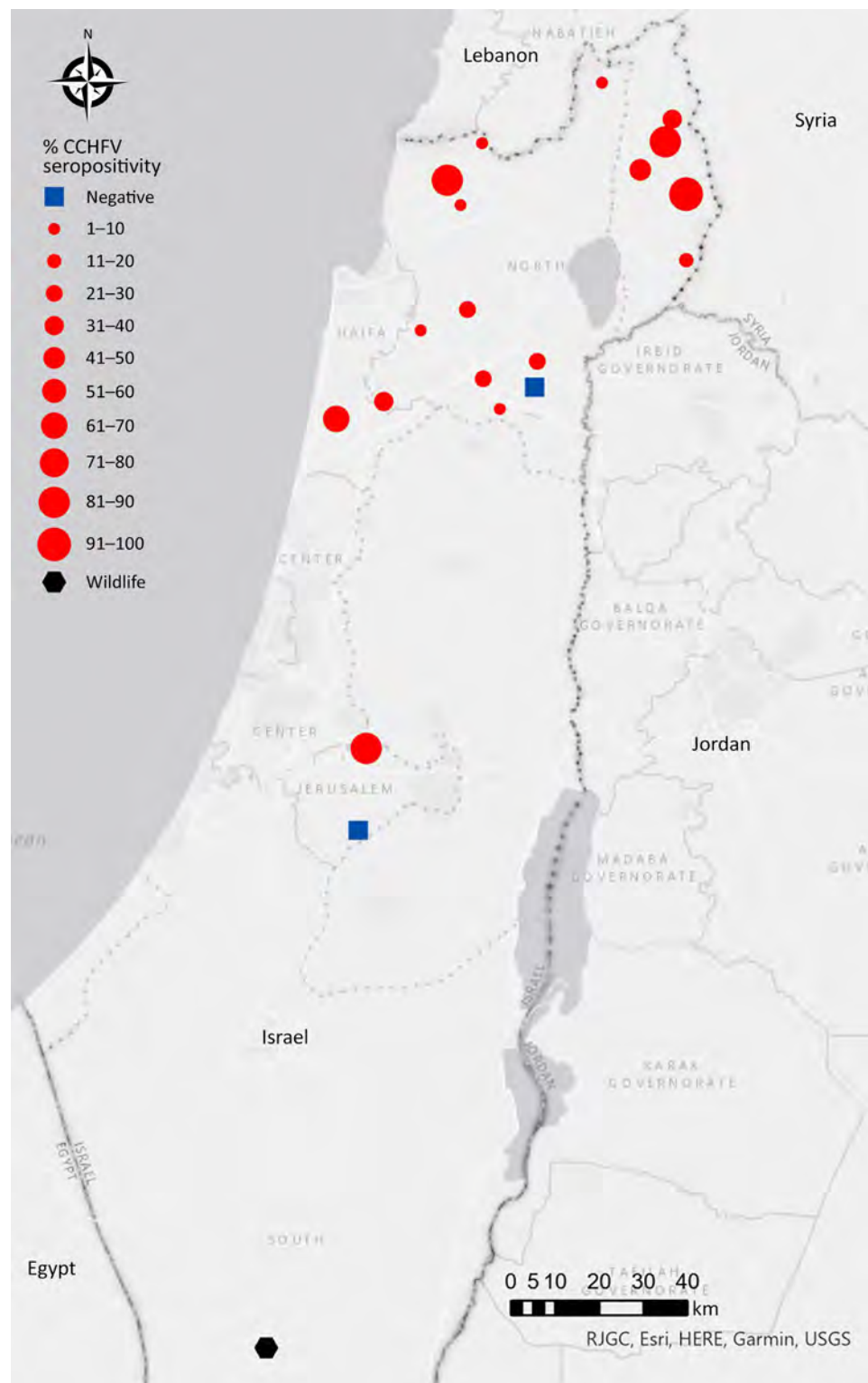

Figure. Distribution of samples seropositive for CCHFV in study of serologic and molecular evidence of CCHFV in cattle and ticks, Israel, April 2024–February 2025. Red dots represent seropositive beef cattle herds. Size of dots correlates with percentage of CCHFV seropositivity. Blue rectangles represent CCHFV seronegative herds. Black hexamer represents 2 of 200 CCHFV seropositive wild animals that were tested. Map created by using ArcGIS software (Esri, https://www.esri.com). CCHFV, Crimean-Congo hemorrhagic fever virus.

sampling of older cows (3–15 years of age) in the herd revealed 100% positive serologic test results (Table). We also tested serum samples that were randomly collected from 200 wild animals dispersed through the country (including boars, foxes, jackals, ibexes, dogs, deer, oryxes, gazelles, and porcupines) during 2023–2024. We found that only 2 samples, from ibexes (*Capra nubiana*) residing in the Negev Desert (southern Israel), were seropositive for CCHFV antibodies (Figure).

We tested for CCHFV RNA in 227 ticks retrieved from 8 cattle herds and 51 ticks retrieved from wildlife by using quantitative reverse transcription PCR targeting 2 regions of the small segment (10). Because we tested each tick individually, we determined a sample to be positive only when both regions were amplified. In addition, the positive samples were validated at an independent facility (The Central Virology Laboratory, Ministry of Health and Sheba Medical Center, Ramat-Gan, Israel). Of the 227 ticks from cattle, 23 (10%) samples collected from northern Israel (Golan Heights and Western Galilee) were positive for CCHFV (Appendix Table 1). Likewise, among 51 ticks collected from wild animals (all sampled from northern Israel), 7 (13%) were positive for CCHFV (Appendix Table 2). All ticks positive for CCHFV belonged to 2 genera, *Hyalomma* and *Rhipicephalus* (Appendix Tables 1, 2). Sanger sequencing of the 181-bp (1,068–1,248 nucleotides at the small segment) amplicons of 10 samples, which we successfully amplified by using endpoint reverse transcription PCR (10), followed by phylogenetic analysis, indicated that the sequences clustered to the Asia-1 genotype (Appendix Figure).

We tested serum samples from 13 persons who had close contact with either CCHFV-positive ticks or seropositive cattle for the presence of CCHF IgG by using ELISA (Euroimmun, https://www.euroimmun.com). All persons tested were seronegative. The study was conducted with the approval of the Shiba Medical Center institutional review board (approval no. 1601–24-SMC).

We present evidence of CCHFV circulation in Israel, expanding the known geographic distribution of CCHFV in the Middle East. We have found serologic evidence of prior exposure to CCHFV in livestock and in wild animals; we also detected CCHFV in the ticks infesting them. Furthermore, the seroprevalence in the cows was found to be comparable to seroprevalence in CCHFV-endemic countries with proven human cases. In addition, the seropositivity prevalence in the cattle and the observation that cows <2 years of age were not seropositive suggest that the virus has been circulating for several years. Still, the route of introduction remains unclear. Our results highlight the importance of raising public and clinical awareness of CCHF, especially among high-risk populations, despite the current absence of human cases.

About the Author

Dr. Rudoler is head of the virology laboratory at the Kimron Veterinary Institute, Israel. His major interests include veterinary public health, zoonotic diseases, and conducting and implementing One Health research projects.

References

1. Hawman DW, Feldmann H. Crimean-Congo haemorrhagic fever virus. Nat Rev Microbiol. 2023;21:463–77. https://doi.org/10.1038/s41579-023-00871-9
2. Frank MG, Weaver G, Raabe V; State of the Clinical Science Working Group of the National Emerging Pathogens Training and Education Center's Special Pathogens Research Network. Crimean-Congo hemorrhagic fever virus for clinicians—virology, pathogenesis, and pathology. Emerg Infect Dis. 2024;30:847–53. https://doi.org/10.3201/eid3005.231646
3. Gargili A, Estrada-Peña A, Spengler JR, Lukashev A, Nuttall PA, Bente DA. The role of ticks in the maintenance and transmission of Crimean-Congo hemorrhagic fever virus: a review of published field and laboratory studies. Antiviral Res. 2017;144:93–119. https://doi.org/10.1016/j.antiviral.2017.05.010
4. Spengler JR, Bergeron É, Rollin PE. Seroepidemiological studies of Crimean-Congo hemorrhagic fever virus in domestic and wild animals. PLoS Negl Trop Dis. 2016;10:e0004210. https://doi.org/10.1371/journal.pntd.0004210
5. Perveen N, Khan G. Crimean-Congo hemorrhagic fever in the Arab world: a systematic review. Front Vet Sci. 2022;9:938601. https://doi.org/10.3389/fvets.2022.938601
6. Messina JP, Wint GRW. The spatial distribution of Crimean-Congo haemorrhagic fever and its potential vectors in Europe and beyond. Insects. 2023;14:771. https://doi.org/10.3390/insects14090771
7. Nurettin C, Engin B, Sukru T, Munir A, Zati V, Aykut O. The seroprevalence of Crimean-Congo hemorrhagic fever in wild and domestic animals: an epidemiological update for domestic animals and first seroevidence in wild animals from Turkiye. Vet Sci. 2022;9:462. https://doi.org/10.3390/vetsci9090462

8. Zohaib A, Saqib M, Athar MA, Hussain MH, Sial AU, Tayyab MH, et al. Crimean-Congo hemorrhagic fever virus in humans and livestock, Pakistan, 2015–2017. Emerg Infect Dis. 2020;26:773–7. https://doi.org/10.3201/eid2604.191154

9. Schulz A, Barry Y, Stoek F, Ba A, Schulz J, Haki ML, et al. Crimean-Congo hemorrhagic fever virus antibody prevalence in Mauritanian livestock (cattle, goats, sheep and camels) is stratified by the animal's age. PLoS Negl Trop Dis. 2021;15:e0009228. https://doi.org/10.1371/journal.pntd.0009228

10. Mazzola LT, Kelly-Cirino C. Diagnostic tests for Crimean-Congo haemorrhagic fever: a widespread tickborne disease. BMJ Glob Health. 2019;4(Suppl 2):e001114. https://doi.org/10.1136/bmjgh-2018-001114

Extensively Drug-Resistant Tuberculosis with Conflicting Resistance Testing Results, Lesotho

Kwonjune J. Seung, Meseret Asfaw, Mikanda Kunda, Llang Bridget Maama-Maime, Joalane Makaka, Mabatloung Mofolo, Stephane Mpinda, Melino Ndayizigiye, Shaheed Vally Omar, Prithiv Prasad, Praharshinie Rupasinghe, Chase Yarbrough, Lawrence Oyewusi

Author affiliations: Brigham and Women's Hospital, Boston, Massachusetts, USA (K. Seung, C. Yarbrough); Partners In Health, Maseru, Lesotho (M. Asfaw, M. Kunda, J. Makaka, M. Mofolo, S. Mpinda, M. Ndayizigiye, P. Prasad); Government of Lesotho Ministry of Health and Social Welfare, Maseru (L.B. Maama-Maime, L. Oyewusi); National Institute for Communicable Diseases, Johannesburg, South Africa (S.V. Omar); Institute of Tropical Medicine, Antwerp, Belgium (P. Rupasinghe)

A patient with extensively drug-resistant tuberculosis in Lesotho recovered successfully after failed treatment with bedaquiline, delamanid, linezolid, and clofazimine. Whole-genome sequencing and broth microdilution testing results were not in agreement, illustrating the urgent need for studies that correlate phenotypic and genotypic resistance testing with clinical response.

New drugs and regimens for treating tuberculosis (TB) have transformed the way in which healthcare providers manage multidrug-resistant (MDR) TB. Bedaquiline, delamanid, and pretomanid are among the newest drugs developed specifically for treating TB. Other drugs, like linezolid and clofazimine, have demonstrated activity against *Mycobacterium tuberculosis* and have therefore gained status as potential treatments for the disease. Healthcare professionals have reported excellent treatment outcomes in patients receiving those drugs, even in low-resource settings that have the highest burden of MDR TB (*1*,*2*). Resistance to those drugs, however, has been increasing faster than access to accurate laboratory resistance testing. Bedaquiline resistance is increasingly common and problematic, given the drug's prominence in most treatment regimens for MDR TB. (*3*).

In 2016, physicians referred a man in his late 30s to the Botsabelo MDR TB referral hospital in Maseru, Lesotho, for suspicion of drug-resistant TB. The man's only previous exacerbation of TB was 2 years earlier, when he received a standard treatment regimen of 4 first-line drugs. At that time, chest radiographs showed bilateral upper lobe infiltrates, more extensive on the right side; PCR testing with Xpert MTB/RIF assay (Cepheid, https://www.cepheid.com) showed resistance to rifampin. He had HIV infection (CD4 115 cells/μL, viral load 20,000 copies/mL), which appeared to be poorly managed because of inconsistent adherence to abacavir, lamivudine, and efavirenz, especially during episodes of binge drinking.

When the patient sought care in 2016, we performed qualitative in vitro testing with GenoType MTBDR*sl* (Hain Lifescience, https://www.hain-lifescience.de), which showed no evidence of mutations conferring resistance to fluoroquinolones or injectables, so we started a standard treatment regimen for MDR TB: pyrazinamide, kanamycin, levofloxacin, prothionamide, cycloserine, and para-aminosalicylic acid (Figure, panel A). Clinical and bacteriologic response was poor. Repeat testing with GenoType MTBDR*sl* showed resistance to fluoroquinolones but not to injectables; we adjusted the drug regimen at month 10 to include bedaquiline and linezolid. At month 14, we added delamanid and clofazimine. Nevertheless, sputum cultures were persistently TB positive. At month 19, BACTEC MGIT (BD, https://www.bd.com) analysis of a sputum isolate sent to the South Africa National Institute for Communicable Diseases (NICD; Johannesburg, South Africa) revealed susceptibility to all second-line TB drugs except moxifloxacin (0.5 μg/mL).
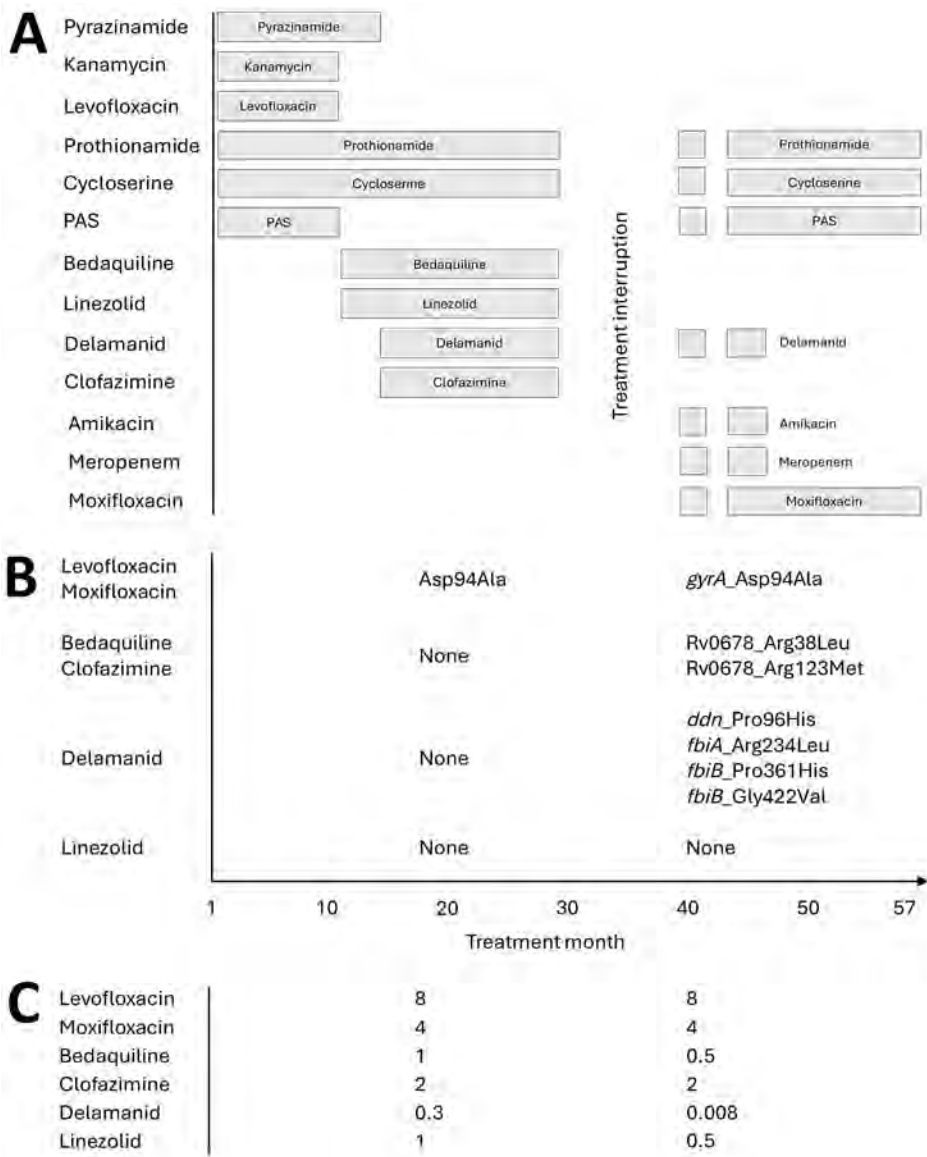
Figure. Data from patient with extensively drug-resistant tuberculosis with conflicting resistance testing results, Lesotho. A) Treatment regimen of the patient. B–C) Drug-resistance mutations (B) and MICs (C) of *Mycobacterium tuberculosis* isolates collected from the patient during months 19 and 42 of treatment. Whole-genome sequence analysis for drug resistance was conducted at the South Africa National Institute for Communicable Diseases (Johannesburg, South Africa), and MIC testing with broth microdilution was conducted at the Institute of Tropical Medicine (Antwerp, Belgium).

After month 29 of follow-up, the patient stopped attending the program, but he returned 8 months later, when his clinical condition worsened. Chest radiographs showed a large, right-sided middle lobe cavity, bilateral lymphadenopathy, and bilateral infiltrates. We consulted thoracic surgeons in Durban, South Africa, about resective surgery, but a right pneumonectomy was not an option because the left lung was also compromised.

In month 42, a sputum isolate sent to NICD confirmed resistance (BACTEC MGIT) to additional second-line drugs, including levofloxacin, moxifloxacin (0.5 µg/mL), bedaquiline, linezolid, and clofazimine. The isolate analysis revealed the TB strain to be susceptible to moxifloxacin at 1.0 µg/mL; delamanid was not tested. We subsequently changed the patient's drug regimen to prothionamide, cycloserine, para-aminosalicylic acid, delamanid, amikacin, meropenem, and high-dose moxifloxacin (800 mg/d). We administered meropenem through a peripheral intravenous tube that was changed every few weeks. The patient improved clinically and bacteriologically, and he completed treatment in month 57, after 5 consecutive negative sputum cultures.

After the patient's recovery, we sent sputum isolates from month 19 and month 42 to NICD, where technicians performed whole-genome sequencing (WGS) analysis (Figure, panel B). We also sent subcultures to the Institute of Tropical Medicine (Antwerp, Belgium) for MIC testing with broth microdilution (Figure, panel C). WGS revealed no resistance mutations for any of these drugs in the month 19 sputum

sample, but the MICs of bedaquiline, clofazimine, and delamanid were above the breakpoints typically considered to be resistant (*4*). In the month 42 sputum sample, WGS found resistance mutations to bedaquiline and clofazimine, consistent with the MIC testing, but there were multiple resistance mutations to delamanid, even though the MIC of delamanid was below the typical breakpoint for resistance. WGS and MIC testing were consistent for fluoroquinolones (resistant) and linezolid (susceptible) in sputum samples from both months.

Complicating interpretation of WGS is the fact that many resistance mutations for the new and repurposed drugs have not yet been discovered. In the patient we treated, who was symptomatic and bacteriologically sputum positive for many months on a regimen containing bedaquiline, clofazimine, delamanid, and linezolid, the mutation conferring resistance to fluoroquinolones, Asp94Ala, is well known, but none of the other mutations found (Figure, panel C) have been previously reported in the scientific literature as conferring resistance to bedaquiline/clofazimine (Rv0678_Arg38Leu, Rv0678_Arg123Met) or delamanid (ddn_Pro96His, fbiA_Arg234Leu, fbiB_Pro361His, fbiB_Gly422Val) (*5*). We considered those to be true resistance mutations because they are located in relevant genes, and the clinical, bacteriologic, and radiologic evidence is consistent with resistance acquisition.

Even with new drugs and regimens, treating MDR TB will continue to be challenging. As both phenotypic and genotypic resistance testing for new and repurposed TB drugs continues to evolve, so must our understanding of how resistance testing correlates with clinical response.

About the Author

Dr. Seung is associate physician at the Division of Global Health Equity at Brigham and Women's Hospital. His primary research interests include drug-resistant TB and the implementation of complex health interventions in resource-limited settings.

References

1. Franke MF, Khan P, Hewison C, Khan U, Huerga H, Seung KJ, et al. Culture conversion in patients treated with bedaquiline and/or delamanid. a prospective multicountry study. Am J Respir Crit Care Med. 2021;203:111–9. https://doi.org/10.1164/rccm.202001-0135OC
2. Guglielmetti L, Khan U, Velásquez GE, Gouillou M, Abubakirov A, Baudin E, et al.; endTB Clinical Trial Team. Oral regimens for rifampin-resistant, fluoroquinolone-susceptible tuberculosis. N Engl J Med. 2025;392:468–82. https://doi.org/10.1056/NEJMoa2400327
3. Perumal R, Bionghi N, Nimmo C, Letsoalo M, Cummings MJ, Hopson M, et al. Baseline and treatment-emergent bedaquiline resistance in drug-resistant tuberculosis: a systematic review and meta-analysis. Eur Respir J. 2023; 62:2300639. https://doi.org/10.1183/13993003.00639-2023
4. Mansjö M, Espinosa-Gongora C, Samanci I, Groenheit R, Werngren J. Performance of a broth microdilution assay for routine minimum inhibitory concentration determination of 14 anti-tuberculous drugs against the *Mycobacterium tuberculosis* complex based on the EUCAST reference protocol. Antimicrob Agents Chemother. 2025;69:e0094624. https://doi.org/10.1128/aac.00946-24
5. World Health Organization. Catalogue of mutations in *Mycobacterium tuberculosis* complex and their association with drug resistance, 2nd ed. Geneva: The Organization; 2023 [cited 2025 Nov 21] https://iris.who.int/handle/10665/374061

Address for correspondence: K.J. Seung, Brigham and Women's Hospital, 75 Francis St, Boston, MA 02115, USA; email: kjseung@gmail.com

Orientia tsutsugamushi Antibodies in Patients with Eschars and Suspected Tickborne Disease

Haley A. Abernathy,[1] Lauryn Ursery,[1] Brooke A. Merdjane, Dana A. Giandomenico, Ross M. Boyce

Author affiliation: University of North Carolina at Chapel Hill, Chapel Hill, North Carolina, USA

To investigate local transmission of *Orientia tsutsugamushi* by chiggers in North Carolina, USA, we tested remnant serum specimens from patients with eschar undergoing testing for suspected tickborne disease. We identified 11 persons with *O. tsutsugamushi* antibodies, including 4 who were positive by both assays; none had severe clinical manifestations consistent with scrub typhus.

[1]These first authors contributed equally to this article.

Scrub typhus, caused by *Orientia tsutsugamushi* bacteria and transmitted by Trombiculid mites, affects >1 million persons each year (*1,2*). Clinical disease is characterized by fever, headache, and eschars. Untreated, case-fatality rates for the disease can exceed 30% (*2,3*).

Most cases of scrub typhus occur in Asia and the Pacific. Although the vectors, commonly known as chiggers, are widely distributed across North America, no autochthonous (i.e., locally acquired) cases have been reported in the United States. In 2023, however, researchers identified *O. tsutsugamushi* in chiggers collected in North Carolina (*4*). To investigate potential transmission to humans in North Carolina, we sought to estimate the seroprevalence of *O. tsutsuguamushi* antibodies and assess the clinical characteristics of persons with evidence of exposure. We hypothesized that cases of eschar are more likely to be caused by endemic tickborne Rickettsiaceae, such as *Rickettsia parkeri* bacteria (*5*).

The protocols of the parent study have been published (*6*). In brief, we collected remanent serum specimens from adult patients undergoing testing for spotted fever group *Rickettsia* or *Ehrlichia* spp. bacteria as part of routine care for acute febrile illness. For the purposes of this study, we selected serum specimens from patients with documented eschar.

We performed serologic testing in parallel by using 2 commercially available kits. We performed all tests according to manufacturers' instructions and ran the tests with the included positive and negative controls. We first tested samples by using IgM-specific indirect immunofluorescence antibody (IFA) assays against *O. tsutsugamushi* (Fuller Laboratories, https://fullerlaboratories.com) (*7*). We diluted samples to a reciprocal titer of 1:64. In parallel, specimens underwent testing with the Scrub Typhus Detect ELISA-based assays that detect IgM and IgG (InBios International Inc., https://inbios.com). We diluted samples to a reciprocal titer of 1:100. The IgG ELISA kit instructions suggested an optical density (OD) cutoff of 0.37, but the IgM kit did not suggest a cutoff. We applied the 0.37 OD cutoff to the IgG results but also applied several IgM and IgG OD cutoffs from existing literature (*8,9*) (Table 1). We estimated seropositivity and used the Clopper-Pearson exact method to calculate 95% CIs.

A total of 138 (5.3%) of 2,593 persons had an eschar documented. Of those, 101 had an adequate sample volume. On the basis of the number of slides and kits available, we selected 87 (86.1%) samples for IFA and 92 (91.1%) samples for ELISA from 83 unique person; some persons had both acute and convalescent samples tested. Of the 83 persons, 35 (42.1%) had illnesses that had been classified as confirmed, probable, or suspected cases of spotted fever group *Rickettsia* (*10*) (Appendix Table 1, https://wwwnc.cdc.gov/EID/article/31/11/25-0763-App.pdf).

By IFA result, we classified 18 (20.6%) of 87 samples as indeterminate (i.e., weakly positive). By ELISA result, 4 (4.3%) of 92 were positive for *O. tsutsugamushi* IgM and 8 (8.9%) of 90 for IgG; no samples were positive for both. None of the 18 samples that were indeterminate by IFA were positive by ELISA. The 8 samples IgG-positive by ELISA results underwent confirmatory IgG IFA testing at Fuller Laboratories (Appendix Table 2). We observed 50% (4 of 8) agreement in IgG reactivity between ELISA and IFA results at an endpoint titer of 1:128.

Of the 11 persons with either a reactive IgG or IgM, 7 (63.6%) reported a tick bite. None of the clinical encounters were associated with travel. Fever and myalgia were the most common clinical syndrome (Table 2). All patients were seen in outpatient settings, and none were hospitalized.

Our study identified North Carolina residents with antibodies reactive against *O. tsutsugamushi* bacteria. However, those results must be interpreted cautiously. The presence of antibodies does not indicate active infection but can be a marker of prior exposure. In addition, in a setting where transmission has not been previously reported, positive results are more likely to be falsely positive because of imperfect test performance. However, the presence of antibodies, especially when indicated by both assays, was unexpected and merits investigation.

Including only persons who had reactive antibodies by both assays (n = 4), our estimate of IgG

Table 1. Seropositivity estimates based on IgM and IgG ELISA at varying optical density thresholds in study of *Orientia tsutsugamushi* bacteria in patients with eschars and suspected tickborne disease, North Carolina, USA, 2020–2022*

Test	Optical density cutoff	Sensitivity	Specificity	Positive, n = 92	% Seropositive (95% CI)
IgG ELISA	0.37	NR	NR	8	8.7 (3.8–16.4)
IgG ELISA (*8*)	1.0	97.5	60	1	1.1 (0.0–5.9)
IgG ELISA (*8*)	1.6	91	75	0	0.0 (0.0–3.9)
IgM ELISA (*8,9*)	0.6	96.4	82.7	2	2.2 (0.3–7.6)
IgM ELISA (*8*)	0.492	97.1	79.1	4	4.3 (1.2–10.8)

*NR, not reported.

Table 2. Demographic, clinical, and laboratory test results of persons with antibodies against *Orientia tsutsugamushi* in study of *O. tsutsugamushi* among patients with eschars and suspected tickborne disease, North Carolina, USA, 2020–2022*

Person no.	Age, y/sex	IFA result	ELISA result	Tick bite	Fever	Headache	Myalgia	Rash	SFGR classification	*Ehrlichia* classification
1	42/M	IgG+	IgG+	Yes		X		X	Probable	Probable
2	48/M	IgG+	IgG+	Yes	X	X	X		NAC	Unknown
3	66/M	IgG+	IgG+	Yes		X	X	X	NAC	Probable
4	55/F	IgG+	IgG+	Unknown	X	X			NAC	NAC
5	76/F	Negative	IgG+	Yes					Probable	Probable
6	64/M	Negative	IgG+	Yes	X		X		Probable	NAC
7	43/F	Negative	IgG+	Unknown					NAC	Unknown
8	60/F	Unknown	IgM+	Yes			X		NAC	Probable
9	44/M	Negative	IgM+	Unknown					Probable	Unknown
10	78/F	Unknown	IgM+	No	X				Unknown	NAC
11	72/F	Unknown	IgM+	Yes	X		X		Probable	Probable

*IFA, immunofluorescence antibody; NAC, not a case (i.e., did not meet Council of State and Territorial Epidemiologists criteria); SFGR, spotted fever group *Rickettsia*; Unk, unknown or not reported; X, sign or symptom present in patient.

seroprevalence is 4.3% (95% CI 1.2%–10.8%) but, depending on the assay and cutoffs applied, might be as high as 8.9. However, if *O. tsutsugamushi* bacteria were being locally transmitted, we would expect cases of severe illness, which we did not observe.

One limitation of this study is its reliance on serologic results and absence of contextual information, including travel histories and clinical outcomes. In addition, most patients did not have convalescent titers drawn, so we were unable to confirm cases.

We believe the current evidence does not support transmission of virulent *O. tsutsugamushi* strains in North Carolina. Further investigation, ideally by using molecular approaches from clinical samples (e.g., eschar swab samples), is needed. Clinicians should maintain a high level of suspicion for *R. parkeri* rickettsiosis, the seroprevalence of which was nearly 10 times greater than *O. tsutsugamushi*, when evaluating patients with arthropod-associated eschars.

Acknowledgments

About the Author

Ms. Abernathy and Ms. Ursery are doctoral students in epidemiology at the University of North Carolina at Chapel Hill Gillings School of Global Public Health. Ms. Abernathy's research interests include the laboratory diagnosis of infectious diseases. Ms. Ursery's research interests include infections in pregnancy and early childhood.

References

1. Rajapakse S, Weeratunga P, Sivayoganathan S, Fernando SD. Clinical manifestations of scrub typhus. Trans R Soc Trop Med Hyg. 2017;111:43–54. https://doi.org/10.1093/trstmh/trx017
2. Bonell A, Lubell Y, Newton PN, Crump JA, Paris DH. Estimating the burden of scrub typhus: a systematic review. PLoS Negl Trop Dis. 2017;11:e0005838. https://doi.org/10.1371/journal.pntd.0005838
3. Wang Q, Ma T, Ding F, Lim A, Takaya S, Saraswati K, et al. Global and regional seroprevalence, incidence, mortality of, and risk factors for scrub typhus: a systematic

review and meta-analysis. Int J Infect Dis. 2024;146:107151. https://doi.org/10.1016/j.ijid.2024.107151

4. Chen K, Travanty NV, Garshong R, Crossley D, Wasserberg G, Apperson CS, et al. Detection of *Orientia* spp. bacteria in field-collected free-living *Eutrombicula* chigger mites, United States. Emerg Infect Dis. 2023;29:1676–9. https://doi.org/10.3201/eid2908.230528

5. Paddock CD, Sumner JW, Comer JA, Zaki SR, Goldsmith CS, Goddard J, et al. *Rickettsia parkeri*: a newly recognized cause of spotted fever rickettsiosis in the United States. Clin Infect Dis. 2004;38:805–11. https://doi.org/10.1086/381894

6. Ursery L, Mansour O, Abernathy H, Wichmann E, Yackley A, Siegler A, et al. Enhanced surveillance for tick-borne rickettsiosis and ehrlichiosis in North Carolina: protocol and preliminary results. PLoS One. 2025; 20:e0320361. https://doi.org/10.1371/journal.pone.0320361

7. Gupta N, Chaudhry R, Thakur CK. Determination of cutoff of ELISA and immunofluorescence assay for scrub typhus. J Glob Infect Dis. 2016;8:97–9. https://doi.org/10.4103/0974-777X.188584

8. Blacksell SD, Tanganuchitcharnchai A, Nawtaisong P, Kantipong P, Laongnualpanich A, Day NP, et al. Diagnostic accuracy of the InBios Scrub Typhus Detect enzyme-linked immunoassay for the detection of IgM antibodies in northern Thailand. Clin Vaccine Immunol. 2015;23:148–54. https://doi.org/10.1128/CVI.00553-15

9. Rawat V, Singh RK, Kumar A, Singh Y, Chaturvedi P, Saxena SR, et al. Diagnostic validation of IgM and IgG ELISA and real-time PCR in detecting scrub typhus infection in endemic regions. J Vector Borne Dis. 2018;55:165–7. https://doi.org/10.4103/0972-9062.242565

10. Council of State and Territorial Epidemiologists. Changes to public health reporting and national notification for spotted fever rickettsiosis (including Rocky Mountain spotted fever). Council of State and Territorial Epidemiologists; 2019.

Address for correspondence: Ross M. Boyce, Division of Infectious Diseases, University of North Carolina at Chapel Hill, CB# 7030, Bioinformatics Building, 130 Mason Farm Rd, Chapel Hill, NC 27599, USA; email: roboyce@med.unc.edu.

Mortality Event in Rainbow Snakes Linked to Snake Fungal Disease, United States

Dane A. Conley, Gaëlle Blanvillain, Jaimie L. Miller, Kate E. Langwig, John D. Kleopfer, Jeffrey M. Lorch,[1] Joseph R. Hoyt[1]

Author affiliations: Virginia Polytechnic Institute and State University, Blacksburg, Virginia, USA (D.A. Conley, G. Blanvillain, K.E. Langwig, J.R. Hoyt); University of Wisconsin–Madison, School of Veterinary Medicine, Madison, Wisconsin, USA (J.L. Miller); Virginia Department of Wildlife Resources, Henrico, Virginia, USA (J.D. Kleopfer); US Geological Survey, National Wildlife Health Center, Madison (J.M. Lorch)

We report mortality in rainbow snakes in Virginia and North Carolina, USA, linked to snake fungal disease caused by *Ophidiomyces ophidiicola*. During 2013–2023, we observed 46 dead rainbow snakes with lesions indicative of snake fungal disease, noted elevated disease severity compared with other species, and recorded fewer live snakes over time.

Detecting and assessing declines in elusive or rare species can be difficult. Early identification of populations in decline can help accelerate intervention strategies and reduce the likelihood of genetic bottlenecks, population extirpation, and trophic disturbances of ecologically important species (1). Snake fungal disease (SFD) is caused by the fungal pathogen *Ophidiomyces ophidiicola* and affects a broad range of snake species (2), causing skin lesions as the fungus invades tissues, sometimes leading to impaired movement, anorexia, and even death (3). Researchers have documented population impacts from SFD in 2 snake species (4,5), but the extent of mortality across snake species is likely underestimated due to the cryptic nature of snakes. We describe a multiyear mortality event associated with SFD in a rare species, the rainbow snake (*Farancia erytrogramma*), in Virginia and North Carolina, USA.

In spring 2019, regional biologists from the Back Bay region of North Carolina and Virginia reported 6 deceased rainbow snakes. In spring of 2020, we found an additional 6 snakes in the same area (Figure 1, panel A). After those events, we gathered additional records of dead rainbow snakes (Appendix Table 1, https://wwwnc.cdc.gov/EID

---

[1]These authors contributed equally to this article.

article/31/11/25-0547-App1.pdf) from the region and began regular surveys and sampling of rainbow snakes and other species for *O. ophidiicola* in 2020–2023 (Appendix).

We captured and swabbed snakes in accordance with previously published protocols (*6*) and used sterile procedures for disinfecting equipment (Appendix). We extracted DNA from and tested samples using quantitative PCR (qPCR) to determine the presence of *O. ophidiicola*, according to established methods (*6*,*7*). To quantify lesion severity for all live-captured snakes, we used an approach integrating snake
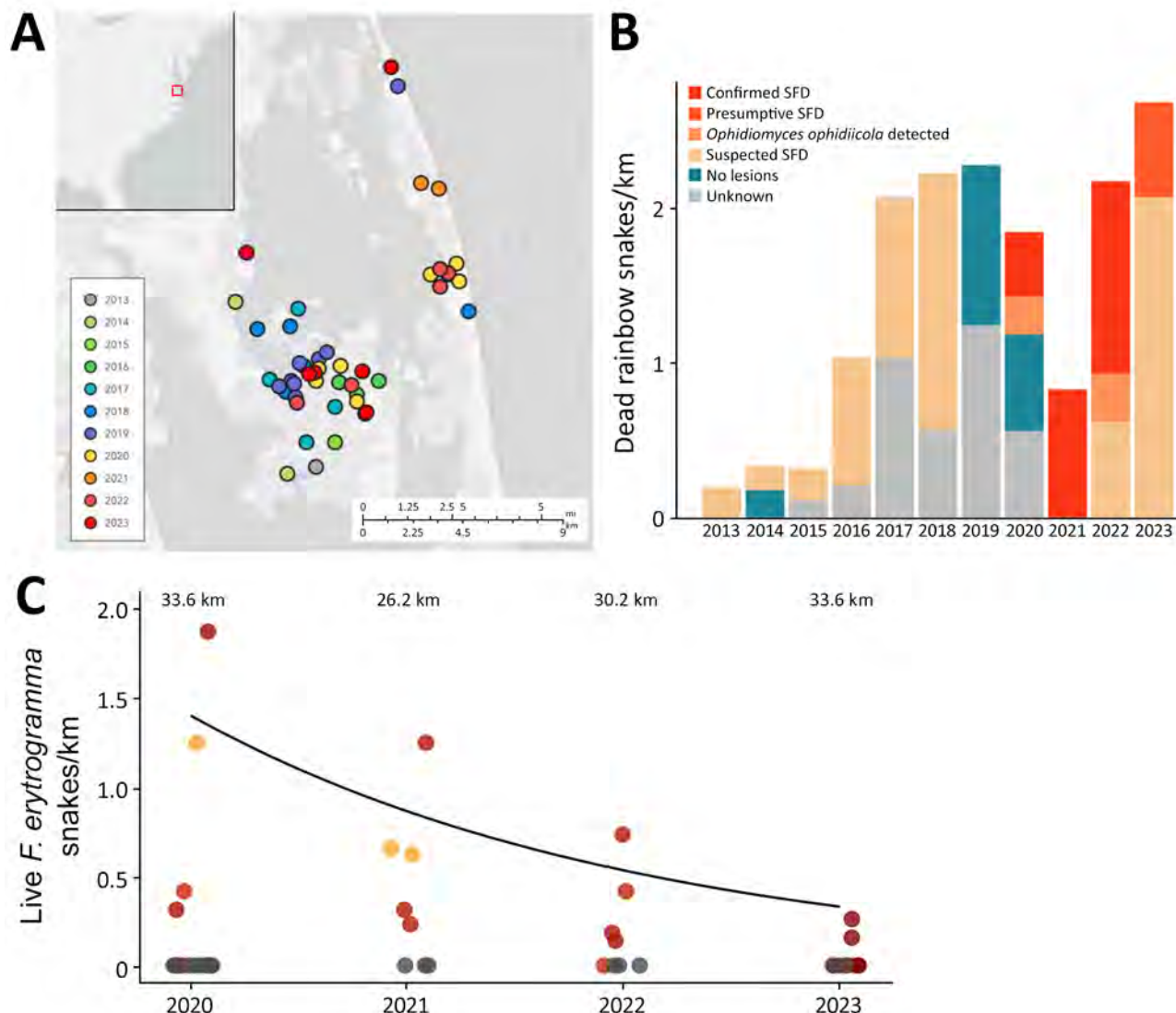
Figure 1. Encounters with dead and live snakes over time from a study of a mortality event in rainbow snakes linked to SFD, United States. A) Map of locations where dead *Farancia erytrogramma* rainbow snakes were observed during 2013–2023. Exact locations were jittered to obscure sensitive habitat. B) Stacked bar plot showing dead rainbow snakes found per kilometer in the Back Bay region of Virginia and North Carolina. Dead snakes characterized based on strength of evidence that they died from SFD: suspected, snakes with characteristic SFD lesions in photographs but no screening for *Ophidiomyces ophidiicola* performed; presumptive, snakes with characteristic SFD lesions, detection of *O. ophidiicola*, but no necropsies performed; confirmed, snakes with characteristic SFD lesions, detection of *O. ophidiicola*, and characteristic histologic lesions confirmed through histology; *O. ophidiicola* detected, snakes with no apparent lesions but tested positive for *O. ophidiicola;* no lesions, snakes with no apparent lesions in photographs and not tested for *O. ophidiicola*; unknown, snakes with no photographs of the dorsal and ventral sides. C) Number of live rainbow snakes encountered in the field per kilometer of transect surveyed with an incorporated 20-coverboard array during 2020–2023 (n = 19; zero-inflated Poisson log-scale year coefficient = −0.482 ± 0.226; p = 0.033) (Appendix Table 3, https://wwwnc.cdc.gov/EID/article/31/11/25-0547-App1.pdf). Total kilometers surveyed per year represented above survey data points. Color shading corresponds to mean infection severity (red is more severe than orange) during sampling event when the species was detected. Gray indicates sampling events without live rainbow snakes detected. SFD, snake fungal disease.
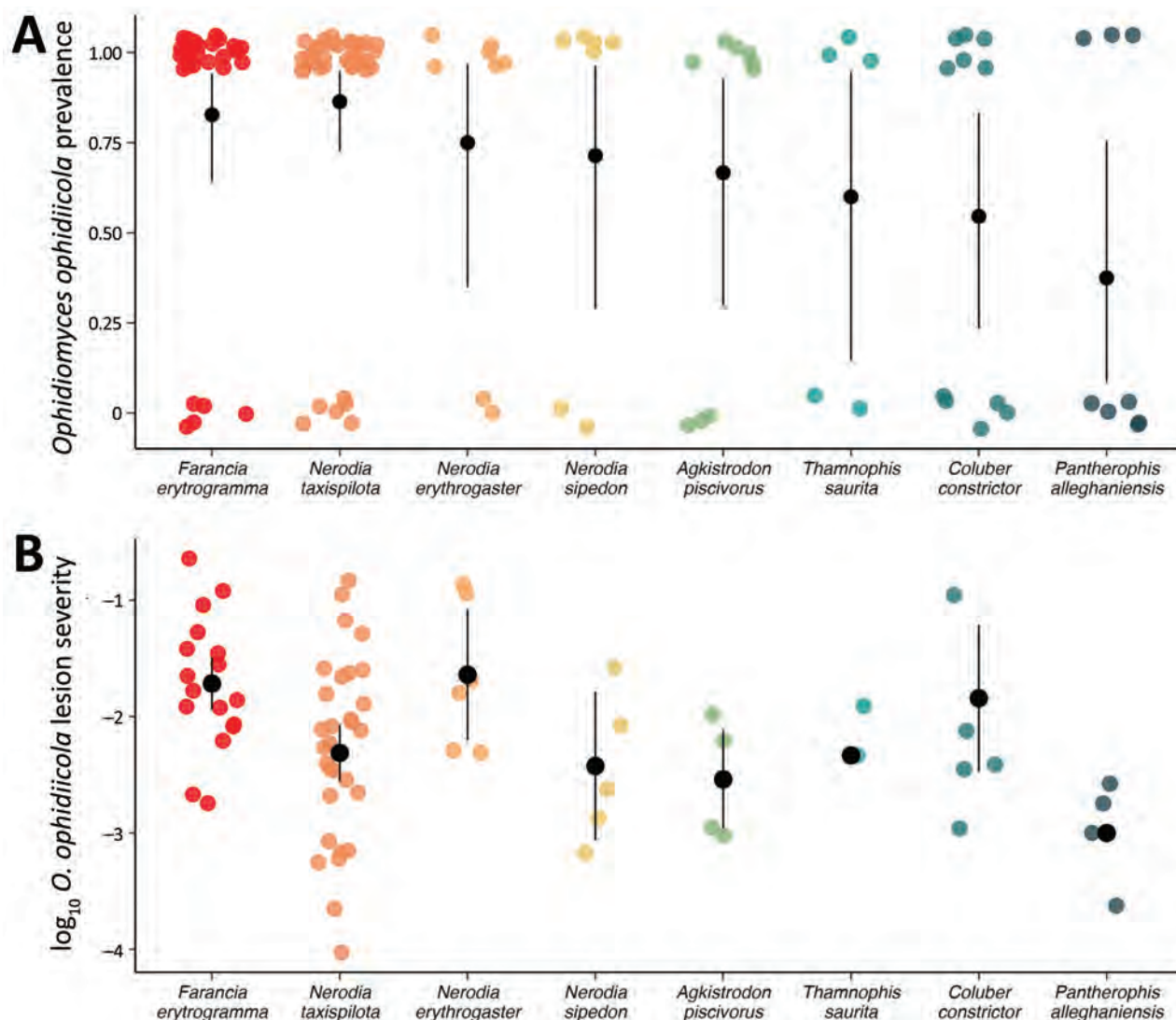
Figure 2. Variation in *Ophidiomyces ophidiicola* infection among snake species from a study of a mortality event in rainbow snakes linked to snake fungal disease, United States. Sampling results during spring (January–June) in 2020–2023 in the Back Bay watershed in Virginia and North Carolina. Black circles and error bars indicate mean lesion severity with 95% CIs. A) Each colored point represents an individual snake sampled and whether it was positive (1) or negative (0) for *O. ophidiicola*. Data points are slightly jittered for visualization purposes. B) Summed lesion severity values accounting for lesion size, lesion progression, and proportion of snake affected (Appendix, https://wwwnc.cdc.gov/EID/article/31/11/25-0547-App1.pdf). Snakes without lesions were omitted.

size, lesion size, and lesion progression (Appendix Table 2, Figure 1).

All dead rainbow snakes screened by qPCR (n = 9) were positive for *O. ophidiicola* and had skin lesions characteristic of SFD (Figure 1, panel B). Necropsies on a subsample (n = 6) indicated all snakes examined had lesions consistent with *O. ophidiicola* infection, including thickening of the epidermis by eosinophilic necrotic cellular debris containing fungal hyphae. Snakes also had invasion by hyphae in deeper tissue, including the dermis (6/6) (Appendix Figure 2, panel A), underlying skeletal muscle (3/6), and in oral and nasal epithelium and tooth pulp (1/6). We also observed hyphae or fi-

brin thrombi within blood vessels in the dermis (5/6). Most snakes (4/6) were in good body condition, had large amounts of fat, and showed no signs of other serious pathologic processes. We considered SFD as the ultimate cause of death in all 6 snakes.

We also examined the number of live rainbow snakes captured over time using sampling data from standardized surveys conducted in 2020–2023 to assess preliminary trends while accounting for effort (Figure 1, panel C). We found a general decrease in the probability of detecting live rainbow snakes over time (log-scale year coefficient = −0.482 ± 0.226; p = 0.033) (Figure 1, panel C; Appendix Tables 3, 4).

A broader comparison of *O. ophidiicola* prevalence and severity of infection among other snakes in the community revealed that rainbow snakes were among the most infected species (Figure 2): *O. ophidiicola* prevalence was 80.1% (95% CI 62.5%–92.5%), and log$_{10}$ lesion severity was −1.71 (95% CI −1.94 to −1.50) (Appendix). Several other snake species also had notably high prevalence of *O. ophidiicola* and did not differ greatly from rainbow snakes (Figure 2, panel A) but were not found dead as part of the ongoing mortality event. Although live rainbow snakes were rare within the broader snake community (total live captures 16.4% [95% CI 11.3%–23%]; n = 25/153), they were disproportionately represented among dead snakes (87.5% [95% CI 52.9%–97.8%]; n = 7/8) found during the same period (2020–2023).

Observing wildlife mortality without obvious cause is rare and can indicate a more serious problem (*8*). We documented mortality of *F. erytrogramma* snakes using photographic, molecular, and histologic evidence, providing support that infection with *O. ophidiicola* are likely responsible. Rainbow snakes are considered a species of conservation concern, and although mortality in the species appeared to be ongoing as of 2023, the full extent of population declines remains uncertain.

O. ophidiicola was likely introduced to the United States in the early 1900s, although new (and possibly more virulent) strains have emerged recently (*9*). Increases in rainbow snake mortality could be the result of the introduction of more virulent strains of *O. ophidiicola* or shifts in environmental conditions since 2014 (*10*), but it is unclear why rainbow snakes appear particularly susceptible to infection (Figure 2). Nonetheless, the observed epizootic from a pathogen that has existed in North America for decades suggests SFD remains a threat to snake populations, which are a critical ecologic component of many ecosystems. Further research on the potential effects of *O. ophidiicola* would help clarify the impacts and trends of this disease on snake populations. Our study highlights the potential impact of disease-causing fungi such as *O. ophidiicola* on unmonitored, cryptic snake species like the rainbow snake.

Acknowledgments

About the Author

Mr. Conley is a PhD student in the Department of Biological Sciences at Virginia Polytechnic Institute and State University. His primary research interests include herpetology, ecology, and infectious disease in wildlife.

References

1. Mörner T, Obendorf DL, Artois M, Woodford MH. Surveillance and monitoring of wildlife diseases. Rev Sci Tech. 2002;21:67–76. https://doi.org/10.20506/rst.21.1.1321

2. Di Nicola MR, Coppari L, Notomista T, Marini D. Ophidiomyces ophidiicola detection and infection: a global review on a potential threat to the world's snake populations. Eur J Wildl Res. 2022;68:64. https://doi.org/10.1007/s10344-022-01612-8

3. Lorch JM, Knowles S, Lankton JS, Michell K, Edwards JL, Kapfer JM, et al. Snake fungal disease: an emerging threat to wild snakes. Philos Trans R Soc Lond B Biol Sci. 2016;371:20150457. https://doi.org/10.1098/rstb.2015.0457

4. Clark RW, Marchand MN, Clifford BJ, Stechert R, Stephens S. Decline of an isolated timber rattlesnake (*Crotalus horridus*) population: interactions between climate change, disease, and loss of genetic diversity. Biol Conserv. 2011;144:886–91. https://doi.org/10.1016/j.biocon.2010.12.001

5. Tetzlaff SJ, Ravesi MJ, Allender MC, Carter ET, DeGregorio BA, Josimovich JM, et al. Snake fungal disease affects behavior of free-ranging massasauga rattlesnakes (*Sistrurus catenatus*). Herpetol Conserv Biol. 2017;12:624–34.

6. Blanvillain G, Lorch JM, Joudrier N, Bury S, Cuenot T, Franzen M, et al. Contribution of host species and pathogen clade to snake fungal disease hotspots in Europe. Commun Biol. 2024;7:440. https://doi.org/10.1038/s42003-024-06092-x

7. Bohuski E, Lorch JM, Griffin KM, Blehert DS. TaqMan real-time polymerase chain reaction for detection of *Ophidiomyces ophiodiicola*, the fungus associated with snake fungal disease. BMC Vet Res. 2015;11:95. https://doi.org/10.1186/s12917-015-0407-8

8. Smith TC, Picco AM, Knapp R. Ranaviruses infect mountain yellow-legged frogs (*Rana muscosa* and *Rana sierrae*) threatened by *Batrachochytrium dendrobatidis*. Herpetol Conserv Biol. 2017;12:149–59.

9. Ladner JT, Palmer JM, Ettinger CL, Stajich JE, Farrell TM, Glorioso BM, et al. The population genetics of the causative agent of snake fungal disease indicate recent introductions to the USA. PLoS Biol. 2022;20:e3001676. https://doi.org/10.1371/journal.pbio.3001676

10. Guthrie AL, Knowles S, Ballmann AE, Lorch JM. Detection of snake fungal disease due to *Ophidiomyces ophiodiicola* in virginia, USA. J Wildl Dis. 2016;52:143–9. https://doi.org/10.7589/2015-04-093.1

Address for correspondence: Dane Conley, Polytechnic Institute and State University, 1015 Life Science Cir, Steger 352, Blacksburg, VA 24061, USA; email: daneaconley@gmail.com

Emergence of Dengue Virus Serotype 3, Lineage III_B.3.2, Angola

Jocelyne Neto de Vasconcelos,[1] Ingra M. Claro,[1] Raissa Heloisa de Araujo Eliodoro,[1] Filipe R.R. Moreira, Amilton Pereira, Luzia Samuel, Esménia Coelho Rocha, Eusébio Manuel, Nelson Mapenzi-Kashali, Fiston Cikaya Kankolongo, Darlan S. Cândido, Jaqueline Goes de Jesus, Gilda Mariano, Sofia Sousa, Carina Clemente, Cláudia Muenga, Ilaria Dorigatti, William M. de Souza, Charles Whittaker, Victoria M. Cox, Wes Hinsley, Nicholas Loman, Joshua Quick, Placide Mbala,[2] Nuno R. Faria,[2] Joana Morais,[2] on behalf of the FEEVIR Consortium[3]

Author affiliations: Centro de Investigação em Saúde de Angola, Bengo, Angola (J.N. de Vasconcelos); Ministry of Health, Luanda, Angola (J.N. de Vasconcelos, A. Pereira, L. Samuel, E. Manuel, J. Morais); Imperial College London, London, UK (J.N. de Vasconcelos, D.S. Cândido, I. Dorigatti, C. Whittaker, V.M. Cox, W. Hinsley, N.R. Faria); Universidade de São Paulo, São Paulo, Brazil (I.M. Claro, R.H. de Araujo Eliodoro, E. Coelho Rocha, J.G. de Jesus, N.R. Faria); University of Kentucky, Lexington, Kentucky, USA (I.M. Claro, W.M. de Souza); Federal University of Rio de Janeiro, Rio de Janeiro, Brazil

[1]These first authors contributed equally to this article.

[2]These senior authors contributed equally to this article.

[3]Members of the group are listed at the end of this article.

(F.R.R. Moreira); Universidade Agostinho Neto, Luanda (E. Manuel, J. Morais); Institut National de Recherche Biomédicale, Kinshasa, Democratic Republic of the Congo (N. Mapenzi-Kashali, F. Cikaya Kankolongo, P. Mbala); Bahiana School of Public Health, Bahia, Brazil (J.G. de Jesus); Cligest Clinic, Luanda (G. Mariano, S. Sousa, C. Clemente, C. Muenga); University of Birmingham, Birmingham, UK (N. Loman, J. Quick); Université de Kinshasa, Kinshasa (P. Mbala)

We detected dengue virus serotype 3 in 11.8% (16/136) of febrile patients in Luanda Province, Angola, during April and July 2024. Our genetic analyses reveal that dengue virus serotype 3 lineage III_B.3.2 probably was imported from the Americas into Angola in late 2022 and then spread through local transmission.

Dengue virus (DENV) is transmitted primarily by *Aedes aegypti* mosquitoes and is the most widespread arbovirus globally (*1*). DENV is classified into 4 serotypes, DENV-1–4, each comprising several genotypes and lineages (*2*). Secondary infection with a heterologous serotype can increase disease severity through antibody-dependent enhancement (*3*).

In Africa, DENV incidence has risen sharply (*4*). Although malaria remains the dominant febrile illness, climate change might be increasing suitability for *Aedes* mosquito–borne arboviruses in the continent. In Angola, dengue became a notifiable disease in 2017. Molecular surveillance has previously confirmed the circulation of DENV-1 (2013) (*5*), and DENV-2 (2018) (*6*). In April 2024, four suspected dengue cases in Luanda Province reported to Angola's Ministry of Health prompted an outbreak investigation.

We tested a convenience sample of 136 febrile patients (median age 33.5 years, interquartile range [IQR] 13–39 years) who visited 3 clinics in Luanda Province during April–November 2024. We tested residual diagnostic samples for DENV, chikungunya virus (CHIKV), and Zika virus (ZIKV) by using real-time reverse transcription PCR (Taqman Arbovirus Triplex Kit; Thermo Fisher Scientific, https://www.thermofisher.com/us/en/home.html.html) at the National Institute for Health Research under Angola's National Arbovirus Surveillance program and in accordance with the National Ethics Committee of the Ministry of Health.

Of 136 samples, 16 (11.8%) were positive for DENV (Figure; Appendix Figure 1, https://wwwnc.cdc.gov/EID/article/31/11/25-1079-App1.pdf). Median cycle threshold was 29.7 (IQR 26.9–32.1),
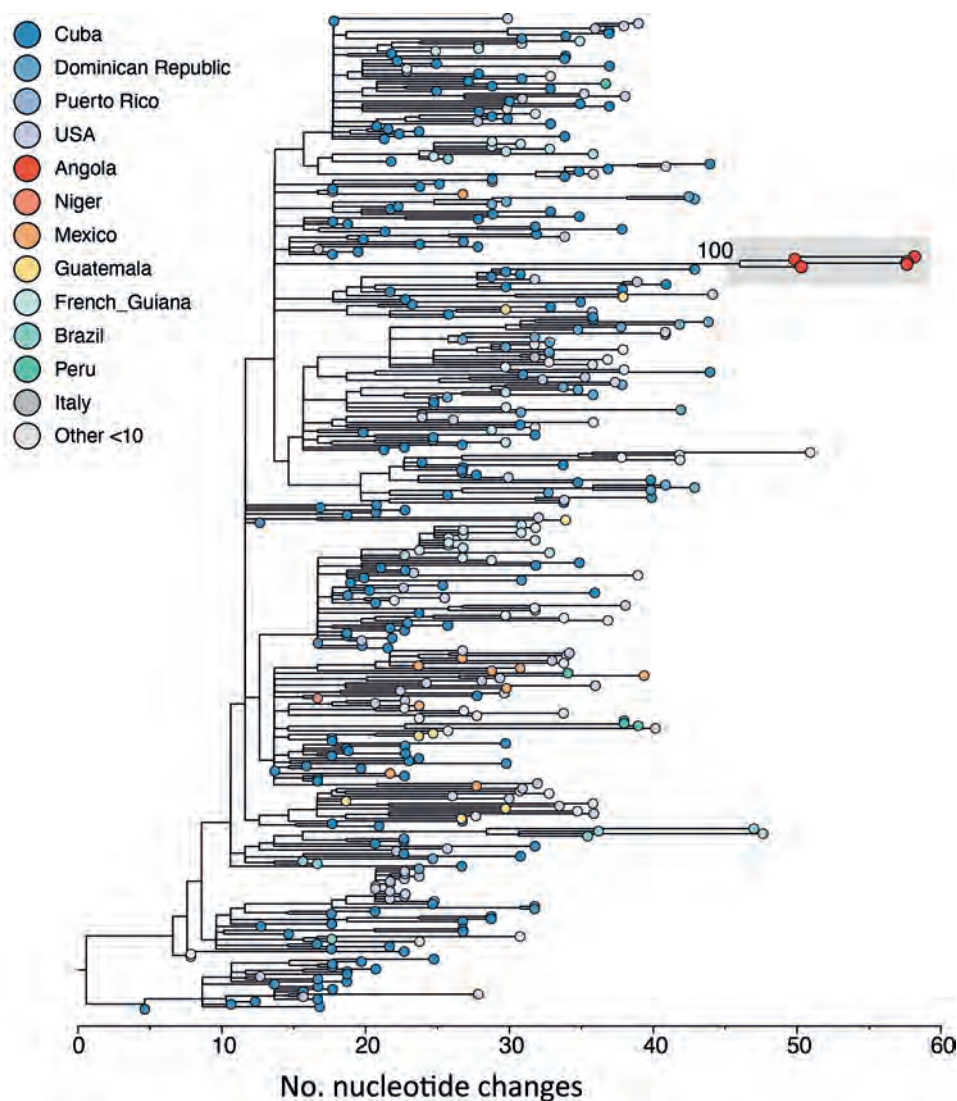
Figure. Maximum-likelihood phylogenetic tree for dengue virus serotype 3, lineage III_B.3.2, Angola. Tips are colored by country of infection. Luanda sequences are shown in red (Appendix Figures 5, 6, https://wwwnc.cdc.gov/EID/article/31/11/25-1079-App1.pdf). Countries with <10 sequences are grouped as other and include Costa Rica (n = 7), Trinidad and Tobago (n = 7), Haiti (n = 4), Guyana (n = 3), Italy (n = 2), El Salvador (n = 2), Saint Lucia (n = 1), Saint Martin (n = 1), Panama (n = 1), Niger (n = 1), and Venezuela (n = 1).

and median patient age was 31.5 years (IQR 10.5–40.5 years). None tested positive for CHIKV or ZIKV. Positive cases were geographically distributed across 3 municipalities in Luanda Province: Luanda (9/16 [56.3%]), Viana (6/16 [37%]), and Talatona (1/16 [6.3%]) (Appendix Table 1). We detected positive cases during April–July 2024 and detected no cases during August–November (dry season). Two positive case-patients required platelet transfusion, consistent with severe dengue and possible secondary infection (Appendix Table). Climatic suitability for *Ae. aegypti* mosquito transmission (index P, lagged +2 months) remained above 1 during September–July, confirming permissive conditions for transmission during the detection window (Figure; Appendix Figure 1).

We attempted sequencing of all 16 positive samples by using a multiplex PCR protocol on

the Oxford Nanopore MinION platform (https://nanoporetech.com) (Appendix). We recovered 6 near-complete and partial DENV-3 sequences (median coverage 37.6%, IQR 21.5%–57.1%) (Figure; Appendix Table). All were classified as DENV-3 lineage III_B.3.2. Lower cycle threshold values correlated with higher horizontal sequencing coverage (r ρ = −0.44; p = 0.1) (Appendix Figure 2). Maximum-likelihood phylogenetic analysis showed Angola sequences clustering into a single clade (bootstrap = 100) (Figure; Appendix). Molecular clock analysis estimated their common ancestor to be around late October 2022 (95% Bayesian CI April 2022–March 2023) (Appendix Figures 4–6).

Phylogenetic analyses revealed that Angola sequences were more closely related to viruses from the Americas (Figure; Appendix Figures 4, 5). However, undersampling and inequities in sequencing capacity

could result in alternative epidemiologic scenarios, so we compared air passenger traffic into Angola (Appendix Figure 6) with lineage III_B.3.2 sampling intensity measured as the number of publicly available genomes for this lineage per million inhabitants in any given country where this lineage had been detected (according to GenBank data as of April 25, 2025). We observed a moderate correlation (Pearson r = 0.55; p = 0.042), suggesting that countries with frequent travel links, particularly Cuba, harbored closely related strains. However, those findings should be interpreted cautiously given limited recent genomic DENV-3 data from several regions, including Brazil (Appendix Figures 7–9).

We document the emergence of DENV-3 lineage III_B.3.2 in Luanda, Angola, where the lineage probably was introduced from the Americas in late 2022, followed by local transmission across Luanda Province. Seasonal detection patterns aligned with climatic suitability for *Aedes* mosquito–borne transmission.

The emergence of DENV-3 in Angola raises concerns about disease severity given prior circulation of DENV-1 and DENV-2. In the absence of large-scale vaccination or vector-control programs, strengthening laboratory and clinical surveillance will be critical for outbreak detection and patient management (*6*). The risk extends beyond Luanda Province, which accounts for 27% of the country's 38 million residents (https://data.worldbank.org/indicator/ SP.POP.TOTL?locations=AO). *Ae. aegypti* mosquitos are widespread in the country (*7*), and climate projections indicate increasingly intense wet seasons in coastal Angola (*8*), further increasing the risk for arboviral transmission.

Given Angola's history of *Aedes* mosquito–borne outbreaks, including yellow fever (2015–2016) (*9*) and Zika virus (2016–2017) (*10*), investment in laboratory capacity, capacity retention, and vector surveillance is urgent. Improved preparedness will help to mitigate the risk for sustained DENV transmission and related public health consequences.

Members of the FEEVIR Consortium: Aracelli Acevedo Colina, Luís Miguel Costa, Rogério Diemba, Reginaldo Samuel, António Cassinda, and Domingos Catraio.

About the Author

Ms. de Vasconcelos is a public health researcher, PhD candidate at Imperial College London, and head of the Centro de Investigação em Saúde de Angola. Her research focuses on epidemiological surveillance and the molecular and genomic characterization of emerging and reemerging infectious diseases in Angola. Dr. Claro is a postdoctoral scholar at the University of Kentucky. Her research focuses on viral genomics and epidemiology of emerging viruses, with an emphasis on developing and improving strategies for detection, preparedness, and response to viral outbreaks affecting humans and animals.

References

1. Lim A, Shearer FM, Sewalk K, Pigott DM, Clarke J, Ghouse A, et al. The overlapping global distribution of dengue, chikungunya, Zika and yellow fever. Nat Commun. 2025;16:3418. https://doi.org/10.1038/s41467-025-58609-5
2. Hill V, Cleemput S, Pereira JS, Gifford RJ, Fonseca V, Tegally H, et al. A new lineage nomenclature to aid genomic surveillance of dengue virus. PLoS Biol. 2024;22:e3002834. https://doi.org/10.1371/journal.pbio.3002834
3. Katzelnick LC, Gresh L, Halloran ME, Mercado JC, Kuan G, Gordon A, et al. Antibody-dependent enhancement of severe dengue disease in humans. Science. 2017;358:929–32. https://doi.org/10.1126/science.aan6836
4. Mercy K, Youm E, Aliddeki D, Faria NR, Kebede Y, Ndembi N. The looming threat of dengue fever: the Africa context. Open Forum Infect Dis. 2024;11:ofae362. https://doi.org/10.1093/ofid/ofae362
5. Centers for Disease Control and Prevention (CDC). Ongoing dengue epidemic - Angola, June 2013. MMWR Morb Mortal Wkly Rep. 2013;62:504–7.

6. Neto Z, Martinez PA, Hill SC, Jandondo D, Thézé J, Mirandela M, et al. Molecular and genomic investigation of an urban outbreak of dengue virus serotype 2 in Angola, 2017-2019. PLoS Negl Trop Dis. 2022;16:e0010255. https://doi.org/10.1371/journal.pntd.0010255

7. Marquetti Fernández M, Arletty T, Cani P, Flores Y. Longitudinal spatial distribution of *Aedes aegypti* (Diptera: Culicidae) during the yellow fever epidemic in Angola, 2016. Glob J Zool. 2019;4:001–6. https://doi.org/10.17352/gjz.000011

8. Soares PMM, Careto JAM, Lima DCA. Future extreme and compound events in Angola: CORDEX-Africa regional climate modelling projections. Weather Clim Extrem. 2024;45:100691. https://doi.org/10.1016/j.wace.2024.100691

9. Kraemer MUG, Faria NR, Reiner RC Jr, Golding N, Nikolay B, Stasse S, et al. Spread of yellow fever virus outbreak in Angola and the Democratic Republic of the Congo 2015-16: a modelling study. Lancet Infect Dis. 2017; 17:330–8. https://doi.org/10.1016/S1473-3099(16)30513-8

10. Hill SC, Vasconcelos J, Neto Z, Jandondo D, Zé-Zé L, Aguiar RS, et al. Emergence of the Asian lineage of Zika virus in Angola: an outbreak investigation. Lancet Infect Dis. 2019;19:1138–47. https://doi.org/10.1016/S1473-3099(19)30293-2

Address for correspondence: Joana Morais, Instituto Nacional de Investigação em Saúde, Rua Amílcar Cabral 96, Maianga, Luanda, Angola; email: jfm.morais9@gmail.com

Yellow Fever Virus in *Aedes albopictus* Mosquitoes from Urban Green Area, São Paulo State, Brazil

Eduardo S. Bergo, Juliana Telles-de-Deus, Luis F. Mucci, Vanessa C. Helfstein, Maria de Jesus C. Nascimento, Nubia R.M.F. Rocha, Anderson de Paula, Lucy S. Villas-Boas, Camila M. Romano, Luzia M.R. Passos, Vera Lucia F. de Camargo-Neves, Karin Kirchgatter

Author affiliations: Pasteur Institute, São Paulo, Brazil (E.S. Bergo, J. Telles-de-Deus, L.F. Mucci, V.C. Helfstein, M.J.C. Nascimento, N.R.M.F. Rocha, V.L.F. de Camargo-Neves, K. Kirchgatter); University of São Paulo, São Paulo (A. de Paula, L.S. Villas-Boas, C.M. Romano); Health Surveillance Department of the Municipality of Ribeirão Preto, São Paulo (L.M.R. Passos)

We detected yellow fever virus by using quantitative PCR in *Aedes albopictus* mosquitoes and isolated the virus in C6/36 cells in 4 of 18 pools, including 118 specimens collected in an urban green area in São Paulo State, Brazil. Additional monitoring to detect shifts in transmission of this species is warranted.

Yellow fever is an infectious disease caused by an RNA virus of the genus *Orthoflavivirus*, family *Flaviviridae* (*1*). Yellow fever virus (YFV) is transmitted to humans and nonhuman primates, the main vertebrate hosts, through bites of mosquitoes from genus *Aedes* in Africa and *Haemagogus* and *Sabethes* in the Americas. The sylvatic cycle occurs in both regions, where vectors, breeding and living in forests, infect nonhuman primates. Human infection is accidental (e.g., when persons enter the forest or stay at forest edges). The urban cycle, common in Africa, involves transmission between *Ae. aegypti* mosquitoes and humans. In the Americas, the last urban transmission occurred in the 1940s, when effective mass vaccination and vector-control campaigns were implemented in cities (*2*).

During 2014–2023, Brazil's main metropolitan regions, including areas with dense, unvaccinated populations, were affected by a major yellow fever epidemic, raising concerns about disease re-urbanization (*3*). In 2017, genetic studies confirmed a new wave spread to areas outside the Amazon rainforest (*4*).

In São Paulo State, the current yellow fever epidemic (2022–2025) has reached 45 municipalities (*5*). The northwest region, which has seasonal climate and fragmented forests, reported fewer human cases and epizootics than the eastern region (*5*). YFV circulation has been documented repeatedly in 2000, 2008, 2016–2018, 2020, and 2024–2025 (*5*). In this northwest region, virus detection in secondary or potential vector species stands out, whereas in more forested regions with higher numbers of human cases and epizootics, *Haemagogus* sp. mosquitoes showed greater infectivity (*6*). We report results of an entomovirologic survey in Ribeirão Preto, São Paulo State, Brazil (≈700,000 inhabitants), conducted after epizootics occurred in nonhuman primates.

On December 25, 2024, four howler monkeys (*Alouatta caraya*) died in forest fragments on the University of São Paulo (USP) campus in Ribeirão Preto. Six days later, 2 more howler monkeys were found dead. All tested positive for YFV at the Adolfo Lutz Institute (São Paulo).

Following Brazil's Ministry of Health guidelines, we conducted entomovirologic surveillance after confirmation of human or epizootic cases to characterize

Table. Nonengorged adult female mosquitoes collected in entomovirologic surveillance for yellow fever virus from an urban green area (University of São Paulo, Ribeirão Preto campus), São Paulo State, Brazil, January 7–9, 2025

Species	No. mosquitoes	Pools analyzed	Positive pools
Aedes albopictus	118	18	4
Ae. scapularis	25	12	0
Ae. serratus	11	5	0
Ae. terrens	2	2	0
Culex (*Culex*) spp.	15	0	0
Haemagogus leucocelaenus	2	2	0
Limatus durhamii	2	2	0
Psorophora ferox	3	3	0
Sabethes albiprivus	30	11	0
Sa. glaucodaemon	1	1	0
Sa. gymnothorax	1	1	0
Sabethes spp.	2	2	0
Total	212	59	4

the eco-epidemiologic context. During January 7–9, 2025, four trained personnel collected adult mosquitoes by using hand nets and suction aspirators at ground level and from 10-m canopy platforms within forest fragments on the university campus during 9 AM–4 PM. We cryopreserved samples in liquid nitrogen, sent them to the Pasteur Institute (São Paulo) for morphologic identification under cold conditions, and then pooled them by species. We tested 59 female pools (197 mosquitoes from 10 species of Aedini and Sabethini tribes) (Table) for YFV RNA by quantitative reverse transcription PCR (qRT-PCR) by using a broad-range flavivirus assay (*7*) and a YFV-specific assay (*8*).

Four pools tested positive for YFV and had high viral loads (cycle threshold [Ct] 19–22 for YFV protocol and 23–25 for pan-flavivirus protocol). We used Sanger sequencing to analyze all PCR products and confirmed YFV by using BLAST (https://blast.ncbi.nlm.nih.gov/Blast.cgi). All positive pools contained only nonengorged *Ae. albopictus* mosquitoes,

collected at ground level with hand nets during January 8–9, 2025 (Table).

To further confirm the virus viability, we performed virus isolation in a Biosafety Level 2 laboratory at the USP Institute of Tropical Medicine by using *Ae. albopictus* mosquito C6/36 cells (Figure, panel A). We cultured cells at 28°C in 5% CO_2 in Leibovitz's L-15 medium with 5% fetal bovine serum. We filtered YFV RNA–positive pool samples (the entire bodies of the insects homogenized in Hanks' balanced salt solution; GIBCO-BRL, https://www.thermofisher.com) through 0.22-µm membranes and inoculated them (100 µL of the filtrate) onto confluent C6/36 monolayers in 24-well plates. After 1-hour adsorption, we added 1 mL medium with 2% fetal bovine serum, 1% streptomycin, and amphotericin B. We incubated cultures 5 days and then conducted 2 passages (P2, P3). We performed daily microscopic monitoring for cytopathic effects. We tested supernatants from P1–P3 for YFV RNA by using qRT-PCR. Virus isolation succeeded in all 4 pools. Pool B3693 showed early cytopathic effects at P1 (Figure, panel B) and had a lower YFV qRT-PCR Ct than the inoculum. The other 3 pools were positive at P2 (Figure, panel C). We confirmed virus isolation by observing cytopathic effects and the decreasing Ct values during passages.

Previous detections of YFV RNA in this species showed only low viral loads (Ct >35), and no virus was cultured (*6*). Our data suggest that *Ae. albopictus* mosquitoes played a central role in virus transmission among nonhuman primates at USP Ribeirão Preto, given its high detection rate (4 of 18 pools), abundance (55.7% of specimens), low *Haemagogus* sp. mosquito density, and no YFV found in *Sabethes albiprivus* mosquitoes (11 pools), a known secondary vector (*9*).
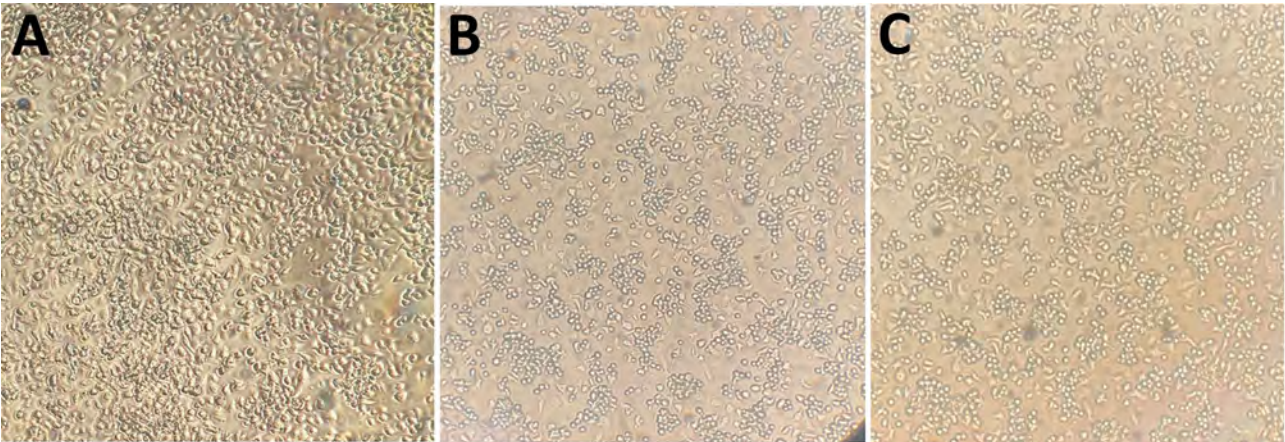

Figure. Optical microscopic analysis of C6/36 cell culture infected by yellow fever virus in *Aedes albopictus* mosquitoes from an urban green area (University of São Paulo, Ribeirão Preto campus), São Paulo State, Brazil. A) Mock (uninfected control cells). B) Yellow fever virus isolated in passage 1, five days postinfection. C) YFV isolated in passage 2, ≈10 days postinfection. Original magnification × 40.

The confirmed vector competence of *Ae. albopictus* mosquitoes for YFV under experimental conditions (*10*), combined with our findings, highlights its potential epidemiologic role at the sylvatic–urban interface. Our findings also underscore the importance of enhancing entomological surveillance in urban green areas to detect shifts in transmission dynamics early and prevent the re-urbanization of yellow fever in Brazil.

About the Author
Dr. Bergo is a scientific researcher at the Vector Section of the Pasteur Institute, Araraquara Unit, São Paulo, Brazil. His research interests include public health, with an emphasis on the ecology of diseases transmitted by insect vectors.

References
1. Postler TS, Beer M, Blitvich BJ, Bukh J, de Lamballerie X, Drexler JF, et al. Renaming of the genus *Flavivirus* to *Orthoflavivirus* and extension of binomial species names within the family Flaviviridae. Arch Virol. 2023;168:224. https://doi.org/10.1007/s00705-023-05835-1
2. Monath TP, Vasconcelos PF. Yellow fever. J Clin Virol. 2015;64:160–73. https://doi.org/10.1016/j.jcv.2014.08.030
3. Giovanetti M, Pinotti F, Zanluca C, Fonseca V, Nakase T, Koishi AC, et al. Genomic epidemiology unveils the dynamics and spatial corridor behind the yellow fever virus outbreak in southern Brazil. Sci Adv. 2023;9:eadg9204. https://doi.org/10.1126/sciadv.adg9204
4. Andrade MS, Campos FS, Oliveira CH, Oliveira RS, Campos AAS, Almeida MAB, et al. Fast surveillance response reveals the introduction of a new yellow fever virus sub-lineage in 2021, in Minas Gerais, Brazil. Mem Inst Oswaldo Cruz. 2022;117:e220127. https://doi.org/10.1590/0074-02760220127
5. Saad LDC, Chiaravalloti-Neto F. Reemergence of yellow fever in the state of São Paulo: the structuring role of surveillance of epizootics in non-human primates in a one health approach. Rev Bras Epidemiol. 2024;27:e240064. https://doi.org/10.1590/1980-549720240064.2
6. Caleiro GS, Vilela LO, Nuevo KMB, Tubaki RM, de Menezes RMT, Mucci LF, et al. Yellow fever virus (YFV) detection in different species of culicids collected during an outbreak in southeastern Brazil, 2016–2019. Trop Med Infect Dis. 2025;10:118. https://doi.org/10.3390/tropicalmed10050118
7. Patel P, Landt O, Kaiser M, Faye O, Koppe T, Lass U, et al. Development of one-step quantitative reverse transcription PCR for the rapid detection of flaviviruses. Virol J. 2013;10:58. https://doi.org/10.1186/1743-422X-10-58
8. Domingo C, Patel P, Yillah J, Weidmann M, Méndez JA, Nakouné ER, et al. Advanced yellow fever virus genome detection in point-of-care facilities and reference laboratories. J Clin Microbiol. 2012;50:4054–60. https://doi.org/10.1128/JCM.01799-12
9. de Oliveira CH, Andrade MS, Campos FS, da C Cardoso J, Gonçalves-Dos-Santos ME, Oliveira RS, et al. Yellow fever virus maintained by *Sabethes* mosquitoes during the dry season in Cerrado, a semiarid region of Brazil, in 2021. Viruses. 2023;15:757. https://doi.org/10.3390/v15030757
10. Couto-Lima D, Madec Y, Bersot MI, Campos SS, Motta MA, Santos FBD, et al. Potential risk of re-emergence of urban transmission of yellow fever virus in Brazil facilitated by competent *Aedes* populations. Sci Rep. 2017;7:4848. https://doi.org/10.1038/s41598-017-05186-3

Address for correspondence: Karin Kirchgatter, Laboratório de Bioquímica e Biologia Molecular, Instituto Pasteur, Rua Paula Sousa 166, São Paulo, São Paulo 01027-000, Brazil; email: karink@usp.br

Molecular Evidence of Dengue Virus Serotype 2 in Travelers Returning to Israel from the Sinai Peninsula

Neta S. Zuckerman,[1] Guy Choshen,[1] Yaniv Lustig, Anna Shoykhet, Keren Friedman, Tatyana Kushnir, Ora Halutz, Hovav Azulay, Victoria Indenbaum,[1] Eli Schwartz[1]

Author affiliations: Tel-Aviv University, Tel Aviv, Israel (N.S. Zuckerman, G. Choshen, Y. Lustig, O. Halutz, E. Schwartz); Sheba Medical Center, Ramat-Gan, Israel (N.S. Zuckerman, Y. Lustig, K. Friedman, T. Kushnir, V. Indenbaum, E. Schwartz); Tel-Aviv University, Tel Aviv, Israel (G. Choshen, Y. Lustig, O. Halutz, E. Schwartz); Meir Medical Center, Kfar-Saba, Israel (G. Choshen, A. Shoykhet); Infectious Disease Institute, Soroka University Medical Center, Beer Sheba, Israel (H. Azulay)

[1]These authors contributed equally to this article.

We report 4 dengue cases in travelers returning to Israel from Sharm-El-Sheikh, Egypt, all confirmed as dengue virus type 2 infections. Phylogenetic analysis showed clustering with strains from Pakistan. Our findings provide molecular evidence of dengue circulation in the Sinai desert, highlighting the need for increased awareness among travelers and health authorities.

Dengue virus (DENV) is the most widespread arbovirus globally; its incidence has increased tenfold in the past 2 decades, largely driven by climate change and globalization (1). Although transmission is well documented in Southeast Asia and the Americas, autochthonous emergence is increasingly reported in nonendemic regions, including Europe.

We report 4 confirmed dengue fever cases in travelers returning to Israel after visiting Sharm El-Sheikh, a desert resort city in South Sinai, Egypt, during April–June 2024. Sharm El-Sheikh has not previously been recognized as an area of dengue transmission, the arid environment of the Sinai Peninsula is considered unfavorable for the DENV primary vectors, *Aedes* mosquitoes.

The cases (Table) were unrelated; travel dates were nonoverlapping and accommodations varied and were located 3–25 km apart. Patients had typical dengue symptoms such as fever, headache, myalgia, and rash. All were hospitalized, received supportive care, and recovered. One patient exhibited meningeal irritation; cerebrospinal fluid testing results were unremarkable, although DENV serotype 2 (DENV-2) RNA was detected by quantitative real-time PCR (cycle threshold 32.5). All samples were collected within 1 week of symptom onset. Serum testing confirmed DENV-2 by multiplex quantitative real-time PCR (2); additional nonstructural protein 1 antigen and IgM/IgG positivity was detected in some cases.

To explore the geographic origin of the DENV-2 cases, we performed DENV whole-genome sequencing. We captured DENV-2 using specific whole-genome primers (https://grubaughlab.com/open-science/amplicon-sequencing); we prepared sequencing libraries using Nextera-XT and ran them on the Illumina NovaSeq (https://www.illumina.com). We generated consensus sequences by mapping to the DENV-2 reference genome (GenBank accession no. NC_001474.2) and deposited resulting sequences into GenBank (Appendix Table, https://wwwnc.cdc.gov/EID/article/31/11/25-0991-App1.xlsx). Use of the samples in this study was approved by the Sheba Medical Center Institutional Review Board (approval no. SMC-6190-19).

Samples yielded sufficient DENV-2 genome coverage, except in the case of patient no. 4 (possibly because of high cycle threshold [34]), which was excluded. Phylogenetic analysis with global DENV-2 sequences (n = 1,492) clustered the Israel sequences within the Cosmopolitan genotype. All 3 sequences formed a distinct cluster, sharing a common ancestor and differing by 32 mutations from the nearest global strain. The closest related sequences were from Pakistan. The only publicly available sequence geographically close to Sinai, from the United Arab Emirates in 2023, clustered separately within another Cosmopolitan lineage with strains from China, India, and Bangladesh (Figure, panel A).

Our findings describe 4 confirmed DENV-2 infections in travelers from Sharm El-Sheikh, Egypt, a city in the arid Sinai Peninsula, previously considered unsuitable for *Aedes* mosquitoes and without previous dengue reports. Genomic analysis showed clustering of cases, likely from a single outbreak, most closely related to strains from Pakistan. Aside from 1 United Arab Emirates 2023 sequence clustering separately, no recent data from Sinai are available, underscoring a major surveillance gap. Those results align with reports of DENV-2 spread along the Red Sea and recent cases in Florence, Italy (8).

During the past 2 decades, *Ae. aegypti* mosquito populations have expanded in Egypt, especially along the Red Sea coast (Figure, panel B), correlating with dengue outbreaks. However, no entomologic data exist for Sinai. The arid climate challenges mosquito survival, but clustering of cases in 1 resort area suggests local adaptation, possibly supported by urban microhabitats (9). Maritime and air travel might drive

Table. Epidemiology and test results of patients in study of molecular evidence of DENV-2 emergence from travelers returning to Israel from the Sinai Peninsula*

Characteristic	Patient 1	Patient 2	Patient 3	Patient 4
Patient age, y/sex	33/M	40/F	45/M	19/M
DENV laboratory diagnostic analysis				
Sample collection date	2024 Apr 22	2024 May 7	2024 Jun 5	2024 Jun 10
Serum quantitative real-time PCR	DENV-2 (Ct 28)	DENV-2 (Ct 26.5)	DENV-2 (Ct 27)	DENV-2 (Ct 34)
Serum EIA IgM	Negative	Negative	Positive	Positive
Serum EIA IgG	Negative	Negative	Positive	Negative
DENV nonstructural protein 1 antigen	Positive	Positive	Negative	Positive

*Ct, cycle threshold; DENV, dengue virus; DENV-2, DENV serotype 2; EIA, enzyme immunoassay.
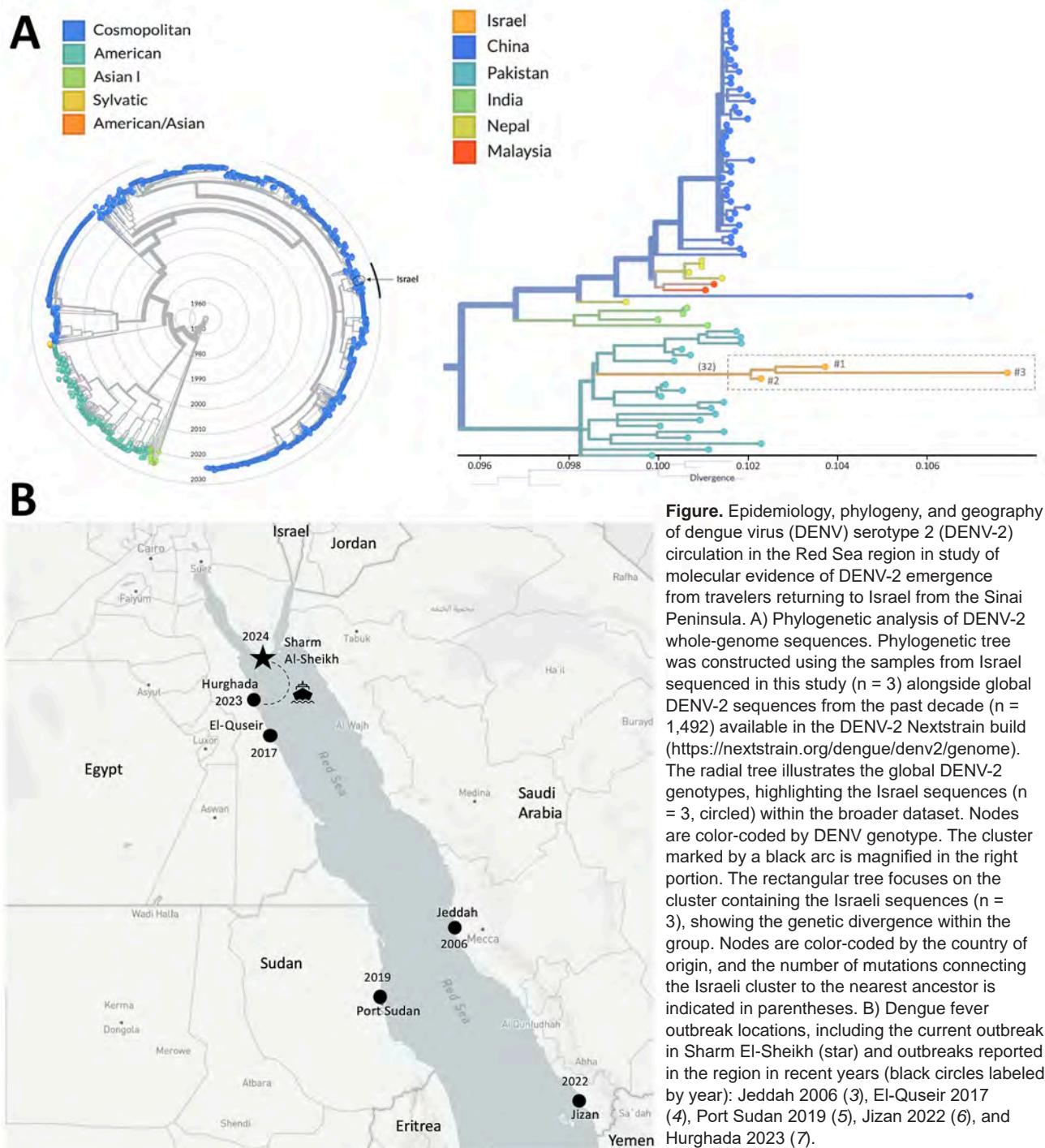
Figure. Epidemiology, phylogeny, and geography of dengue virus (DENV) serotype 2 (DENV-2) circulation in the Red Sea region in study of molecular evidence of DENV-2 emergence from travelers returning to Israel from the Sinai Peninsula. A) Phylogenetic analysis of DENV-2 whole-genome sequences. Phylogenetic tree was constructed using the samples from Israel sequenced in this study (n = 3) alongside global DENV-2 sequences from the past decade (n = 1,492) available in the DENV-2 Nextstrain build (https://nextstrain.org/dengue/denv2/genome). The radial tree illustrates the global DENV-2 genotypes, highlighting the Israel sequences (n = 3, circled) within the broader dataset. Nodes are color-coded by DENV genotype. The cluster marked by a black arc is magnified in the right portion. The rectangular tree focuses on the cluster containing the Israeli sequences (n = 3), showing the genetic divergence within the group. Nodes are color-coded by the country of origin, and the number of mutations connecting the Israeli cluster to the nearest ancestor is indicated in parentheses. B) Dengue fever outbreak locations, including the current outbreak in Sharm El-Sheikh (star) and outbreaks reported in the region in recent years (black circles labeled by year): Jeddah 2006 (*3*), El-Quseir 2017 (*4*), Port Sudan 2019 (*5*), Jizan 2022 (*6*), and Hurghada 2023 (*7*).

repeated introductions of *Ae. aegypti* mosquitos and DENV into the Red Sea region. However, the pattern of DENV-2 outbreaks in Red Sea port cities support maritime transport as a key driver of spread (*6,7,10*). The daily ferries from Hurghada, where dengue recently emerged, to Sharm El-Sheikh might be especially relevant (Figure, panel B). Genetic data from a 2019 Jizan outbreak and strains from Saudi Arabia (1992–2014) further suggest multiple introductions linked to an imported DENV-2 variant genetically similar to strains from Malaysia, Singapore, Korea, and China (*6*). Additional analyses from the DENV-2 strains isolated in Saudi Arabia during 1992–2014 reveal strong clustering with viruses from countries that contribute the largest numbers of Hajj and Umrah pilgrims: Indonesia, Pakistan, and India (*10*). Indeed, phylogenetic

analysis shows that our dengue sequences are closest to recent strains from Pakistan. However, the scarcity of sequences from Egypt and neighboring regions limits inference on viral origin, circulation, and distribution, and observed variability suggests undersampling and additional undetected cases.

This report of 4 cases over 3 months in different localities of Sharm El-Sheikh suggests sustained DENV-2 transmission and emphasizes the importance of enhanced vector surveillance and control, providing an alert to public health authorities. The genetic data presented might help address gaps in regional DENV sequence reporting and contribute to understanding its molecular epidemiology and origins.

About the Author

Dr. Zuckerman leads the Bioinformatics and Genomics Center at Israel's Central Virology Laboratory, Ministry of Health, and is affiliated with Tel Aviv University's School of Public Health. Her work focuses on genomic surveillance, molecular epidemiology, and bioinformatics applications in the study of viral pathogens

References

1. World Health Organization. Dengue and severe dengue [2025 Mar 1]. https://www.who.int/news-room/fact-sheets/detail/dengue-and-severe-dengue.
2. Santiago GA, Vergne E, Quiles Y, Cosme J, Vazquez J, Medina JF, et al. Analytical and clinical performance of the CDC real time RT-PCR assay for detection and typing of dengue virus. PLoS Negl Trop Dis. 2013;7:e2311. https://doi.org/10.1371/journal.pntd.0002311
3. Kholedi AAN, Balubaid O, Milaat W, Kabbash IA, Ibrahim A. Factors associated with the spread of dengue fever in Jeddah Governorate, Saudi Arabia. East Mediterr Health J. 2012;18:15–23. https://doi.org/10.26719/2012.18.1.15
4. El-Kady AM, Osman HA, Alemam MF, Marghani D, Shanawaz MA, Wakid MH, et al. Circulation of dengue virus serotype 2 in humans and mosquitoes during an outbreak in El Quseir City, Egypt. Infect Drug Resist. 2022;15:2713–21. https://doi.org/10.2147/IDR.S360675
5. Desogi M, Ali M, Gindeel N, Khalid F, Abdelraheem M, Alnaby A, et al. Detection of dengue virus serotype 4 in Sudan. East Mediterr Health J. 2023;29:436–41. https://doi.org/10.26719/emhj.23.041
6. Dafalla O, Abdulhaq AA, Almutairi H, Noureldin E, Ghzwani J, Mashi O, et al. The emergence of an imported variant of dengue virus serotype 2 in the Jazan region, southwestern Saudi Arabia. Trop Dis Travel Med Vaccines. 2023;9:5. https://doi.org/10.1186/s40794-023-00188-8
7. Frank C, Lachmann R, Wilking H, Stark K. Increase in dengue fever in travellers returning from Egypt, Germany 2023. Euro Surveill. 2024;29:2400042. https://doi.org/10.2807/1560-7917.ES.2024.29.5.2400042
8. Manciulli T, Zammarchi L, Lagi F, Fiorelli C, Mencarini J, Fognani M, et al. Emergence of dengue fever: sentinel travellers uncover outbreak in Sharm El-Sheikh, Egypt, May 2024. J Travel Med. 2024;31:taae080. https://doi.org/10.1093/jtm/taae080
9. Newman EA, Feng X, Onland JD, Walker KR, Young S, Smith K, et al. Defining the roles of local precipitation and anthropogenic water sources in driving the abundance of *Aedes aegypti*, an emerging disease vector in urban, arid landscapes. Sci Rep. 2024;14:2058. https://doi.org/10.1038/s41598-023-50346-3
10. El-Kafrawy SA, Sohrab SS, Ela SA, Abd-Alla AM, Alhabbab R, Farraj SA, et al. Multiple introductions of dengue 2 virus strains into Saudi Arabia from 1992 to 2014. Vector Borne Zoonotic Dis. 2016;16:391–9. https://doi.org/10.1089/vbz.2015.1911

Address for correspondence: Neta S. Zuckerman, Central Virology Laboratory, Sheba Medical Center, 2 Derech Sheba, Ramat-Gan, Israel; email: neta.zuckerman@sheba.health.gov.il

Anna Mary Robertson ("Grandma") Moses (1860–1961), *May, Making Soap, Washing Sheep, 1870* (1945). Oil on Masonite, 17.24 in × 23.94 in × 2 in/43.79 cm × 60.81 cm × 5.08 cm. Copyright © Grandma Moses Properties Co. New York. Digital image from the Kallir Research Institute, 156 W 56th St, New York, NY, USA.

Viewing Rural Life through a Public Health Lens

Nkuchia M. M'ikanatha, David P. Welliver, Byron Breedlove

This month's cover features Grandma Moses's painting *May, Making Soap, Washing Sheep, 1870*, a vibrant 1945 depiction of rural life by one of America's most recognized folk artists. The painting typifies the artist's extraordinary ability to recall and illustrate the many activities of farm life. Anna Mary Robertson (later fondly known as Grandma Moses) provides a window into the routines of a family farm, where human contact with animals occurred regularly, interactions that can heighten the risk for transmitting zoonotic diseases.

Anna Mary Robertson was born in 1860 in Greenwich in upstate New York and grew up on a farm where she, along with her siblings, contributed to family chores. In her autobiography, *My Life's History*, Moses recalled a happy childhood with limited schooling. She began working for neighbors for wages at age 12 years. Although she was inclined to painting, Moses lacked the time to develop her artistic talent during her youth and married life.

Anna Mary married Thomas Salmon Moses, an agricultural laborer, in 1887. The couple spent about 2 decades in Virginia's Shenandoah Valley before

Author affiliations: Pennsylvania Department of Health, Harrisburg, Pennsylvania, USA (N.M. M'ikanatha); Clarific Services, Rochester, Minnesota, USA (D.P. Welliver); Centers for Disease Control and Prevention (retired), Atlanta, Georgia, USA (B. Breedlove)

settling on a farm in Eagle Bridge, New York, near her birthplace. They named the farm Mount Nebo. Loneliness after her husband's death in the late 1920s, arthritis (which hindered her ability to stitch embroidery), and her sister's urging probably motivated Moses, then a septuagenarian, to begin painting.

Tapping into her childhood experiences in a rural setting, Grandma Moses brought numerous authentic details into each of her creations. For example, describing the painting that appears on this month's cover, she wrote: "Back in the 1870s the farmers would always wash the sheep after a few hot days before shearing, and the wives would make up the year's supply of hard and soft soap, used on wash day, and [for] house cleaning." In producing soap on their farm from lanolin extracted from sheep's wool, Moses and her family continued a practice dating back millennia. Evidence of this enduring method, combining animal fats with wood ash, can be found in various ancient texts from civilizations including Roman, Greek, and Egyptian.

Beginning in her late 70s, until well into her centennial year, Moses created more than 1,500 paintings, a remarkable feat noted by the Smithsonian American Art Museum (Washington, DC). Her success is largely attributed to Otto Kallir, an art dealer who, after escaping Nazi persecution in Austria in 1938, established Galerie St. Etienne (New York, New York). Kallir championed Moses's work, beginning with a pivotal 1940 exhibition. He meticulously cataloged her paintings and offered crucial insight into her creative process, writing in *Grandma Moses American Primitive*: "The pleasure [she] takes in making a picture, the playful imagination. . . it remains always fresh and fascinating." The catalog from an exhibit in the National Museum of Women in the Arts (Washington, DC) says that Moses rendered pleasant bucolic scenes and figures that evoked "a world that existed primarily in her imagination."

Grandma Moses's nostalgic art depicting "how it used to be" captivated audiences, leading to her widespread recognition beginning in 1940. An early *New York Herald Tribune* report on her October exhibition at Galerie St. Etienne quickly popularized her nickname, "Grandma Moses," solidifying her public persona. Her work became widely accessible and instantly recognizable to millions of Americans, reproduced on holiday cards, dinner plates, and curtain fabrics. Her appearances on a *Time* magazine cover in 1953 and a 1955 *See it Now* episode hosted by Edward R. Murrow further propelled Grandma Moses into her status as a national icon. Her artwork is held by major institutions, including the Galerie St. Etienne,

the Smithsonian American Art Museum, the Metropolitan Museum of Art (New York, New York), and the Bennington Museum (Bennington, Vermont), the last of which maintains the largest public collection of her paintings. In addition, her painting *July Fourth* (1951), a gift to President Harry S. Truman, is part of the White House collection.

In *May, Making Soap, Washing Sheep, 1870*, set against bucolic landscapes with rolling hills, the depiction of people and animals in a homestead environment mirrors themes explored by the *Emerging Infectious Diseases* journal. The bonneted woman tending to a boiling cauldron evokes a bygone era when family chores included soapmaking and washing sheep before shearing. Nostalgic scenes such as this profoundly resonate, somewhat surprisingly, with topics addressed by *Emerging Infectious Diseases*.

Soap washes away not only dirt and grime but also invisible viruses and bacteria that are on skin. It does not kill microscopic pathogens, but the combination of soap and water helps remove them, thus helping also to reduce illness or infection. "Soap and water and common sense are the best disinfectants," according to a quotation attributed to Canadian physician William Osler, one of the "Big Four" founding professors of Johns Hopkins Hospital (Baltimore, Maryland) and sometimes referred to as the father of modern medicine.

On the other hand, in some instances, although less frequently, people washing sheep can inhale *Bacillus anthracis*, a spore-forming, drug-resistant bacterium associated with high fatality rates in humans and animals. This bacterium's spores, however, typically enter the body of workers handling infected sheep, most commonly through carcasses, hides, wool, or contaminated soil, by way of a cut, scratch, or abrasion on the skin. Human contact with sheep, as shown in Grandma Moses's work, also poses a risk for zoonotic diseases such as Q fever, a highly infectious pathogen.

The presence of domestic fowl, which appear to be ducks or geese, visible near the house introduces an array of other zoonotic risks. For example, Psittacosis (*Chlamydophila psittaci*), an atypical pneumonia, is transmitted to humans by inhaling aerosolized dried droppings from infected birds, an occupational risk highlighted by outbreaks on duck farms. More broadly, the fowl might also harbor parasites, including various tapeworms and protozoa. Furthermore, these birds pose a risk for viral diseases, most notably avian influenza ("bird flu"), such as the circulating H5N1 strain of highly pathogenic avian influenza virus. The presence of that

virus is being actively monitored in domestic fowl and livestock across the United States.

In another vignette, chickens gather in front of a gray barn, near a man bent next to a small white structure, with a child in a maroon dress standing nearby. Backyard poultry and their eggs have been associated with outbreaks of emerging drug-resistant strains of *Salmonella infantis*. Other animals present, including a barking dog and horses near the main house on the left, could, without proper precautions, increase the transmission of zoonotic agents such as *Campylobacter* bacteria and *Giardia duodenalis* parasites.

Grandma Moses's naive style is unquestionably aesthetically pleasing and rewarding. Caution is prudent because the farm landscape in the painting also represents a shared ecosystem for humans, domestic animals (including pets), and microbes. Within this space, known zoonotic pathogens are always present, which underscores the need for integrated One Health surveillance and response.

Bibliography

1. Kallir Research Institute. Grandma Moses. American, 1860–1961 [cited 2025 Jun 30]. https://www.kallirresearch.org/artists/grandma-moses/biography
2. National Museum of Women in the Arts. Grandma Moses (Anna Mary Robertson Moses) [cited 2025 Jun 6]. https://nmwa.org/art/collection/calhoun
3. Moses G. Grandma Moses: my life's history. New York: Harper & Brothers; 1951.
4. American Folk Art Museum. Anna Mary Robertson Moses [cited 2025 Jun 6]. https://folkartmuseum.org/grandma-moses
5. Smithsonian American Art Museum. Grandma Moses [cited 2025 Mar 1]. https://americanart.si.edu/artist/grandma-moses-5826
6. Bennington Museum. Grandma Moses [cited 2025 Mar 1]. https://benningtonmuseum.org/grandma-moses
7. The White House Historical Association. July Fourth [cited 2025 June 30]. https://www.whitehousehistory.org/photos/july-fourth
8. Kallir O. Grandma Moses. New York: Abrams; 1973.
9. EBSCO Information Services. Grandma Moses [cited 2025 Jun 3]. https://www.ebsco.com/research-starters/history/grandma-moses
10. Guidoccio J. Honoring Grandma Moses. 2018 Sep 7 [cited 2025 Jun 3]. https://joanneguidoccio.com/2018/09/07/honoring-grandma-moses
11. Centers for Disease Control and Prevention. Handwashing facts. 2024 Apr 17 [cited 2025 Jun 30]. https://www.cdc.gov/clean-hands/data-research/facts-stats/?CDC_AAref_Val=https://www.cdc.gov/handwashing/why-handwashing.html
12. Doctors of British Columbia. Soap, water, and common sense are the best disinfectants—Sir William Osler. President's blog. 2020 Jan 28 [cited 2025 Jun 3]. https://www.doctorsofbc.ca/presidents-blog/2020/soap-water-common-sense-are-best-disinfectants-sir-william-osler
13. The Johns Hopkins University. The founding physicians. William Osler (1849–1919) [cited 2025 Jun 30]. https://www.hopkinsmedicine.org/about/history/history-of-jhh/founding-physicians#osler
14. World Health Organization. Anthrax. 2016 Nov 18 [cited 2025 Jun 30]. https://www.who.int/europe/news-room/questions-and-answers/item/anthrax
15. Laroucau K, de Barbeyrac B, Vorimore F, Clerc M, Bertin C, Harkinezhad T, et al. Chlamydial infections in duck farms associated with human cases of psittacosis in France. Vet Microbiol. 2009;135:82–9. https://doi.org/10.1016/j.vetmic.2008.09.048
16. US Department of Agriculture. Highly pathogenic avian influenza detections in livestock. 2025 Jul 30 [cited 2025 Nov 15]. https://www.aphis.usda.gov/h5n1-hpai
17. Centers for Disease Control and Prevention. Backyard poultry. 2025 Jul 18 [cited 2025 Jun 30]. https://www.cdc.gov/healthy-pets/about/backyard-poultry.html
18. Caddey B, Fisher S, Barkema HW, Nobrega DB. Companions in antimicrobial resistance: examining transmission of common antimicrobial-resistant organisms between people and their dogs, cats, and horses. Clin Microbiol Rev. 2025;38:e0014622. https://doi.org/10.1128/cmr.00146-22

Address for correspondence: Nkuchia M. M'ikanatha, Bureau of Epidemiology, Rm 933 H&W Bldg, 625 Forster St, Harrisburg, PA 17120-0701, USA; email: nmikanatha@pa.gov, nmikanatha@gmail.com

EMERGING INFECTIOUS DISEASES®

Upcoming Issue • Zoonotic Infections

Complete list of articles in the December issue at
https://wwwnc.cdc.gov/eid/#issue-327

Earning CME Credit

To obtain credit, you should first read the journal article. After reading the article, you should be able to answer the following, related, multiple-choice questions. To complete the questions (with a minimum 75% passing score) and earn continuing medical education (CME) credit, please go to http://www.medscape.org/journal/eid. Credit cannot be obtained for tests completed on paper, although you may use the worksheet below to keep a record of your answers.

You must be a registered user on http://www.medscape.org. If you are not registered on http://www.medscape.org, please click on the "Register" link on the right hand side of the website.

Only one answer is correct for each question. Once you successfully answer all post-test questions, you will be able to view and/or print your certificate. For questions regarding this activity, contact the accredited provider, CME@medscape.net. For technical assistance, contact CME@medscape.net. American Medical Association's Physician's Recognition Award (AMA PRA) credits are accepted in the US as evidence of participation in CME activities. For further information on this award, please go to https://www.ama-assn.org. The AMA has determined that physicians not licensed in the US who participate in this CME activity are eligible for AMA PRA Category 1 Credits™. Through agreements that the AMA has made with agencies in some countries, AMA PRA credit may be acceptable as evidence of participation in CME activities. If you are not licensed in the US, please complete the questions online, print the AMA PRA CME credit certificate, and present it to your national medical association for review.

Article Title

Haematospirillum jordaniae Infections after Recreational Exposure to River Water, Pennsylvania, USA, 2020

CME Questions

1. Which of the following statements regarding previous findings of *Haematospirillum jordaniae* infection is most accurate?

A. It is generally fast-growing on culture
B. It is gram-positive
C. It has affected women and men equally
D. It has usually been diagnosed during the summer and fall

2. What was the common exposure associated with *H. jordaniae* infection among 3 of the 4 patients in the current study?

A. Exposure to farm animals
B. Intravenous drug use
C. Drinking unpasteurized milk
D. Minor trauma in fresh water

3. All of the following were laboratory abnormalities identified in all 4 cases of *H. jordaniae* infection in the current study except

A. Elevated serum creatinine
B. Thrombocytosis
C. Neutrophilia
D. Leukocytosis

4. What were the outcomes of the 4 patients with *H. jordaniae* infection in the current study?

A. The mortality rate was ~ 33%
B. About half of the patients required surgical debridement
C. Most patients required admission to the intensive care unit
D. Patients experienced recovery with a combination of parenteral and oral antibiotics

2026

CDC YELLOW BOOK

Health Information for International Travel

Launch of CDC Yellow Book 2026– A Trusted Travel Medicine Resource

CDC is pleased to announce the launch of the **CDC Yellow Book 2026**. The CDC Yellow Book is a resource containing the U.S. government's travel medicine recommendations and has been trusted by the travel medicine community for over 50 years. Healthcare professionals can use the print and digital versions to find the most up-to-date travel medicine information to better serve their patients' healthcare needs.

The CDC Yellow Book is available online now at www.cdc.gov/yellowbook and in print starting in June 2025 through Oxford University Press and other major online booksellers.